

CENTRAL LIBRARY

TEZPUR DIST.

Accession No. T 308

Date _____

HYPERBRANCHED EPOXY NANOCOMPOSITES FOR BIOMEDICAL APPLICATIONS

A thesis submitted in partial fulfillment of the requirements for
the degree of
Doctor of Philosophy

Shaswat Barua

Registration No. TZ121481 of 2012



School of Sciences
Department of Chemical Sciences
Tezpur University
Napaam, Tezpur - 784028
Assam, India

Dedicated

To

Maa Dua

ABSTRACT

Biomaterials are developed to address basic problems associated with human health and wellbeing. They have been utilized for the reconstruction of damaged tissues and organs, prevention of microbial infections and decrement drug-toxicity. With the development of biomaterials, polymeric ones attained popularity because of their inertness to physiological environment, tunable properties and the control over their fabrication. The chronology continues with the emergence of synthetic catheters, artificial organs, biomedical devices and implants, surgical sealants, safety tools etc. Epoxy based biomaterials were designed for utilizing as root canal sealers, biological glue and surgical sealants. These resins have immense potential for biomedical applications owing to their excellent adhesive strength, resistance to corrosion and high mechanical performance. A few epoxy based commercial products are available, which could not find sustained utility due to their brittleness and toxicity.

Thus, scientists had to think beyond the conventional epoxy systems. At this juncture, epoxy resin with hyperbranched architecture may be utilized for combating the shortcomings of the prevailing systems. In the present investigation hyperbranched epoxy was synthesized by using a biocompatible moiety, glycerol. Different analytical and spectroscopic techniques confirmed the structure of the synthesized epoxy. *In vitro* biocompatibility was examined for the hyperbranched epoxy system. Further, *Homalomena aromatica* rhizome oil modified bentonite and OMMT clay were incorporated into the hyperbranched matrix to attain property enhancement of the nanocomposite systems. *In vitro* and *in vivo* studies established the compatibility of the material with mammalian system. The nanocomposite supported the growth and proliferation of dermatocytes, without induction of any toxic effect. The material also exhibited antimicrobial efficacy against bacteria and fungi. Again, 'green' silver nanoparticles decorated modified OMMT nanocomposite showed tremendous mechanical properties and antimicrobial activity. Its *in vivo* implantation fostered wound healing in wistar rats. Further, a highly efficient antimicrobial implantable material was designed based on hyperbranched epoxy/reduced graphene oxide-silver-curcumin nanocomposite. The material strongly inhibited the growth of bacteria, fungi and microalgae on its surface and showed excellent biocompatibility.

Another carbon based nanomaterial; multiwalled carbon nanotube was utilized to fabricate a high performing nanocomposite. This carbon nanotubes-CuO-nystatin nanocomposite exhibited good biocompatibility to mammalian systems and showed antimicrobial efficacy against bacteria, fungi and microalgae. Moreover, a 'CuO nanoparticles decorated nanofibrillar cellulose' nanocomposite was utilized to prepare an implantable muscle tissue scaffold, which also revealed strong inhibitory effect against surgical site microorganisms. Thus, glycerol based hyperbranched epoxy nanocomposites presented in this thesis can be endorsed as multifaceted biomaterials with advantageous attributes over the prevailing materials in the domain.

DECLARATION

I do hereby declare that the thesis entitled "*Hyperbranched epoxy nanocomposites for biomedical applications*", submitted to the Department of Chemical Sciences, Tezpur University, is a record of original research work carried out by me. All sources of assistance have been assigned with due acknowledgment. I also declare that neither this work as a whole nor a part of it has been submitted to any other University or Institute for any other degree, diploma or award.

Place: Tezpur University, Tezpur

Shaswat Barua
(Shaswat Barua)

Date: 05/01/2015



TEZPUR UNIVERSITY

Ph: 03712-267004

(A Central University established by an Act of Parliament) 03712-267005

NAPAAM, TEZPUR-784028

Fax: 03712-267006

DISTRICT: SONITPUR:: ASSAM:: INDIA

03712-267005

E-mail: nkarak@tezu.ernet.in

CERTIFICATE

This is to certify that the thesis entitled “*Hyperbranched epoxy nanocomposites for biomedical applications*” submitted to Tezpur University in the Department of Chemical Sciences under the School of Sciences, in partial fulfilment for the award of the degree of Doctor of Philosophy in Science, is a record of research work carried out by Mr. Shaswat Barua under my personal supervision and guidance.

All helps received by him from various sources have been duly acknowledged. No part of this thesis has been reproduced elsewhere for award of any other degree.

(Dr. Niranjana Karak)

Professor

Department of Chemical Sciences

School of Sciences

Tezpur University

Place: Tezpur University, Tezpur

Date: 05/01/2015



TEZPUR UNIVERSITY

Ph: 03712-267004

(A Central University established by an Act of Parliament) 03712-267005

NAPAAM, TEZPUR-784028

Fax: 03712-267006

DISTRICT: SONITPUR:: ASSAM:: INDIA

03712-267005

CERTIFICATE

This is to certify that the thesis entitled "*Hyperbranched epoxy nanocomposites for biomedical applications*" submitted to Tezpur University in the Department of Chemical Sciences under the School of Sciences, in partial fulfilment for the award of the degree of Doctor of Philosophy in Science, has been examined by us on .../.../... and found to be satisfactory.

The committee recommends for the award of the degree of Doctor of Philosophy.

Niranjana Karak
Principal Supervisor

Dr. Pradip

External Examiner

Date: 11/03/2015

Date: March 11, 2015

PREFACE

Polymer based biomaterials have been explored for finding out apt options in the domain of tissue engineering and regenerative medicine. Epoxy based biomaterials are utilized for number of medical utilities, while their toxicity demands improvement of the prevailing systems. To overcome the demerits of the conventional epoxy systems like toxicity, brittleness etc; the concept of hyperbranched architecture was introduced. Again, formation of nanocomposites bestows fascinating properties to polymeric systems. Thus, it is quite interesting to collaborate the pros of polymer science and nanotechnology for fabricating high performance, non-toxic biomaterials based on hyperbranched epoxy nanocomposites.

Delving into the possible perspectives in this domain, glycerol based biocompatible hyperbranched epoxy and its nanocomposites were endorsed for various potential biomedical applications in this thesis. Incorporation of *Homalomena aromatica* rhizome oil modified bentonite and OMMT clay, silver decorated modified OMMT clay, reduced graphene oxide-silver-curcumin, carbon nanotubes-CuO-nystatin and nanofibrillar cellulose-CuO conferred the nanocomposites with excellent antimicrobial efficacy, good biocompatibility and adequate mechanical performance to be suitable for a range of biomedical utilities.

Date: 05/01/2015

Place: Tezpur University, Tezpur

Shaswat Barua
(Shaswat Barua)

ACKNOWLEDGMENT

It is really a great pleasure to express my gratitude to the people who have influenced and encouraged me directly or indirectly over the course of my studies and my life in general.

First of all, I would like to express my deep sense of gratitude to my supervisor Dr. Niranjan Karak, Professor, Department of Chemical Sciences, Tezpur University for his guidance, teachings, support, tolerance and advices throughout my Ph.D. work. My whole research career is highly indebted to his sincere efforts.

I would also like to express my sincere gratitude and humble respect to my doctoral committee members Prof. R.C. Deka and Dr. R. Borah, Department of Chemical Sciences, Tezpur University for their timely help and advises.

It is my pleasant duty to acknowledge with thanks the cooperation and support extended to me by the Tezpur University fraternity.

It is of great pleasure to acknowledge the present and former Heads of the Department, Prof. R.C. Deka, Prof. N. Karak and Prof. R.K. Dutta for giving me the opportunity to work on my topic and valuable advises throughout my stay at Tezpur University.

I extend my gratitude to Prof. A.K. Buragohain, Prof. B.K. Konwar and Dr. M. Mandal, Department of Molecular Biology and Biotechnology and Dr. P. Chattopadhyay, Defence Research Laboratory, Tezpur for their cooperation during the course of my biological works. I have the pleasure to acknowledge Dr. S.S. Bhattacharya, Department of Environmental Science, Tezpur University for his kind help regarding the statistical analysis of my data.

I am immensely grateful to Prof. N. S. Islam, Prof. S.K. Dolui, Prof. T.K. Maji, Prof. R.K. Dutta, Prof. R.C. Deka, Dr. A.K. Phukan, Dr. A. J. Thakur, Dr. R. Bora, Dr. P. Puzari, Dr. P. Bharali, Dr. N.M. Gogoi, Dr. K.K. Bania, Dr. S.K. Das, Dr. S. Pratihar and Dr. B.K. Sharma, faculty members of Department of Chemical Sciences, Tezpur University for their valuable suggestions and advices.

My heartfelt thanks go to my senior lab-mates Dr. Harekrishna Deka, Dr. Uday Konwar, Dr. Buddhadeb Roy, Dr. Rocktotpal Konwarh, Dr. Hemjyoti Kalita and Dr. Gautam Das for their manifold help and active co-operation. I would also like to thank my group members Dr. Harsha S.N., Dr. Sujata Pramanik, Beauty Das, Suman Thakur, Bibekananda De, Satyabrat Gogoi, Purnima Baruah, Rituparna Duwarah and Deepshikha Hazarika for their constant inspiration and help during my Ph.D. work.

I would like to offer my sincere thanks to Dr. Biren Gohain, Mr. Nipu Dutta, Mr. Raju K. Borah, Mr. Sankur Phukan, Mr. Rajen Borah, Mr. Biraj Borah, Mr. Arup Chakrabarty, Mr. Manaranjan Sarma, Mr. Ratan Baruah and Mr. Prakash Kurmi for instrumental and experimental helps. DRL Tezpur, IIT Kharagpur, NEHU Shillong, Viswa Bharati West Bengal and other institutions are highly acknowledged for their help in analyzing and testing works.

I would like to thank also the office staffs of Department of Chemical Sciences, Tezpur University, Ms Babita Das, Mr. Hemanta Gogoi and Mr. Bubul Das for their kind help during my Ph.D. work.

I wish to thank all my friends, research scholars of Department of Chemical Sciences, Tezpur University for their help and support during the course of my work. I would like to appreciate Dr. Vijay K. Das, Ms. Papia Dutta, Mrs. Lipika Aidew, Mrs. Nilakshi Baruah, Mr. Bhaskarjyoti Gogoi for their help and suggestions.

I am also grateful to NRB, India for financial support.

I take this opportunity to express my sincere gratitude to Mrs. Susmita Karak for her great affection, which I continue to enjoy during my stay at Tezpur University.

Finally, I owe heartfelt gratitude to my parents and all of my family members for their blessings, support and constant inspiration. I am thankful to all my relatives and well-wisher for their encouragement. The endless love of them will always be in my heart that will inspire me in every step of my future life.

Place : Tezpur University, Tezpur

Date : 05/01/2015

Shaswat Barua
(Shaswat Barua)

CONTENTS

<i>Content</i>	<i>Page No.</i>
Abstract.....	i
Declaration.....	iii
Certificate of Supervisor.....	iv
Certificate of Examiners.....	v
Preface.....	vi
Acknowledgement.....	vii
Contents.....	ix
List of Abbreviations and Symbols.....	xvii
List of Tables.....	xx
List of Figures.....	xxi
List of Schemes.....	xxv

Chapter 1

GENERAL INTRODUCTION

Highlights

1.1. Introduction	1-2
1.2. Background of biomaterials.....	1-4
1.3. Materials and methods.....	1-6
1.3.1. Materials.....	1-6
1.3.1.1. Epoxy	1-6
1.3.1.2. Nanomaterials	1-12
1.3.2. Methods.....	1-18
1.3.2.1. Epoxy resin.....	1-18
1.3.2.2. Nanocomposites	1-23
1.4. Characterization and analysis	1-25
1.4.1. Epoxy resin	1-25

1.4.2. Nanomaterials and nanocomposites.....	1-26
1.4.3. Biological testing for biomaterials.....	1-29
1.4.3.1. Cytocompatibility test.....	1-29
1.4.3.2. Cell adhesion assay.....	1-29
1.4.3.3. <i>In vivo</i> compatibility test.....	1-30
1.4.4. Statistical analysis.....	1-31
1.5. Properties.....	1-31
1.5.1. Rheological.....	1-31
1.5.2. Mechanical.....	1-32
1.5.3. Thermal.....	1-32
1.5.4. Biological properties.....	1-33
1.5.4.1. Biocompatibility.....	1-33
1.5.4.2. Cell adhesion.....	1-34
1.5.4.3. Antimicrobial activity.....	1-35
1.5.4.4. Biodegradation.....	1-36
1.6. Applications.....	1-39
1.6.1. Dental sealing.....	1-39
1.6.2. Antimicrobial coatings.....	1-40
1.6.3. Tissue engineering.....	1-41
1.6.4. Miscellaneous.....	1-42
1.7. Scopes and objectives of the present investigation.....	1-43
1.8. Plan of research.....	1-43

References

Chapter 2

Highlights

2.1. Introduction.....	2-2
2.2. Experimental.....	2-3
2.2.1. Materials.....	2-3
2.2.2. Instruments.....	2-6
2.2.3. Methods.....	2-7
2.2.3.1. Synthesis of HGE.....	2-7

2.2.3.2.	Curing study of the resins	2-8
2.2.3.3.	Evaluation of physical properties.....	2-8
2.2.3.4.	<i>In vitro</i> biocompatibility assessment	2-9
2.2.3.5.	Statistical analysis.....	2-10
2.3.	Results and discussion	2-10
2.3.1.	Synthesis of HGE.....	2-10
2.3.2.	FTIR study	2-10
2.3.3.	¹ H NMR and ¹³ C NMR studies.....	2-11
2.3.4.	XRD study	2-14
2.3.5.	Physical properties of HGE	2-14
2.3.6.	Rheological behavior	2-14
2.3.7.	Curing study and mechanical performance.....	2-15
2.3.8.	Thermal study	2-18
2.3.9.	Chemical resistance	2-19
2.3.10.	<i>In vitro</i> biocompatibility assessment	2-19
2.4.	Conclusion	2-20
References		

Chapter 3

Highlights

3.1.	Introduction	3-2
3.2.	Experimental.....	3-3
3.2.1.	Materials.....	3-3
3.2.2.	Animals	3-4
3.2.3.	Instruments	3-4
3.2.4.	Methods.....	3-5
3.2.4.1.	Modification of nanoclay.....	3-5
3.2.4.2.	Preparation of the NC	3-5
3.2.4.3.	<i>In vitro</i> Biocompatibility assessment.....	3-6
3.2.4.4.	<i>In vivo</i> biocompatibility assessment	3-6
3.2.4.5.	Antibacterial activity test	3-7

3.2.4.6. Statistical analysis	3-8
3.3. Results and discussion	3-8
3.3.1. Preparation of the NC	3-8
3.3.2. Characterization	3-8
3.3.2.1. FTIR study.....	3-8
3.3.2.1. X-ray diffraction analysis	3-10
3.3.2.3. Morphology of the NC	3-11
3.3.3. Curing study and mechanical performance.....	3-12
3.3.4. Thermal study	3-13
3.3.5. <i>In vitro</i> biocompatibility assessment	3-14
3.3.6. <i>In vivo</i> biocompatibility assessment	3-15
3.3.7. Cell attachment and proliferation.....	3-16
3.3.8. Antimicrobial activity	3-17
3.4. Conclusion	3-19
References	

Chapter 4

Highlights

4.1. Introduction	4-2
4.2. Experimental.....	4-3
4.2.1. Materials.....	4-3
4.2.2. Animals	4-4
4.2.3. Instruments	4-4
4.2.4. Methods.....	4-5
4.2.4.1. Preparation of AgNP.....	4-5
4.2.4.2. Preparation of AgOM	4-5
4.2.4.3. Preparation of NC	4-5
4.2.4.4. <i>In vitro</i> biocompatibility assessment	4-6
4.2.4.5. Antimicrobial assays.....	4-6
4.2.4.6. Creation of wound and wound healing analysis	4-7
4.2.4.7. Hematological and histopathological examinations	4-7

4.2.4.8. Statistical analysis.....	4-8
4.3. Results and discussion.....	4-8
4.3.1. Preparation of AgNP.....	4-8
4.3.2. Preparation of HGCS.....	4-8
4.3.3. Characterization.....	4-9
4.3.3.1. UV-visible spectroscopy.....	4-10
4.3.3.2. FTIR study.....	4-10
4.3.3.3. XRD analysis.....	4-11
4.3.3.4. Morphological study.....	4-12
4.3.4. Curing study and mechanical properties.....	4-13
4.3.5. <i>In vitro</i> biocompatibility assessment.....	4-15
4.3.6. Antimicrobial assays.....	4-16
4.3.7. Wound healing analysis.....	4-19
4.3.8. Hematological and histopathological examinations.....	4-19
4.4. Conclusion.....	4-22
References	

Chapter 5

Highlights

5.1. Introduction.....	5-2
5.2. Experimental.....	5-3
5.2.1. Materials.....	5-3
5.2.2. Animals.....	5-4
5.2.3. Instruments.....	5-4
5.2.4. Methods.....	5-5
5.2.4.1. Preparation of Ag-RGO.....	5-5
5.2.4.2. Preparation of Ag-RGO-Cur.....	5-5
5.2.4.3. Preparation of the NC.....	5-6
5.2.4.4. <i>In vitro</i> biocompatibility assessment.....	5-6
5.2.4.5. <i>In vivo</i> biocompatibility assessment.....	5-6
5.2.4.6. Antimicrobial assays.....	5-7

5.2.4.7. Statistical analysis	5-8
5.3. Results and discussion	5-8
5.3.1. Preparation of Ag-RGO	5-8
5.3.2. Preparation of HGGS	5-9
5.3.3. Characterization	5-10
5.3.3.1. UV-visible spectroscopy	5-10
5.3.3.2. FTIR study.....	5-11
5.3.3.3. XRD analysis.....	5-12
5.3.3.4. Morphological study	5-13
5.3.4. Curing study and mechanical performance.....	5-14
5.3.5. <i>In vitro</i> biocompatibility test.....	5-16
5.3.6. <i>In vivo</i> biocompatibility test.....	5-17
5.3.7. Antimicrobial assays	5-20
5.4. Conclusion	5-24
References	

Chapter 6

Highlights

6.1. Introduction	6-2
6.2. Experimental.....	6-3
6.2.1. Materials.....	6-3
6.2.2. Animals	6-5
6.2.3. Instruments	6-5
6.2.4. Methods.....	6-5
6.2.4.1. Preparation of CNT-CuO-Nys	6-5
6.2.4.2. Preparation of NC	6-6
6.2.4.3. Antimicrobial assays.....	6-6
6.2.4.4. <i>In vitro</i> biocompatibility assessment	6-7
6.2.4.5. <i>In vivo</i> biocompatibility assessment	6-7
6.2.4.6. Statistical analysis.....	6-7
6.3. Results and discussion	6-7

6.3.1. Preparation of HGCC.....	6-8
6.3.2. Characterization	6-9
6.3.2.1. UV-visible spectroscopy	6-9
6.3.2.2. FTIR study.....	6-10
6.3.2.3. XRD analysis.....	6-10
6.3.2.4. Morphological study	6-11
6.3.3. Curing study and mechanical performance.....	6-12
6.3.4. Antimicrobial assay	6-13
6.3.5. <i>In vitro</i> biocompatibility assessment	6-16
6.3.6. <i>In vivo</i> biocompatibility assessment	6-17
6.4. Conclusion.....	6-19
References	

Chapter 7

Highlights

7.1. Introduction	7-2
7.2. Experimental.....	7-3
7.2.1. Materials.....	7-3
7.2.2. Animals	7-5
7.2.3. Instruments	7-5
7.2.4. Methods.....	7-5
7.2.4.1. Isolation of NFC from <i>C. esculenta</i> stems.....	7-5
7.2.4.2. Preparation of CuO-NFC	7-6
7.2.4.3. Preparation of NC	7-6
7.2.4.4. <i>In vitro</i> biocompatibility assessment	7-6
7.2.4.5. Adhesion of L6 muscle cells on HGCNF3 scaffold	7-7
7.2.4.6. <i>In vivo</i> implantation of HGCNF3 and host response.....	7-7
7.2.4.7. Antimicrobial assays.....	7-8
7.2.4.8. Statistical analysis	7-8
7.3. Results and discussion	7-8

7.3.1. Preparation of CuO-NFC	7-8
7.3.2. Characterization	7-9
7.3.2.1. UV-visible spectroscopy	7-9
7.3.2.2. FTIR study.....	7-10
7.3.2.3. XRD analysis.....	7-11
7.3.2.4. Morphological study	7-12
7.3.3. Curing study and performance of HGCNF	7-12
7.3.4. <i>In vitro</i> biocompatibility assessment	7-14
7.3.5. Adhesion of L6 muscle cells on HGCNF3 scaffold	7-15
7.3.6. <i>In vivo</i> implantation of HGCNF3 and host response	7-16
7.3.7. Antimicrobial assay	7-18
7.4. Conclusion.....	7-20

References

Chapter 8

Highlights

8.1. Summary and conclusions.....	8-2
8.2. Future scopes.....	8-4

List of Publications.....	P-1
----------------------------------	------------

LIST OF ABBREVIATIONS AND SYMBOLS

ANOVA	analysis of variance
ASTM	American Society for Testing and Materials
ATCC	American Type Culture Collection
ATRP	atom transfer radical polymerization
BPA	bisphenol A
CFU	colony-forming unit
Cm	centimeter(s)
CNT	carbon nanotubes
DB	degree of branching
DMSO	dimethyl sulfoxide
DMTA	dynamic mechanical thermal analyzer
DNA	deoxyribonucleic acid
DSC	differential scanning calorimetry
ECM	extracellular matrix
EDTA	Ethylenediaminetetraacetic acid
Eq	equivalent
FTIR	fourier transform infrared
G	gram(s)
H	hour(s)
HE	hyperbranched epoxy
HRTEM	high resolution transmission electron microscope
Kg	kilogram(s)
kV	kilo-volt
LSD	least significant difference
M	meter(s)
meqv	mili equivalent

MHz	megahertz
Min	minute(s)
mL	milli litre(s)
Mm	milli meter(s)
M_n	number average molecular weight
Mol	mole
MPa	megapascal
MW	multi walled
M_w	weight average molecular weight
N	Newton
NC	nanocomposite
NFC	nanofibrillar cellulose
Nm	nanometer
NMR	nuclear magnetic resonance
OMMT	organically modified montmorillonite
Pas	pascal second
PBS	phosphate buffer saline
RGO	reduced graphene oxide
RPM	rotation per minute
S	second(s)
SEM	scanning electron microscope
SW	single walled
TEM	transmission electron microscope
TGA	thermogravimetric analysis
UTM	universal testing machine
UV	ultraviolet
XRD	X-ray diffraction
Mg	micro gram(s)
μ L	micro liter(s)
Mm	micro meter(s)
μ M	micro molar(s)

%

percentage

°C

degree centigrade

LIST OF TABLES

Table 1.1: Diols commonly used for epoxy synthesis with their structures and applications

Table 1.2: Some branch generating units used for HE synthesis

Table 1.3: Curing agents used for epoxy crosslinking

Table 1.4: A few commercially available epoxy based biomaterials

Table 2.1. Chemical compositions, yield and a few physical properties of HGE

Table 2.2: Curing parameters and performance of HGE and BPAE

Table 2.3: Change in weight (%) of the thermosets in different chemical media

Table 3.1: Curing parameters and performance of HGE5 and its NC

Table 3.2: Hematological parameters of the control and HGEMC implanted rats

Table 3.3: MIC values ($\mu\text{g/mL}$) for the nanocomposites

Table 3.4: Antimicrobial activity of the nanocomposites as zone of inhibition

Table 4.1: Curing parameters and performance of HGE5 and HGCS

Table 4.2: Antimicrobial activity (CFU mL^{-1})

Table 4.3: Percentage of wound contraction

Table 4.4: Hematological parameters after 21 days of implantation

Table 5.1: Curing parameters and performance of HGE5 and HGGS

Table 5.2: Hematological parameters of the control and HGGS3 implanted rats

Table 5.3: Liver function, kidney and lipid profiles of HGG3 implanted rats

Table 5.4: MIC ($\mu\text{g/mL}$) of the nanomaterials against bacteria and fungus

Table 5.5: CFU/mL count for *in vivo* antimicrobial assay against *S. aureus*

Table 6.1: Curing parameters and performance of HGE5 and HGCC

Table 6.2: Hematological parameters of HGCC3 implanted rats

Table 7.1: Curing parameters and performance of HGE5 and HGCNF

Table 7.2: Hematological parameters of HGNFC3 implanted rats

LIST OF FIGURES

- Figure 1.1: Potential applications of hyperbranched epoxy nanocomposites
- Figure 2.1: Structure of glycerol
- Figure 2.2: Structure of bisphenol A
- Figure 2.3: Structure of epichlorohydrin
- Figure 2.4: FTIR spectra of HGE resins
- Figure 2.5: ^1H NMR spectra of (a) HGE5, (b) HGE15, (c) HGE25 and (d) assignment of protons
- Figure 2.6: ^{13}C NMR spectra of (a) HGE5, (b) HGE15 and (c) HGE25, indicating the D, L, T units (insets) and (d) assignment of carbons
- Figure 2.7: XRD patterns of HGE
- Figure 2.8. Variation of shear viscosity of HGE and BPAE resins against (a) shear stress under constant temperature, (b) temperature under constant stress, (c) temperature under constant stress for BPAE and (d) time at constant stress and temperature
- Figure 2.9: TGA thermograms of HGE and BPAE thermosets
- Figure 2.10: Cell viability (%) of the cardiac and liver cell lines as evaluated by MTT assay
- Figure 3.1: FTIR spectra of (a) bentonite, modified bentonite and HGEB and (b) OMMT, M-OMMT, HGEC and HGEMC; and XRD patterns of (c) OMMT, M-OMMT, HGEC and HGEMC and (d) bentonite, modified bentonite and HGEB
- Figure 3.2: SEM micrographs of (a) HGE5, (b) HGEB, (c) HGEC and (d) HGEMC
- Figure 3.3: TEM micrographs of (a) pristine clay, (b) HGEB, (c) HGEC and (d) HGEMC
- Figure 3.4: (a) TGA thermograms of HGE5 and its NC and (b) Cell viability (%) of cardiac and liver cell lines
- Figure 3.5: Representative histological sections of skin, liver, brain and heart of control (a-d) and HGEMC implanted (e-h) groups
- Figure 3.6: SEM micrographs of adherence and proliferation of the dermatocytes on (a) HGE5 and (b) HGEMC
- Figure 3.7: Representative antimicrobial activity of the nanocomposites against (a) *S. aureus*, (b) *E. coli* and (c) *C. albicans*

Figure 3.8: Interaction of *E. coli* with (a) HGE5 and (b) HGEMC (red arrows show denatured bacterial cells)

Figure 4.1: UV-visible spectra of (a) AgNP and *T. occidentalis* leaf extract and (b) AgOM and HGCS

Figure 4.2: FTIR spectra of cured and uncured HGCS5

Figure 4.3: XRD patterns of (a) AgNP and (b) AgOM and HGCS

Figure 4.4: SEM micrographs of (a) HGE5 and (b) HGCS5

Figure 4.5: TEM micrographs of (a) AgNP and (b-c) HGCS5

Figure 4.6: Cytotoxicity assessment (% cell viability) of (a) AgNP and (b) AgOM, HGEMC and HGCS

Figure 4.7: Antibacterial activity of the prepared AgNP against (a) *S. aureus* and (b) *E. coli*

Figure 4.8: SEM images of *E. coli* cells incubated with (a) HGE5, (b) HGCS1, (c) HGCS3 and (d) HGCS5

Figure 4.9: MIC values against *S. aureus*, *E. coli* and *C. albicans*

Figure 4.10: (a) Creation of wound, (b) HGCS5 scaffold implantation and wound contraction on (c) 0 day, (d) 7 days, (e) 14 days and (f) 21 days

Figure 4.11: SEM image, showing the adherence of dermatocytes on the surface of HGCS5

Figure 4.12: Hematoxylin and eosin stained histopathological sections of skin, showing contraction of the wound at (a) 7 (b) 14 and (c) 21 days after surgery

Figure 4.13: Representative histopathological sections of HGCS5 treated rats: (a) heart, (b) liver and (c) brain

Figure 5.1: UV-visible spectra of GO and Ag-RGO

Figure 5.2: (a) UV-visible spectra of curcumin, Ag-RGO and Ag-RGO-Cur, (b) deconvoluted spectrum of curcumin, (C) deconvoluted spectrum of Ag-RGO-Cur and (d) spectra of HGGs

Figure 5.3: FTIR spectra of (a) GO and Ag-RGO and (b) Curcumin, Ag-RGO-Cur and the cured and uncured HGGs3

Figure 5.4: XRD patterns of (a) Ag-RGO, (b) Ag-RGO-Cur and (c) HGGs

Figure 5.5: HRTEM images of (a) Ag-RGO, Inset: histogram of the size distribution of AgNP, (b) a nanoparticle residing between sheets of RGO, (c) distribution of Ag-

RGO-Cur in HGGS3 and (d) RGO sheet with lattice fringe spacing of 0.68 nm over AgNP

Figure 5.6: Microscopic images of trypan blue stained PBMC (control and treated)

Figure 5.7: Cell survival (%) of (a) PBMC and (b) primary cardiac cell line of wistar rat

Figure 5.8: Representative histopathological sections of skin (a) 7, (b) 15 and (c) 30 days to post implantation and (d) kidney, (e) liver and (f) heart sections of the implanted rats

Figure 5.9: Representative antimicrobial activity of the nanomaterials against (a) *S. aureus*, (b) *E. coli* and (c) *C. albicans*

Figure 5.10: MIC against *S. aureus* and *C. albicans*

Figure 5.11: Inhibition of growth of (a) *S. aureus* (b) *C. albicans* and (c) *Chlorella* sp. in presence of HGGS3

Figure 5.12: Antimicrobial activity of HGGS3 in the proximities of *S. aureus*, *C. albicans* and *Chlorella* sp.

Figure 5.13: (a) Severe infection on un-implanted rat, (b) no sign of infection on HGGS3 implanted rat and SEM micrographs of (c) un-implanted skin, (d) implanted skin

Figure 6.1: UV-visible spectra of (a) CuO, (b) Nystatin and (c) MWCNT, CNT-CuO, CNT-CuO-Nys, HGCC3

Figure 6.2: (a) FTIR spectra of modified CNT, CNT-CuO, CNT-CuO-Nys and thermosetting HGCC and (b) XRD patterns of CNT-CuO-Nys and HGCC

Figure 6.3: TEM micrographs of (a) pristine MWCNT, (b) distribution of CNT-CuO-Nys within HGCC matrix (onset: particle size distribution histogram), (c) and (d) CuO nanoparticles inside the tubule of MWCNT

Figure 6.4: MIC of pristine CNT, CNT-CuO, CNT-CuO-Nys and HGCC against *S. aureus* and *C. albicans*

Figure 6.5: Inhibition of growth of (a) *S. aureus*, (b) *C. albicans*; SEM images of cell morphology alteration of (c) *S. aureus*, and (d) *C. albicans* adhered on HGCC3 and (e, f) growth of *S. aureus* and (g, h) *C. albicans* in the close vicinity of HGE5 and HGCC3 respectively

Figure 6.6: (a) Growth inhibition of *Chlorella* sp. in presence of pristine epoxy and HGCC3, (b) SEM micrographs of microalgal cells, adhered onto HGCC3 surface, and (c and d) growth of the microalga in the proximity of HGE5 and HGCC3

Figure 6.7: Cell viability (%) of the rat primary heart cells

Figure 6.8: Representative histopathological sections of (a) skin, (b) liver, (c) brain and (d) heart of HGCC3 implanted rat

Figure 7.1: UV-visible spectra of CuO-NFC and HGCNF

Figure 7.2: FTIR spectra of (a) base treated fibers (1), acid treated fibers (2) and NFC (3), (b) CuO-NFC and (c) cured and uncured HGCNF3

Figure 7.3: XRD patterns for (a) NFC, (b) CuO-NFC and (c) HGCNF

Figure 7.4: TEM images of (a-b) Distribution of CuO-NFC within the matrix, (c) Enlarged area of a and (d) particles size distribution histogram

Figure 7.5: Microscopic images of Trypan Blue stained PBMC treated with NFC and CuO-NFC

Figure 7.6: Cell survival (%) of (a) PBMC and (b) rat primary liver cells

Figure 7.7: (a-d) Inverted microscope images of L6 cells adhered onto HGCNF3 on 1st to 4th day of incubation and (e-h) SEM images of L6 cells adhered onto HGCNF3 on 1st to 4th day of incubation

Figure 7.8: Growth rate of L6 cells on the surface of HGCNF3

Figure 7.9: Histopathological sections of (a) skin, (b) kidney (c) liver and (d) brain of HGCNF3 implanted rat

Figure 7.10: MIC values against *S. aureus*, *E. coli* and *C. albicans*

Figure 7.11: Zones of inhibition against (a) *S. aureus*, (b) *E. coli* and (c) *C. albicans*

Figure 7.12: SEM micrographs of *S. aureus* adhered to HGE5 and HGCNF

LIST OF SCHEMES

- Scheme 1.1: Formation of diglycidyl ether epoxy
- Scheme 1.2: Synthesis of glycerol by Glycerol-To-Epichlorohydrin process
- Scheme 1.3: A model self condensing ring opening polymerization reaction
- Scheme 1.4: Proton transfer polymerization reaction
- Scheme 1.5: A model $A_2 + B_3$ reaction
- Scheme 2.1: Reduction of MTT to formazan by mitochondrial reductase
- Scheme 2.2: Synthesis of HGE
- Scheme 2.3: Crosslinking of HGE with poly(amido amine)
- Scheme 3.1: Schematic representation for the preparation of HGE5/M-OMMT nanocomposite
- Scheme 4.1: Plausible mechanism of reduction of Ag^+ , by *T. occidentalis* leaf extract
- Scheme 4.2: Schematic representation for the fabrication of HGCS
- Scheme 5.1: A probable mechanism for the simultaneous reduction of GO and Ag^+ by the *C. esculenta* leaf extract
- Scheme 5.2: Preparative protocol of HGGS
- Scheme 6.1: Preparative protocol of HGCC
- Scheme 6.2: Probable mechanism of *in situ* formation of CuO nanoparticles
- Scheme 7.1: Schematic protocol for the preparation of HGCNF

Chapter 1

General introduction

Highlights

In this chapter a general introduction of the present investigation is highlighted. This encompasses a brief report on epoxy nanocomposites, with special reference to their biomedical applicability. Role of different nanomaterials in the property improvement of polymers is also included in this chapter. Moreover, materials and methods for preparation of epoxy nanocomposites are briefed herein. Important analytical, spectroscopic or microscopic techniques, such as FTIR, XRD, TGA, DSC, SEM and TEM are described in context of characterization of polymeric nanocomposites. Various properties such as mechanical, thermal, physico-chemical, especially biological properties like biocompatibility, antimicrobial efficacy, biodegradability etc. of polymeric nanocomposites are elaborated here. This chapter also describes the application of epoxy nanocomposites in different domains of biomedical applications. The scopes, objectives and plans for the present investigation are mentioned in this chapter.

Chapter 1

1.1. Introduction

Responsibility of materials scientists is not only to provide next-generation materials to the society, but also to address basic problems associated with human health and wellbeing through the material development. Thus, a great demand on the advancement of biomaterial research has opened newer avenues. A genius collaboration of material science with chemistry, biology, medical science and nanotechnology is inevitable for the development of such biomaterials. Biomaterials find utility in the reconstruction of damaged tissues and organs, prevention of microbial infections, curing of congenital or cosmetic anomalies and decrement of drug-toxicity.¹ With the evolution of biomaterials, the concern regarding their toxicity and effectiveness raises concurrently.² This leads to a great room for research in this domain. Thus, fabrication of metallic, ceramics and polymeric biomaterials has been explored extensively.³

In the chronology of development, biomaterials come across a systematic evolution, which resulted implantable bone joints, artificial heart, kidney etc.⁴ Despite the success of metals and ceramic based biomaterials, some lacunas such as inadequate flexibility, corrosion etc. remain unabated. In this respect, polymeric biomaterials are able to attract great attention because of their inertness to physiological environment, light weight, tunable properties and most importantly the control over their fabrications.¹ These biomaterials can be tailored as per the service requirements by judicious approaches. Polymer can resist corrosion, offers excellent flexibility with body movement and diminishes the probability of infection.⁵ Further, biocompatibility of natural polymers is well understood by the scientific community. Again, in case of synthetic ones, compatibility can be achieved by selecting suitable building units. Thus, different polymers have been utilized for a myriad of biomedical applications in recent time. Polymers like polyurethane, natural rubber, polyacrylates, epoxy, polylactic acid etc. were found to be suitable for different biomedical utilities.⁶ Utility of polymers has started from 19th century with the development of nylon based synthetic sutures.⁷ The journey continues with the emergence of synthetic catheters, artificial organs, biomedical devices and implants, surgical sealants, safety tools etc. Biocompatible thermoplastic polymers such as polyurethane are extensively explored for designing different scaffold materials.⁸ Again, epoxy based adhesives were synthesized for fabricating root canal sealers, biological glue

Chapter 1

and surgical sealants.⁹⁻¹¹ However, biocompatibility issues did not favor their sustained utility.¹² Epoxy resins have immense potential for biomedical applications owing to their excellent adhesive strength, resistance to corrosion and high mechanical performance. A few commercial products emerged out of the incessant efforts to modify epoxy with biocompatible moieties and to confer flexibility to the thermosetting matrix.¹³

Thus, efforts have been made to redesign the existing polymers to satisfy the ever increasing demand of polymeric biomaterials. In this endeavor, scientists have introduced highly branched polymers, like (i) dendrimer, a perfectly regular, 3D structure and (ii) hyperbranched polymers, less perfect with missing branches in their structure. Hyperbranched ones attained popularity because of mass scale production by easy preparative methods. Hyperbranched epoxy (HE) resins are associated with some unique properties like high solubility, low viscosity, high reactivity and shorter curing time, which make their industrial production possible.¹⁴

Again, the concept of multifunctional polymeric materials started to emerge with the advancement of technological aspects. Hence, composite materials came into the picture to improve the properties of the prevailing polymers and to acquire some allied beneficial attributes. Concept of nanotechnology further helped to overtake the conventional composite systems. Different nanomaterials are being used to prepare nanocomposites (NC) with extraordinary properties.¹⁴ Nanoclay is regarded as one of the cost efficient nanomaterials that proved its utility in augmenting thermo-mechanical behavior of pristine epoxy systems.¹⁵ Biocompatibility of the nanoclay made it a good candidate in biomedical domain. Again, metal nanoparticles such as silver, copper, copper oxide (CuO), iron oxide etc. were also utilized to fabricate highly promising antimicrobial polymeric NC.¹⁶⁻¹⁸ However, their compatibility with biological systems aroused questions regarding their applicability in biomedical field. Further, carbon based nanomaterials, like carbon nanotubes (CNT), graphene and reduced graphene oxides (RGO) have immense potential in biomaterial science.^{19,20} Targeted drugs and protein delivery, controlled release of therapeutics and disease diagnosis are some credits accounted by such carbon based nanomaterials.^{21,22} However, the on-going campaign for utilizing sustainable raw materials, motivated the researchers to explore the global vicinity for finding out bioresources, in cost

Chapter 1

efficient ways. In this context, nanofibrillar cellulose (NFC) draws attention of the scientists for fabricating, NFC based biomaterials.²³

Polymeric NC based biomaterials are therefore at the height of exploration in the evolving realm of biomaterial science, where lots of possibilities are awaited.

1.2. Background of biomaterials

Much historical evidences were found regarding the use of biomaterials in ancient times to cure human ailments.²⁴ Metal and ceramic based biomaterials occupied the principal place for a long time. Stainless steel, titanium, tantalum, platinum, cobalt-chromium etc. based alloys were used for joint arthroplasty, dental implants, pacemaker, cardiac valve manufacturing etc. Poor corrosion resistance, need of repeated surgery and prone to surgical site infections urges upon the researchers to think beyond the metallic biomaterials.²⁵⁻²⁷ Consequently, calcium phosphate, zirconia, aluminium oxide etc. based ceramics were designed to fabricate dental and orthopedic implants, facial grafts, bone cement etc.^{25, 28, 29} Again, their catastrophic failure, toxicity and poor processing flexibility restricted their use in biomedical applications. Subsequently, emergence of polymeric biomaterials revolutionized the domain and opened newer trails to prepare easily processable, light weight, biocompatible, corrosion resistant and infection preventing biomaterials.³⁰

Amongst different polymeric biomaterials, epoxy occupies a great share. It is a widely used thermosetting polymer prepared by reacting an epoxide resin with an appropriate hardener. This class of polymeric materials has tremendous use in industrial applications. Epoxy resins contain more than one oxirane moieties per molecule in their oligomeric structures.³¹ Conventional diglycidyl ether based epoxy resins are synthesized by reacting bisphenol A with epichlorohydrin. In 1930, the first epoxy resin was simultaneously synthesized in Switzerland and U.S.A., though the first synthetic attempt was made by Lindmann of Germany in 1891 by reacting hydroquinone and epichlorohydrin.³² Commercial production began during 1940s and consequently thousand tons of different types of epoxy resin have been synthesized till date. During this period, diglycidyl ether of bisphenol A based epoxy attained utmost popularity due to ease of

Chapter 1

preparation and good mechanical strength. Biomedical aspects of epoxy resins were proved by the formulation of different root canal sealers.¹¹

The prime drawback of epoxy thermosets is their inherent brittleness, which creates tremendous problem for biological utility. At this juncture; HE proved their primacy over the conventional epoxy systems, in regard of various material properties, including flexibility.³³ Concept of hyperbranched polymers started during early 1900s. Different multifunctional moieties were used for synthesizing hyperbranched polymers with different attributes.¹⁴ Tartaric acid (A_2B_2) and glycerol were first reacted to obtain a hyperbranched resin.³⁴ Since then myriads of starting materials were explored which could react to form highly branched polymers.^{35,36} Emrick and his group in 1999, first reported the synthesis of a HE resin via proton transfer mechanism.³⁷ Concurrently, Chang et al. employed a base catalyzed polymerization reaction to obtain an aromatic HE.³⁸ Again, AB_n and $A_2 + B_3$ monomers were used by Emrick in 2000 to synthesize hyperbranched aromatic and aliphatic polyether epoxies.³⁹ In the same year, Gong and Frechet reported an epoxy terminated hyperbranched polyester.⁴⁰ Hyperbranched polyester with carboxylic end groups was utilized by Wang et al. in 2002 to prepare a hyperbranched polymer with terminal epoxy functionalities.⁴¹ Huang and his group reported the synthesis of epoxy-functionalized hyperbranched poly(phenylene oxide) in 2011.⁴² Again, in 2013, Luo et al. applied an epoxy ended hyperbranched polymer for reinforcement of conventional epoxy resin.⁴³ Roy and Karak reported another epoxy terminated hyperbranched polyether polyol in 2012.⁴⁴ The same group synthesized a novel HE, by using triethanol amine and bisphenol A in a facile manner.³³

Limitations of polymeric materials were tried to overcome by preparing suitable composite systems. Composites are referred to as the materials comprising of two or more distinct phases in macro or micro scale. Beneficial attributes of each material contribute to the resultant composite.¹⁴ Emergence of nanotechnology has taken over the domain of composite science and put forward newer materials, termed as NC.¹⁴ Superiority of NC lies in their light weight, excellent barrier properties, reinforcement of mechanical performance and most interestingly conferment of many fascinating biological attributes.¹⁸ By definition, NC can be referred to as the 'multiphase solid material, where one of the phases has one, two or all dimensions of <100 nanometer (nm)'. Polymeric NC can be primarily

Chapter 1

categorized as intercalated or exfoliated ones.⁴⁵ The former represents the penetration of polymeric chains in a regular crystallographic mode within the nanomaterials, whereas in the latter, nanomaterials lose their identical orientation and form a continuous dispersion in the polymer phase.¹⁴ Interfacial interaction amongst the materials and their mixing strategy govern the type of NC formed. A myriad of literature is found at present time regarding the applicability of polymeric NC in biomedical domains such as tissue engineering, antimicrobial coatings, dental prosthesis etc.^{46, 47, 13}

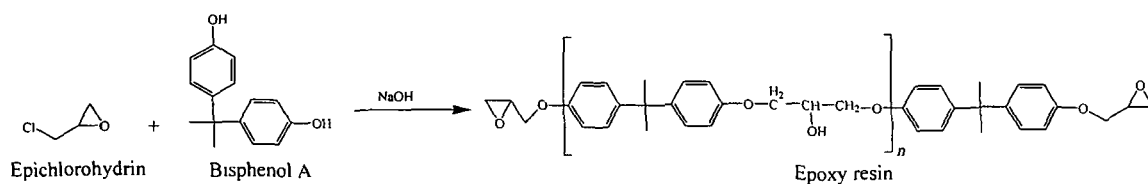
1.3. Materials and methods

1.3.1. Materials

Development of high performance, biologically important polymer NC has been continuing with the introduction of newer materials to the scientific community. Epoxy based NC are the vital point of attraction in the present investigation because of their much desired relevant attributes.

1.3.1.1. Epoxy

Epoxy is a versatile polymeric material which could occupy a giant space amongst the industrial polymers. Due to excellent material properties and adhesive strength epoxy NC systems were studied extensively.⁴⁸ Commercially important diglycidyl ether epoxy resins are prepared by reacting bisphenol A with excess of epichlorohydrin in presence of a base as shown in **Scheme 1.1**.



Scheme 1.1: Formation of diglycidyl ether epoxy

Again, novolacs of epoxidized phenol, cresols, resorcinol, catechol, ethyl phenols, hydroquinone and t-butyl phenols are non-bisphenol A type epoxy resins. Epoxidation of such novolacs are carried out with excess amount of epichlorohydrin to evade the branching which is generated by the reaction between phenolic hydroxyls and glycidylated

Chapter 1

phenol groups. Again, non-glycidyl ether epoxies are of two kinds; the cyclic aliphatic epoxy with ring structures and the aliphatic epoxy resins with linear structures. A few, commercially available resins of the former class are dicyclopentadiene dioxide, vinyl cyclohexene dioxide, ERL-4299 (wpeISO-210), ERL-4206 (wpe70-76), ERL-4229 (wpe131-143) etc. Examples of the other class are epoxidised oils, polyglycol diepoxides, epoxidised diene polymers etc.⁴⁹ Vegetable oil-based epoxy resins are prepared by epoxidation of unsaturated fatty acids and glycerol esters catalyzed by peracids.⁵⁰

A brief account of different components used in epoxy synthesis is presented below.

Diol

Bisphenol A (2, 2 bis(4-hydroxyphenyl) propane, BPA) is the most widely used aromatic diol in epoxy synthesis.⁵¹ A list of aromatic diols used for the synthesis of epoxy resins and their applications are given in Table 1.1. Presence of aromatic moieties in the structural backbones confers excellent strength and thermostability.⁴⁴ Again, sulfone groups of bisphenol S help to shorten the curing time and offers corrosion resistance to the resin.⁵² Another diol, bis(4-hydroxyphenyl)methane helps in synthesizing low viscosity epoxy resins.⁵³ Bis(dichlorovinylidene)diphenol (bisphenol C) and 4,4'-isopropylidene bis(2, 6-dibromophenol) (tetrabromobisphenol A) are used to obtain flame retardant epoxy resins.⁵⁴ Fluorinated epoxy resins were synthesized for anticorrosive coating applications, by using another class of diol, which includes hexafluorobisphenol A (hexafluoroisopropylidene diphenol).⁵⁵ However, use of halogenated precursors raises the production cost and creates toxic wastes, which obstacles their path for commercialization. Most of the epoxy based glues, used for biomedical sealing is generally synthesized by using BPA. In this respect, endodontic sealers such as AH-plus, AH26 etc. are worth to be mentioned.


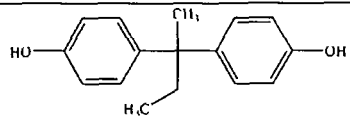
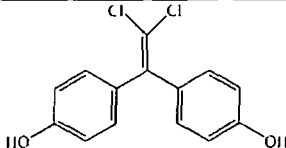
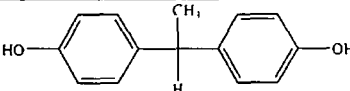
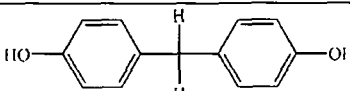
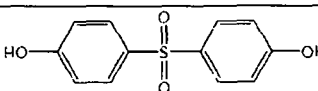
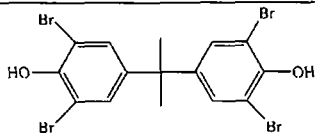
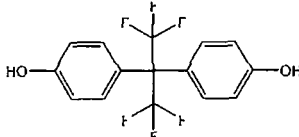
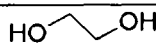
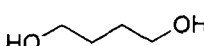
Branch generating unit

Different branched generating units are used to synthesize epoxy terminated hyperbranched polymers. Emrick et al. in 1999, used 1,1,1-tris(hydroxymethyl)ethane as the branch generating unit for synthesizing HE, by reacting with 1,2,7,8-diepoxyoctane.³⁷ In the next year, diepoxyphenol was prepared from commercially available dimethyl 5-hydroxyisophthalate, by the same group.³⁹ This diepoxyphenol subsequently undergone a

Chapter 1

chloride-catalyzed proton transfer polymerization reaction to yield the HE. Further, 4,4-bis(hydroxyphenyl)valeric acid based moieties are also used for HE synthesis.⁴⁰ In the year 2011, Chen and co-workers used another multifunctional moiety, tris(2-hydroxyethyl)-isocyanurate for synthesizing HE with heterocyclic N atoms.⁵⁶

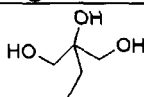
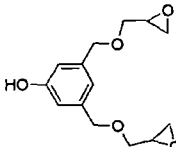
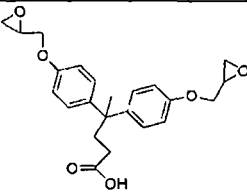
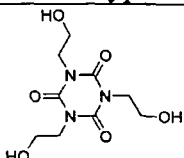
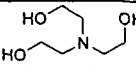
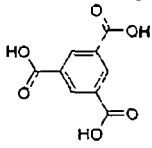
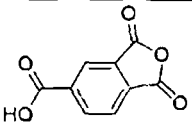
Table 1.1: Diols commonly used for epoxy synthesis with their structures and applications

Name	Structure	Major application
Bisphenol A		Coatings on metal products
Bisphenol B		Water proof coatings
Bisphenol C		Flame retardant epoxy coatings
Bisphenol E		Resin-injection repair of advanced composites
Bisphenol F		Functional diluents in solvent free coatings
Bisphenol S		Fast-drying epoxy glues
Tetrabromobisphenol A		Electronic enclosures, flame retardant epoxy
Hexafluorobisphenol A		High solid coatings, adhesives and laminates, low dielectric materials
Ethylene glycol		Low viscosity epoxy resin
Butane diol		Low viscosity epoxy resin

Chapter 1

Some other multifunctional moieties like triethanol amine, 1,3,5-benzene tricarboxylic acid, trimellitic anhydride etc. have been used to design branching units for HE.^{33, 57, 58} Moreover, some other moieties are used by researchers to obtain HE, either directly or by modification of different hyperbranched polymers.⁴⁴ Tris(2-hydroxyethyl)-isocyanurate based HE resins are suitable for biomedical antimicrobial coatings. A list of branch generating units used for HE synthesis is provided in Table 1.2.

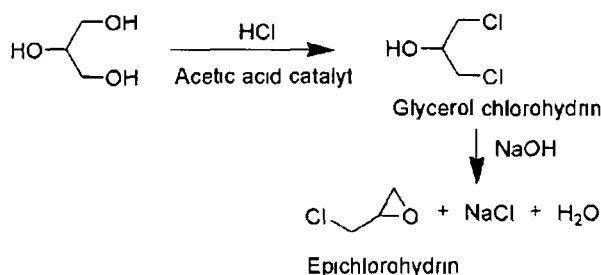
Table 1.2: Some branch generating units used for HE synthesis

Branch generating unit	Starting material	Reference
 1,1,1-tris(hydroxymethyl)ethane	Commercially available	37
 Diepoxyphenol	Dimethyl 5-hydroxyisophthalate	39
 4,4-bis(oxiranylmethoxyphenyl)valeric acid	4,4-bis(hydroxyphenyl)valeric acid	40
 Tris(2-hydroxyethyl)isocyanurate	Commercially available	56
 Triethanolamine	Commercially available	33
 Tricarboxylic acid	Commercially available	57
 Trimellitic anhydride	Commercially available	58

Chapter 1

Epichlorohydrin

The most important component for epoxy synthesis is the oxirane precursor. Epichlorohydrin is the abundantly used precursor, with an organochloro chain and an oxirane moiety. This is manufactured from the reaction between allyl chloride and hypochlorous acid, in presence of a base (NaOH) via two step pathways. Now a days, bio-based epichlorohydrin is synthesized from glycerol by the use of Glycerol-To-Epichlorohydrin process (GTO).⁵⁹ In this process, glycerol is reacted with HCl, in presence of acetic acid as catalyst. Glycerol chlorohydrin formed in this reaction is further treated with NaOH to yield epichlorohydrin (Scheme 1.2). Such epichlorohydrin is commercially available under the trademark Epicerol[®], under the banner of Solvay Chemicals. Fourcade et al. synthesized renewable resource based epoxy by taking Epicerol[®] as the oxirane precursor.⁶⁰



Scheme 1.2: Synthesis of glycerol by Glycerol-To-Epichlorohydrin process

Catalyst

Polycondensation reaction is employed for synthesizing epoxy resins. Diols are less reactive and hence catalysts are used, which can facilitate the removal of the active hydrogen from the diol and enhances the reactivity.⁶¹ Catalysts that are used for this purpose include sodium hydroxide (NaOH), potassium hydroxide (KOH), lithium hydroxide (LiOH), calcium hydroxide (Ca(OH)₂), sodium carbonate (Na₂CO₃), potassium carbonate (K₂CO₃), calcium carbonate (CaCO₃), sodium bicarbonate (NaHCO₃), potassium bicarbonate (KHCO₃), lithium bicarbonate (LiHCO₃), calcium bicarbonate (Ca(HCO₃)₂) etc. However, NaOH is the most widely used catalyst for epoxy synthesis.⁶² Further, Markovitz used coordination compounds, containing acetylacetonate (acac) ligand

Chapter 1

as a catalyst for commercial epoxy ERL 4221.⁶³ Reddy et al. revealed that Cu(II) containing coordination compound catalyzed epoxy resins show longer storage time. However, reverse effect was witnessed for catalysts, containing Co(III) and Ni(II).⁶⁴

Again, choice of catalyst plays a significant role in the epoxidation of vegetable oils or olefinic double bonds. Percarboxylic acid based epoxidation reactions are catalyzed by acids or enzymes.⁶⁵ Peroxide mediated epoxidation involves transition metal based catalysts. Hypohalous acids are employed for epoxidation with halohydrins. Despite, the availability of myriads of catalysts, peracetic acid has attracted copious attention for the synthesis of non-glycidyl epoxy resins. Moreover, inorganic acids, like H₂SO₄, HCl, HNO₃, H₃PO₄ etc. can also be utilized for epoxidation reaction.^{66,67}

Curing agent

Epoxy resins are mixed with appropriate hardeners or curing agents to form three dimensional network. The first category of curing agents are the active hydrogen containing compounds such as amines, hydroxyls, acids, acid anhydrides, amides etc. Highly strained oxirane ring of the resin opens up in presence of reactive hydrogen of the curing agent and forms rigid, entangled, horny structure with high mechanical strength. Amongst different amines, aliphatic ones are the most reactive, followed by the cycloaliphatic and aromatic ones. A tertiary amine, 1-ethyl-3-(3-dimethylaminopropyl)carbodiimide is used as a crosslinker in endodontic sealing.⁶⁸ Again, cystamine was used to cure an epoxy based scaffold with excellent biocompatibility as tested *in vitro* and *in vivo*.⁶⁹ Different types of amine curing agents used to crosslink epoxy resins are given in Table 1.3.

Acid anhydrides are also explored to a great extent for curing epoxy resins. Their crosslinked products have immense use in the field of electronic devices. They provide low dielectric constant, which is beneficial to insulate various electronic appliances, circuits etc.⁶¹ Polybasic acids or acid anhydrides are basically used for coating applications. Diethylenetriamine, triethylenetetraamine, poly(amido amine) etc. are used for advanced engineering applications.

The next category curing agents includes tertiary amines, metal alkoxides, imidazoles, halides and fluoroborates of tin, zinc, iron etc. which in combination with acid

Chapter 1

or acid anhydride enhances the epoxy curing reaction. Boron trifluoride (BF_3) is another vital catalyst which causes instant gelation of epoxy resin.⁶¹

Reactive crosslinkers, like melamine, phenol and urea-formaldehyde resins have also been used to cure epoxy resins. Amongst the aforesaid curing agents, active hydrogen containing ones have found wide commercial importance. Very recently; bio-based hardener systems are introduced to cure epoxy resins.⁷⁰ Aliphatic carboxylic acids such as sebacic acid, citric acid, succinic acid and adipic acid in presence of tetrabutyl ammonium bromide, methyl imidazole etc. catalysts are also used for the same purpose.⁷⁰ Researchers have observed that the use of bio-based curing agents renders biodegradable properties to the synthetic diglycidyl ether based epoxy.⁷¹ Application of such crosslinkers are beneficial for vulcanization of epoxidized natural rubber, liquid crystalline epoxy elastomers etc.

Further, a considerable interest has been paid to fabricate photo-cured epoxy resins by choosing appropriate crosslinkers. Aryl diazonium and diaryl iodonium salts are used as photo-initiators in such approaches. Photo-induced crosslinking process decreases the curing time and temperature.⁷² Again, microwave oxygen plasma is used for curing solid and liquid epoxy.^{73, 74}

1.3.1.2. Nanomaterials

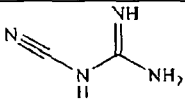
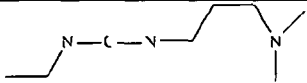
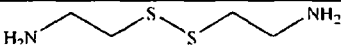
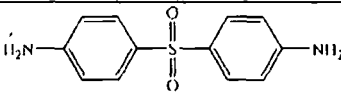
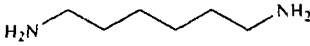
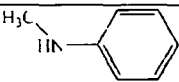
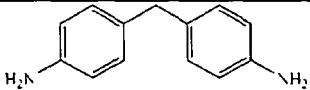
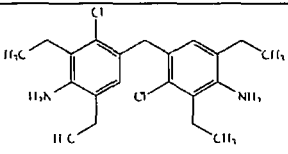
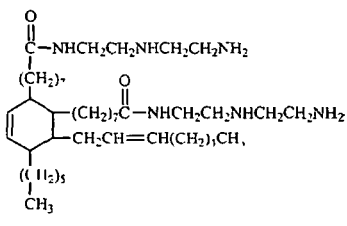
Amongst all reinforcing agents, nanomaterials proved their superiority in case of polymer NC. These nanomaterials contribute some exceptional attributes to the polymeric NC. High surface to volume ratio and physico-chemical properties of the nanomaterials show many interesting activities at bio-nano interface. For last two decades, extensive research works have been carried out to explore different novel nanomaterials. In broader sense these materials could be categorized into three classes, viz. zero, one and two dimensional nanomaterials. Their utility in polymer NC is briefly accounted below.

Zero dimensional nanomaterial

Nanoparticles, quantum dots and nanoclusters represent the category of zero dimensional nanomaterials. These nanomaterials have all the three dimensions in nanometer range.

Chapter 1

Table 1.3: Curing agents used for epoxy crosslinking

Name	Structure	Advantage	References
Dicyandiamide		Good viscoelastic properties	75
1-ethyl-3-(3-dimethylaminopropyl) carbodiimide		Fast endodontic sealing	68
Cystamine		Biocompatibility	69
Diamino diphenyl sulfone		Decreases curing temperature	76
Hexamethylene diamine		Good thermal stability	77
Methylaniline		Good physical and dielectric properties	78
Diamino diphenyl methane		Enhanced mechanical property	79
4,4-methylene bis(3-chloro-2,6-diethylaniline)		Good abrasion resistant	80
Fatty amido amines		Low temperature curing, high mechanical property	33

Chapter 1

Zero dimensional nanomaterials may be of different shapes, with amorphous or crystalline structure and may be composed of different chemical elements.⁸¹ Nanoparticles are the most studied nanomaterials, which can be prepared by various physical and chemical methods. Recently, 'green' route mediated synthesis of nanoparticles has gained utmost attention because of the ease of preparation, use of non-toxic reducing agents in cost efficient manner.⁸² Different biological entities like plant, bacteria, enzymes etc. are explored extensively for the preparation of metal nanoparticles. Many attractive properties were shown by silver, gold, copper, copper oxide, iron oxide, zinc oxide and titanium oxide nanoparticles.⁸³⁻⁸⁹

Silver nanoparticles (AgNP) are at the top of interest because of their exquisite biological activities and ease of preparation. Sodium borohydride, sodium sulfite, ascorbate, hydrazine hydrate, elemental hydrogen, dimethylaminoborane, dimethyl formamide, sodium citrate, glucose, fructose, lactose sucrose etc. are used by various research groups for reducing silver ions. However, these reducing agents are either toxic or expensive.⁹⁰⁻⁹⁴ In the quest of 'going green', researchers have tried various routes like microwave irradiation, use of ionic liquids, plant extracts, micorbes etc. for reducing silver ions.⁸² Amongst these, use of plant extract for the reduction process has attained copious attention of the community because of its economic viability, ease of processing, especially impartment of many interesting biological activities to the nanoparticles. Recent reports and reviews showcase various greener strategies for preparation of silver nanoparticles. Leaf extracts of *Cinnamomum camphora*, *Aloe vera*, *Capsicum annuum*, *Medicago sativa*, *Pelargonium graveolens*, *Emblica officinalis*, *Mimosa pudica*, *Nelumbo nucifera*, *Tinospora cordifolia*, *Eclipta prostrate*, *Ocimum tenuiflorum*, *Solanum tricobatum*, *Syzygium cumini*, *Centella asiatica*, *Pulicaria glutinosa* etc. have been used to prepare AgNP with different shapes and sizes. Again, some researchers reported the preparation of stable AgNP using various fruit extracts such as *Vitis vinifera*, *Carica papaya* L., *Emblica Officinalis*, *Tanacetum vulgare*, Pear fruit, *Lantana camara* etc.⁸² The vital feature for choosing a plant based reducing agents are the availability of the plant and applicability of the nanoparticles.

Broad spectrum antimicrobial activity of AgNP endorses it as a potential candidate for different biomedical and cosmetic products, viz dental resin composites, bone cement,

Chapter 1

wound dressing material, toothpaste, shampoo, water sanitizer, antimicrobial textiles etc.⁹⁵ Antimicrobial activity of AgNP is significantly high from AgNO₃, which has been treated as an efficient antimicrobial agent for long time.

Again, copper and copper oxide (CuO) nanoparticles are semiconductor materials generally with monoclinic lattice structure. These have potential use in high temperature superconductors, batteries, solar energy cells, photovoltaic cells, gas sensors, catalysis etc.^{86, 87} Moreover, these nanoparticles also possess efficient antimicrobial activity. Copper and CuO are used in a number of commercial antimicrobial agents like Super KL K90 Red, Nordox etc.⁹⁶ However, the toxicity to human health and environment restricted their sustained applicability. Therefore, 'greener' routes were adopted to synthesize such nanoparticles, which showed better compatibility at bio-nano-interface.⁸⁶ As compared to AgNP, very few literature reports are found on the preparation of 'green' route mediated CuO nanoparticles. Preparation of pure metallic copper nanoparticles is very difficult, as it is highly susceptible to oxidation in the atmosphere.⁹⁷ Thus, CuO nanoparticles with similar attributes have been synthesized by researchers via different approaches.

Further, nanocrystals, semiconductor quantum dots, fullerene etc. have been explored for different biological fields like diagnostics and therapeutics.⁹⁸⁻¹⁰⁰ In recent time, newly added carbon dots have immense potential as fluorescent biomarkers in advanced disease diagnosis technique.¹⁰¹

One dimensional nanomaterial

Two dimensions of this class of nanomaterials are in nanometer range, while the third is in micrometer. They encompass nanofibers, nanotubes, nanorods, nanowires etc.

The most exciting one dimensional nanomaterials are the nanotubes, with hollow tubular structures. Extraordinary mechanical, electrical and physico-chemical properties have endorsed CNT as the central point of attraction amongst them. CNT are composed of sp² hybridized carbons rolled up to form tubules.⁸¹ Number of graphitic layers in their structures, classifies them as single walled (SW), double walled (DW) and multiwalled (MW) CNT. From the last two decades, different techniques were reported for synthesizing CNT. Primary synthetic approaches include laser ablation, chemical vapor deposition, arc discharge etc.^{81,102} During synthesis, amorphous carbon particles, fullerene and metal

Chapter 1

catalysts remain as impurities. Chemical vapor deposition method is widely used to obtain CNT with minimal impurity and to achieve large scale production.

CNT based drug delivery systems have been explored by the researchers. Conjugation of drugs with CNT and their controlled delivery is another aspect of application. High surface area of the nanotubes enhances the activity of drugs or biomolecules by synergistic effect and protects them from absurd physiological environment.¹⁰³ CNT-biomolecule conjugate systems could be used as biochemical sensors, such as enzyme electrode, DNA sensor etc.¹⁰⁴ Moreover, importance of CNT is also understood in the domain of tissue engineering and regenerative medicines. Again, decoration or coating of metal/metal oxide nanoparticles on CNT surface confers excellent antimicrobial efficacy, interesting optical and electrical properties. In this quest, silver, gold, nickel oxide, copper oxide and zinc oxide nanoparticles were anchored on CNT surface by various chemical, physical or sonochemical methods.¹⁰⁵ Ultrasonication is regarded as one of the efficient 'green' tools to anchor nanoparticles on CNT. The same technique showed proficiency in immobilizing biomolecules and drug onto CNT.

Nanofibers represent another type of one dimensional nanomaterials, where fiber diameters ranges from 1-100 nm, while their length falls into micrometer regime. Carbon nanofibers are formed of graphene layers arranged as stacked cones. These fibers are prepared by vapor deposition method, in presence of transition metal catalyst. They have potential applicability as reinforcing material in composites, oil field remediation and in electrodes.⁸¹ Amongst the nanofibers, NFC gained utmost attention because of its natural abundance, cost efficient isolation methods and compatibility with biological systems. Literature reveals limited number of approaches for isolating NFC from nature and industrial waste.²³ Apart from plants, certain non-pathogenic bacteria, algae and fungi found in fruits, vegetables etc. have been used to isolate NFC.^{106, 107} Fiber size depends on the type of feedstock and isolation procedure. Generally, chemico-mechanical treatment is given to the isolated fibers followed by soaking in HCl. NFC coated metal nanoparticles showed excellent antimicrobial activity.⁸⁷ Thus, AgNP coated textiles are launched to prevent microbial infections.¹⁰⁸ Another vital application of AgNP coated cellulose is in wound dressing materials.¹⁰⁹

Chapter 1

Two dimensional nanomaterial

Two dimensional nanomaterials are those, which have only one dimension in nanometer range. Such materials include nanoclay, nanofilms, graphene, RGO etc. Nanoclays are layered silicates, with tetrahedrally bound Si atoms to an octahedrally shared edge of $\text{Al}(\text{OH})_3$ or $\text{Mg}(\text{OH})_2$. Layered nanosilicates possess very high aspect ratio with about 1 nm thick layers. These layers are stacked by weaker physical forces like van der Waals to form a gallery.¹¹⁰ Some widely used nanoclay include nacrite, antigorite, montmorillonite, bentonite, beidellite, kolinite, hectorite, illite, taenolite, saponite, talc, lizardite, halloysite, octosilicate, kenyaite, magadite, brucite, berlinite etc.

Nanoclays are the natural cation exchangers, which can replace inorganic cations with organic onium ions. This renders hydrophobic character to hydrophilic nanoclay that makes them compatible with polymer matrices. Quaternary alkylammonium and alkylphosphonium compounds are widely used for clay modification. This increases the interlayer spacing, which again allows the polymeric chains to enter the clay galleries. This type of interaction offers high mechanical properties to the NC.¹¹¹ However, such modifications require costly modifying agents and high temperature treatment for long time. Contrarily, Phua et al. recently modified nanoclay with the hormone, dopamine.¹¹² Again, nanoclay, like saponite and montmorillonite can exchange cations with some drug molecules. Smectites and kaolinites are used for sustained drug release applications.¹¹³ Further, nanoclay provides a highly active surface for adsorption of different drugs or biomolecules and enhances their water solubility.

Another widely used two dimensional nanomaterial is graphene. This is a single atom thick sheet of carbon atoms, packed in honeycomb fashion with sp^2 hybridization. Theoretically, graphene was established during 1940s. However, successful identification of graphene was achieved by Geim and co-workers, in 2004. Graphene exhibits various interesting properties that have potential use in nanomedicine, catalysis, electronics and material science.^{22, 114} Dispersion of graphene in polymer matrix is a difficult task. Thus, different approaches such as electrochemical, chemical and sono-chemical techniques have been put forward to functionalize graphene surface. RGO, also exhibits similar attributes as that of graphene. However, RGO can be obtained easily from graphene oxide by cost efficient approaches. Several methods are attempted to reduce graphene oxide by using

Chapter 1

direct reduction with sodium borohydride, hydroquinone, hydrazine etc.¹¹⁵ However, retention of such agents in trace amount in the RGO may induce toxic affect to biological systems. Hence, newer methodologies are explored by researchers under the dictates of 'green' chemistry tenets. In this vein, plant extract mediated synthesis of RGO is of prime interest.¹¹⁶

1.3.2. Methods

1.3.2.1. Epoxy resin

Different processes are used for synthesizing epoxy resins. Some well known processes are briefly described below.

Taffy process

Epichlorohydrin and BPA are reacted in this process in presence of a stoichiometric amount of NaOH. In this process, one organic and one aqueous phase are present. The organic phase contains the epoxy resin, the viscosity of which increases with time. The reaction is carried out with an excess amount of epichlorohydrin.

Commercially, this process is used to prepare high molecular weight epoxy resins. The resin is recovered from the reaction mixture after the removal of unreacted epichlorohydrin and water by vacuum drying. During the reaction, 20-50% NaOH is added very slowly to catalyze the reaction. NaOH is used for enhancing the basicity of the reaction medium as well as for nucleophilic ring opening reaction of the oxirane moiety of epichlorohydrin. The initial phase undergoes an exothermic coupling reaction, which further goes through a dehydrochlorination step for completion. These two reactions can be carried out separately with the help of quaternary ammonium salts, which behave as phase transfer catalysts. Upon completion of the coupling reaction, dehydrochlorination reaction starts on addition of NaOH.¹¹⁷

Fusion process

Low molecular weight liquid epoxy resin is reacted with additional amount of BPA to obtain high molecular weight resin, in 'fusion' process. This process is superior to the taffy

Chapter 1

process in terms of processability. Fusion process is carried out by reacting the compounds containing 2-4 hydroxyl functionalities with low ($M_n = 370-500$) or moderate ($M_n = 500-1,000$) molecular weight epoxy resins. This process is also termed as advancement process, as it propagates through a step-growth polymerization process.

Commercially this process is more predominant because of easier isolation of the product and non-requirement of any solvent. Dihydric or polyhydric phenols are reacted with a liquid epoxy at about 150-190 °C, in this process, in presence of a catalyst. The reaction temperature is set as per the required epoxy equivalent. High molecular weight epoxy synthesis often encounters reaction temperature above 200 °C.

Choice of catalyst plays a major role in defining the structure of the final product. Generally, inorganic bases like KOH, NaOH, Na_2CO_3 , LiOH, quaternary ammonium salts etc. are used as catalysts in this process. However, this kind of catalysts may impart ionic impurity to the final product, which restricted various advanced applications. Thus, phosphonium halides, organic phosphine or phosphonium salt of carboxylic acids are used for selective reactions.

Processes for synthesis of HE resin

With the evolution of advanced materials, hyperbranched polymers have taken a significant place in the domain of polymer science. Synthesis of HE is much simpler than that of dendrimers. However, availability and scaling up difficulties of AB_n type monomers led to the use of $A_2 + B_3$ ones for synthesizing HE.³³ Such epoxies with desired architecture along with the combination of aliphatic and aromatic moieties are synthesized to overcome the inherent brittleness of conventional linear epoxy systems. Further, chemical transformations are also possible by a broad range of ring opening reactions in such systems.

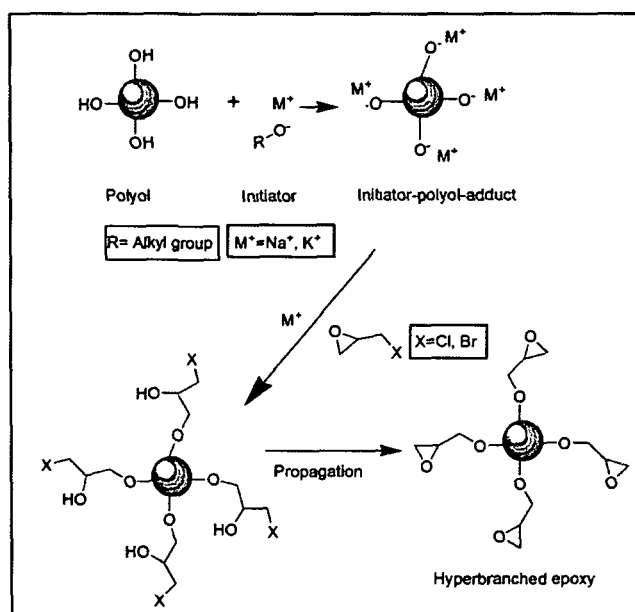
Again, single and double monomer technologies are employed for HE synthesis. The first one involves polymerization of AB_n or latent AB_n monomers. This is again subdivided into four categories, viz. (i) polycondensation of AB_n monomers, (ii) self condensing vinyl polymerization (SCVP), (iii) self condensing ring opening polymerization (SCROP) and (iv) proton transfer polymerization. Double monomer methodology involves polymerization of two types of monomers directly to obtain HE. This can again be

Chapter 1

categorized into two classes. Classical polymerization using A_2 and B_3 monomers generates AB_n intermediate *in situ* by couple monomer technology. The important methodologies used for synthesizing hyperbranched polymers are briefed below.

Self condensing ring opening polymerization (SCROP)

In this approach, monomers (latent AB_n) as such do not contain branching points; rather they are generated during propagation of the reaction. This approach is also termed as 'multibranching ring opening polymerization'. Initiators are added to generate some active sites which help in controlling the molecular weight of the product. A typical representative reaction is shown in Scheme 1.3, which depicts the reaction between a polyol and an oxirane precursor, by using an alkoxide initiator. The reaction propagates via the addition of monomer. This approach is not explored widely for synthesizing HE resins.¹¹⁸



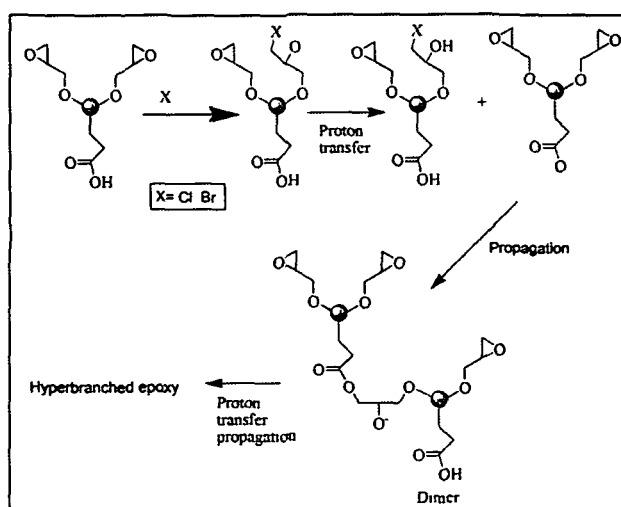
Scheme 1.3: A model self condensing ring opening polymerization reaction

Proton-transfer polymerization

This approach is a typical example of single monomer methodology. HE, polyol, polysiloxanes etc. are reported to be synthesized via this method.¹¹⁹ A hyperbranched poly(hydroxyether) with two epoxy and one phenolic hydroxyl group was prepared from

Chapter 1

AB_n monomer in 1999 by Chang et al.³⁸ This involved proton transfer polymerization reaction. The reaction was initiated by adding a base to abstract phenolic hydrogen, followed by the addition of phenolate anion to epoxy ring. The reaction generated a dimer containing a secondary alkoxide. This dimer does not undergo a proton exchange reaction with an AB_n monomer to get a phenolate anion and a neutral dimer, which further propagates to generate the epoxy terminated hyperbranched polymer. Gong and Frechet in 2000 synthesized an epoxy terminated hyperbranched polyester by similar proton transfer polymerization.⁴⁰ The starting monomer, 4,4-bis(oxiranylmethoxyphenyl)valeric acid was prepared from 4,4-bis(hydroxyphenyl)valeric acid and Bu_4NBr was used as the reaction initiator. This approach led to a hyperbranched polyester with terminal epoxy groups with $M_w = 44,000$ g/mol and $PDI = 5.9$. In the same year Emrick et al. employed a chloride-catalyzed proton transfer polymerization to obtain hyperbranched aromatic and aliphatic polyether epoxies.³⁷ AB_n and $A_2 + B_3$ monomers were used to obtain the aromatic and the aliphatic products respectively. Aromatic HE with high molecular weight can be synthesized by using diepoxyphenol (as AB_2 monomer) and tetra-*n*-butylammonium chloride (Bu_4NCl) as the nucleophilic catalyst. This catalyst was used to avoid crosslinking during the synthetic process. Trimethylolpropane triglycidyl and BPA were reacted by Ma et al. via proton transfer polymerization catalyzed by tetrabutylammonium bromide.¹²⁰ A model reaction is shown in Scheme 1.4.

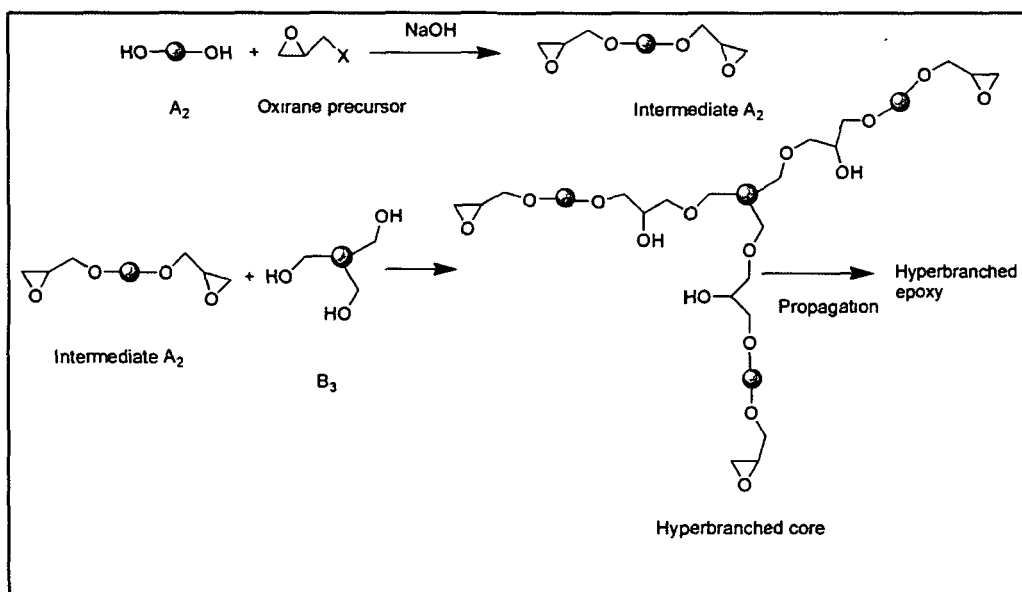


Scheme 1.4: Proton transfer polymerization reaction

Chapter 1

$A_2 + B_3$ approach

Use of A_2 and B_3 monomers gained popularity because of the unavailability of AB_n type monomers. This approach is cost efficient because of the involvement and availability of bi and tri functional monomers. Jikei was the first to synthesize hyperbranched polymer by $A_2 + B_3$ approach.¹²¹ In 1999, Emrick et al. used 1,2,7,8-diepoxyoctane and 1,1,1-tris(hydroxymethyl)ethane as the A_2 and B_3 monomers respectively to obtain an epoxy terminated hyperbranched polyester.³⁷ Again in 2005, 1,3,5-benzene tricarboxylic acid and diglycidyl ether of BPA were used by Maruyama et al. to synthesize hyperbranched polyester epoxy by $A_2 + B_3$ approach.⁵⁷ In 2007, Murli et al. synthesized epoxy terminated photoactive hyperbranched benzylidene polyester.¹²² De and Karak in 2013 reported a tough HE, synthesized by using triethanol amine and BPA.³³ The same group further reported the epoxidation of a hyperbranched polyester polyol, derived from castor oil.⁴⁴ A model $A_2 + B_3$ reaction is shown in Scheme 1.5.



Scheme 1.5: A model $A_2 + B_3$ reaction

HE can be also be synthesized by the modification of terminal functionalities of a hyperbranched polymer, by indirect method. Hydrosilylation of 1,1,3,5,5-pentamethyl-1,5-divinyltrisiloxane, followed by epoxidation yielded an epoxy terminated polysiloxysilanes as reported by Yokomachi et al.¹²³ In another approach, Zhang and co-workers reported the

Chapter 1

synthesis of a low viscosity liquid aromatic polyester HE resin to toughen commercial epoxy.¹²⁴ Fu and his group reported a HE resin, synthesized by reacting carboxyl terminated hyperbranched polyester and epichlorohydrin.¹²⁵ Again, Chen et al. reported a heterocyclic HE resin containing nitrogen, prepared by the reaction of dimethylol propionic acid and tris(2-hydroxyethyl)isocyanurate.⁵⁶ A new epoxy-functionalized hyperbranched poly(phenylene oxide) was synthesized by Huang et al. by reacting hyperbranched poly(phenylene oxide) with epichlorohydrin.⁴² Literature reports a few other approaches carried out to synthesize HE resins.¹²⁶

1.3.2.2. Nanocomposites

Limitations of polymers can be overcome by preparing polymeric NC as stated earlier. Different approaches are used till date for fabrication of such materials. Some widely used methodologies are *in situ*, melt mixing, solution techniques etc. These techniques are briefly stated below.

In situ technique

This is one of the most widely used methods for the preparation of polymeric NC. Preparation of exfoliated polymer NC has been reported by many researchers by using this approach.¹²⁷⁻¹²⁹ Prepolymer or polymer precursors are reacted in presence of the nanomaterial to form *in situ* polymer NC. Insertion of monomer/prepolymer chains into the platelets of the nanomaterials allows extensive mixing, interaction and distribution of the nanomaterials within the polymeric matrix. This method is widely adopted for preparing exfoliated polymer-clay NC. Monomer or prepolymer migrates into the galleries of the nanoclay and delaminates the clay layers which resulted in a disordered exfoliated structure. Park et al. thoroughly studied the mechanism of exfoliation of *in situ* generated epoxy clay NC.¹³⁰ CNT or graphene based NC are also prepared by *in situ* technique.^{131, 132} Chain growth of the polymer in the nanotubes' side walls or on the graphene layers helps in uniform dispersion of the nanomaterials within the matrix. Bao et al. prepared a graphene oxide/epoxy NC and witnessed enhanced mechanical behavior.¹³³ Again, Li et al. reported a polyurethane/graphene oxide/epoxy NC with excellent thermal and mechanical attributes.¹³⁴ *In situ* technique was also employed to prepare carbon nanofiber based epoxy

Chapter 1

NC. Diffusion of pre-polymer or polymer precursors through nanomaterials and presence of different secondary interactions forms stable and well dispersed epoxy NC in this technique. High surface energy of the nanomaterials helps in attracting the epoxy to diffuse through them which swell the nanomaterials. Then, the epoxy chains start to grow within the nanomaterials and result in highly exfoliated NC.

Solution technique

In solution technique, nanomaterials are dispersed in suitable solvents and mixed with polymeric solution by vigorous mechanical shear force followed by ultrasonic energy. NC is obtained by precipitation or evaporation of the solvent after adequate mixing. In this method, first the solvent molecules swell and help to disperse the nanomaterials. Then, epoxy chains replace the solvent molecules to obtain stable NC. In this process, the total entropy decreases due to the confinement of the chains, which is again compensated by desorption of solvent molecules resulting in intercalated NC. Intercalated/exfoliated or partially exfoliated epoxy clay NC are reported in this context.^{135, 136}

This technique is again useful for the preparation of metal nanoparticles based epoxy NC.¹⁶ Silver, iron oxide, copper oxide etc. nanoparticles can be well dispersed in a number of organic solvents, which also dissolve epoxy resin. Again, carbon based nanomaterials form good dispersion in some selective organic solvents after surface functionalization. Such functionalized CNT, graphene etc. are successfully used by different researchers to prepare high performing epoxy NC.^{137, 138}

Despite wide advantages, this method has limited industrial utility. The main cause behind this is the need of a large amount of volatile organic solvents to scale up the process. Release of toxic waste to the environment is an allied disadvantage.¹³⁹

Melt Mixing

This technique is generally employed to prepare thermoplastic polymer based NC. The polymer and the nanomaterials are mixed mechanically beyond the softening point of the polymer under dynamic or static condition. This method has industrial utility as it does not necessitate the use of toxic organic solvents. Polymer clay NC are widely prepared by using this approach.¹⁴⁰ In molten state, polymer can crawl into the galleries of the layered

Chapter 1

silicates and forms intercalated or exfoliated NC. This is governed by the degree of penetration of the polymeric chains to the interlayer spacing of the clay. Melt mixing process needs conventional instrumentations such as injection molding, extruder, kneader, Brabender, plasticorder etc. Thus, environment friendly technique, conventional instrumentation and efficient mixing of the components make this technique industrially suitable, especially to prepare intercalated polymer clay NC. However, in this process the temperature should be kept below the decomposition temperature of the components.

The aforementioned approaches are the generally explored ones in context of polymeric NC preparation. Various other methods like template synthesis, sol-gel process, ball milling, plasma treatment, thermal decomposition etc. are also employed in the preparation and fabrication of polymer NC.¹⁴¹⁻¹⁴³ The method is selected as per the stature of the polymer and the nanomaterials.

1.4. Characterization and analysis

Different analytical and spectroscopic techniques are used for the characterization of polymer, nanomaterials and polymeric NC as described briefly underneath.

1.4.1. Epoxy resin

Physical properties like viscosity, molecular weight, epoxy equivalent, hydroxyl value etc. of epoxy resin are determined by the standard methods. Epoxy equivalent is defined as the amount of resin in gram required to obtain one equivalent of epoxy group. This is generally determined by treating epoxy resin with HBr or by hydrohalogenation of epoxy in pyridine medium [ASTM D 1652-73].¹⁴⁴ Hydroxyl value is referred to as the amount in milligram of KOH or NaOH, equivalent to the hydroxyl content of one gram of the resin. Hydroxyl value is generally determined by acetylation of the free hydroxyl groups of the resin with acetic anhydride in pyridine medium.¹⁴⁵ Again, viscosity is a vital parameter of the resin that governs the processing of the thermoset. It is usually measured by Brookfield or Ford cup or Redwood viscometer under ambient conditions. Rheological behavior of epoxy resin provides viscoelastic character of the resin under high shear and temperature gradient.¹³⁷ Molecular weight of epoxy is determined by gel permeation chromatography or by vapor pressure osmometry.

Chapter 1

Chemical structure and functionalities of epoxy resin are determined by FTIR and NMR techniques. FTIR spectrum of a typical resinous epoxy system shows sharp bands at around 920 and 830 cm^{-1} for the oxirane ring.³³ However, exact structure can be elucidated from ^1H and ^{13}C NMR spectral analyses. Different types of protons and carbons clarifies the structural identity of the resin, NMR technique is greatly useful for ensuring the branched structure in a HE system. The signature remark of a particular HE can be shown by its degree of branching.³⁶ This is calculated by using the Frechet's equation as follows

$$\text{DB} = (\text{D} + \text{T})/(\text{D} + \text{T} + \text{L}) \quad (1.1)$$

where, D, T and L are the number of dendritic, terminal and linear units respectively, present in the hyperbranched structure.

1.4.2. Nanomaterials and nanocomposites

Physical and chemical characteristics of nanomaterials and polymer NC are done by using different analytical, spectroscopic and microscopic tools like UV-visible spectroscopy, X-ray diffraction analysis, scanning and transmission electron microscopy, atomic force microscopy (AFM), raman spectrophotometry etc.

UV-visible

This is one of the vital tools used for characterizing metal nanoparticles based epoxy NC. Metal or metal oxide nanoparticles show typical surface plasmon resonance (SPR) peaks in UV-visible region. Such peak arises due to the interaction of the surface electrons of nanoparticles with the incident UV radiation.¹⁴⁶ Thus, it is very useful to determine the presence of a particular type of nanoparticles within the epoxy NC. Further, this technique is also helpful for carbon based nanomaterials like graphene, RGO etc., which show distinct spectral identity due to π - π^* and n - π^* transitions of electrons upon exposure to UV radiation.¹¹⁵ Bare CNT generally does not show any characteristic peak in the spectrum because of the difficulty in dispersing the pristine nanotubes in any liquid medium.

FTIR

Chapter 1

Another characterization technique used broadly is FTIR spectroscopy. This is highly useful in identifying the chemical interaction of nanomaterials with polymeric matrix. FTIR also sets evidence for modification of hydrophilic clay with appropriate modifying agent. De and Karak recently observed that the characteristic interlayer H₂O bending band of hydrophilic bentonite clay shifted from 1641 to 1565 cm⁻¹, when modified with aliphatic poly(amido-amine).¹⁴⁷ Again, surface modification of CNT and RGO was analyzed by FTIR technique.¹¹⁵ This tool is also helpful for indentifying the existence of inter- and intra-molecular hydrogen bonding, which is very common for cellulose based nanomaterials.¹⁴⁸ However, special IR technique like Attenuated total reflection infrared (ATR-IR) is used for advanced characterization of polymeric NC much easily.¹⁴⁹

NMR

NMR is a useful technique for structural characterization of polymer NC. Si-solid state NMR elaborates important information regarding polymer clay NC.¹⁵⁰ Again, ¹³C solid state NMR provides useful facts about the surface chemistry and morphology of NC. Free volume in polymer NC has also been determined by ¹²⁹Xe NMR technique.¹⁵¹

XRD

Crystallinity of nanomaterials and polymer NC is studied by XRD. Wide angle X-ray diffraction (WAXD) analysis and small-angle X-ray scattering (SAXS) techniques are available in this context; while the former has broad utility because of easy availability and simple operational method. XRD provides information of state of crystallinity for layered silicates, metal nanoparticles, CNT, graphene, RGO etc.^{16, 115, 152} In case of epoxy clay NC, this is regarded as the preliminary tool to ascertain the structure like exfoliated or intercalated. The interlayer *d*-spacing calculated from the basal reflection peaks provides the extent of delamination of the clay layers upon interaction with the epoxy matrix.^{16, 147} The *d*-spacing is determined by using the Bragg's law, $n\lambda = 2d\sin\theta$, where, *n* is the order of plane, λ is the wave length of the incident radiation and θ corresponds to the diffraction or glancing angle. Metal or metal oxide nanoparticles show distinctive Bragg's reflection planes which implicate the lattice structure of the metal.⁸⁴ However, WAXD technique can

Chapter 1

only provide preliminary information regarding the distribution of nanomaterials; while this cannot be considered as concrete until further characterizations are done.¹⁵³

While SAXS utilizes very low incident angle of radiation (typically $<3^\circ$), which is helpful to elucidate the size and shape of inhomogeneities, present in a polymer NC. Neutron scattering (SANS) is preferred in some cases, because cold neutrons can enter into thick samples. This provides the conformation of polymeric chains within NC, thus depicting their structure.¹⁵⁴

Electron microscopy

Electron microscopy has a strong impact on polymeric NC research. SEM is used to a great extent in this context, because of its versatile imaging modes, excellent resolution, easy sample preparation and simple interpretation of images. SEM is broadly used in the domain of biomaterial research to observe cell attachment on the materials, morphology of drug treated or untreated cells etc.¹⁸ Further, texture of microbes-degraded polymeric films can be visualized from SEM micrographs.¹⁵⁵ In this microscopic techniques high energy electrons are produced which interact with the surface of the samples analyzed. Thus, SEM provides clear picture of the surface morphology of a polymeric NC.

Other two vital microscopic techniques are scanning tunnelling microscopy (STM) and atomic force microscopy (AFM). They use sharp tip to determine the tunneling current and tip-sample interaction respectively. They are termed as scanning probe microscopy (SPM), which is a useful tool to characterize polymeric NC as well as biological samples.¹⁵⁶

Further, TEM is considered as the vital instrumentation for characterization of polymer NC. TEM helps in elucidating the distribution of nanomaterials within NC. It provides clear images of the structure and size of different phases present in the NC system. It allows a beam of high energy electrons to transmit through a very thin specimen, which shows internal structure of the sample. TEM has immense utility in the domain of the nanotechnology and nanobiotechnology. Literature showcase TEM micrographs of clay, metal nanoparticles, CNT, RGO and graphene based epoxy NC, which provided their distribution and shape-size accord within the matrices.^{16, 115, 147, 152} Many researchers have utilized this tool for characterizing biological samples such as bacteria, fungi, different

Chapter 1

cells, cell-biomaterials-interaction etc.^{18, 155} Karak and co-workers reported distribution and interaction of silver decorated clay within HE matrices.¹⁶ The same group utilized high resolution TEM for characterizing luminescent carbon oxide dots based HE NC.¹⁵⁷

Besides, DSC provides glass transition (T_g) and melting temperatures (T_m) of polymer and their NC. This technique is widely used to study the curing behavior of epoxy resins with temperature and time in presence of an appropriate hardener.¹⁵⁸ Crosslinking reaction, phase separation, first and second order transition, degree of crystallinity, coefficient of thermal expansion etc. are the vital attributes explored by DMA thermal technique under dynamic conditions.¹⁵⁹

1.4.3. Biological testing for biomaterials

1.4.3.1. Cytocompatibility test

Cytocompatibility is the basic requirement for any biomaterial. Different cytocompatibility assays like direct contact method, extract assay etc. are recommended by ASTM and ISO. Direct contact method is the simplest one to use in case of polymeric biomaterials. In this method, polymer or polymeric NC films are incubated with specific cell lines. Percentage survival of cells in presence of the tested materials is checked generally by using MTT dye. Microscopic analysis of cell morphology is observed by using dyes, like trypan blue.^{160, 161}

Another such cell survival assay used widely is the agar diffusion method. Agar, enriched with the cell culture medium is used as a barrier between cells and sample. Soluble product is diffused in the agar and comes in contact with the cells. Cell viability is calculated by observing the effected zones by using appropriate dyes. Toxicity of the degraded products of biomaterials can be detected by elusion assay.¹⁶²

1.4.3.2. Cell adhesion assay

Cell adherence on the surface of a biomaterial is calculated by seeding the cells onto it. Number of adhered cells is determined by subtracting the non-adhered cells from the total number of cells initially seeded. Quantitatively, number of cells is calculated haemocytometrically.¹⁶⁰ MTT dye and radioactive labeling is also used to measure the cell viability. Adherence, growth and proliferation of cells on the biomaterial-surface are

Chapter 1

observed by microscopic analysis. SEM is a vital technique in this context. Other optical microscopic techniques are also used for analyzing cell morphology, after staining with appropriate dyes. DAPI (4',6-diamidino-2-phenylindole), 7-AAD (7-Aminoactinomycin D), Propidium iodide, JC-1 etc. fluorescent dyes are generally used for staining.

1.4.3.3. In vivo compatibility test

Two important parameters, *viz* hematology and histopathology are usually scrutinized for ascertaining *in vivo* compatibility of biomaterials. Karak and co-workers analyzed *in vivo* compatibility of polymeric NC by implanting the biomaterials subcutaneously within wistar rat. They observed hematological parameters of the implanted rats during their experiment, by collecting blood from orbital sinus vein.¹⁸ Macrophage (matured monocytes), neutrophil or lymphocytes counts of the implanted rats indicates the immunogenesis after implantation of a foreign polymeric material into the body. Thus, hematological parameters can indicate the preliminary immune response for an implantable biomaterial. These parameters are compared with that of a control group, which implicates the induction of any kind of toxicity to the host body.

The other important aspect of biocompatibility can be monitored by histopathological studies. Major organs of the test animal are extracted after certain period of implantation. These organs are fixed in 2.5% gluteraldehyde or 10% formaldehyde solution, followed by dehydration in increasing alcohol gradient (70-100%). Then, the organs are sectioned with the help of microtome. Finally histological sections are observed under microscope after staining with an appropriate dye. Hematoxylin and eosin are widely used in combination for staining histological sections.¹⁸

Lipid and kidney profiles as well as liver function tests are also performed as a part of *in vivo* compatibility assessment, by analyzing the serum biochemistry of the implanted animals. These tests scrutinize the abnormality of lipid, liver and nephrotoxicity induced in the animal body after implantation of a biomaterial.^{18, 163}

In-vivo tissue regeneration study is generally carried out by creating wound or crack at particular sites of the animal body. Subsequent implantation of the polymeric biomaterial to the wound site and continuous monitoring of healing, constitute the experimental

Chapter 1

process. Hematology and histopathological parameters are observed to examine the progress of the healing process.¹⁶⁴

1.4.4. Statistical analysis

Statistical analysis of results is very much relevant to achieve the real significance of biological data. Obtained data are generally presented as mean \pm standard deviation (SD) from the triplicate results. Analysis of variance (ANOVA, one or two way) is carried out to understand real deviations amongst the results. Least significant difference (LSD) test is further performed to determine the significant differences amongst the data. SPSS, Minitab, DesignExpert etc. are some of the softwares used for statistical analysis of biological results.

1.5. Properties

Various properties of pristine polymer and their enhancement in polymeric NC systems are interesting to study. Properties of epoxy and epoxy based NC are studied by different research groups.^{165, 166} Karak and co-workers observed property improvement of HE systems upon formation of NC.^{16, 147} Some significant properties of polymeric NC are discussed in this section.

1.5.1. Rheological

Study of the rheological behavior of a resinous material is very important for its processing and industrial applications. Rheological properties are referred to as the properties of a material that are related to the deformation and fluidity of the material under application of an external stress. The changes in shear viscosity under variable temperature and stress are generally studied. Viscosity of an epoxy resin is associated with the segmental density, intermolecular entanglement and inter or intramolecular hydrogen bonding.¹⁶⁷ Liquid epoxy behaves as an ideal Newtonian fluid. The limited applied shear force also cannot cause any structural change of the resin. Again, researchers have found favorable rheological properties for HE.¹⁶⁸ Moreover; this is helpful to determine the dispersion quality of a nanomaterial within the polymer matrix. In most of the cases, viscosity increases with increase in amount of the nanomaterial loading.¹⁶⁹

Chapter 1

1.5.2. Mechanical

Mechanical strength and flexibility are two important features to be present in an ideal biomaterial. It is well understood by the scientific community that mechanical performance of an epoxy system increases dramatically upon NC formation. Very low level (<5 weight%) of nanomaterials incorporation can augment mechanical strength to multi-fold than the pristine matrix. Even in few cases this augmentation is accompanied by a simultaneous increment of elongation at break though in most of the cases, the value decreases.¹⁵⁷ Tensile strength usually increased with increase in loading of nano-reinforcing agents, up to a critical dose. Better interaction of the nanomaterials with the polymeric matrix aids to such increment. Thus, exfoliated NC shows higher strength as compared to the intercalated one. High surface activity of nanomaterials facilitates the load bearing capacity of the polymer, thereby reinforcing the NC system. De and Karak recently showed 50% increment of tensile strength of HE upon 3 weight% loading of modified bentonite clay.¹⁴⁷ Similar observation was made by the same group upon incorporation of 5 weight% octadecyl amine-modified montmorillonite clay into HE matrix.¹⁶ CNT and graphene based epoxy NC were studied, where 35.4% increment of tensile strength was observed.¹⁷⁰

Again, incorporation of 0.5 weight% of luminescent carbon oxide dots to HE matrix enhanced the tensile strength as well as elongation at break.¹⁵⁷ Elongation at break implicates the strain that a material can endure before the point of break. Many reports show that this property decreases in case of NC as compared to the pristine matrix.¹⁷¹ This is attributed to the restriction of mobility of polymeric chains upon formation of NC.

Another important mechanical property is the impact resistance, which signifies the strength and flexibility of the polymeric material. In most of the cases, impact strength increases with the increase of loading of the nanomaterial up to a certain value. Again, scratch hardness is an important mechanical attribute, which indicates the resistance of the material to plastic deformation due to friction created by a sharp object under dynamic conditions. Other types of hardness are indentation hardness and rebound hardness. Hardness increases with increase in interaction of the nanomaterials with the epoxy matrix as well as in crosslinking density.¹⁷²

1.5.3. Thermal

Chapter 1

The most important thermal property of a polymer is its stability at elevated temperature. Thus, TGA is the most widely used technique to measure the onset temperature of degradation of a polymeric material as well as NC. In general, two step degradation patterns are witnessed in case of epoxy thermosets. This is because of the presence of both aliphatic and aromatic moieties in the structure, which degrades at different temperature ranges. The aliphatic moieties show the onset degradation temperature at around 200-250 °C, while the aromatic ones generally start degrading at around 450-500 °C. Literature demonstrated that HE shows better thermostability than their linear analogs.^{33, 147, 172} Thermal stability of NC increases to significant extent as compared to the pristine epoxy. Curing kinetics of epoxy resins in presence of a hardener can be evaluated through DSC technique.¹⁵⁸ Dimensional stability of a material can be determined by calculating the coefficient of thermal expansion (CTE) with TMA. Further, viscoelastic properties of epoxy are analyzed by DMA/DMTA. Incorporation of nanomaterials augments the thermal stability as such the nanomaterials serve as heat insulators. These nanomaterials also act as the mass transport barrier for volatiles generated during the decomposition process. This is also attributed to the decrease in T_g value due to the restriction of polymeric chain mobility in case of NC.¹⁴¹

1.5.4. Biological properties

1.5.4.1. Biocompatibility

In vitro biocompatibility

Preliminary *in vitro* biocompatibility of polymeric materials is assayed by calculating the cell survival rate in presence of the test materials. Recent literature showcased that MTT assay is the most widely used technique in this regard.¹⁸ Different polymers and their NC are designed to gain excellent biocompatibility by tailoring their architecture. Polyurethanes are one of the most explored polymers in the biomedical domain.¹⁷³ Epoxy based biomaterials also showed potential utility in a number of biomedical applications. However, in maximum cases cytotoxicity stood as the barrier between theory and practice. Reports demonstrated that fast cured epoxy is immensely used as a dental sealer; while

Chapter 1

prolonged prevalence of the material induced acute toxicity to human oral fibroblast.¹⁷⁴ Therefore, researchers tried to synthesize cytocompatible epoxy, by incorporating benign moieties to the structural backbone. Another major concern is the compatibility of nanomaterials with biological systems. Metal nanoparticles showed severe toxicity to many cell lines as tested *in vitro*.¹⁷⁵ Contrarily, green route mediated synthesis of such nanoparticles exhibited promising cell compatibility. Further, toxicity of nanomaterials like graphene, CNT etc. is dramatically diminished after incorporation of these materials into polymer matrices.¹⁶⁴ Thus, polymeric NC provides higher cytocompatibility than the bare nanomaterials. Epoxy based NC are studied to a limited extent to understand their cytocompatibility profiles.

In vivo biocompatibility

Implantable biomaterials demand positive host response, without inducing immunogenesis. Hematological parameters are regarded as the indicators of such immune response.¹⁷⁶ Levels of macrophage (matured monocytes), neutrophil or lymphocytes show the initial immunity generated after implantation of a biomaterial. Karak and co-workers demonstrated that no immune response was induced in rats after implantation of hyperbranched polyurethane based NC.¹⁶⁴ However, to affirm the compatibility of the biomaterial with *in vivo* systems, histopathological study is a prerequisite. There is a probability of leaching out of the nanomaterials from the polymer matrix, which can enter the blood stream and reach different parts of the body. Hence, histology of major organs, such as skin, heart, liver, kidney, brain etc. gives the real picture of the material's compatibility. Nelson et al. examined the histology of epoxy based human dental enamel.¹⁷⁷ Many researchers have shown compatibility of implantable tissue scaffolds by histological studies.¹⁷⁸ Such study provides information regarding angiogenesis, neovascularization, irregularity in cell morphology and capsule formation around the implant site.^{179, 180} However, *in vivo* test is performed only after obtaining successful results in *in vitro* test of the material.

1.5.4.2. Cell adhesion

Chapter 1

A biomaterial used for tissue engineering applications provides a surface, which could support the adhesion, growth and proliferation of cells. Different polymers and polymeric NC are being used for adhering cells.^{18, 164} Inadequate bonding between cells and the polymer results in inflammation, capsule formation, thrombosis etc. Continuous endeavors have been made to utilize suitable polymeric materials as scaffolds for regeneration of different types of tissues. Tissue engineering is referred to as 'application of the principles and methods of engineering and life sciences towards the fundamental understanding of structure-function relationships in normal and pathological mammalian tissues and the development of biological substitutes that restore, maintain or improve tissue function'.¹⁸¹ Polyurethane, polyglycolic acid (PGA), polylactic acid (PLLA), polycaprolactone (PCL), chitosan-based polysaccharides, polyphosphazenes, polyfumarate, polyorthoester, poly(glycerol sebacate), polypyrrole, polyarylates, poly(ether ester amide), poly(amido amine) etc. are used for anchoring different types of cells.¹⁸² Epoxy compounds are used for crosslinking of different kinds of other polymeric materials which showed excellent cell adhesion.¹⁸³ However, epoxy based tissue scaffold is very rare in literature.⁷⁰

1.5.4.3. Antimicrobial activity

In vitro antimicrobial activity

Antimicrobial polymeric NC have immense utility in the domain of material science as well as biomedical research. Metal nanoparticles based NC show proficient inhibitory effect against bacteria and fungus. Silver and copper oxide nanoparticles and their polymeric NC exhibited both bacteriostatic and bactericidal properties against a number of pathogenic bacteria, like *Staphylococcus aureus*, *Bacillus subtilis*, *Escherichia coli*, *Pseudomonas aeruginosa*, *Mycobacterium smegmatis*, *Trichophyton rubrum* etc.¹⁶ Microbial infection resistant polymeric materials are useful in fabricating infection resistant scaffolds or coating over conventional metal implants. Saravanan et al. fabricated a chitosan-hydroxyapatite-silver based NC for bone tissue regeneration which showed promising antibacterial activity against *Staphylococcus aureus* and *Escherichia coli*.¹⁸⁴ However, very few polymers show antimicrobial attributes in their pristine form. Phosphorylcholine containing antifouling epoxy coatings are used for fabricating optical biosensor.¹⁸⁵

Chapter 1

Incorporation of nanomaterials, primarily metal nanoparticles confer high efficacy to polymeric NC to prevent microbial fouling. A large number of NC with antimicrobial activity are studied. Metal-chelated epoxy resins are reported by Nishat and co-workers, which exhibited good inhibitory effect against *Staphylococcus aureus*, *Escherichia coli*, *Bacillus subtilis*, Mucor yeast and *Candida albicans*.¹⁸⁶ Lai et al. showed the zones of growth inhibition of epoxy-resin-based endodontic sealers against the common endodontic pathogens, *Staphylococcus aureus*, *Streptococcus mutans*, *Streptococcus sanguis* and *Escherichia coli*.¹⁸⁷ Similar observations were made by Yasuda and her group.¹⁸⁸ Again, TiO₂-Ag and Al₂O₃-Ag based epoxy NC produced strong antibacterial properties when tested with *Staphylococcus epidermidis* and *Escherichia coli*.¹⁸⁹ Further, silver embedded hyperbranched epoxy/clay NC reported by Karak and his group inhibited the growth of both Gram positive and negative bacteria.¹⁶

Further, epoxy based NC are studied for their potential utility in the domain of advanced antifouling marine coatings. With such an effort, Schif et al. fabricated a slow release copper impregnated modified epoxy coating.¹⁹⁰ Wang and co-workers reported a polyaniline and epoxy resin based corrosion resistant, antifouling coating.¹⁹¹ Different other polymers such as polyesters, polyurethane, polyamides etc. based NC were explored for designing non-toxic antifouling coatings.¹⁹²

In vivo antimicrobial activity

In vivo antimicrobial activity is an essential property for implantable polymeric biomaterials. However, very limited number of reports are found where *in vivo* activity has been addressed thoroughly. Deitch et al. studied the *in vitro* and *in vivo* antimicrobial efficacy of silver coated nylon cloth against *Streptococcus aureus*, *Pseudomonas aeruginosa* and *Candida albicans*.¹⁹³ Literature on such study for epoxy based NC is not reported.

1.5.4.4. Biodegradation

Biodegradable biomaterials are at the height of attraction because of their sustainability and compatibility with host systems. Use of biodegradable feedstock for polymeric biomaterials also satisfies the environmental aspects. In case of implantable polymeric scaffolds, the

Chapter 1

materials degrade after serving the purpose of tissue regeneration inside the body, which overrules the need of repeated surgery. Physiological fluids, which include water, enzymes and different salts, are mainly responsible for polymer degradation. Trypsin, esterase, papain etc. are some examples of enzymes which help in the degradation process of polymeric biomaterials.¹⁹⁴ Reported works suggested that degradation rate of a polymer increases after formation of NC. Presence of nanomaterials within the matrix initiate many catalytic activities, which enhance the rate of degradation.^{195, 196} However, the extent of degradation depends on the chemical linkages present in the polymeric NC. The degradation process involves different steps such as water absorption, fragmentation of structural moieties etc.

Another path for polymeric degradation is the one caused by microorganisms. This ensures that the polymeric biomaterials would be degraded after disposal to the environmental conditions. Available literature pointed out that vegetable oil based polymers and their NC are more susceptible to microbial biodegradation. In this context, biodegradable hyperbranched polyurethanes, polyesters and epoxy based NC are reported by different research groups.^{172, 197, 198}

Besides the above properties, some allied aspects associated to epoxy based NC are shortly described below.

Barrier properties

Barrier properties of a polymer significantly increase upon formation of NC. Inorganic nanomaterials provide very high surface area to volume ratio which amends the diffusion pathways of different penetrating molecules. Rate of diffusion of a penetrating molecule further depends on the degree of dispersion of the nanomaterials. High aspect ratio provided by nanoclay generally diminishes the gas permeability in NC.¹⁹⁹ Kim and co-workers reported the improved gas barrier property of graphene/polyurethane NC; whereas Takahashi et al. describes the same for butyl rubber/vermiculite NC based coatings.^{200, 201} Further, Kim et al. in 2005, investigated the moisture barrier properties of organoclay-epoxy NC.²⁰² Guadagno and group analyzed the transport properties, sorption and diffusion of water vapor of MWCNT based epoxy NC.²⁰³

Chapter 1

Flame retardancy

Flame retardant compounds are incorporated to polymeric matrices to increase the ignition temperature and to slow down the decomposition. Epoxy NC, with very little amount of nanomaterials, like clay, CNT etc. may exhibit flame retardant behavior as described in literature.^{204, 205}

Optical properties

Transparency of a polymeric NC is very important for many advanced applications. It is the physical property of a material which allows the transmission of light. Various polymeric NC are reported with excellent transparency. Epoxy based clay NC are generally transparent up to a certain loading percentage of the nanomaterial.¹⁴¹ However, CNT or graphene based epoxy NC lost their transparency even at very low level of loading. Transmittance of a NC film is quantitatively determined by UV-visible spectroscopy. Other interesting optical properties, like fluorescence, luminescence, non-linearity etc. are also exhibited by polymeric NC. Recently, carbon oxide nanodots impregnated HE with high luminescent properties was reported.¹⁵⁷ Further, metal quantum dots impart interesting optical properties when incorporated within polymeric matrix. Now a days, different nanomaterials are explored to obtain fascinating optical properties of polymeric NC, which have immense industrial applicability.

Electrical properties

A material, which allows the flow of current, is a good conductor and the one which opposes that is regarded as an insulator. Most of the polymers, in their pristine forms act as insulators, mainly due to their covalent nature and lack of electronic pathway. Epoxy thermosets with low dielectric constant are useful for many applications, such as semiconductor devices, circuit boards, electronic packaging, microelectronic devices etc. Further, incorporation of nanomaterials confers interesting attributes to epoxy systems. Wang and Chen studied the dielectric behavior, space charge and dielectric breakdown of SiO₂/Al₂O₃ based epoxy NC.²⁰⁶ Carbon based nanomaterials also help in altering the electrical properties of a polymer. Wang et al. in 2008 observed high conductivity in a CNT based epoxy NC.²⁰⁷

Chapter 1

1.6. Applications

As formation of NC improves various material properties of epoxy, it is quite interesting to study their applicability by incorporating different nanomaterials to the matrix. Epoxy based biomaterials gained commercial impetus from long time. However due to a number of demerits their sustainability has been hindered. Moreover, epoxy/NC based biomaterials are explored to a minimum extent. Importance of epoxy in the field of biomedical research is highlighted earlier. Epoxy thermosets and their NC used in various applications are described below.

A brief list of commercially available epoxy based biomaterials is presented in Table 1.4.

Table 1.4: A few commercially available epoxy based biomaterials

Material	Applications	Merit/Demerit	Reference
EX-131, EX-810, EX-313 and EX-512 (Denacol [®] , Nagase Chemicals, Ltd., Osaka, Japan).	Bioprotheses, Fixatives	Superiority to gluteraldehyde fixatives.	208
Hysol W-795, Hysol EA 9696, Hysol PL 795 etc. (Henkel, Malaysia)	Insulators in biomedical sensors	Low dielectric constant, high adhesive strength. Poor host compatibility	209
Intergard 269 (Akzo Nobel, USA)	Biomedical and marine coatings	Low-VOC, low viscosity, highly flexible	210
AH Plus, AH26 (Dentsply Maillefer, Ballaigues, Switzerland), Acroseal (Septodont, France)	Dental root canal sealers	Quick sealing capacity, low leakage. Severe cytotoxicity.	211

1.6.1. Dental sealing

Chapter 1

Dental sealers or fissure sealants are referred to as a dental treatment measure, where a polymeric sealing material is added to the dental pitch of the molar or premolar teeth. Epoxy based dental sealers are used to a great degree. Eick et al. scrutinized the properties of spiroorthocarbonates and epoxy co-polymer dental sealers, as a non-shrinking matrices.²¹² AH26, AH-Plus (Dentsply Maillefer, Ballaigues, Switzerland), Acroseal (Septodont, Saint-Maur des Fosse's, France) etc. are some of the epoxy resin based commercial dental sealers for root canal therapy. AH-plus is a BPA based epoxy glue, which is applied along with hexamethylene tetraamine and bismuth oxide. Bismuth oxide is used for radiographic contrast. Again, AH26 is a highly water resistant sealer, which releases trace amount of formaldehyde that acts as an antibacterial agent. However, cytotoxicity of the prevailing sealers raised a serious concern amongst the researchers regarding the application of the same. Azar et al. demonstrated that AH-plus exhibited better compatibility with human fibroblasts as compared to two common endodontic sealers AH26 and zinc oxide-eugenol.¹⁷⁴ Contrarily, Miletic and co-workers observed that AH-plus showed significant cytotoxicity against human cervical carcinoma (HeLa) cells and skin fibroblasts (L929) in comparison to another available sealer, RoekoSeal Automix (RSA).²¹³ Another observation made by Huang et al. revealed that two epoxy based root canal sealers, induced cytotoxicity to human osteoblast cell line and U2OS cells.¹¹ Kostoryz and group demonstrated that ERL-4206 and UVR-6105 resins (epoxy based sealers) showed severe toxicity to L929 cells, which is diminished by the addition of a spiroorthocarbonate.¹³

The aforementioned facts implicates that there is a great demand for non-toxic endodontic sealants. Thus, there are lots of scopes to develop such sealers. Incorporation of multifunctional nanomaterials may confer good cytocompatibility as well as antimicrobial activity to such endodontic sealers.

1.6.2. Antimicrobial coatings

Microbial contamination and infections are serious problems associated with biomedical implants, food packaging, implant coatings, marine coatings etc.¹⁹² Microorganisms form biofilms over medical devices and implants, which induce infections at surgical sites. Further, material surfaces, constantly exposed to aquatic conditions are highly susceptible to marine microbes and algae. Therefore, antimicrobial thin film coatings are on high

Chapter 1

demand to protect such surfaces, thereby enhancing the service life. Biocides impregnated coatings have been used for last two-three decades for such purpose. Still, their toxicity to health and non-target marine organisms stood as a barrier between development and applicability.²¹⁴

Epoxy is a widely used binder in coating industries. Different polymers were blended with epoxy to attain high mechanical performance of the coating. Sharmin and co-workers synthesized corrosion resistant epoxy-polyols and epoxy-polyurethane for antimicrobial coating application.²¹⁵ Abdullayev et al. prepared silver and halloysite based epoxy NC for developing antibacterial composite coating against *Staphylococcus aureus* and *Escherichia coli*.²¹⁶ Silver and copper/copper oxide based composite coatings are investigated as antimicrobial coating materials to prevent microbial fouling. Chae and group put forwarded a phosphorylcholine based antifouling epoxy coating for optical biosensor application.¹⁸⁵ Further, agar diffusion method carried out by Zafar et al. revealed the potential inhibitory effect of epoxy-acrylic-oleic acid coating against bacteria and fungi.²¹⁶ Activity of silver-zeolite-epoxy NC was analyzed by Cowan et al. against *Escherichia coli*, *Staphylococcus aureus*, *Pseudomonas aeruginosa*, and *Listeria monocytogenes*.²¹⁷ *Staphylococcus aureus* is mostly responsible for creating surgical site or hospital acquired infections. Therefore, epoxy NC based coatings with inhibitory effect to this bacterium can protect the medical devices and implants or surgical equipments from acute infection. In this regard, different nanomaterials based epoxy NC were prepared and patented.²¹⁸

1.6.3. Tissue engineering

Tissue engineering is an emerging area that could significantly contribute to regenerate the damaged tissues. In broader aspects, tissue engineering is assimilated in the category of regenerative medicines. This is an interdisciplinary branch, where engineering, biology, physics, chemistry and biotechnology collaborate. Scaffold materials are regarded as the basic platform of tissue engineering. In due course of development, polymeric scaffolds are gaining significant impetus, because of their tunable properties. Thermoplastic polymers and their NC are widely explored for tissue engineering applications. However, very limited reports are found where thermosetting polymers are utilized to regenerate tissues.

Chapter 1

Hamid et al. recently showed the potential of epoxy-amine synthesized hydrogel scaffolds for soft tissue engineering.⁷⁰ Again, Ovsianikov and his group used epoxy-based (SU8) materials for microfabrication of three dimensional tissue scaffolds.²¹⁹

1.6.4. Miscellaneous

Excluding the above fields of applications, epoxy NC have immense utility in various domains of science and technology. Carbon nanomaterials based epoxy NC are used in light weight badminton and tennis rackets, hockey sticks etc. With the development of materials people become concerned about their degradability when disposed to environment. Non-degradable polymeric materials play the giant role in land and water pollution all over the globe. Consequently, research on biodegradable polymers got the momentum. Vegetable oil based high performance epoxy and their NC are reported in literature, which showed good degradability in physiological fluids as well as by microorganisms. Biodegradable polymeric NC are desired for scaffold material as they nullify the requirement of repeated surgery. Further, surgical equipments, medical devices, food industries, hospital appliances etc. are some of the application areas for biodegradable polymeric NC.

Based on the above discussions, prospective applications of HE NC are depicted in Figure 1.1.

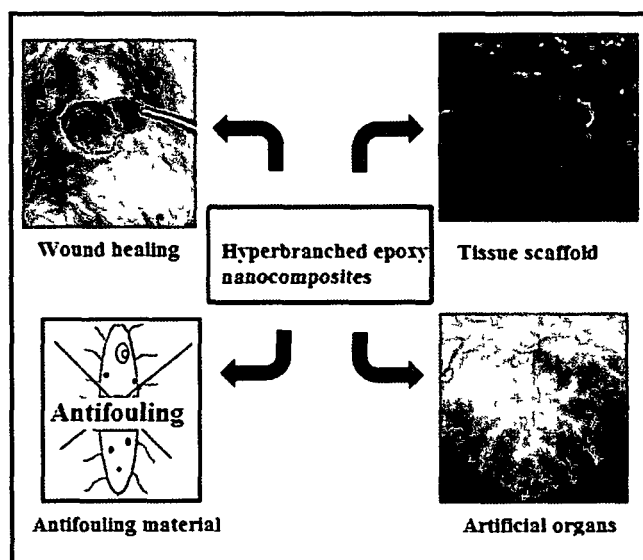


Figure 1.1: Potential applications of hyperbranched epoxy nanocomposites

Chapter 1

1.7. Scopes and objectives of the present investigation

From the above discussions, it can be visualized that HE based NC have lots of potential in the realm of biomedical research. Literature reports the use of epoxy in various domains of biomedical applications. They are basically used in endodontic sealers, biosealants, bioprotheses, insulating biomedical sensors etc. However, epoxy NC based tissue scaffolds are rarely explored. Thus, it opens a new arena for research to use biocompatible HE based high performing NC as multifunctional biomaterials.

Scrutinizing the above facts, the main objectives of the present investigation are made as follows,

1. To synthesize HE resins using a biocompatible polyol core unit.
2. To characterize the synthesized HE using different analytical and spectroscopic techniques.
3. To evaluate the properties including biocompatibility of the synthesized HE resins.
4. To prepare the NC of the HE with nanoclay, CNT, RGO, NFC, metal nanoparticles etc.
5. To characterize the prepared NC using different analytical and spectroscopic techniques.
6. To evaluate the properties including biocompatibility of the prepared NC and optimize the performance for possible potential applications.

1.8. Plan of research

In order to implement and achieve the goal of the objectives, the proposed work has been planned in the following manner

- i) A thorough literature survey on the field biocompatible epoxy and NC will be conducted.
- ii) The HE resin will be synthesized by using a polyol core unit through an $A_2 + B_3$ approach.
- iii) The synthesized resin will be characterized by using different analytical and spectroscopic techniques such as determination of epoxy equivalent, FTIR, NMR etc.
- iv) Properties like physical, chemical, mechanical and the biocompatibility of the HE resin will be evaluated.
- v) HE NC will be prepared by solution technique as reported in literature using commercial organophilic nanoclay, CNT, RGO, NFC, metal nanoparticles etc. The plant mediated preparation of metal nanoparticles will also be attempted.

Chapter 1

- vi) The prepared NC will be characterized by UV, XRD, SEM and TEM analyses.
- vii) Biocompatibility of the HE NC will be tested both *in vitro* and *in vivo*.
- viii) Performance of the NC will be investigated by measuring tensile strength, elongation at break, adhesive strength, biological attributes etc. and the best studied NC will be utilized for possible biomedical applications in each case.

References

1. Severian, D. *Polymeric Biomaterials*, Marcel Dekker, Inc. New York, 2002.
2. John, A. *Artif. Organs* **1** (1), 53--57, 1977.
3. Huebsch, N. & Mooney, D.J. *Nature* **462** (26), 426--432, 2009.
4. Park, J.B. & Bronzino, J.D. *Biomaterials-Principles and Applications*, CRC Press LLC, USA, 2003.
5. Angelova, N. & Hunkeler, D. *Trends Biotechnol.* **17**, 409--421, 1999.
6. Ulery, B.D., et al. *Polym. Sci., Part B: Polym. Phys.* **49** (12), 832--864, 2011.
7. Modjarrad, K. & Ebnesajjad, S. *Handbook of Polymer Applications in Medicine and Medical Devices*, e-book, Elsevier, 2013.
8. Kalita, S.J. *Nanostructured Biomaterials* Springer, New York, 2008.
9. Determan, M.D., et al. *Gentle to skin adhesive*, US Patent No. 0212325, September 1, 2011.
10. Wen, L., et al. *Soybean Sci.* **1**, 1--33, 2010.
11. Huang, T.H., et al. *Biomaterials* **23** (1), 77--83, 2002.
12. Rathee, M., et al. *Indian J. Endocrinol. Metab.* **16** (3) 339--342, 2012.
13. Kostoryz, E.L., et al. *Dent. Mater.* **15** (5), 363--373, 1999.
14. Karak, N. *Fundamentals of Polymers*, PHI Learning Private Limited, New Delhi, 2010.
15. Kiliaris, P. & Papaspyrides, C.D. *Prog. Polym. Sci.* **35** (7), 902--958, 2010.
16. Roy, B., et al. *Bioresour. Technol.* **127**, 175--180, 2013.
17. Cioffi, N., et al. *Chem. Mater.* **17** (21), 5255--5262, 2005.
18. Das, B., et al. *Biomed. Mater.* **8** (3), 035003--035014, 2013.
19. Jell, G., et al. *J. Mater. Chem.* **18** (16), 1865--1872, 2008.
20. Wei, J., et al. *Nanotechnol.* **23** (33), 335707--335713, 2012.
21. Spear, R.L. & Camero, R.E. *Int. J. Mater. Form.* **1** (2), 127--133, 2008.

Chapter 1

22. Yang, Y., et al. *Mater. Today* **16** (10), 365--373, 2013.
23. Abdul Khalil, H.P.S., et al. *Carbohydr. Polym.* **87** (2) 963--979, 2012.
24. Migonney, V. *History of Biomaterials*, Wiley and Sons, New York, 2014.
25. Temenoff J.S. & Mikos, A.G. *Biomaterials: The Interaction of Biology and Material Science*, Prentice Hall, USA, 2008.
26. Roach, P., et al. *J. Mater. Sci: Mater. Med.* **18** (7), 1263--1277, 2007.
27. Nasab, M.B., et al. *Trends Biomater. Artif. Organs* **24** (2), 69--82, 2010.
28. Mantripragada, V.P., et al. *J. Biomed. Mater. Res. A* **101** (11), 3349--3364, 2013.
29. Sarkar, R. & Banerjee, G. *Interceram.* **59**, 98--102, 2010.
30. Ebevele, R.O. *Polymer Science and Technology*, CRC Press, Boca Raton, 2000.
31. Selvaraj, M., et al. *Prog. Org. Coat.* **67** (3), 339--347, 2010.
32. Rocks, J. *Characterization of novel co-anhydride cured epoxy resins*, Ph. D. Thesis, Queensland University of Technology, Switzerland, 2004.
33. De, B. & Karak, N. *J. Mater. Chem. A* **1** (2), 348--353, 2013.
34. Kienle, R.H. & Hovey, A.G. *J. Am. Chem. Soc.* **51** (2), 509--519, 1929.
35. Kim, Y.H. & Webster, O.W. *Polym. Prepr.* **29** (2), 310--311, 1988.
36. Kim, Y.H. & Webster, O.W. *J. Am. Chem. Soc.* **112** (11), 4592--4593, 1990.
37. Emrick, T., et al. *Macromolecules* **32** (19), 6380--6382, 1999.
38. Chang, H-T. & Frechet, J.M.J. *J. Am. Chem. Soc.* **121** (10), 2313--2314, 1999.
39. Emrick, T., et al. *J. Polym. Sci. Part A: Polym. Chem.* **38** (S1), 4850--4869, 2000.
40. Gong, C. & Frechet, J.M.J. *Macromolecules* **33** (14), 4997--4999, 2000.
41. Wang, X. & Feast, W.J. *Chin. J. Polym. Sci.* **20** (6), 585--590, 2002.
42. Huang, P., et al. *J. Appl. Polym. Sci.* **123** (4), 2351--2359, 2011.
43. Luo, L., et al. *J. Appl. Polym. Sci.* **130** (2), 1064--1073, 2013.
44. Roy, B. & Karak, N. *J. Mater. Res.* **27** (14), 1806--1814, 2012.
45. Anandhan, S. & Bandyopadhyay S. *Polymer Nanocomposites: From Synthesis to Applications, in Nanocomposites and Polymers with Analytical Methods*, J. Cuppoletti, ed., InTech, Europe, 2011, 3--28.
46. Mei, L.L., et al. *J. Inorg. Mater.* **28** (8), 811--817, 2013.
47. Fu, G., et al. *J. Phys. Chem. B* **109** (18), 8889--8898, 2005.
48. Liu, F., et al. *Polym. Int.* **58** (8), 912--918, 2009.

Chapter 1

49. Unnikrishnan, K.P. *Studies on the toughening of epoxy resins*, Ph. D. Thesis, Cochin University of Science and Technology, 2012.
50. Goud, V.V., et al. *Chem. Eng. Sci.* **62** (15), 4065--4076, 2007.
51. Choy, I-C. & Plazek, D.J. *J. Polym. Sci., Part B: Polym. Phys.* **24** (6) 1303--1320, 1986.
52. Bansal, R., et al. *Macromol. Mater. Eng.* **117** (2), 211--218, 1983.
53. Elmore, J., et al. *Stable aqueous epoxy dispersions*, US Patent No. **4315044**, February 9, 1982.
54. Birnbaum, L.S. & Staskal, D.F. *Environ. Health Perspect.* **112** (1), 9--17, 2004.
55. Twardowski, T.E. & Geil, P.H. *J. Appl. Polym. Sci.* **41** (5-6), 1047--1054, 1990.
56. Chen, S., et al. *J. Appl. Polym. Sci.* **123** (6), 3261--3269, 2012.
57. Maruyama, K., et al. *J. Polym. Sci., Part A: Polym. Chem.* **43** (19), 4642--4653, 2005.
58. Zhang, D., et al. *Macromol. Chem. Phys.* **210** (13-14), 1159--1166, 2009.
59. Bell, B.M. *CLEAN – Soil Air Water*, **36** (8), 657--661, 2008.
60. Fourcade, D., et al. *Green Chem.* **15** (12), 910-918, 2013.
61. Lee, H. & Neville, K. *Handbook of Epoxy Resins*, McGraw-Hill Inc., New York, 1967, reprinted 1982.
62. Potter, W.G. *Epoxide resins*, Springer-Verlag, New York, 1970.
63. Markovitz, M. *Hardenable composition consisting of an epoxy resin and a metal acetylacetonate*, US Patent No. **3,812,214**, May 21, 1974.
64. Reddy, P.V. & Nanje Gowda, N.M. *J. Appl. Polym. Sci.* **53** (10), 1307--1314, 1994.
65. Abdullah, B.M. & Salimon, J. *J. Appl. Sci.* **10** (15), 1545--1553, 2010.
66. Dinda, S., et al. *Bioresour. Technol.* **99** (9), 3737--3744, 2008.
67. Salunkhe, D.K., et al. *Legume Lipids, in Chemistry and Biochemistry of Legumes*, Edward Arnold Pub. Ltd., London, 1983.
68. Carvalho, C.N., et al. *Dent. Mater.* **29** (4), e79--e79, 2013
69. Shechter, L. & Wynstra, J. *Ind. Eng. Chem.* **48** (1), 86--93, 1956.
70. Hamid, Z.A.A., et al. *Biomaterials* **31** (25), 6454--6467, 2010.
71. Mahendran, A., et al. *J. Therm. Anal. Calorim.* **107** (3), 989--998, 2012.
72. Zuo-Guang, Z., et al. *J. Appl. Polym. Sci.* **94** (5), 2217--2222, 2004.
73. Loos, A.C. & Springer, G.S. *J. Compos. Mater.* **17**, 135--169, 1983.
74. Kondyurin, A. & Lauke, B. *Eur. Polym. J.* **40** (8), 1915--1923, 2004.

Chapter 1

75. Amdouni, N., et al. *Polymer* **31** (7), 1245--1253, 1990.
76. Babayevsky, P.G. & Gillham, J.K. *J. Appl. Polym. Sci.* **17** (7), 2067--2088, 1973.
77. Yeganeh, H., et al. *Eur. Polym. J.* **41** (10), 2370--2379, 2005.
78. Bilow, N. *J. Appl. Polym. Sci.* **12** (1), 175--190, 1968.
79. Woo, E.M., et al. *J. Mater. Sci.* **22** (10), 3665--3671, 1987.
80. Hong, S. *Airfoil leading edge coatings*, US Patent No. 0011935 A1, January 9, 2014.
81. Fahlman, B.D. *Material Chemistry*, 2nd ed., Kindle edition, Springer, New York, 2011.
82. Kumar, V. & Yadav, S.K. *J. Chem. Technol. Biotechnol.* **84** (2), 151--157, 2009.
83. Ghule, K., et al. *J. Nanosci. Nanotechnol.* **6** (12), 3746--3751, 2006.
84. Konwarh, R., et al. *Colloids Surf., B* **81** (2), 578--586, 2010.
85. Sharma, V.K., et al. *Adv. Colloid Interface Sci.* **145** (1-2), 83--96, 2009.
86. Hořary, S. et al. *Dig. J. Nanomater. Bios.* **7** (3), 999--1005, 2012.
87. Jia, B., et al. *ACS Appl. Mater. Interfaces*, **4** (6), 2897--2902, 2012.
88. Brayner, R. et al. *Langmuir* **26** (9), 6522--6528, 2010.
89. Chen, S. & Mao, S.S. *Chem. Rev.* **107** (7), 2891--2959, 2007.
90. Lo'pez-Miranda, A., et al. *J. Nanopart. Res.* **14**, 1101--1112, 2012.
91. Guzmán, M.G., et al. *World Acad. Sci., Eng. Technol.* **27**, 575--582, 2009.
92. Hartlieb, K.J., et al. *Green. Chem.* **12** (6), 1012--1017, 2010.
93. Pastoriza-Santos, I., et al. *Pure Appl. Chem.* **72** (1-2), 83--90, 2000.
94. Sahoo, P.K., et al. *Def. Sci. J.* **59** (4), 447--455, 2009.
95. Prabhu, S. & Poulouse, E.K. *Int. Nano Lett.* **2**, 32--41, 2012.
96. Anyaogu, K.C., et al. *Langmuir* **24** (8), 4340--4346, 2008.
97. Yang, J.G., et al. *Chem. Lett.* **35** (10), 1190--1191, 2006.
98. Yu, W.W., et al. *Biochem. Biophys. Res. Commun.* **348**, 781--786, 2006.
99. Yaghini, E., et al. *Nanomedicine* **4** (3), 353--363, 2009.
100. Chen, J., et al. *Theranostics* **2** (3), 238--250, 2012.
101. Yang, S.T. *J. Am. Chem. Soc.* **131** (32), 11308--11309, 2009.
102. Petrovic, Z.S. *Polym. Rev.* **48** (1), 109--155, 2008.
103. Yang, W., et al. *Nanotechnology* **18** (41), 412001--412013, 2007.
104. Zhang, W., et al. *Nanoscale Res. Lett.* **6**, 555--577, 2011.
105. Satishkumar, B.C., et al. *J. Phys. D: Appl. Phys.* **29** (12), 3173--3176, 1996.

Chapter 1

106. Alemdar, A. & Sain, M. *Bioresour. Technol.* **99** (6), 1664--1671, 2008.
107. Kramer, F., et al. *Macromol. Symp.* **244** (1), 136--148, 2006.
108. Wu, J., et al. *Carbohydr. Polym.* **102** (1), 762--771, 2014.
109. Lee, H.J., et al. *J. Mater. Sci.* **38** (10), 2199--2204, 2003.
110. Paul, D.R. & Robeson, L.M. *Polymer* **49** (15), 3187--3204, 2008.
111. Jordan, J. *Mater. Sci. Eng. A* **393**, 1--11, 2005.
112. Phua, S.L., et al. *ACS Appl. Mater. Interfaces* **4** (9), 4571--4578, 2012.
113. Suresh, R., et al. *Int. J. Pharm. Sci. Nanotech.* **3** (2), 901--905, 2010.
114. Zhu, Y., et al. *Adv. Mater.* **22** (35), 3906--3924, 2010.
115. Thakur, S. & Karak, N. *Carbon* **50** (14), 5331--5339, 2012.
116. Kulia, T., et al. *Prog. Mater. Sci.* **57** (7), 1061--1105, 2012.
117. Liaw, D-J. & Shen, W.C. *Macromol. Mater. Eng.* **199** (1), 171--190, 1992.
118. Goodwin, A. & Baskaran, D. *Macromolecules* **45** (24), 9657--9665, 2012.
119. Gong, C.G. & Frechet, J.M.J. *J. Polym. Sci. Part A: Polym. Chem.* **38** (16), 2970--2978, 2000.
120. Ma, L., et al. *Chin. J. Polym. Sci.* **29** (3), 300--307, 2011.
121. Jikei, M., et al. *Macromolecules* **32** (6), 2061--2064, 1999.
122. Murali, M., et al. *J. Polym. Sci. Part A: Polym. Chem.* **45** (14), 3116--3123, 2007.
123. Yokomachi, K., et al. *Polym. J.* **40** (3), 198--204, 2008.
124. Zhang, D., et al. *Polym. Compos.* **30** (7), 918--925, 2009.
125. Fu, J-F., et al. *Polym. Adv. Technol.* **19** (11), 1597--1607, 2008.
126. Xavier, F-F., et al. *React. Funct. Polym.* **70** (10), 798--806, 2010.
127. Okada, A., et al. *Composite material and process for manufacturing same*, **US Patent No. 4739007**, April 19, 1988.
128. Okada, A., et al. *Mater. Res. Soc. Proc.* **171** (8), 45--50, 1990.
129. Kojima, Y., et al. *J. Appl. Polym. Sci.* **49** (7), 1259--1264, 1993.
130. Park, J.H. & Jana, S. C. *Macromolecules* **36** (8), 2758--2768, 2003.
131. Verdejo, R., et al. *J. Biomed. Mater. Res. A.* **88** (1), 65--73, 2009.
132. Wang, X., et al. *J. Mater. Chem.* **21** (1), 4222--4227, 2011.
133. Bao, C., et al. *J. Mater. Chem.* **21** (35), 13290--13298, 2011.
134. Li, Y., et al. *Mater. Design* **47** (15), 850--856, 2013.

Chapter 1

135. Ruiz-Hitzky, E. & Aranda, P. *Adv. Mater.* **2** (11), 545--547, 1990.
136. Wu, J. & Lerner, M.M. *Chem. Mater.* **5** (6), 835--838, 1993.
137. Kim, J.A., et al. *Carbon* **44** (10), 1898--1905, 2006.
138. Teng, C-C., et al. *Carbon* **49** (15), 5107--5116, 2011.
139. Vaia, R.A. & Giannelis, E.P. *Macromolecules* **30** (25), 7990--7999, 1997.
140. Vaia, R.A. et al. *Chem. Mater.* **5** (12), 1694--1696, 1993.
141. Zou, H., et al. *Chem. Rev.* **108** (9), 3893--3957, 2008.
142. Alexandre, M. & Dubois, P. *Mater. Sci. Eng. R* **28** (1-2), 1--63, 2000.
143. Carrado, K.A. *Appl. Clay Sci.* **17** (1-2), 1--23, 2000.
144. Jahn, H. & Goetzky, P. *Epoxy Resins Chemistry and Technology*, C.A. May et al. eds., 2nd ed., Marcel Dekker Inc., New York, 1988, 1049-1087.
145. Moghimi, A., et al. *Eur. Polym. J.* **49** (1), 228--234, 2013.
146. Eustis, S. & El-Sayed, M.A. *Chem. Soc. Rev.* **35** (3), 209--217, 2006.
147. De, B. & Karak, N. *J. Appl. Polym. Sci.* **131** (1), 40327--40334, 2014.
148. Kondo, T. *J. Polym. Sci., Part B: Polym. Phys.* **35** (4), 717--723, 1997.
149. Sun, D.H., et al. *Macromolecules* **38** (13), 5617--5624, 2005.
150. KICKELBICK, G. *In hybrid materials. Synthesis, Characterization, and Applications*, Wiley-VCH: Weinheim, Germany, 2007, Chapter 1.
151. Merkel, T.C., et al. *Macromolecules* **36** (2), 353--358, 2003.
152. Pramanik, S., et al. *J. Phys. Chem. C* **117** (47), 25097--25107, 2013.
153. Ray, S.S. & Okamoto, M. *Progress Polym. Sci.* **28** (11), 1539--1641, 2003.
154. Li, R., et al. *J. Synchrotron Radiat.* **18** (5), 697--701, 2011.
155. De, B., et al. *ACS Sustainable Chem. Eng.* **2** (3), 445--453, 2013.
156. Zanetti, M., et al. *Macromol. Mater. Eng.* **279** (1), 1--9, 2000.
157. De, B., et al. *ACS Appl. Mater. Interfaces* **5** (20), 10027--10034, 2013.
158. Vyazovkin, S. *Macromolecules* **29** (6), 1867--1873, 1996.
159. Duan, J., et al. *J. Polym. Res.* **16** (1), 45--54, 2009.
160. Temenoff J.S. & Mikos, A.G. *Biomaterials: The Interaction of Biology and Material Science*, Prentice Hall, USA, 2008.

Chapter 1

161. Marois, Y. & Guidoin, R. *Biocompatibility of Polyurethanes, in Biomedical Applications of Polyurethanes*, P. Vermette et. al, eds., Landes Bioscience, Georgetown, Austin, 2011, 77--96.
162. Shalaby, S.W. & Burg K.J.L. *Absorbable and Biodegradable polymers*, CRC Press, Boca Raton, 2004.
163. Banerjee, S. et al. *Int. J. Toxicol.* **32** (4), 308--313, 2013.
164. Das, B. et al. *J. Mater. Chem. B* **1** (33), 4115--4126, 2013.
165. Allaoui, A. *Compos. Sci. Technol.* **62** (15), 1993--2015, 2002.
166. Gojny, F.H. et al. *Chem. Phys. Lett.* **370**, 820--824, 2003.
167. Sun, F., et al. *Ind. Eng. Chem. Res.* **51** (1), 240--247, 2012.
168. Roy, B., & Karak, N. *Polym. Bull.* **68**, 2299--2312, 2012.
169. Mohan, T.P., et al. *Polym. Int.* **54** (12), 1653--1659, 2005.
170. Yang, S-Y., et al. *Carbon* **49** (3) 793--803, 2011.
171. Jia, Q.M., et al. *Polym. Adv. Technol.* **17**, 168--173, 2006.
172. Das, G. & Karak, N. *Polym. Degrad. Stab.* **94** (11), 1948--1954, 2009.
173. Sirivisoot, S. & Harrison, B.S. *Int. J. Nanomed.* **6**, 2483--2497, 2011.
174. Azar, N.G., et al. *J. Endodont.* **26** (8), 462--465, 2000.
175. Navarro, E., et al. *Environ. Sci. Technol.* **42** (23), 8959--8964, 2008.
176. Rihovi, B. *Adv. Drug Delivery Rev.* **21** (2), 157--176, 1996.
177. Nelson, D.G.A., et al. *Caries. Res.* **21** (5), 411--426, 1987.
178. Caropreso, S., et al. *J. Micro.* **199** (3), 244--247, 2000.
179. Pharaon, M.R., et al. *Tissue Engineering, in Plastic and Reconstructive Surgery* M.Z. Siemionow & M. Eisenmann-Klein, eds., Springer-Verlag, London , 2010.
180. Gunatillake, P.A. & Adhikari, R. *Eur. Cells Mater.* **5**, 1--16, 2003.
181. Sachlos, E. & Czernuszka, J.T. *Eur. Cells Mater.* **5**, 29--40, 2003.
182. Martina, M. & Hutmacher, D.W. *Polym. Int.* **56** (2), 145--157, 2007.
183. Chevally, B. & Herbage, D. *Med. Biol. Eng. Comput.* **38**, 211--218, 2000.
184. Saravanan, S., et al. *Int. J. Biol. Macromol.* **49** (2), 188--193, 2011.
185. Chae, K.H., et al. *Sens. Actuators, B* **124** (1), 153--160, 2007.
186. Nishat, N., et al. *J. Appl. Polym. Sci.* **101** (3), 1347--1355, 2006.
187. Lai, C-C., et al. *Clin. Oral Invest.* **5**, 236--239, 2001.

Chapter 1

188. Yasuda, Y., et al. *J. Oral Sci.* **50** (3), 309--313, 2008.
189. Bala, T., et al. *J. Colloid Interface Sci.* **356** (2), 395--403, 2011.
190. Schiff, K., et al. *Mar. Pollut. Bull.* **48** (3-4), 371--377, 2004.
191. Wang, X-H., et al. *Synth. Met.* **102** (1-3), 1377--1380, 1999.
192. Banerjee, I., et al. *Adv. Mater.* **23** (6), 690--718, 2011.
193. Deitch, E.A., et al. *J. Trauma* **27** (3), 301--304, 1987.
194. Lamba, N.M.K. Woodhouse, K.A. & Cooper, S.L. *Polyurethane in Biomedical Application*, CRC Press, Boca Raton, 1997.
195. Mishra, A., et al. *Acta. Biomater.* **10** (5), 2133--2146, 2014.
196. Okamoto, M. *Mater. Sci. Technol.* **22** (7), 756--779, 2006.
197. Deka, H., et al. *Carbon* **48** (7), 2013--2022, 2010.
198. Konwar, U., et al. *Polym. Degrad. Stab.* **94** (2), 2221--2230, 2009.
199. Cong, H.L., et al. *Sep. Purif. Technol.* **55**, 281--291, 2007.
200. Kim, H., et al. *Chem. Mater.* **22** (11), 3441--3450, 2010.
201. Takahashi, S., et al. *Polymer* **47** (9), 3083--3093, 2006.
202. Kim, J-K., et al. *Compos. Sci. Technol.* **65** (5) 805--813, 2005.
203. Guadagno, L., et al. *Carbon* **47** (1), 2419--2430, 2009.
204. Morgan, A.B. & Wilkie, C.A. *Flame Retardant Polymer Nanocomposites*, ed., John Wiley & Sons: Hoboken, NJ, 2007.
205. Bourbigot, S. & Duquesne, S. *J. Mater. Chem.* **17** (22), 2283--2300, 2007.
206. Wang, Q. & Chen, G. *Adv. Mater. Res.* **1** (1), 93--107, 2012.
207. Wang, Q., et al. *Compos. Sci. Technol.* **68** (7), 1644--1648, 2008.
208. Sung, H-W., et al. *J. Biomed. Mater. Res. (Appl. Biomater)* **33**, 177--186, 1996.
209. Ko, W.H., et al. *IEEE T. Electron. Des.* **26** (12), 1896--1905, 1979.
210. Peres, R.S., et al. *Mater. Res.* **17** (3), 720--727, 2014.
211. Pameijer, C.H. & Zmener, O. *Dent. Clin. N. Am.* **54**, 325--344, 2010.
212. Eick, J.D., et al. *Dent. Mater.* **9** (2), 123--127, 1993.
213. Miletic, I., et al. *J. Endod.* **31** (4), 307--309, 2005.
214. Chesworth, J.C., et al. *Aquat. Toxicol.* **66** (3), 293--305, 2004.
215. Sharmin, E., et al. *Int. J. Biol. Macromol.* **40** (5), 407--422, 2007.
216. Abdullayev, E., et al. *ACS Appl. Mater. Interfaces* **3** (10), 4040--4046, 2011.

Chapter 1

217. Zafar, S., et al. *J. Appl. Polym. Sci.* **113** (2), 827--838, 2009.
218. Kirwan, L.T. *Electro-surgical forceps having recessed irrigation channel US Patent No. 6,228,084 B1*, May 8, 2001.
219. Ovsianikov, A., et al. *J. Tissue Eng. Regen. Med.* **1** (6), 443--449, 2007.

Synthesis, characterization and property evaluation of glycerol based hyperbranched epoxy

Highlights

This chapter deals with the synthesis, characterization and property evaluation of a glycerol based HE. Three HE resins were synthesized by varying percentage of an environmentally benign reactant, glycerol used as a B₃ moiety by a single step polycondensation reaction, following an A₂ + B₃ approach. The chemical structures were authenticated from FTIR, ¹H and ¹³C NMR studies. Viscoelastic properties of the resins were studied by rheometric analysis. The poly(amido amine) cured HE thermosets exhibited higher mechanical performance, thermal stability as well as adhesive strength as that of a linear analogous epoxy system. Further, excellent chemical resistance was witnessed for the thermosets. Most interestingly, the synthesized glycerol based HE exhibited *in vitro* biocompatibility to primary liver and heart cell lines of wistar rat.

Parts of the chapter are published in

Barua S., Dutta, G. & Karak, N. *Chem. Eng. Sci.* **95**, 138--147, 2013.

Chapter 2

2.1. Introduction

Chapter 1 clearly pointed out that lots of scopes are waiting for the development of hyperbranched polymers and their NC, in respect of biomedical applicability. Epoxy resins are associated with notable properties, such as excellent chemical and solvent resistance, good thermal and electrical properties, high tensile and adhesive strength etc., which make them good candidates for various applications.¹ However, the commercially used diglycidyl ether epoxy of BPA suffers from the demerit like brittleness, which restricts its advanced uses. Thus, modification of epoxy resins is done by various means to achieve desired properties. Blending with flexible polymers like rubber, polyesters etc. imparts good toughness to epoxy resins.²⁻⁵ Moreover, hyperbranched architecture provides epoxy some superiorities like low solution and melt-viscosity, high solubility, good processability, good reactivity and faster curing time compared to its linear analog.⁶ The highly branched structure with a large number of reactive end groups help in crosslinking reaction and thereby improving their properties like reduced shrinkage and increased thermal stability, toughness etc.⁷⁻¹³

However, relatively low number of reactants are found in literature for synthesizing HE resin.^{14, 15} Reported aliphatic hyperbranched polyester epoxy resins possess high viscosity and thereby create difficulty in processing.¹⁶ Chapter 1 also demonstrated the use of different multifunctional moieties to generate branching units in HE. Some previously reported HE are synthesized from toxic reagents and monomers. As an example, triethanol amine based compounds showed liver hemangiosarcoma in mice.¹⁷ Again, 1,2,7,8-diepoxyoctane is considered as a toxic reagent by United States Environmental Protection Agency.¹⁸ Further, Venables observed pulmonary edema and subsequent hemorrhage caused by trimellitic anhydride based resins.¹⁹ Biocompatible epoxy resins are used in a range of biomedical products like surgical tapes, bioadhesives, root canal sealers etc.²⁰⁻²² With due course of time, many such products are banned due to sustaining toxicity.^{23, 24} Therefore, biocompatibility is the vital requirement for a HE based biomaterial, which can be achieved by utilizing benign starting materials. In this context glycerol may an apt option as a branch generating unit with 'green' credentials and hence, the resultant HE might be used for various biomedical applications.

Chapter 2

Glycerol has been used for various medicinal and cosmetic products for long time.²⁵ Moreover, researchers found that glycerol treatment could diminish the possibility of acute stroke.²⁶ Glycerol based hyperbranched polyester, polyether, polyurethane etc. are reported by different research groups.^{27, 28} However, the synthesis of glycerol based hyperbranched epoxy (HGE) resin is not yet reported.

Different approaches like proton transfer polymerization, end group modification, atom transfer radical polymerization (ATRP) etc. are explored for the synthesis of HE.^{29, 30} Amongst different strategies, $A_2 + B_3$ polycondensation approach gained impetus, because of easy availability of the monomers. In the present investigation, glycerol and BPA were reacted with epichlorohydrin by following the strategy of a controlled polycondensation reaction. Further, characterization and property evaluation of the materials were also described in this chapter. Another important study was carried out for scrutinizing the *in vitro* biocompatibility of the synthesized materials.

2.2. Experimental

2.2.1. Materials

Glycerol was procured from Merck, India. Its purity is 99% and molecular weight is 90.09 g/mol. It is a colorless and odorless polyol compound, containing three hydroxyl groups. Glycerol is soluble in water and behaves as a hygroscopic viscous liquid. Density, melting and boiling points of glycerol are 1.26 g/mL, 17.8 and 290 °C respectively. Along with the petroleum based feedstock, glycerol is obtained from renewable resources like, vegetable oils. It is also the bi-product of biodiesel. Glycerol (Figure 2.1) is used in different pharmaceutical formulations. Here, it was used as the B_3 monomer for HGE synthesis.

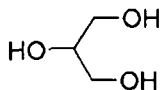


Figure 2.1: Structure of glycerol

BPA was obtained from Merck, India. Its melting and boiling points are 158-159 °C and 220 °C respectively. It is the most widely used aromatic diol for epoxy synthesis. BPA

Chapter 2

based epoxy resins are used in surface coating over metallic articles and devices. Moreover, epoxy sealers containing BPA as starting material, are used in endodontic treatments. In this investigation, BPA (Figure 2.2) was used as a reactant.

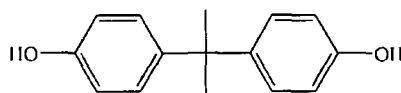


Figure 2.2: Structure of bisphenol A

Epichlorohydrin was obtained from Merck, India. Molecular weight and density of epichlorohydrin are 92.52 g/mol and 1.18 g/cm³ respectively. This is used as the oxirane precursor in diglycidyl ether epoxies. It has further utility in paper and food industries. Here, epichlorohydrin (Figure 2.3) was taken as a reactant for synthesizing HGE.

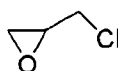


Figure 2.3: Structure of epichlorohydrin

Tetrahydrofuran (THF) was procured from Merck, India, with 99.5% purity (Cu 0.0001%, Fe 0.0001%, Pb 0.0001% and non-volatile substances like 0.002% are present as impurities). Its boiling point and density are 65-67 °C and 0.886-0.88 g/cm³ respectively. THF is a broadly used industrial solvent, which can dissolve a range of polar and non-polar compounds. This solvent is purified by keeping overnight with sodium wire followed by distillation. One of the main applications of THF is as an industrial solvent for poly(vinyl chloride) and in varnishes. In this study, it was used to isolate epoxy resin from the reaction mixture.

Toluene was bought from Merck, India with 99.5% purity (Impurities like 0.04% water, 0.003% non-volatile matter and 0.0005% sulfur compounds (CS₂) are present). Its molecular weight, density and boiling points are 92.14 g/mol, 0.860-0.866 g/cm³ at 25 °C and 110-111 °C respectively. Toluene was used here for recrystallizing BPA.

Potassium hydroxide (KOH) was purchased from Merck, India, with 97% purity. Molecular weight of KOH is 56.11 g/mol. It is widely used in soap and detergent industries. KOH was used to determine hydroxyl value of HGE.

Chapter 2

Maleic anhydride was obtained from Merck, India. This is the acid anhydride of maleic acid. It has broad utility in polymer industries. Molecular weight and density of maleic anhydride are 98.06 g/mol and 1.48 g/cm³ respectively. Its melting and boiling points are 52.8 and 202 °C respectively. In this work, it was used for hydroxyl value determination of HGE.

Triethylamine (TEA) was procured from Merck, India. TEA is a volatile liquid with strong fishy odor. It is produced by alkylation of ammonia with ethanol. It has wide applications as a base in organic synthesis. Molecular weight and density of TEA are 101.19 g mol⁻¹ and 0.7255 g/cm³ respectively. Its melting and boiling points are -114.70 and 88.6-89.8 °C respectively. Here, it was used as a base catalyst in the determination of hydroxyl value of the synthesized resins.

Hydrochloric acid (HCl) was obtained from Merck, India. This is a strong acid with molecular weight 36.46 g/mol. HCl is industrially used in the production of vinyl chloride, diphenyl methylene diisocyanate, toluene diisocyanate etc. In the present investigation, it was used to determine the epoxy equivalent of the synthesized HGE resins.

Sodium sulphate (Na₂SO₄, anhydrous) was purchased from Merck, India (purity 99.5%), with molecular weight 142.04 g/mol and density 2.664 g/cm³. This is largely used in home laundry detergent powder. Another broad utility of Na₂SO₄ is in glass industries. Here it was used as a desiccant to remove traces of water from the epoxy resins.

Sodium chloride (NaCl) crystals, with 99.5% purity were procured from Merck, India. Molecular weight and density of NaCl are 58.44 g/mol and 2.16 g/cm³ respectively. NaCl is used for a broad spectrum of industrial purposes such as textiles and dyeing, oil and gas, pulp and paper, leather and rubber manufacturing etc. Its saturated solution was used as a demulsifying agent in the present study.

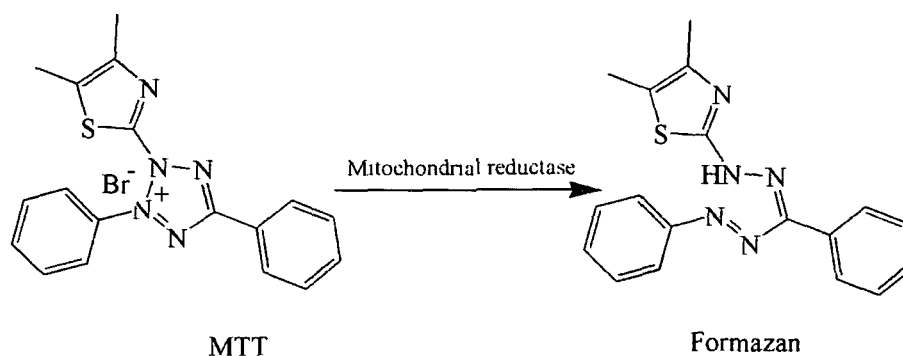
Sodium hydroxide (NaOH) was purchased from Merck, India, with 97% purity. Molecular weight of NaOH is 40.0 g/mol. It is used in various industries such as paper, textile, water, detergent, soap etc., mainly as a strong base. Here it is used as the base in the polycondensation reaction for synthesizing HGE.

Poly(amido amine) (HY 840, Ciba-Geigy, India) was procured from Hindustan Ciba Geigy Ltd. India, with amine value of 6.6-7.5 eq/kg. Its viscosity and density are 10-

Chapter 2

25 Pas and 0.98 g/cm^3 at $25 \text{ }^\circ\text{C}$ respectively. It is used as the crosslinking agent to cure HGE.

William medium, low-glucose Dulbecco's modified Eagle medium (DMEM), fetal bovine serum (FBS) and 3-(4, 5-dimethylthiazol-2-yl)-2, 5-diphenyltetrazolium bromide (MTT) were procured from Sigma Aldrich, Germany and used as such for the *in vitro* biocompatibility assay. Mitochondrial reductase, the enzyme present in cells can reduce MTT to formazan. This bears a purple color which indicates the cell viability. Dead cells cannot produce such enzymes and thus their solutions remain colorless when incubated with MTT. However, quantitatively, percentage of cell viability is calculated from UV absorbance at around 540 nm. Scheme 2.1 indicates the reduction of MTT by the cellular enzyme. This assay is generally carried out in dark, as MTT is highly sensitive to light.



Scheme 2.1: Reduction of MTT to formazan by mitochondrial reductase

2.2.2. Instruments

FTIR spectra of HGE were taken in a FTIR spectrophotometer (Impact-410, Nicolet, USA) after mixing with KBr pellets. Chemical functionalities associated with HGE are analyzed by this technique. ^1H and ^{13}C NMR spectra of the resins were recorded to detect different protons and carbon atoms present in the HGE structure. Spectra were recorded in a FTNMR spectrometer (400 MHz, JEOL, Japan) by dissolving the resins in d_6 -DMSO and using TMS as the internal standard. TGA was carried out in a thermal analyzer (Shimadzu USA, TG 50) with a heating rate of $10 \text{ }^\circ\text{C/min}$, under constant nitrogen flow (30 mL/min). TGA analysis was carried out to study the degradation of the thermosets at elevated temperature. The viscoelastic behavior of the resins was tested in a controlled strain

Chapter 2

rheometer (CVO 100) equipped with parallel plate geometry. Variations in the shear viscosity of HGE resins against shear stress, temperature and time were observed by rheological study. X-ray diffraction (XRD) patterns of HGE thermosets were recorded in a 'Miniflex' (Rigaku Corporation, Japan) diffractometer.

Tensile strength, elongation at break and lap shear tensile adhesive strength of the thermosetting HGE were measured in a Universal Testing Machine (UTM, WDW10, Jinan, China, load cell 5-10 kN, with a crosshead speed of 10-50 mm min⁻¹). The polymeric film is placed between the grips of UTM, equipped with an extensometer. The machine applies a load on the film and the attached software records the mechanical behavior of the same. For the mechanical test (ASTM D 882), rectangular films were taken with dimension of 60 × 10 × 0.3 mm³. Overlapping wood surfaces (25 × 25 × 0.3 mm³) were prepared by applying the material at the interfaces for determining the lap-shear tensile adhesive strength according to ASTM D4896-01. Before, applying the adhesive, wood substrates were washed with acetone followed by toluene to remove dirt, grease etc. They were further polished with sand paper (grit number 60) as per ASTM 906. Scratch hardness of the thermosets was recorded in a scratch hardness tester (Model No. 705, Sheen, UK) associated with a stylus accessory (ASTM G171). Impact strength was tested by the standard falling weight (ball) method (ASTM D 1709) in an Impact tester (S. C. Dey Co. Kolkata, India). In this test, a weight of 850 g is allowed to fall onto the film coated on a steel plate from minimum to maximum falling heights. The maximum height was taken as the impact resistance up to which the film was not damaged. A mandrel with diameter 1-100 mm was used to test the bending of the films (standard ASTM D 522).

2.2.3. Methods

2.2.3.1. Synthesis of HGE

HGE resin was synthesized by taking required amount of glycerol and BPA with epichlorohydrin (1:2 mol ratios with respect to the total hydroxyl groups of glycerol and BPA) in a reactor fitted with a condenser, a pressure equalizing funnel and a stirrer. The reaction temperature was maintained at 110 °C. A 5 N aqueous solution of NaOH

Chapter 2

(equivalent to the hydroxyl groups) was added very slowly to the reaction mixture through the pressure equalizing funnel. The viscous mass formed after 3 h of continuous reaction was separated with the help of a separating funnel. The organic layer was washed with brine solution followed by water for several times. Finally, the resin was collected in THF and dried at 70 °C for 24 h in a vacuum oven. By using exactly the same methodology three resins were synthesized by varying the glycerol amount. The resins with 5, 15 and 25 weight% of glycerol were coded as HGE5, HGE15 and HGE25 respectively. These three systems would be collectively termed as HGE in this chapter. A BPA based epoxy without glycerol (BPAE) was prepared under the same reaction conditions for comparative study.

2.2.3.2. *Curing study of the resins*

Homogenous mixtures of the resin with poly(amido amine) hardener were prepared in a glass beaker at room temperature by hand stirring for 20 min. The amount of hardener was taken in equimolar quantity to the epoxy equivalent of the resins. The mixture was cast at ambient temperature on commercially available mild steel strips (150 mm × 100 mm × 1.44 mm) or glass plates (75 mm × 25 mm × 1.75 mm) for determination of mechanical properties. The uniformly coated plates were kept at room temperature for 48 h and then the films were cured in an oven at specified temperature for the desired period of time. The average thickness of the films was measured by a pen tester (Sheen instrument Ltd., UK).

Swelling test was performed by immersing weighed amount of the cured films in sufficient amount of THF. After 48 h, the weight of the swollen film was taken. The swelling value (%) was determined from the weight of dry and swelled films, using the following equation

$$\text{Swelling (\%)} = \frac{(W_s - W_d) \times 100}{W_d} \quad (2.1)$$

where, W_s and W_d are the weights of the swelled and dry films respectively.

2.2.3.3. *Evaluation of physical properties*

Different physical properties such as solubility, hydroxyl value, epoxy equivalent, drying time etc. of the HGE resins were determined by following the standard methods.¹⁵ Solubility of the resins was checked by dissolving a pinch of the sample in about 1 mL of

Chapter 2

solvent at room temperature and by observing the solubility for consecutive 2 days under the same condition.

Hydroxyl value was determined by treating the resins with 10 mL, 0.2 M maleic anhydride and 1 mL, 1 M TEA under reflux condition.³¹ Finally, it was titrated with 0.1 M KOH and the volume required for neutralization is recorded (T). A blank treatment was also run without sample and the volume of KOH required for neutralization is noted (B). Hydroxyl value was calculated by the following formula

$$\text{Hydroxyl value} = \frac{[\text{Equivalent weight of KOH} \times (B - T) \times \text{Normality of KOH}]}{\text{Weight of the resin}} \quad (2.2)$$

Epoxy equivalent weight was determined by refluxing the resins with 10 mL, 2 N HCl in 20 mL of ethanol for 90 min.³² After titrating the mixture with 0.5 N NaOH, the epoxy equivalent was calculated by the following formula. Volume of NaOH for neutralization is determined (T). Here also, volume of NaOH for blank treatment was measured (B).

$$\text{Epoxy equivalent} = \frac{(\text{Sample weight} \times 1000) \times \text{Normality of NaOH}}{(B - T)} \quad (2.3)$$

Chemical resistance of the films was tested in a number of chemical media according to ASTM D 543-67. Weighed amount of dry films were immersed in each medium (150 mL) for the specified time. The chemical resistance was determined by measuring the change in weight of each film after completion of the test period.

2.2.3.4. *In vitro* biocompatibility assessment

For *in vitro* biocompatibility assessment, MTT assay was carried out against primary liver and heart cell lines of wistar rat. These organs were isolated, flushed out and re-suspended in William medium and low-glucose DMEM respectively, supplemented with 10% FBS. The cell counting was done by using the trypan blue exclusion test. Then the cells were cultured in 96 well plates for 24 h under 5% CO₂ flow at 37 °C inside an incubator. Pieces of the films (5 mm × 5 mm × 0.3 mm) were kept in the culture wells in triplicates both for the cardiac and liver primary cell lines, separately and incubated for another 24 h. Wells without treatment of samples was taken as the control. Then, 50 μL of MTT was added to

Chapter 2

each well. After 8 h, blue crystals of formazan were formed in the wells. The crystals were dissolved in 40 μL of DMSO and UV spectra were taken at 540 nm. The absorbance was compared with that of the control and cell viability percentage was calculated for each case by using the formula given below

$$\text{Cell viability (\%)} = \frac{\text{Absorbance of the sample} - \text{Absorbance of the blank}}{\text{Absorbance of the control} - \text{Absorbance of the blank}} \quad (2.4)$$

Cell viability for the control was taken as 100% and the others were calculated accordingly.

2.2.3.5. Statistical analysis

Data were presented as mean \pm SD from the triplicate results. One way ANOVA was applied to determine the LSD.

2.3. Results and discussion

2.3.1. Synthesis of HGE

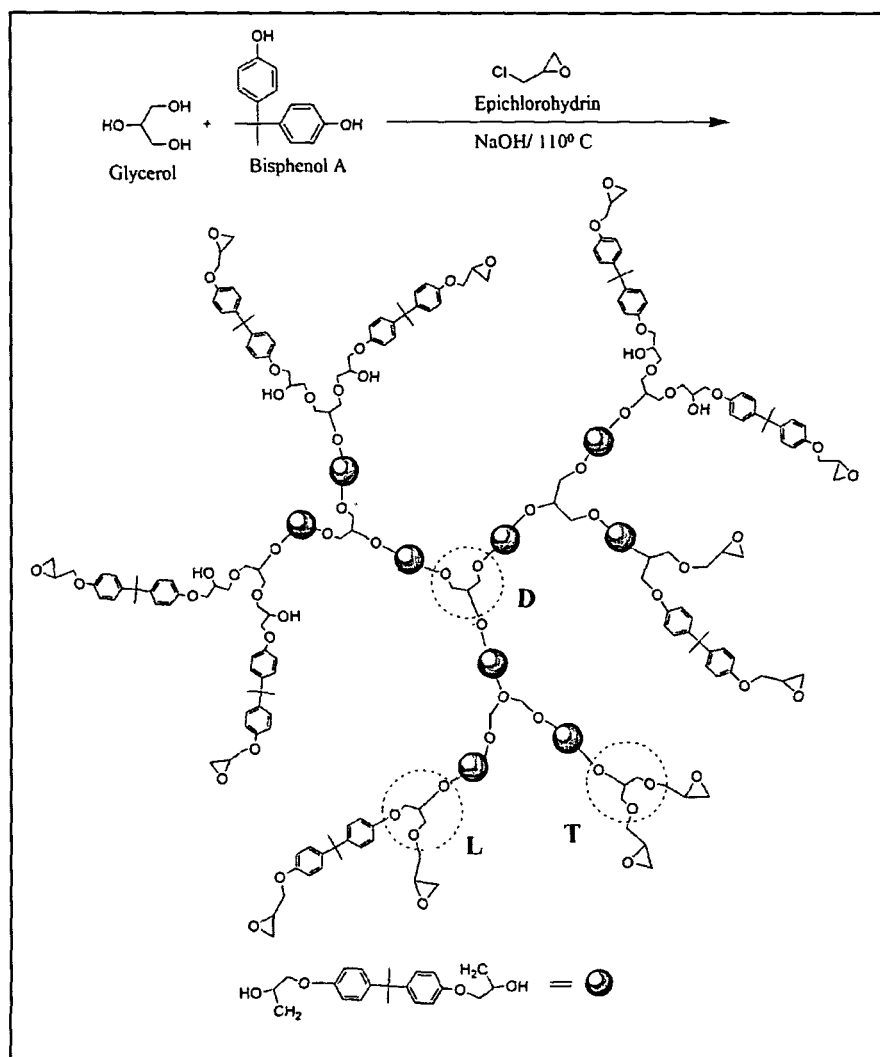
Three HGE resins have been synthesized by polycondensation reaction using an $A_2 + B_3$ approach. BPA and three different amounts of glycerol were reacted with epichlorohydrin in presence of an alkali to yield HGE (Scheme 2.2). The composition of the components was taken in such a way that the hydroxyl to epichlorohydrin ratio remains constant as given in Table 2.1. At first, an intermediate diglycidyl ether of BPA was formed in the reaction mixture, as the activity of BPA towards epichlorohydrin is greater than that of glycerol. Then, the desired HGE resin was obtained by the reaction between the diglycidyl ether of BPA (A_2) and glycerol (B_3). It was observed that the viscosity of the resin increases with the increase of reaction time; hence the reaction was carried out for 3 h to obtain the desired viscosity and epoxy equivalent.

2.3.2. FTIR study

The chemical linkages predicted in the structure of the epoxy resin as shown in Scheme 2.2 was confirmed by FTIR analysis (Figure 2.4). The bands for asymmetric vibrations of epoxy ring appeared at around 914 and 832 cm^{-1} .⁶ Presence of a sharp absorption band at

Chapter 2

1035 cm^{-1} confirmed the alkyl-aryl ether groups in the resin. Similarly, the band observed at 1241 cm^{-1} is due to the presence of aryl ether linkage in the structure of the resin. Further, the band at 1608 cm^{-1} is assigned to the aromatic -C=C- stretching vibrations. Bands at 2964-2877 and 3050 cm^{-1} are the representative features for the aliphatic and aromatic -C-H stretching respectively. The -O-H stretching vibration is evident from the band at 3441 cm^{-1} .³³



Scheme 2.2: Synthesis of HGE

2.3.3. ¹H NMR and ¹³C NMR studies

Chapter 2

The ^1H NMR spectra (Figure 2.5) of HGE confirmed the structures of the resins. Chemical shift values at δ 1.61 ppm are due to the methyl protons of BPA moieties. The $-\text{OH}$ protons associated with the glycerol moiety showed a chemical shift value at δ 2.14 ppm.²⁸ Presence of the oxirane protons was confirmed by the three chemical shift values at δ 2.71, 2.72 and 3.13 ppm. The protons attached to the substituted glycerol unit in the resins were observed at δ 3.30–3.90 ppm. Two types of phenyl protons associated with the BPA moieties were observed at δ 6.81 and 7.23 ppm for ortho and meta protons respectively.¹⁵

Similarly, the carbons with different atmosphere present in the structure of HGE were confirmed by the ^{13}C NMR spectra (Figure. 2.6). Signals at δ 30.97 and δ 41.66 ppm are due to the methyl and the quarternary carbon of BPA respectively. The characteristic signals for the oxirane ring carbons were observed at δ 44.68 and 50.43 ppm. The BPA carbons attached directly to the $-\text{O}-$ linkage was observed with the signal at δ 143.2 ppm. The signals at δ 113.97, 127.73 and 156.26 ppm are due to the different carbons of the BPA moiety.¹⁵

Dendritic (D) (δ 68.68 ppm), linear (L) (δ 68.49 ppm) and terminal (T) (δ 67.9 ppm) units are the trisubstituted, disubstituted and monosubstituted glycerol units, represented in Figure 2.6.²⁸ The degree of branching calculated (by using Fréchet's equation) for HGE5 was 0.88, which established the hyperbranched structure for the resin. Degree of branching for HGE15 and HGE25 were 0.78 and 0.70 respectively and the corresponding peaks for dendritic, linear and terminal units of the resins are shown in Figure 2.6 separately.

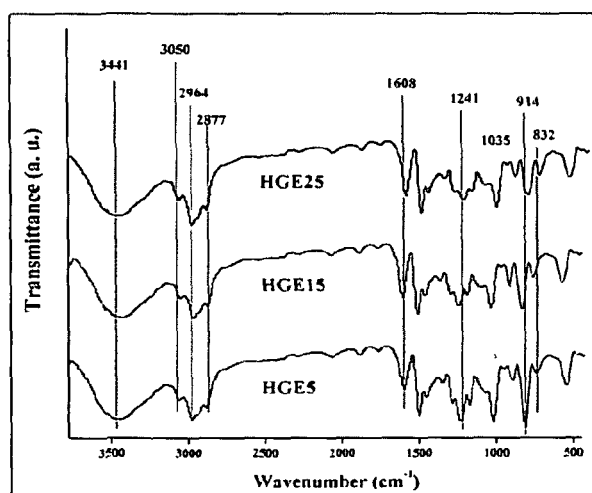


Figure 2.4: FTIR spectra of HGE resins

Chapter 2

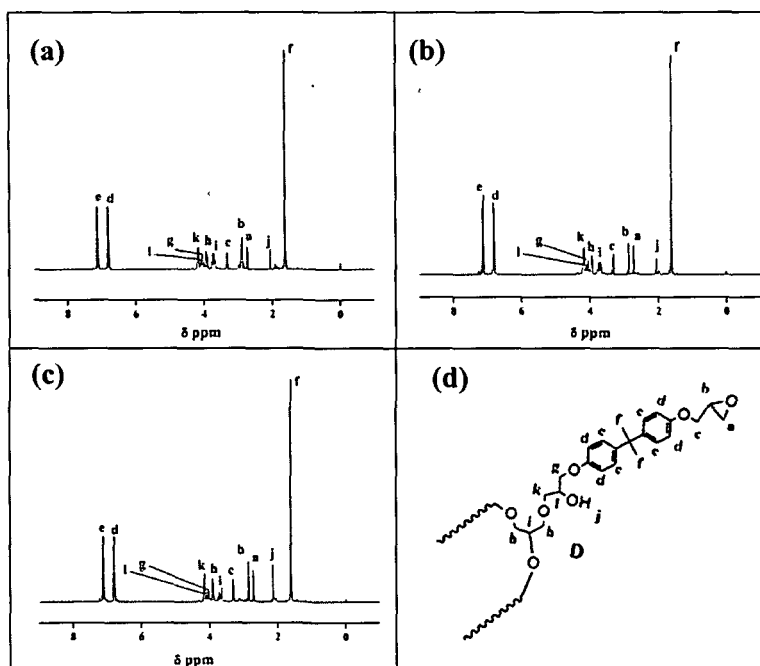


Figure 2.5: ¹H NMR spectra of (a) HGE5, (b) HGE15, (c) HGE25 and (d) assignment of protons

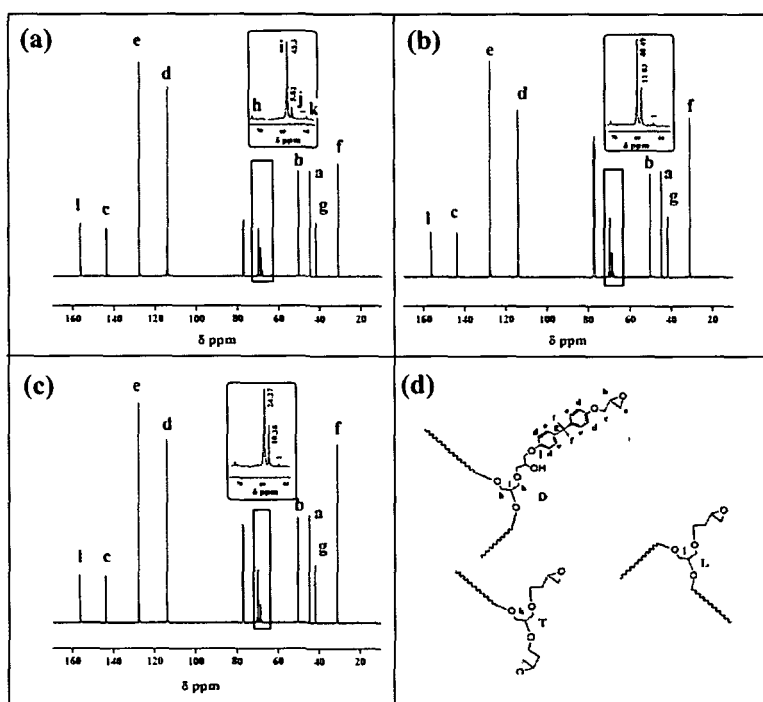


Figure 2.6: ¹³C NMR spectra of (a) HGE5, (b) HGE15 and (c) HGE25, indicating the D, L, T units (insets) and (d) assignment of carbons

Chapter 2

2.3.4. XRD study

The XRD patterns for HGE showed no sign of crystallinity in the samples (Figure 2.7). This is because of the amorphous nature of the building blocks. However, the broad diffraction peaks around $2\theta=21^\circ$ were observed for the amorphous hyperbranched matrix.

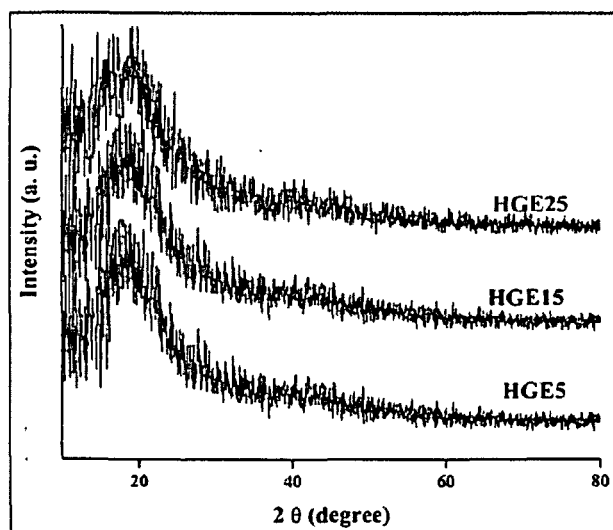


Figure 2.7: XRD patterns of HGE

2.3.5. Physical properties of HGE

The synthesized hyperbranched resins appeared to be odorless and colorless sticky masses. The values for the physical properties like hydroxyl value and epoxy equivalent of the resins are given in Table 2.1. HGE5 possesses the lowest epoxy equivalent and therefore, the highest number of epoxy groups is present in its structure. From solubility studies, it has been found that HGE were soluble in most of the common organic solvents such as dichloromethane, chloroform, acetone, ethanol, dimethylacetamide, dimethylformamide, dimethyl sulfoxide etc. However, their solubility was poor in hydrocarbon solvents, water and methanol. The good solubility might be owing to the presence of higher number of polar functionalities and flexible aliphatic moieties in the structure of the resins.¹⁵

2.3.6. Rheological behavior

All the hyperbranched resins as well as BPAE showed constant flow behavior against studied shear stress and time (Figure 2.8), as the applied shear force did not cause any

Chapter 2

structural change to the resins.³⁴ Shear viscosity also remained unaltered with the increase of shear rate up to 200 Pas. On application of temperature gradient, viscosity decreased for the resins. Molecular mobility of the chains increased on increasing the temperature which causes decrease in the viscosity. Viscosity of a resin is usually associated with segmental density, intermolecular entanglement of chains and inter or intramolecular hydrogen bonding.³⁵ HE generally exhibits low viscosity due to globular kind of structure with no entanglement. Under a constant shear stress of 100 Pa, viscosity remains almost constant with time for HGE5 (18 Pas), HGE15 (20 Pas) and HGE25 (39 Pas). Viscosity of HGE5 is only 18 Pas which is much lower than the value of BPA based epoxy without glycerol (200 Pas for BPAE). High DB and low viscosity, exhibited by HGE are the desired basic characteristics of hyperbranched resins.³⁶

Table 2.1. Chemical compositions, yield and a few physical properties of HGE

Code	Composition (mol)		Yield (%)	Hydroxyl value (mg KOH/g)	Epoxy equivalent (g/eq)
	Glycerol	Bisphenol A			
HGE5	0.0108	0.0833	97.28	100.77	248.15
HGE15	0.0325	0.0745	95.92	165.96	342.5
HGE25	0.0542	0.0658	95.23	277.59	505.32

2.3.7. Curing study and mechanical performance

Curing of a resin with proper hardener is a prerequisite for the evaluation of various performance characteristics of it. In the curing process, the liquid resin is transformed into a solid form by the chemical crosslinking reactions with a hardener.¹⁵ Highly strained oxirane rings of the epoxy resin readily open up in presence of a labile proton of the amine hardener. Poly(amido amine) is a resinous hardener system largely used for the curing of epoxy resin, which is a polycondensation product of diethylene triamine with dimmer acid. This contains labile amino protons that readily react with epoxy groups at high temperature to form crosslinked three dimensional network structures. The crosslinking process is shown in Scheme 2.3. Curing time (at 120 °C) with swelling percentages for HGE as well as BPAE are shown in Table 2.2.

Chapter 2

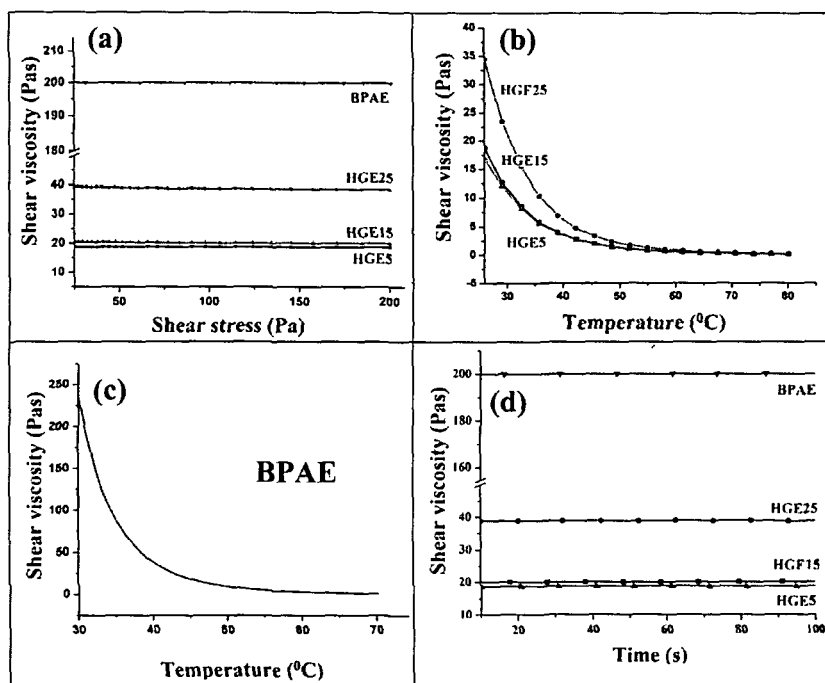
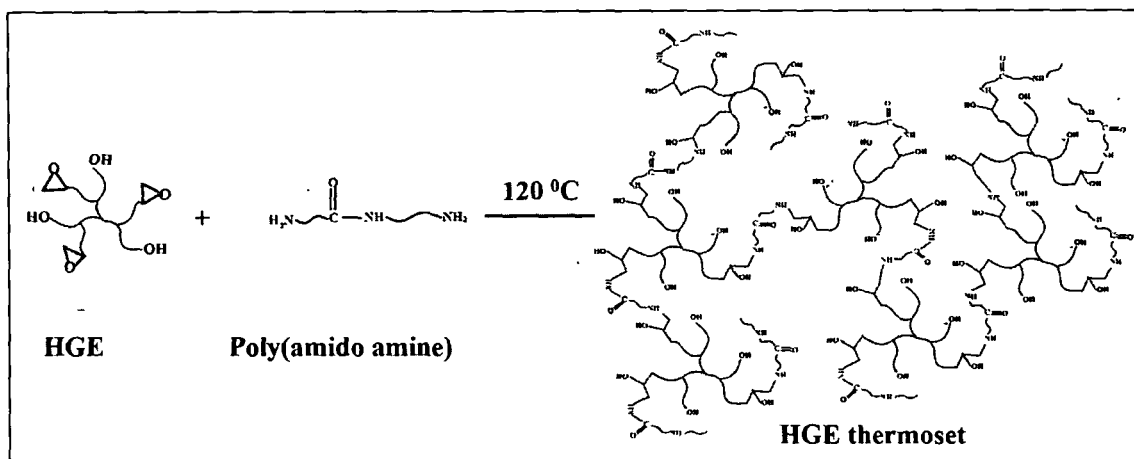


Figure 2.8. Variation of shear viscosity of HGE and BPAE resins against (a) shear stress under constant temperature, (b) temperature under constant stress, (c) temperature under constant stress for BPAE and (d) time at constant stress and temperature

Mechanical properties were evaluated by measuring the tensile strength, elongation at break, impact resistance, scratch hardness and bending of the thermosets (Table 2.2). The highest tensile strength of HGE5 is because of adequate crosslinking, as evident from the swelling value, which is due to the presence of the highest percentage of aromatic moiety (BPA) and also the lowest epoxy equivalent.¹⁵ On the other hand, the elongation percentage decreased as the percentage of the aromatic moiety was increased. BPAE showed good tensile strength, but very poor elongation value, which implicates the poor flexibility of BPAE.¹ HGE contrarily, exhibited high tensile strength with good elongation at break. The bending test confirmed sufficient flexibility of all the thermosets up to the lowest diameter of the mandrel (1 mm) without any fracture, which is four times superior to BPAE. Again, impact resistance and scratch hardness were found to be similar in all the cases (impact resistance and scratch hardness were above 1 m and 10 kg respectively, as these are the

Chapter 2

maximum limits of the used instruments). Due to the brittle nature, BPAE exhibited less impact strength and scratch hardness.



Scheme 2.3: Crosslinking of HGE with poly(amido amine)

Table 2.2: Curing parameters and performance of HGE and BPAE

Property	HGE5	HGE15	HGE25	BPAE	LSD
Curing time at 120 °C (min)	24 ± 0.58	40±0.12	32±0.81	28.5±0.67	0.83
Swelling (%)	22.67 ± 0.43	26±.028	24±0.31	26±0.56	0.71
Tensile strength (MPa)	38.49 ± 0.84	30±0.23	23.7±0.74	32.7±0.87	0.31
Elongation at break (%)	21.30 ± 0.57	25.27±0.4	28.6±0.57	6.5±0.7	0.54
Impact resistance (m)*	>1	>1	>1	0.4	-
Scratch hardness (kg)*	>10	>10	>10	0.7	-
Bending (mm)*	<1	<1	<1	<4	-
Adhesive strength (MPa)	768	710	621	422	34.69

*Instrumental limits: Scratch hardness=10 kg, Impact resistance=1 m and bending test mandrel=1 mm

Again, excellent lap shear tensile adhesive strength was observed for HGE. HGE5 exhibited the highest adhesive strength amongst the studied compositions. This is due to the large number of polar epoxy and hydroxyl groups that helped in strong interaction with the substrates.^{15 30} In case of BPAE, the adhesive strength was less than the hyperbranched

Chapter 2

counterparts. This is attributed to the large number of functionalities present in the hyperbranched epoxies. Data provided in Table 2.2 are significantly different ($>LSD$ value) in each case with $p < 0.05$.

2.3.8. Thermal study

Relative thermal stability of the thermosets is shown in Figure 2.9. In all the cases it was observed that the epoxy thermosets exhibited two step degradation patterns, which can be directly attributed to the presence of both aliphatic and aromatic moieties in the structure of the thermosets.³⁴ The onset temperatures were 286, 275 and 254 °C for HGE5, HGE15 and HGE25 respectively. This is ascribed to the increase of aromatic moieties from HGE25 to HGE5.

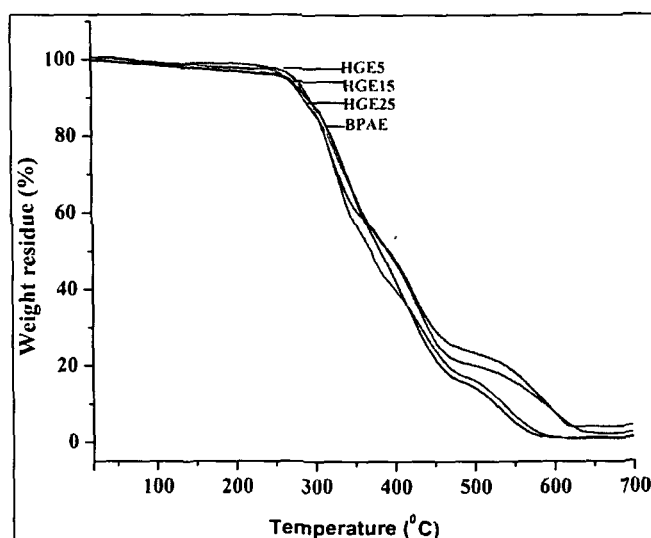


Figure 2.9: TGA thermograms of HGE and BPAE thermosets

The second step of degradation commences at around 529, 504 and 492 °C for HGE5, HGE15 and HGE25 respectively. The highest thermostability of HGE5 is due to the increase in percentage of the aromatic moiety (BPA) and the highest crosslink density, as authenticated from the swelling value (Table 2.2).¹⁵ Slightly better thermostability was observed for BPAE, which is because of the presence of more aromatic moiety in the structure. The second step of degradation for BPAE occurred at around 540 °C. HGE5 retained a weight residue of 4.6%, at 700 °C, which were 1.8%, 1.2% and 4.8% for HGE15, HGE25 and BPAE respectively.

Chapter 2

HGE25 and BPAE respectively. The highly thermostable BPA moiety again plays the role for this variation.

2.3.9. Chemical resistance

Chemical resistance of HGE was determined under different chemical environments (Table 2.3) such as 3% aqueous NaOH (pH 9), 20% aqueous EtOH, 10% aqueous HCl (pH 5), 10% aqueous NaCl and water after exposure of 30 days and the changes of weights were recorded. All the films exhibited very good chemical resistance in almost all the tested environments. The excellent chemical resistance of the films is owing to the presence of good crosslinking and presence of aromatic moiety in the structure.¹⁵ Good chemical resistance is a vital feature of epoxy thermosets.

Table 2.3: Change in weight (%) of the thermosets in different chemical media

Chemical medium	HGE5	HGE15	HGE25
3% aq NaOH	-0.068±0.56	-0.082±0.72	-0.091±0.37
20% aq EtOH	+0.003±0.17	+0.007±0.63	+0.009±0.48
10% aq HCl	-0.003±0.53	-0.006±0.47	-0.008±0.71
10% aq NaCl	+0.002±0.62	+0.005±0.38	+0.008±0.18
Water	+0.010±0.51	+0.012±0.81	+0.015±0.43

2.3.10. *In vitro* biocompatibility assessment

MTT assay is performed to evaluate the percentage of cell survival when incubated with a test material. For, polymeric film samples, direct contact is the best method to assay the cytocompatibility.³⁷ Biocompatibility of glycerol is well known to the scientific community. Thus, presence of glycerol backbone in the structure of the hyperbranched polymer is expected to confer good compatibility to the resultant material.²⁵ Thus, HGE thermosets exhibited excellent cell compatibility as tested *in vitro* (Figure 2.10).

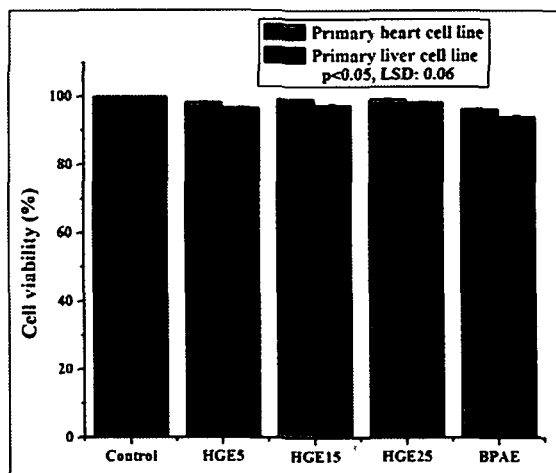


Figure 2.10: Cell viability (%) of the cardiac and liver cell lines as evaluated by MTT assay

Very subtle differences were witnessed amongst the three HGE. However, BPAE showed less compatibility as compared to the hyperbranched counterparts. In all the cases, it was quite clear that the materials are more compatible to the heart cells than the primary hepatocytes (liver cells).³⁷ Cell survival rate is not significantly different from each other, implicating that they have similar biocompatibility against the tested cell lines ($p < 0.05$). Thus, MTT assay proved the *in vitro* biocompatibility of the synthesized HGE.

2.4. Conclusion

HGE resins with varying amount (weight%) of the glycerol moiety were successfully synthesized. Different analytical and spectroscopic characterizations confirmed the chemical structure of the HGE resins. Presence of both aliphatic and aromatic moieties in the structures imparts high strength and flexibility. Excellent lap shear tensile adhesive strength and chemical resistance were observed for the HGE thermosets. The study also confirmed the superiority of the HGE thermosets over the linear analog. Moreover, the synthesized HGE thermosets proved adequate cytocompatibility for primary heart and liver cell lines of wistar rat. This high performance, biocompatible HGE can be endorsed to different advanced biomedical applications, after scrutinizing their compatibility *in vivo* with clinical trials.

Chapter 2

References

1. Ray, D., et al. *Ind. Eng. Chem. Res.* **51** (6), 2603--2608, 2012.
2. Qi, G., et al. *Polym. Chem.* **2** (6), 1271--1274, 2011.
3. Ratna, D. & Banthia, A. K. *Polym. Int.* **49** (3), 281--287, 2000.
4. Frigione, M. & Calo, E. *J. Appl. Polym. Sci.* **107** (3), 1744--1758, 2007.
5. Shin, S.M., et al. *J. Appl. Polym. Sci.* **78** (14), 2464--2473, 2000.
6. Zhang, D. & Jia, D. *Eur. Polym. J.* **42** (3), 711--714, 2006.
7. Dabritz, F., et al. *Polymer* **52** (25), 5723--5731, 2011.
8. Dabritz, F., et al. *J. Polym. Sci. A Polym. Chem.* **50** (10), 1979--1990, 2012.
9. Deb, K., et al. *Chem. Eng. Sci.* **59** (20), 4261--4277, 2004.
10. Sangermano, M., et al. *Polymer* **52** (10), 2103--2109, 2011.
11. Blanco, I., et al. *Polym. Eng. Sci.* **46** (11), 1502--1511, 2006.
12. Jena, K.K. & Raju, K.V.S.N. *Ind. Eng. Chem. Res.* **47** (23), 9214--9224, 2008.
13. Foix, D., et al. *Polym. Degrad. Stab.* **95** (4), 445--452, 2010.
14. Mezzenga, R., et al. *Macromolecules* **33** (12), 4373--4379, 2000.
15. De, B. & Karak, N. *J. Mater. Chem. A* **1** (2), 348--353, 2013.
16. Gong, C. & Frechet, J.M.J. *Macromolecules* **33** (14), 4997--4999, 2000.
17. National Toxicology Program report, *Toxicology and carcinogenesis studies of triethanolamine*, U.S. Department of Health and Human Services, May 2004.
18. United States Environmental Protection Agency Science Inventory, *Development of an in situ toxicity assay system using recombinant baculoviruses*, 2014.
19. Venables, K.M. *Brit. J. Ind. Med.* **46** (4), 222--232, 1989.
20. Determan, M.D., et al. *Gentle to skin adhesive*, US Patent No. 0212325, September 1, 2011.
21. Wen, L., et al. *Soybean Sci.* **1**, 1--33, 2010.
22. Huang, T.H., et al. *Biomaterials* **23** (1), 77--83, 2002.
23. Kostoryz, E.L., et al. *Dent. Mater.* **15** (5), 363--373, 1999.
24. Azar, N.G., et al. *J. Endodont.* **26** (8), 462--465, 2000.
25. Behr, A., et al. *Green Chem.* **10** (1), 13--30, 2008.
26. Berger, C., et al. *Stroke* **36**, e4--e6, 2005.

Chapter 2

27. Wyatt, V.T., et al. *J. Am. Oil Chem. Soc.* **83** (12), 1033--1039, 2006.
28. Sunder, A., et al. *Macromolecules* **33** (2), 309--314, 2000.
29. Emrick, T., et al. *J. Polym. Sci., Part A: Polym. Chem.* **38** (S1), 4850--4869, 2000.
30. Coessens, V., et al. *Macromol. Rapid Commun.* **21** (2), 103--109, 2000.
31. Evtushenko, Y.M., et al. *J. Anal. Chem.* **56** (11), 1035--1037, 2001.
32. He, Z., et al. *Anal. Methods* **6** (12), 4257--4261, 2014.
32. Hawker, C.J., et al. *J. Am. Chem. Soc.* **113** (12), 4583--4588, 1991.
34. Konwar, U. & Karak, N. *J. Polym. Environ.* **19** (1), 90--99, 2011.
35. Sun, F., et al. *Ind. Eng. Chem. Res.* **51** (1), 240--247, 2012.
36. Zagar, E., et al. *Macromol. Chem. Phys.* **208** (13), 1379--1387, 2007.
37. Das, B., et al. *Biomed. Mater.* **8** (3), 035003--035014, 2013.

Hyperbranched epoxy/clay nanocomposite as an antimicrobial biomaterial

Highlights

This chapter includes the preparation and characterization of an antimicrobial, implantable glycerol based hyperbranched epoxy/clay NC. Three thermosetting NC were prepared with *Homalomena aromatica* rhizome oil-modified bentonite and octadecylamine modified montmorillonite clay. FTIR, XRD, SEM and TEM analyses confirmed the presence of strong interfacial interaction between clay layers and epoxy matrix. Poly(amido amine) cured NC thermosets exhibited high mechanical and adhesive strength as well as high thermostability. Biocompatibility of the NC was validated by *in vitro* and *in vivo* assays. The material supported the growth and proliferation of dermatocytes without inducing any toxicity to the host organs as tested against wistar rat. Furthermore, the investigation revealed the inhibitory effect of the NC against *Staphylococcus aureus*, *Escherichia coli* and *Candida albicans*, the microorganisms responsible for many infectious diseases.

Parts of the chapter are published in

Barua, S., Dutta, N., Karmakar, S., Chattopadhyay, P., Aidew, L., Buragohain, A.K. & Karak, N. *Biomed. Mater.* 9 (2), 025006--025019, 2014.

Chapter 3

3.1. Introduction

The previous chapter documented the potential of HGE as a biocompatible, tough polymeric material. Biocompatible polymers are used in a range of implantable biomaterials.¹ In this respect, development of artificial skin is pertinent to mention. It is an important option for the treatment of severe wounds or injuries of skin. This also opens new opportunity for curing coetaneous ulcers, burns, congenital anomalies etc.² The most important part of artificial skin is the scaffold which supports the rapid regeneration and proliferation of skin tissues.³ However, available skin scaffolds suffer a range of demerits such as poor strength, toxicity to the host tissue etc. Polymeric scaffolds as 'extracellular matrix' (ECM) are gaining impetus in recent times because of many advantageous properties.⁴ Thus, biocompatible polymeric materials with adequate strength may be a good addition to tissue engineering research. Previous discussions adequately clarify that epoxy has lots of potential for biomedical applications. However, acute cytotoxicity of the prevailing epoxy based biomaterials, restrict their path for sustained utility.⁵ Therefore, high performance and non-toxic epoxy is desired for a myriad of biomedical utilities. It is well understood from Chapter 2 that HGE are superior to their linear analog with respect to their overall performance and HGE5 is the best amongst them. Consequently, biocompatible HGE5 with adequate strength is expected to support the growth of tissues by acting as a scaffold material.

Again, nanoreinforcement of polymers helps to fabricate novel NC to shape out new generation materials. Nanoclay is one of the cost-efficient and most widely used nanomaterials in the manufacturing of high performance epoxy NC.^{6, 7} Use of layered silicates is well known in the domain of biomedical research. Schiraldi et al. reported a silica-based hybrid material which showed excellent cell adhesion and proliferation in case of murine fibroblasts and osteoblasts.⁸ Hosseini et al. reported an organomodified-nanoclay based silicone rubber NC, as a biomaterial with enhanced cell behavior.⁹ Further, nanoclay-loaded polymer matrix has been used as a bone tissue scaffold.¹⁰ However, no report is found where HE/clay NC is used as a scaffold material.

Further, modification of clay is required for good compatibility and strong interaction with the epoxy matrix.¹¹ Such modification is generally achieved by the exchange of cations which needs high temperature, costly reagents and long time.¹² On the

Chapter 3

contrary, Phua et al. demonstrated the use of dopamine-modified nanoclay for a polyether polyurethane NC.¹³ Therefore, modification of clay with a readily available bio-based compound by cost efficient method would be a good proposition.

Homalomena aromatica (Sugandh Mantri) is an important medicinal plant found widely in the forests of Asia and the southwestern Pacific. The rhizome oil of *H. aromatica* contains about 96.1% total oil, where linalool is the major component. This oil is well-reported to possess efficient antimicrobial and insecticidal activities.¹⁴ In this investigation, modification of clay was carried out with this oil. It is assumed that incorporation of the oil would offer improved compatibility of the nanoclay with HGE matrix as well as it would impart antimicrobial effect to the NC. Biomedical materials face various microbial infections when surgically implanted within the host body.¹⁵ Therefore, a suitable tissue scaffold with efficient antimicrobial activity can prevent the material from microbial attack.

HGE5/clay NC with promising antimicrobial activity, therefore, is presented here as a potential tissue-scaffold material. The study also focuses on the impact of the oil on the modification of the hydrophilic and hydrophobic nanoclays.

3.2. Experimental

3.2.1. Materials

The chemicals and reagents such as glycerol, BPA, epichlorohydrin, THF, toluene, sodium hydroxide, poly(amido amine) were of the same specification as mentioned in Chapter 2, section 2.2.1.

Bentonite clay was procured from Sigma Aldrich, Germany. The hydrophilic clay is a form of aluminium phyllosilicates. Different types of bentonite clays are commercially available, which are named after the predominant element present like potassium, sodium, calcium and aluminium. This clay is widely used in drilling fluids, iron and steel foundries, absorbents etc. Further, bentonite impregnated epoxy NC are extensively studied for various applications.

Octadecylamine-modified (25-30% w/w) montmorillonite (OMMT) clay was purchased from Sigma Aldrich, Germany. This is a soft phyllosilicate mineral, belonging to the smectite family. Its cation exchange capacity is 90 meqv/100 g.

Chapter 3

H. aromatica rhizome oil was obtained from Assam Aroma and Herbs, Pvt. Ltd., India. This plant belongs to the Araceae family. It is a good source of essential oils. Its vapor pressure and flash point are 0.5 mm of Hg at 25 °C and 66.67 °C respectively. Linalool, T-muurolol, α -selinene, viridiflorol, γ -Muurolene, M-cymene, α -cadinol, terpene-4-ol, δ -cadinene and spatulenol are the identified components of rhizome oil. It has broad medicinal utility as antimicrobial, antidepressant, antiseptic, analgesic, sedative, anti-inflammatory, antispasmodic agents etc.¹⁶

William medium and low-glucose DMEM medium, MTT etc. used for *in vitro* biocompatibility assessment were of same grade as described in Chapter 2, section 2.2.1. Further, the microbial strains, viz. *Staphylococcus aureus* (ATCC 11632), *Escherichia coli* (ATCC 10536) and *Candida albicans* (ATCC 1023), needed for antimicrobial activity assays were obtained from the Department of Molecular Biology and Biotechnology, Tezpur University, Assam. Other media and agars such as nutrient broth, potato dextrose broth, Muller Hinton agar etc. for microbial culture were provided by the same department.

3.2.2. Animals

Male wistar rats, weighing 200-250 g, were provided by the Laboratory Animal Resources, Division of Pharmaceutical Technology, Defence Research Laboratory, Tezpur, Assam, India. The animals were kept within a temperature range of 22-26 °C with 12 h alteration of light and dark cycles and given adequate nutrition with water *ad libitum*. Animal experiments were performed according to the Principles of Laboratory Animal care (NIH publication 85-23, revised 1985) and approved by the Institutional Animal Ethics Committee.

3.2.3. Instruments

FTIR, XRD and TGA analyses were performed under the same conditions and by using the same instruments as referred to in Chapter 2, section 2.2.2. Surface texture of NC and the bacterial adhesion on their surfaces were studied by a scanning electron microscope (SEM, JEOL, JSM-6390LV, Japan). All the samples were characterized after coated with platinum. For biological samples, prescribed protocol was followed.¹⁷ Distribution of nanoclay within HGE5 matrix was studied by using a JEOL, JEM 2100 high resolution

Chapter 3

transmission electron microscope (HRTEM) at an operating voltage of 200 kV. Very dilute solution of the NC was mounted on a carbon coated copper grid and high magnification images were captured. An ultrasonicator (Hielscher, UP200S, Germany) was used to disperse the nanomaterials within the HGE5 matrix, at an amplitude of 60% with 0.5 cycle. Tensile strength, elongation at break, lap shear tensile adhesive strength, scratch hardness, impact resistance and bending of the NC were studied by using the same instruments under same test conditions as stated in Chapter 2, section 2.2.2.

3.3.4. Methods

3.3.4.1. Modification of nanoclay

Hydrophilic bentonite clay (0.5 g) was swelled in 3 mL of ethyl acetate. *H. aromatica* oil (1 mL) was dissolved in ethyl acetate and added dropwise into the dispersed clay. The dispersion was stirred at 40 °C for 24 h. The clay was then washed with ethyl acetate to remove the unused oil and kept for drying in an oven at 45 °C. OMMT clay was modified with the oil by following the same approach.

3.3.4.2. Preparation of the NC

To determine the effect of the oil on clay-HGE5 interaction, three systems were considered, viz. OMMT/HGE5 NC (HGEC), *H. aromatica* oil-modified OMMT/HGE5 NC (HGEMC) and *H. aromatica* oil-modified bentonite clay/HGE5 NC (HGEB). In each case, 5 weight% (with respect to HGE5) of the nanoclay was swelled in 5 mL of THF by using a magnetic stirrer for 2 h at room temperature, followed by ultrasonication for 15 min. Swelled nanoclay was mixed with HGE5 resin, by the help of a magnetic stirrer at 50 °C for 2 h. Further dispersion of nanoclay with the matrix was assisted by 30 min of ultrasonication. Unmodified bentonite clay/HGE5 NC was also prepared which showed distinct phase separation on curing. Therefore, this was not considered for further studies. The prepared NC were degassed under vacuum for 24 h. Curing of the NC were done by mixing with required amount of poly(amido amine), using the same procedure as described in Chapter 2, section 2.2.3.2. Percentage of crosslinking was estimated by swelling the films in THF for 48 h with the same method as stated in that section.

Chapter 3

3.3.4.3. *In vitro* Biocompatibility assessment

In vitro biocompatibility of the materials was evaluated by MTT assay as stated in the Chapter 2, section 2.3.4. In this test, pieces of NC films (5 mm × 5 mm × 0.02 mm each) were kept in the culture wells of a 96 well plate, along with OMMT and modified OMMT (MOMMT) in triplicates, separately for the cardiac and liver primary cell lines. The plate was incubated at 37 °C for 24 h inside a CO₂ incubator, at the flow rate of 5%. Wells without the treatment of samples was taken as the control. MTT was added after 24 h to each well, followed by the addition of DMSO (40 μL). Cell survival rate was calculated after taking the absorbances according to the formula as mentioned in Chapter 2, section 2.3.4.

3.3.4.4. *In vivo* biocompatibility assessment

The test animals (total number of animals, n = 6 nos) were anesthetized by injecting sodium phenobarbitone (Neon Lab, India) peritoneally (50 mg per kg body weight of the rats) according to the standard protocol.¹⁸ HGEMC films (5 mm × 5 mm × 0.25 mm) were subcutaneously implanted within wistar rats (in triplicate) by a ventral surgery. A group of rats (n = 6) were kept as control, without any implantation. The hematological parameters were evaluated for both the groups at 0, 15 and 30 post implantation days. Animals were fasted overnight before collecting the blood samples. Blood was collected in a non-vacuum blood collection tube, containing K3 EDTA (Peerless Biotech, India) by using a 75 mm heparinized capillary tube (Hematocrit capillary, Himedia, India) through the orbital sinus vein puncture technique from the retro orbital sinus of rats.¹⁹ Samples were analyzed within 60 min from collection. Hematological parameters like white blood cell (WBC) count, WBC differential counts (i.e. lymphocyte (Lym), monocyte (Mon), neutrophil (Neu), eosinophil (Eo) and basophil (Ba) counts), RBC count, mean corpuscular volume (MCV), hematocrit (Hct), mean corpuscular hemoglobin (MCH), mean corpuscular hemoglobin concentration (MCHC), hemoglobin (Hb) concentration and platelet (Pct) were scrutinized by an Automatic Hemato analyzer (MS-4, Melet Schloesing Laboratories, Osny, France).

The rats were sacrificed 30 days after implantation by cervical dislocation and the organs (brain, heart, liver and skin) were collected in normal saline. These were fixed in formaldehyde solution (10%) for 24 h and dehydrated with varying alcohol percentages.

Chapter 3

Finally they were embedded by paraffin and fine sections were prepared using a microtome. Sections were examined microscopically after staining with hematoxylin and eosin.

3.3.4.5. Antibacterial activity test

The minimum inhibitory concentration (MIC) of the nanomaterials and the NC was determined by using micro-dilution technique.²⁰ Stock solutions of the samples were prepared at a concentration of 20 mg mL⁻¹ and diluted with 1% DMSO to yield a final concentration ranging from 100-500 µg mL⁻¹. Then, 100 µL of the samples in various concentrations were added in the wells along with 100 µL of the bacterial inoculums, corresponding to 10⁷ CFU mL⁻¹. Ampicillin and nystatin were taken as the positive controls for bacteria and fungus respectively, while 1% DMSO was used as the negative control. The plates were then incubated at 37 °C for 16 h for the bacteria. For *C. albicans*, the plate was incubated for 48 h at 28 °C. After incubation, 40 µL of MTT solution (0.2 mg mL⁻¹) was added into each well. Formation of blue color indicated bacterial growth and no change in color signified the growth inhibition.

Zones of inhibition for each microorganism were estimated at the MIC value of each sample. For samples (HGE5, HGEC and OMMT), not showing any inhibition effect, the concentration was taken as 500 µg mL⁻¹. The bacterial strains were cultured in nutrient broth (HiMedia, India) and incubated at 37 °C for overnight. *C. albicans* was grown in potato dextrose broth (HiMedia, India) for 48 h at 28 °C. Inoculums of the culture for agar well diffusion assay were adjusted to 10⁵ colony forming unit (CFU) per mL. The suspensions of the inoculums were mixed and spread over Mueller Hinton agar (MHA) plates. The samples were diluted with 1% sterile DMSO to a concentration equal to the MIC values. Wells were bored on the plates with diameters of 8 mm. Then, 40 µL of the samples were added in the respective wells, along with the positive control (ampicillin/nystatin). Diameters of the zones were measured by using a zone scale (Himedia, India) after 24 and 48 h of incubation. The experiment was done in triplicates.

E. coli strain was selected to study the adhesion of the bacterium onto the HGEMC surface. The strain was cultured in nutrient broth for 24 h. Then, it was centrifuged and re-suspended in PBS. Pieces of HGE5 and HGEMC films (5 mm × 5 mm × 0.25 mm) were

Chapter 3

immersed in the culture medium and incubated for 16 h. After incubation the films were rinsed in PBS and 2.5% glutaraldehyde was used to fix the samples. The films were dehydrated by increasing the alcohol gradient (70-100%). SEM micrographs were taken for the dehydrated films. This test was performed to observe the adhesion of the bacteria onto the surfaces of the films, as well as to study the interaction bacteria and the NC.

3.3.4.6. Statistical analysis

Evaluated data were presented as mean±SD for triplicate results. Significant difference (LSD) was measured for the data, with the help of one or two way ANOVA.

3.3. Results and discussion

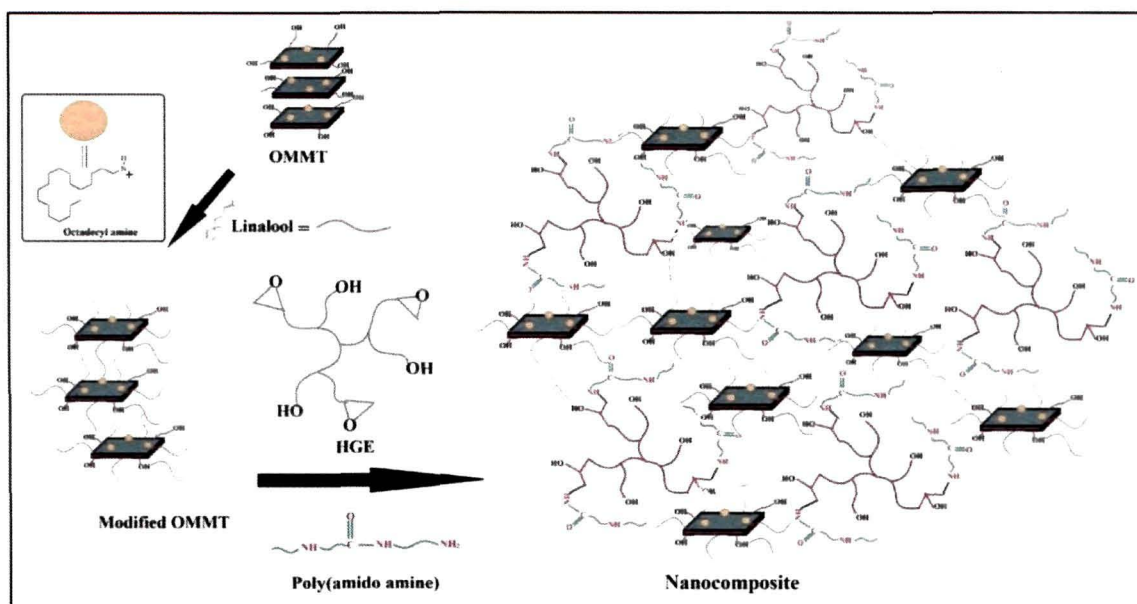
3.3.1. Preparation of the NC

A uniform and stable dispersion of clay layers in the polymer matrix contributes to the advancement of materials properties. Due to their high surface energy, nanoclay layers have an affinity to agglomerate by self organization mechanism. In the present approach, the clays were modified with *H. aromatica* oil as stated above. This approach was adopted to make the bentonite clay compatible with the HGE5 matrix. The major component of the oil is linalool, which may get adsorbed on the surface of nanoclay, owing to its surface hydroxyl groups. Moreover, the surface functionalities of HGE5, including the reactive oxirane group, can easily interact with the nanoclay. Mechanical shearing and ultrasonication further aid to the delamination or intercalation of clay layers. OMMT clay surface was also modified by the same oil. This was done to evaluate whether the clay-HGE5 interaction was enhanced by surface adsorption of the oil components. Scheme 3.1 pictorially depicts the possible interactions between nanoclay and HGE5.

3.3.2. Characterization

3.3.2.1. FTIR study

In the FTIR spectrum of HGEB, bands indicating asymmetric vibrations of the epoxy group appeared at 912 and 838 cm^{-1} (Figure 3.1a), which was not observed in the other spectra.



Scheme 3.1: Schematic representation for the preparation of HGE5/M-OMMT nanocomposite

Characteristic bands at 3452 cm^{-1} were for the stretching frequencies of $-\text{OH}$ groups of freely bonded water molecules on the bentonite surfaces. The interlayer H_2O bending was observed at 1638 cm^{-1} for the unmodified bentonite. Shifting of this band to 1614 and 1605 cm^{-1} was witnessed in the modified clay and HGE5 respectively. However, peak sharpness was noticed in case of the modified clay and HGE5, because of the presence of $-\text{C}=\text{C}-$ stretching band of the unsaturated components of the oil at this region.²¹ This clarifies the interaction of clay with *H. aromatica* oil and HGE5. Bands at 1514 and 2957 cm^{-1} were observed in case of the modified bentonite clay, which were absent in the pristine one. These are for the $-\text{C}-\text{H}$ stretching vibration of different components of the modifying agent.²¹ The tetrahedral bending modes of $\text{Si}-\text{O}-\text{Al}$ and $\text{Si}-\text{O}-\text{Si}$ stretching were observed at 525 and at 450 cm^{-1} . The intense broad band at around 1028 cm^{-1} was due to the $\text{Si}-\text{O}$ stretching frequencies.

FTIR spectra were also recorded for OMMT and M-OMMT (Figure 3.1 b). For the pristine OMMT, bands at 3627 and 3417 cm^{-1} were observed for the stretching vibrations of the $-\text{OH}$ groups of the water molecules present in the interlayer. In M-OMMT, these bands shifted to 3606 and 3494 cm^{-1} . The $-\text{C}=\text{C}-$ stretching vibrational bands were

Chapter 3

observed at 1623, 1612 and 1605 cm^{-1} for M-OMMT, HGEC and HGEMC respectively, which were due to the adsorption of the oil onto the clay surface.²¹ It is ascribed to the interaction of the clay with the oil and further with the HGE5 matrix. The tetrahedral bending mode for Si–O–Al was witnessed at 511 cm^{-1} . The band at 1022 cm^{-1} was for the Si–O stretching frequency of clay. Asymmetric vibrations for the epoxy group appeared at around 908 and 832 cm^{-1} for HGEC and HGEMC.

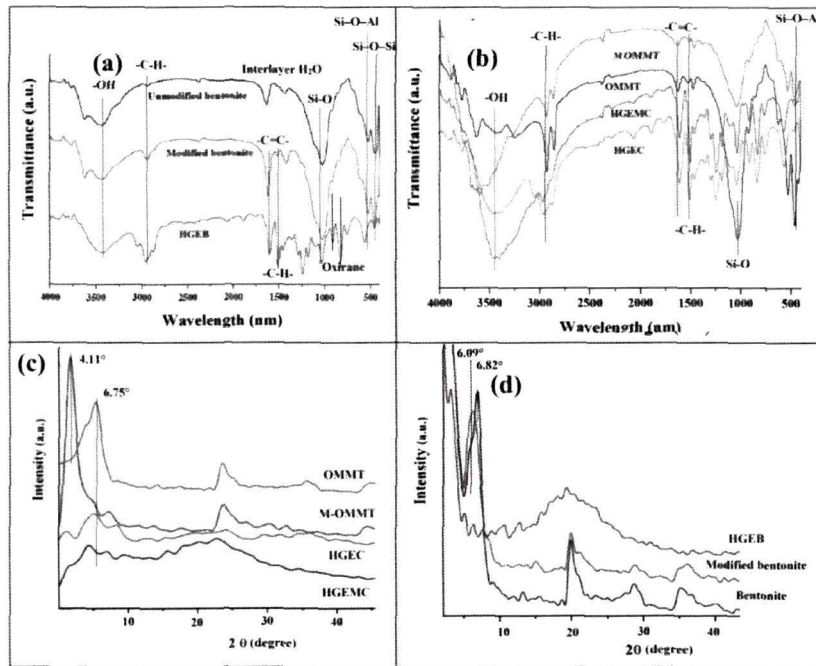


Figure 3.1: FTIR spectra of (a) bentonite, modified bentonite and HGEB and (b) OMMT, M-OMMT, HGEC and HGEMC; and XRD patterns of (c) OMMT, M-OMMT, HGEC and HGEMC and (d) bentonite, modified bentonite and HGEB

3.3.2.2. X-ray diffraction analysis

The XRD pattern showed the shifting of the peak from 2θ value 6.75° (OMMT) to 4.11° (M-OMMT) as shown in Figure 3.1c. This corresponds to the increase in basal spacing from 1.308 to 2.11 nm, which ascertains the delamination of the clay layers upon interaction with the oil. HGEC and HGEMC exhibited a kind of partially exfoliated behavior, as the peak was diminished to a considerable extent.⁶ This confirmed the presence of strong interaction between M-OMMT and HGE5 matrix.

Chapter 3

Again, XRD patterns of modified and unmodified bentonite clay and HGE5 are shown in Figure 3.1 (d). For pristine bentonite clay, the basal spacing is 1.29 nm, as calculated from the peak position (2θ value 6.82°) in the diffractogram using Bragg's equation. *H. aromatica* oil-modified bentonite showed an increase in the basal spacing (1.45 nm), which corresponds to the peak at 2θ value 6.09° . This implicates the intercalation of clay layers as a result of modification.¹¹ Furthermore, this imparts an organophilic behavior to the nanoclay. The d -spacing of the clay layers in HGE5 was 2.81 nm. This delamination demonstrated the insertion of HGE5 chains into the basal spacing of the modified clay and formed an intercalated NC.

3.3.2.3. Morphology of the NC

The surface morphology of HGE5 was smooth as observed in the SEM image (Figure 3.2 a). Contrarily, in case of NC, rough surfaces were observed (Figures 3.2 b-d). This depicts the dispersed clay layers in the epoxy matrix.¹¹ The micrographs of NC show that the nanosized silicate galleries interact with HGE5. This study also revealed the existence of porous structures on the surfaces of the nanoclays with irregular shape and size.

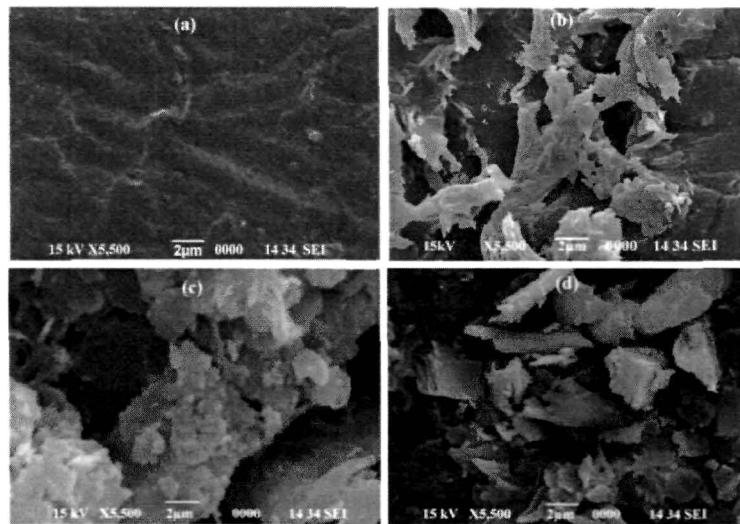


Figure 3.2: SEM micrographs of (a) HGE5, (b) HGE5, (c) HGE5 and (d) HGE5

Again, intercalation of HGE5 chains between the clay layers was evident from the TEM micrographs (Figure 3.3).^{6, 11} The interlayer spacing of the clay layers in HGE5 (2.75 nm) increased than that of the pristine nanoclay (1.32 nm), which is very close to the value

calculated from the XRD pattern (2.81 nm). In case of HGEC and HGEMC, TEM images showed partial exfoliation of the clay layers, which were again in agreement with the XRD patterns. This study ascertains a strong interaction of the nanomaterials with HGE5 matrix.

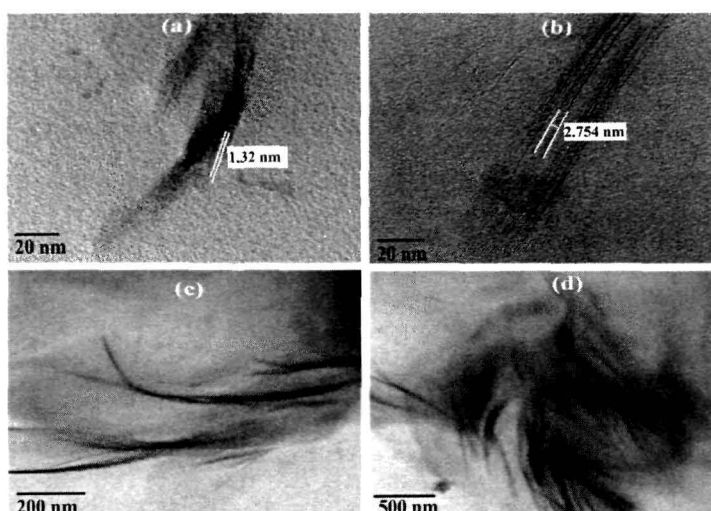


Figure 3.3: TEM micrographs of (a) pristine clay, (b) HGEB, (c) HGEC and (d) HGEMC

3.3.3. Curing study and mechanical performance

It is demonstrated in Chapter 2, that time required for the curing of HGE5 resin is less than that of its linear analog, due to the presence of high surface functionalities. Again, the clay-hydroxyl groups and the amine group of the hardener helps to enhance the rate of curing reaction in the present case. The hard drying time at 120 °C was determined for the NC (Table 3.1). It was observed that curing time decreased for the NC as compared to the pristine one. Again, HGEC and HGEMC took even less time than the HGEB. This is because of the stronger interaction of M-OMMT layers with HGE5, due to the long chain octadecylamine present within the clay nanostructures.

Mechanical properties were analyzed by determining the tensile strength, elongation at break, impact resistance, scratch hardness and bending values of the thermosetting NC (Table 3.1). Tensile strength of HGE5 was found to be improved significantly in HGEMC. This augmentation is due to the adequate crosslinking and dispersion pattern of the clay layers in the epoxy matrix. Intercalation of the clay layers within the matrix reinforces the mechanical properties in the NC.¹¹ Further, exfoliation of the nanoclay showed superior

Chapter 3

properties in HGEC and HGEMC. However, loading of nanoclay above 5 weight% showed a distinct phase separation in the system. Elongation at break decreased linearly with increase in tensile strength. This is due to the restriction on the segmental motion of HGE5 chains upon interaction with clay nanostructures.⁶ Flexibility of the NC was excellent as evident from the bending values, which is attributed to the presence of the aliphatic glycerol moiety in the backbone structure. Scratch hardness was above 10 kg, as this is the maximum limit of the instrument. Impact resistance was more than 1m, which could not be measured due to the instrumental limit (Limit of the instrument= 1m).

Again, lap shear tensile adhesive strength was excellent as tested on wood substrates (Table 3.1). HGEMC showed the highest strength amongst the studied NC, due to the efficient interaction of M-OMMT with HGE5, as observed from the TEM images. However, in every case, NC exhibited better properties than the pristine polymer. For each case, significant difference (>LSD and $p < 0.05$) was witnessed amongst the data.

Table 3.1: Curing parameters and performance of HGE5 and its NC

Property	HGE5 [#]	HGEB	HGEC	HGEMC	LSD
Curing time at 120 °C (min)	24±0.58	20±0.55	16±0.26	15±0.21	0.54
Swelling (%)	22.6±0.43	25.1±0.89	26.5±0.46	26.4±0.21	0.87
Tensile strength (MPa)	38.4±0.84	44.4±0.68	50.2±0.86	54.1±0.96	0.34
Elongation at break (%)	21.3±0.57	19.6±0.33	17.8±0.51	16.9±0.50	0.74
Impact resistance (m)*	>1	>1	>1	>1	-
Scratch hardness (kg)*	>10	>10	>10	>10	-
Bending (mm)*	<1	<1	<1	<1	-
Adhesive strength (MPa)	768	1141±1.5	1623±2.52	1880±2.0	28.69

*Instrumental limits: Scratch hardness=10 kg, Impact resistance=1 m and bending test mandrel=1 mm

[#]As reported in Chapter 2, Table 2.2.

3.3.4. Thermal study

The relative thermal stability of the thermosetting NC is shown in Figure 3.4 a. This shows two step degradation patterns for all NC, as well as for the pristine thermoset. This can be

Chapter 3

attributed to the existence of both aliphatic and aromatic groups in the structure of HGE5.¹¹ The onset temperature for the pristine thermoset and HGE5 were 255 and 278 °C, whereas for HGEC and HGEMC, it was 297 and 305 °C respectively. Augmentation in the thermal stability is due to the interaction of the thermostable clay layers with HGE5. Therefore, HGEC and HGEMC exhibited better stability than the others, due to the exfoliation of the clay within the matrix.

The second step of degradation began at around 495 °C for the pristine thermoset. This was observed at around 539, 555 and 609 °C for HGE5, HGEC and HGEMC respectively. HGEMC retained a weight residue of 17.2%, at 700 °C. These were 15.3% and 12.1% for HGEC and HGE5 respectively, whereas for the pristine polymer only 8% residue remained. This proves that HGEMC is the best NC amongst all, in terms of toughness, thermostability and allied material properties.

3.3.5. *In vitro* biocompatibility assessment

In vitro cell compatibility assay established that HGE5 as well as the NC are compatible to both cardiac and liver cell lines of wistar rat (Figure 3.4 b). Presence of the biocompatible moiety, glycerol, in the backbone structure of HGE5 conferred excellent biocompatibility as demonstrated in Chapter 2, section 2.3.9. Moreover, literature reports showcase that bentonite and OMMT clay are quite compatible with biological systems.²² Hence, the NC are well expected to be biocompatible. The average cell viability observed was above 90% (<LSD value and $p < 0.05$) for all the cases. However, the test samples showed better compatibility with cardiac cell line as compared to the liver.

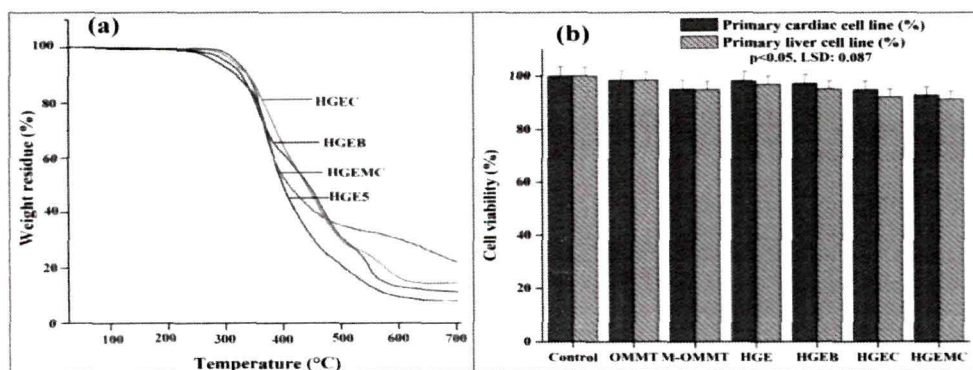


Figure 3.4: (a) TGA thermograms of HGE5 and its NC and (b) Cell viability (%) of cardiac and liver cell lines

Chapter 3

3.3.6. *In vivo biocompatibility assessment*

To observe the potential of the prepared NC as an implantable biomaterial, subcutaneous implantation was done within wistar rats. Blood was collected at 0, 15 and 30 days of implantation from each group as mentioned above. The hematological parameters were evaluated for the animals under experimental observation and the data were compared with the control (Table 3.2). The results suggest that there was no such difference of the blood parameters with time for the implanted animals. This indicated that the implanted material had no drastic effect on the blood parameters, which govern many physiological conditions.¹ An increase in the level of monocytes, neutrophil, eosinophil etc. implicates immunogenesis of the body against any xenobiotic material, which is not observed in the present case.³

Table 3.2: Hematological parameters of the control and HGEMC implanted rats

Parameter	0 day		15 days		30 days	
	Control	HGEMC	Control	HGEMC	Control	HGEMC
WBC	10.5±0.3	11.8±0.4	11.2±0.34	11.8±0.6	11.9±0.52	11.9±0.43
Lym (%)	42.2±0.1	41.9±0.6	43.8±0.79	42.6±0.6	40.6±0.23	41.4±0.73
Mon (%)	8.5±0.69	8.2±0.86	8.9±0.26	8.6±0.21	9.3±0.15	8.4±0.21
Neu (%)	48.1±0.5	48.7±0.9	46.8±0.98	45.4±0.6	46.3±0.65	44.7±0.44
Eo (%)	3.0±0.69	3.8±0.71	3.7±0.29	4.4±0.41	3.1±0.53	3.9±0.54
Ba (%)	0.3±0.53	0.3±0.71	0.3±0.35	0.3±0.44	0.3±0.43	0.3±0.53
RBC (m/mm ³)	7.9±0.38	6.5±0.21	7.5±0.33	6.15±0.2	7.1±0.32	6.1±0.63
MCV (fl)	51.9±0.6	51.1±0.6	54.1±0.54	55.4±0.4	51.2±0.54	53.1±0.56
Hct (%)	45.1±0.8	44.4±0.9	44.7±0.62	41.2±0.4	41.3±0.12	42.4±0.29
MCH (pg)	19.2±0.3	19.1±0.1	18.2±0.84	17.9±0.2	16.3±0.62	17.3±0.18
MCHC (g/dL)	29.9±0.4	29.5±0.9	29.8±0.41	28.5±0.1	29.3±0.41	28.1±0.54
Hb (g/dL)	14.2±0.1	13.5±0.9	14.8±0.19	12.9±0.6	12.5±0.28	12.5±0.51

Chapter 3

To understand the effect of implantation on the major organs of the tested animal, histopathological study was carried out. Representative histological images of the skin, liver, brain and heart tissues of both the groups, after 30 days of implantation are presented in Figure 3.5. This shows that the skin sections of the control as well as the treated group exhibited almost similar cellular arrangements.^{1, 3} Same observations were witnessed for the liver, brain and heart tissues. There was no abnormality or damage seen in the histomorphological organization of tissues after implantation of HGEMC film.

Thus, the *in vitro* and *in vivo* biocompatibility assays showed the potential of HGEMC as an implantable biomaterial, without induction of toxicity to the host system.

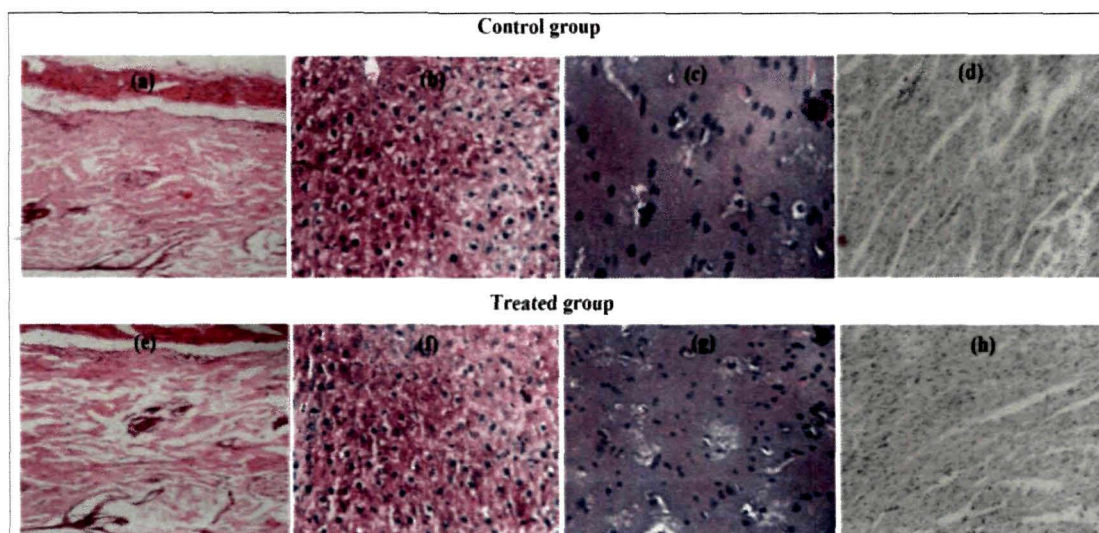


Figure 3.5: Representative histological sections of skin, liver, brain and heart of control (a-d) and HGEMC implanted (e-h) groups

3.3.7. Cell attachment and proliferation

The HGE5 and HGEMC films were analyzed after 30 days of implantation. The films were then fixed in gluteraldehyde (2.5%) and SEM micrographs were taken (Figure 3.6). The images showed the adherence of dermatocytes on the films. However, cell adherence was higher on HGEMC than the pristine matrix. This is because the nanoclay provides a rough surface with porous structure (evident from SEM images), which helped in anchoring of the cells.¹ Further, it can be well assumed that HGEMC offers a compatible and tough matrix which could support the growth and proliferation of the dermal (skin) cells.

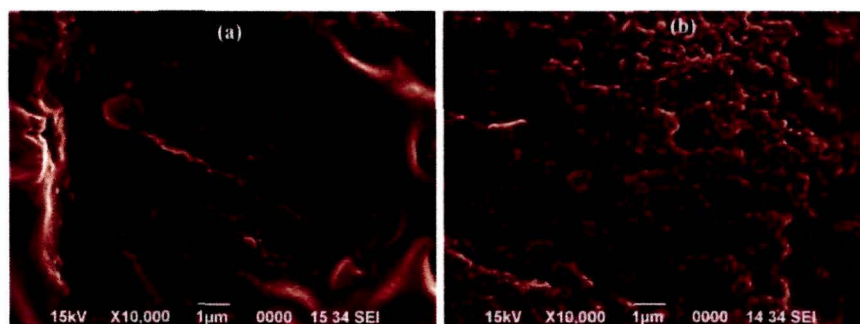


Figure 3.6: SEM micrographs of adherence and proliferation of the dermatocytes on (a) HGE5 and (b) HGEMC

3.3.8. Antimicrobial activity

According to the traditional knowledge, *H. aromatica* oil has promising antimicrobial effect.¹⁶ Therefore, in the present investigation, interest was paid to see its activity, in the NC, against the above-mentioned microorganisms. MIC values for the tested microorganisms are presented in Table 3.3. It is clearly visible that the oil has imparted antimicrobial activity to the modified clay, which is again reflected in HGEB and HGEMC. However, HGEC did not show any inhibitory effect, as the material is lack of the oil. This validates the idea of using the oil to modify the nanoclay. Again, HGEB and HGEMC exhibited almost similar inhibitory action which is basically due to the presence of M-OMMT within their matrices.

Table 3.3: MIC values ($\mu\text{g/mL}$) for the nanocomposites

Microorganism	HGE	OMMT	HGEC	M-OMMT	HGEB	HGEMC
<i>S. aureus</i>	>500	>500	>500	300 \pm 0.53	290 \pm 0.91	290 \pm 0.28
<i>E. coli</i>	>500	>500	>500	125 \pm 0.21	125 \pm 0.8	130 \pm 0.41
<i>M. Smegmatis</i>	>500	>500	>500	350 \pm 0.98	350 \pm 0.31	320 \pm 0.55
<i>C. albicans</i>	>500	>500	>500	130 \pm 0.38	125 \pm 0.19	125 \pm 0.95

The zones of inhibition were measured for each microorganism, taking the material concentration at their MIC values (Table 3.4). Here also M-OMMT, HGEB and HGEMC

Chapter 3

exhibited good efficacy against the microbial species (Figure 3.7). This again indicated that M-OMMT imparted the activity to the NC. However, the effect was different for different microbes. Stronger inhibitory effect was witnessed for the Gram negative bacterium; *E.coli* as compared to the Gram positive one, *S. aureus*. This may be due to the differential surface morphology of the microorganisms and their response to the material.²³ Further, the material showed profound antifungal activity against *C. albicans*. HGEMC exhibited excellent biocompatibility as well as the best material properties amongst the prepared NC. Therefore, HGEMC was only considered for further studies.

Table 3.4: Antimicrobial activity of the nanocomposites as zone of inhibition

Microbes	Zones of inhibition (mm)						
	HGE	OMMT	M-OMMT	HGEC	HGEB	HGEMC	Antibiotic
<i>S. aureus</i>	0	0	14±0.48	0	16±0.28	13±0.40	25±0.63
<i>M. smegmatis</i>	0	0	12±0.93	0	150±0.59	13±0.92	29±0.24
<i>E.coli</i>	0	0	26±0.74	0	25±0.74	28±0.87	33±0.56
<i>C. albicans</i>	0	0	25±0.41	0	28±0.81	25±0.29	34±0.95

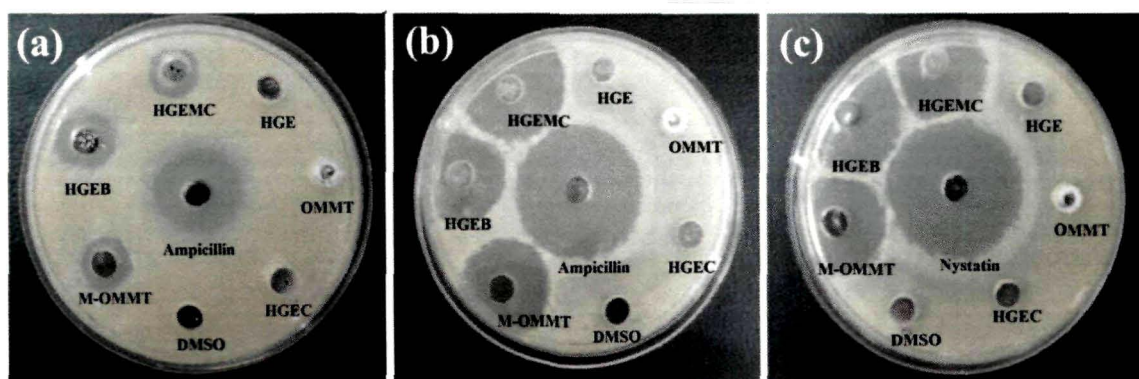


Figure 3.7: Representative antimicrobial activity of the nanocomposites against (a) *S. aureus*, (b) *E. coli* and (c) *C. albicans*

Adhesion of *E. coli* on HGE5 and HGEMC surfaces is shown in Figure 3.8. Sufficient amount bacteria were adhered onto the surfaces of both the films. However, in case of HGEMC, morphology of the adhered bacteria altered, which can be clearly

Chapter 3

visualized from the SEM micrographs.²⁴ This ascertains the death of bacterial cells upon interaction with the HGEMC surface. Further, no biofilm was formed during the process of interaction. This suggested that the material holds strong antibacterial property that is basically imparted by the oil as mentioned above. These micrographs clarify three facts; (1) the bacteria can adhere to the surface of HGEMC, (2) upon interaction with the surface bacterial cells denature and (3) the bacteria could not form any type of biofilm to protect themselves from the drastic environment, which is due to the surface properties of HGEMC film. Thus, this biocompatible, high performance NC with good antibacterial efficacy may be used as an infection resistant, implantable biomaterial.

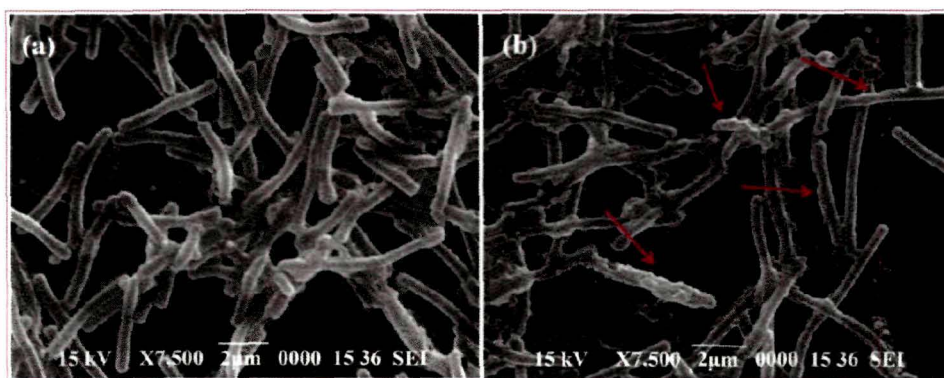


Figure 3.8: Interaction of *E. coli* with (a) HGE5 and (b) HGEMC (red arrows show denatured bacterial cells)

3.4. Conclusion

HGE5 based NC were prepared with *H. aromatica* rhizome oil-modified bentonite and OMMT clay. The NC exhibited good tensile and adhesive strength as well as high thermostability. However, HGEMC exhibited superior material properties than either of HGE5 and HGEC. This proved the positive impact of the oil on the modification of the clay surfaces. Again, *in vitro* and *in vivo* studies revealed the biocompatibility of the material. HGEMC supported the growth and proliferation of dermatocytes (skin cells) on its surface, without inducing any toxic effect to the host. Further, they could inhibit the growth of both Gram-positive and negative bacteria as well as fungi. Thus, this study demonstrates the potentiality of HGEMC as a high performance, biocompatible, antimicrobial implantable biomaterial.

Chapter 3

References

1. Das, B., et al. *Biomed. Mater.* **8** (3), 035003--035014, 2013.
2. Someya, T., et al. *Proc. Natl. Acad. Sci.* **101** (27), 9966--9970, 2004.
3. Ma, J., et al. *Biomaterials* **22** (4), 331--336, 2001.
4. Oh, S.H. & Lee, J.H. *Biomed. Mater.* **8** (1), 014101--014116, 2013.
5. Azar, N.G., et al. *J. Endodont.* **26** (8), 462--465, 2000.
6. Deka, H. & Karak, N. *Polym. Adv. Technol.* **22** (6), 973--980, 2009.
7. Kiliaris, P. & Papaspyrides, C.D. *Prog. Polym. Sci.* **35** (7), 902--958, 2013.
8. Schiraldi, C., et al. *Biomaterials* **25** (17), 3645--3653, 2004.
9. Hosseini, M.S., et al. *World Acad. Sci., Eng. Technol.* **60**, 1159--1162, 2011.
10. Katti, K.S., et al. *Biomed. Mater.* **3** (3), 034122--034133, 2011.
11. Das, G. & Karak, N. *Polym. Degrad. Stab.* **94** (11), 1948--1954, 2009.
12. Pramanik, S., et al. *RSC Adv.* **3** (14) 4574--4581, 2013.
13. Phua, S.L., et al. *ACS Appl. Mater. Interfaces* **4** (9) 4571--4578, 2012.
14. Singh, G., et al. *Flavour Fragr. J.* **15** (4), 278--280, 2000.
15. Murata, H., et al. *Surf. Sci.* **570** (1-2), 111--118, 2004.
16. Policegoudra, R.S., et al. *J. Mycol. Med.* **22** (1), 83--87, 2012.
17. Rose, S.F., et al. *J. Mater. Sci. Mater. Med.* **16** (11), 1003--1015, 2005.
18. Das, B., et al. *Macromol. Biosci.* **13** (1), 126--139, 2012.
19. Banerjee, S., et al. *Int. J. Toxicol.* **32** (4) 308--313, 2013.
20. Newton, S.M., et al. *J. Ethnopharmacol.* **79** (1), 57--67, 2002.
21. Shukla, A. & Srivastava, A.K. *J. Macromol. Sci. A* **40** (1), 61--80, 2003.
22. Wang, M-C., et al. *ACS Appl. Mater. Interfaces* **4** (1), 338--350, 2012.
23. Konwarh, R., et al. *Colloids Surf., B* **81** (2), 578--586, 2010.
24. Basu, A., et al. *J. Mater. Chem. B* **1** (37), 4746--4755, 2013.

Hyperbranched epoxy/clay-silver nanocomposite as an infection resistant scaffold material

Highlights

This chapter demonstrates the preparation and characterization of a hyperbranched epoxy/clay-silver NC based infection-resistant tough implantable scaffold material. 'Green' silver nanoparticles embedded NC with varying percentages of nanoparticles were prepared by an *ex-situ* technique. Interaction of the clay-silver nanohybrid with hyperbranched epoxy matrix was studied by FTIR, XRD, SEM and TEM analyses. The thermosetting NC demonstrated improvement of mechanical properties compared to the pristine polymeric system. The NC surface inhibited the growth of antibiotic-resistant microbes such as *Staphylococcus aureus*, *Escherichia coli* and *Candida albicans* which are mostly responsible for surgical infections. The material is highly compatible with primary liver and cardiac cell lines of wistar rat. *In vivo* implantation of the material fostered wound healing in wistar rat. Hematological and histopathological parameters of the tested animals confirmed the compatibility of the scaffold with the *in vivo* system.

Parts of the chapter are published in

Barua, S., Konwarh, R., Bhattacharya, S.S., Das, P., Devi, K.S.P., Maiti, T.K., Mandal, M., Karak, N. *Colloids Surf., B* **105**, 37--42, 2013.

Barua S., Chattopadhyay, P., Aidew, L., Buragohain, A.K. & Karak, N. *Polym. Int.* DOI: 10.1002/pi.4790, 2014.

Chapter 4

4.1. Introduction

Skin, the largest organ of human body, has to withstand various environmental conditions as well as physical and chemical hazards. The previous chapter proved the potentiality of HGEMC, as a scaffold that could also inhibit microbial infection. However, keeping into account the mortality rate associated with surgical/hospital related infections, the material further needs stronger antimicrobial efficacy. In this regard, incorporation of metal nanoparticles to the matrix is a good proposition. Metal nanoparticles find their utility in important areas of material science and biomedical domain.^{1, 2} Amongst them, silver is an attractive candidate due to its excellent antimicrobial activity against a broad spectrum of pathogenic microbes.^{3, 4} Although, chemical methods for preparation of silver nanoparticles (AgNP) are popular as their large scale production is possible, yet there is a chance of residual toxicity of the chemicals and reagents to biological systems. Thus, the idea of plant extract mediated synthesis of AgNP emerged, which conferred interesting biological attributes to the nanoparticles. Different leaf extracts were utilized to reduce silver salts, amongst which *Emblica officinalis*, *Mimosa pudica*, *Nelumbo nucifera*, *Tinospora cordifolia*, *Eclipta prostrate*, *Ocimum tenuiflorum* are to mention a few.⁵ 'Green' AgNP showed profound inhibitory effect against *Staphylococcus aureus*, *Escherichia coli*, *Klebsiella pneumonia*, *Fusarium oxysporum*, *Chromobacterium violaceum*, *Streptococcus faecalis*, *Aspergillus niger*, *Salmonella typhi*, *Fusarium accuminatum*, *Candida albicans* etc. as reported in literature.⁶ In the present investigation, yet another phyto-resource, *Thuja occidentalis* is explored for the preparation of AgNP. *T. occidentalis* is an evergreen coniferous tree, in the cypress family, Cupressaceae with wide applications in homeopathy and evidence-based phytotherapy. It is pertinent to mention that a number of *in vitro* and *in vivo* studies bear testimony to *Thuja*'s immunopharmacological potential and antiviral action.⁷

Even though a number of reports are available on bio-resource based preparation of AgNP, not many have addressed their toxicity issues.¹ Tunable antibacterial coatings with AgNP, generated through *in situ* route, which support mammalian cell growth, have been developed.⁸ Such reports on the utility of nanoparticles call for the assessment of their biocompatibility. Deciphering molecular events that regulate bioaccumulation and toxicity of nanoparticles is quite perplexing.

Chapter 4

Moreover, metal nanoparticles supported on solid surfaces not only stabilize the nanoparticles, but also dictate many important properties.⁹ Thus, AgNP anchored on clay surfaces may be utilized for various advanced applications. In this regard, Ahmed et al. prepared montmorillonite-silver nanohybrid and found potential antibacterial properties of the material.¹⁰ Similar nanohybrid was prepared by Shameli and co-workers, by γ -irradiation technique.¹¹ Further, a few researchers have reported efficient antimicrobial activity of silver-clay based polymer NC. To exemplify, Shameli et al. in 2010, reported an antimicrobial silver-montmorillonite/chitosan NC.¹² Interesting material and biological attributes were witnessed for a silver-clay HE NC as reported by Roy et al, in 2013.⁹ Chapter 3 showed that the porous surface provided by HGEMC is efficient to anchor on skin cells. Hence, it is expected to fabricate an infection resistant scaffold material, by incorporating silver-clay nanohybrid (AgOM) into the HGE5 matrix.

Acute and chronic infections generally occur upon insertion of implants into the host body.¹³ Modification of such implants with infection-preventing surfaces may address this problem. With such an approach, de Mel et al. fabricated silver NC based implant material for blood contacting tissues.¹⁴ Again, An et al. reported an antimicrobial silver NC with chitosan graft methyl acrylate.¹⁵ However, mechanical strength was compromised in such cases. Therefore, biocompatibility, infection resistance and high mechanical attributes are the three qualities that are tried to impart to the present NC and related studies were performed.

4.2. Experimental

4.2.1. Materials

Silver nitrate (AgNO_3) was procured from Merck, India (with 99.8% purity). This has been widely used as the precursor for preparation of AgNP. AgNO_3 is prepared by reacting metallic silver with nitric acid (hot/cold). Its melting point is 212 °C and molecular weight is 169.6 g/mol. It has proven antimicrobial activity against a broad range of microorganisms.

Chapter 4

Thuja leaves were collected from Tezpur University campus (Assam, India). About 2 g of the leaves were washed with de-ionized water and ground in a domestic blender. The ground mass was dried at room temperature.

The chemicals and reagents such as glycerol, BPA, epichlorohydrin, THF, toluene, sodium hydroxide, poly(amido amine), OMMT clay, *H. aromatica* etc. oil were of the same grade as mentioned in Chapter 2, section 2.2.1 and Chapter 3, section 3.2.1. M-OMMT was prepared as described in the previous chapter.

L929 cell line was obtained from Department of Biotechnology, Indian Institute of Technology, Kharagpur, India. William medium and low-glucose DMEM medium, MTT etc. required for the *in vitro* biocompatibility assessment were of the same grade as described in Chapter 2, section 2.2.1. Microbial strains, like *Staphylococcus aureus* (ATCC 11632), *Escherichia coli* (ATCC 10536) and *Candida albicans* (ATCC 1023), along with the required media and agar were obtained from the Department of Molecular Biology and Biotechnology, Tezpur University, Assam.

4.2.2. Animals

Wistar rats were obtained from Laboratory Animal Resources, Division of Pharmaceutical Technology, Defence Research Laboratory, Tezpur, Assam, India. Animals were fed and looked after as described in Chapter 3, section 3.2.2. Animal studies were carried out with due approval from the Institutional Animal Ethics Committee.

4.2.3. Instruments

FTIR, XRD and SEM analyses were performed under the same conditions by using the same instruments as mentioned in Chapter 2, section 2.2.2. Distribution and shape size accord of AgNP in the prepared NC were analyzed by using the TEM as mentioned in Chapter 3, section 3.2.3. AgNP were dispersed in water by using an ultrasonicator of same the specification as stated in Chapter 3, section 3.2.3. UV-visible spectra of the dispersed AgNP were recorded in a UV-visible spectrophotometer, UV-2550 (Shimadzu, Japan). NC were dispersed in THF and spectra were taken in the instrument.

Tensile strength, elongation at break, lap shear tensile adhesive strength of NC were measured in the UTM, as described in Chapter 2, section 2.2.2. Film samples of similar

Chapter 4

dimension were prepared. The resinous NC were mixed with poly(amido amine) hardener and applied in the overlapping surfaces of wood substrates for tensile adhesive strength test. Scratch hardness, impact resistance and bending of the NC were determined by using the same instruments under the same conditions as described in that section.

4.3.4. Methods

4.3.4.1. Preparation of AgNP

The aqueous leaf extract was prepared by stirring the ground leaves for about 20 min in 50 mL of water at 50 °C, followed by filtration through a muslin cloth. AgNO₃ (0.01 M) solution was prepared by dissolving the required amount of silver salt in 25 mL of millipore water. The aqueous leaf extract (2 mL) was added to the AgNO₃ solution and allowed to stir for 4 h at room temperature. Completion of the reduction process was indicated by a change in color of the transparent solution to dark brown. The suspension was washed several times with water to remove the undesired components. Finally, it was washed with acetone and dried in an oven.

4.3.4.2. Preparation of AgOM

An amount of 5 weight% of the modified clay (M-OMMT) with respect to HGE5 resin was swelled in THF under mechanical stirring for 3 h at room temperature followed by ultrasonication for 10 min. The prepared AgNP were dispersed in THF in varying amounts (1, 3 and 5 weight% with respect to the resin) and added to the above clay slurry. This mixture was allowed to stir for another 5 h at room temperature for homogenization. This was further subjected to ultrasonication for 15 min. AgOM thus formed was washed with THF by centrifugation and allowed to dry at 45 °C for 24 h.

4.3.4.3. Preparation of NC

AgOM suspension was prepared in THF by the assistance of magnetic stirring and ultrasonication. HGE5 resin was mixed with AgOM suspension according to the above mentioned ratios and stirred for 3 h at room temperature, followed by 10 min of ultrasonication. These NC were then degassed under vacuum. They were encoded as

Chapter 4

HGCS1, HGCS3 and HGCS5 where digits are as per the weight percentages of AgNP within the matrix. These NC are referred to as HGCS in general in this chapter.

4.3.4.4. *In vitro* biocompatibility assessment

L929 cells (1×10^4 cells/mL) were seeded into a 96 well plate. Cell suspension of 180 μ L was added to each well and allowed to stand for 4 h. Concentration of AgNP was adjusted as 10-100 μ g/mL and pipetted in the wells against the control wells. DMEM was taken as the culture medium. Culture was incubated for 72 h at 37 °C in a 5% CO₂ incubator and cell survival was estimated by MTT assay as described in Chapter 2, section 2.3.4. All the experiments were performed twice in triplicates and the average was recorded as cell-viability percentage in comparison with the control experiment, while AgNP untreated controls were considered as 100% viable.

Cytocompatibility of HGCS was examined with primary heart and liver cell lines of wistar rat. Heart and liver were extracted from the sacrificed rat. The cell survival assay was carried out by following the same protocol as stated in Chapter 2, section 2.3.4.

4.3.4.5. *Antimicrobial assays*

The antimicrobial activity of the plant extract and AgNP were individually tested against the Gram positive species *S. aureus* and the Gram negative species *E. coli*. The mentioned bacterial strains were cultured overnight in nutrient broth at 37 °C. Inoculums of the microbial culture for agar well diffusion assay were adjusted to 10^5 colony forming unit (CFU) per mL. The inoculum suspension was mixed properly and spread over Mueller Hinton agar (MHA) plates and wells were bored. In the respective wells, 40 μ L of the plant extract/nanoparticles were poured along with the positive control. Ampicillin and gentamicin (10 μ g/mL) were used as positive control for Gram positive and negative bacteria respectively. The diameter of zones of inhibition was measured by using a zone scale (HiMedia, India) after 18 h of incubation at 37 °C.

Again, to study the infection-preventing capability of HGCS surfaces, *E. coli* strain was considered. The bacterial strain was cultured in nutrient broth (HiMedia, India) for 24 h. This was re-suspended in PBS after centrifugation. Small pieces of HGCS (1 mm \times 1 mm \times 0.25 mm) were immersed in the culture medium and incubation was carried out for

Chapter 4

16 h. Then the films were taken out and rinsed in PBS. The films were fixed with 2.5% glutaraldehyde and dehydrated with alcohol. SEM micrographs were taken to understand the interaction of the bacteria with the film surface. Again, *S. aureus* and *C. albicans* are the microorganisms involve in hospital-acquired infections.¹⁶ Thus, MIC were determined for AgNP, AgOM and HGCS against the microbial strains, *S. aureus*, *E. coli* and *C. albicans* by following the same protocol as described in Chapter 3, section 3.3.4.5. To quantify the antimicrobial efficacy of the samples, counts of colony forming units (CFU) were taken at the MIC. The test samples at their MIC were incubated with the strains for 12 h in case of the bacteria and 24 h for *C. albicans* and smeared onto agar plates. CFU per milliliter for the samples was determined and compared with that of the control.

4.3.4.6. Creation of wound and wound healing analysis

To analyze the efficiency of HGCS5 as a skin tissue scaffold, two groups (each containing six animals) of wistar rats were used. Animals were anesthetized by peritoneally injecting sodium phenobarbitone as described in Chapter 3, section 3.2.2. A circular wound (ca. 20 mm in diameter) was made on the dorsal side of each animal. In the treated group, HGCS5 scaffold (UV-sterilized) was implanted in the wound area so that it was visible from outside. The untreated group was kept as control to observe the healing process in absence of the scaffold.

Epithelialization with time was photographed (by a Nikon Coolpix-S3000 camera) at 0, 7, 14 and 21 days. The diameter of the wound site was determined by using the Fiji 13 software, where desired length can be measured by comparing with a standard length and the percentage wound healing was determined with the formula.¹⁷

$$\text{Percentage wound contraction} = \frac{a_0 - a_n}{a_0} \times 100 \quad (4.1)$$

where, a_n is the unhealed area of the wound on the n^{th} day and a_0 is the initial wound area on the day of surgery.

4.3.4.7. Hematological and histopathological examinations

Animals were kept for 21 days to observe the reconstruction of skin at the wound sites. After 21 days, the animals were fasted overnight before collecting blood samples. The

Chapter 4

hematological parameters were measured for both the groups according to the procedure described in Chapter 3, section 3.3.4.4. Wound granulation tissues were collected on postoperative days 7, 14 and 21, by sacrificing the test animals. They were fixed in 10% formaldehyde and embedded by paraffin. Fine sections were prepared with a microtome and stained with hematoxylin and eosin. Histopathological study was carried out under a microscope to analyze the cellular organization, inflammation, vascularization etc. To study the compatibility of the scaffold material under *in vivo* conditions, other major organs (brain, heart and liver) were also considered for histopathological examination. Similarly, stained sections were prepared and studied under a microscope.

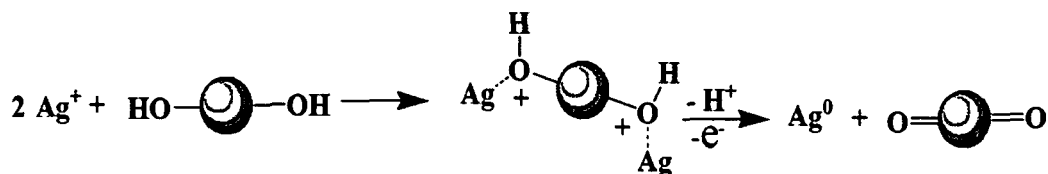
4.3.4.8. Statistical analysis

Data were presented as mean \pm SD, from the triplicate experimental results. LSD was determined by one or two way ANOVA to evaluate the significant difference amongst the results.

4.3. Results and discussion

4.3.1. Preparation of AgNP

The 'green' AgNP were prepared by using the Thuja leaf extract. The plant extract is a store-house of many natural polyphenolic compounds. Such polyphenols form complexes with metal ions, thereby releasing a good number of electrons and protons. Such electrons take part in the reduction process of Ag^+ to Ag^0 . The plausible mechanism of reduction is pictorially presented in Scheme 4.1.

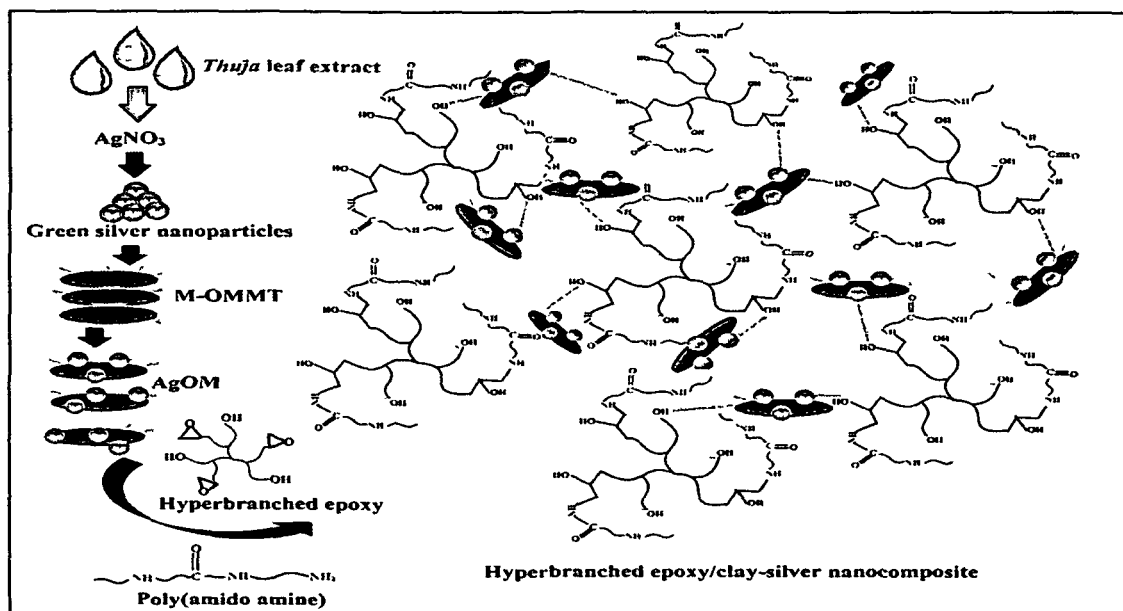


Scheme 4.1: Plausible mechanism of reduction of Ag^+ , by *T. occidentalis* leaf extract

4.3.2. Preparation of HGCS

Chapter 4

Interaction of clay layers with HGE5 depends on the accessibility of polymer to the galleries of the nanoclay. The primary factors that facilitate the interfacial interaction between polymer and clay are van der Waals forces. Other forces that govern the extent of interaction are the binding interaction of the epoxy and silicon basal surface and physicochemical bonding between clay hydroxyl groups and the functionalities of HGE5. The oxirane ring opens up when reacted with poly(amido amine) hardener and takes part in the curing reaction. In the previous chapter, it was observed that M-OMMT formed a partially exfoliated structure by interacting with the HGE5 matrix. In the present investigation, the nanohybrid system (AgOM) was prepared by anchoring *T. occidentalis* leaf extract (aqueous) mediated 'green' AgNP onto the M-OMMT surface. Electrostatic forces basically dictate the interaction between metal nanoparticles and clay. This AgOM is expected to perform dual duties; first to enhance the mechanical properties of HGCS and to protect the proposed implant from microbial infections. Thus, incorporation of AgOM to HGE5 can form a stable NC with the aforementioned properties. Moreover, biocompatibility is a major concern in this study. The fabrication procedure of HGCS is schematically presented in Scheme 4.2.



Scheme 4.2: Schematic representation for the fabrication of HGCS

4.3.3. Characterization

4.3.3.1. UV-visible spectroscopy

The UV-visible spectrophotometric analysis vouched for the successful green-route mediated generation of AgNP. The peak at around 420 nm in the spectrum was observed which indicates the formation of AgNP (Figure 4.1 a). The corresponding surface plasmon resonance (SPR) is attributed to the collective oscillation of electron gas in the particles with a periodic change in the electronic density at the surface. A couple of parameters like particle size, shape, dielectric constant of the medium and surface adsorbed species determine the position and shape of the plasmon absorption.

Again, the presence of AgNP in AgOM and in HGCS was demonstrated by the UV-visible spectra in Figure 4.1 b. Peaks at around 429 nm confirmed this fact. HGCS also exhibited the characteristic SPR peak in the same range. High aspect ratio of the clay layers prevented the agglomeration of nanoparticles.¹⁸ Further, HGE5 chains supported the stable dispersion of the nanohybrid within the matrix.

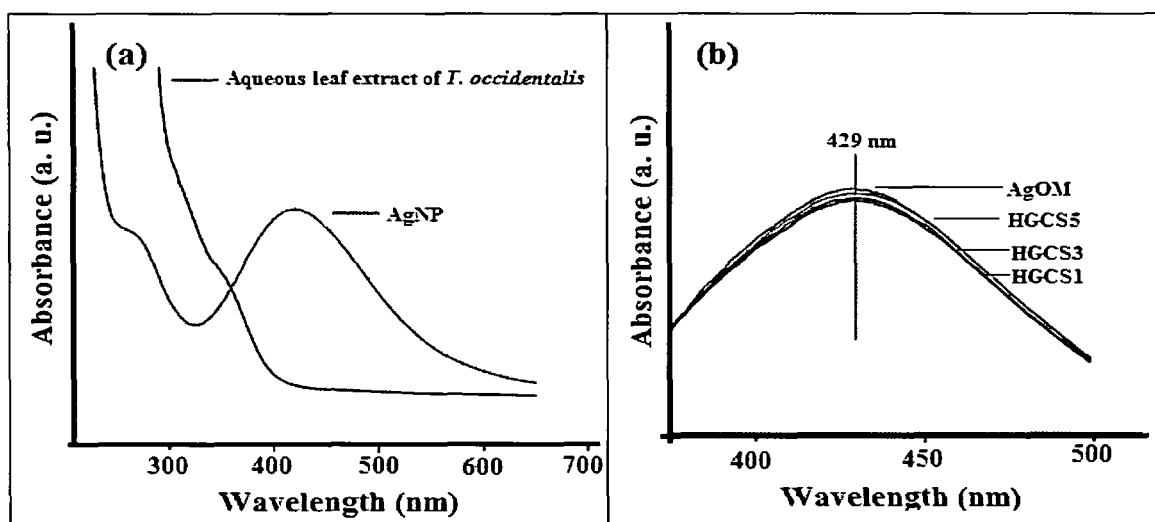


Figure 4.1: UV-visible spectra of (a) AgNP and *T. occidentalis* leaf extract and (b) AgOM and HGCS

4.3.3.2. FTIR study

The FTIR spectra showed the structural features of cured and uncured HGCS5 (Figure 4.2). In case of M-OMMT, a broad band was observed at around 3494 cm^{-1} as reported in Chapter 3. This is due to -OH stretching of Si-OH and Al-OH linkages of the nanoclay. This band was shifted to 3419 cm^{-1} in HGCS5. This is a clear indication of the interaction

Chapter 4

between clay and AgNP with the HGE5 matrix. The -C=C- stretching vibrational band was observed at around 1672 cm^{-1} for the unsaturated components of *H. aromatica* oil. Bending modes at $530\text{-}550$ and 442 cm^{-1} were observed for Si-O-Al and Si-O-Si linkages respectively. The broad band at 1038 cm^{-1} is for the Si-O stretching frequencies. The asymmetric vibrational bands of the epoxy ring were observed at around 915 and 839 cm^{-1} . These bands were absent in case of the HGCS5 thermoset, which clearly indicates the successful crosslinking of the resin with the hardener which is also supported by the swelling values (Table 4.1).

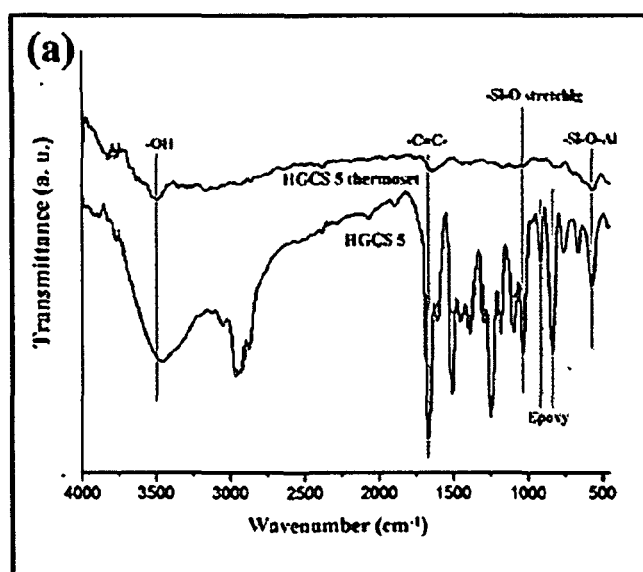


Figure 4.2: FTIR spectra of cured and uncured HGCS5

4.3.3.3. XRD analysis

The X-ray diffractogram of AgNP showed distinct peaks at 2θ values of about 38 , 44.3 , 64.4 and 77.4° , representing the (111), (200), (220) and (311) Bragg reflections planes of face-centered cubic (fcc) structure of silver (Figure 4.3 a). The indexed peaks were compared with JCPDS data file (89-3722). Scherrer's formula was used for determining the average crystallite size of the nanoparticles

$$D = \frac{K\alpha}{\beta\cos\theta} \quad (4.2)$$

where, D represents the crystallite domain size, K is the Scherrer's constant (0.9) in the present case, α , the wavelength of the used X-ray is equal to 1.574 nm ; β is half width

maximum height peak and θ is the diffraction angle. The crystallite average domain size of the prepared nanoparticles was found to be 11 nm.

Again, XRD patterns of AgOM showed peaks at 2θ values of 36° , 44° , 64° and 74° (Figure 4.3 b). These correspond to the Bragg reflection planes (111), (200), (220) and (311) respectively for the fcc structure of silver.⁴ Except for the first one (with subtle shifting), the other peaks are not prominent in HGCS, which may be due to the embedded particles within the nanoclay. These peaks were not observed in case of HGCS. This indicates the presence of strong interaction between nanomaterials and HGE5. This is attributed to the small amount of nanomaterials within the polymer. M-OMMT showed a sharp peak at 2θ value of 4.11° as observed in the previous chapter. This peak is absent in HGCS which may be due to the AgNP embedded in clay layers within the epoxy matrix. Mechanical stirring and ultrasonication help in dispersing AgOM within the matrix. The broad peak at around 2θ value 20° is due to the amorphous nature of HGE5.

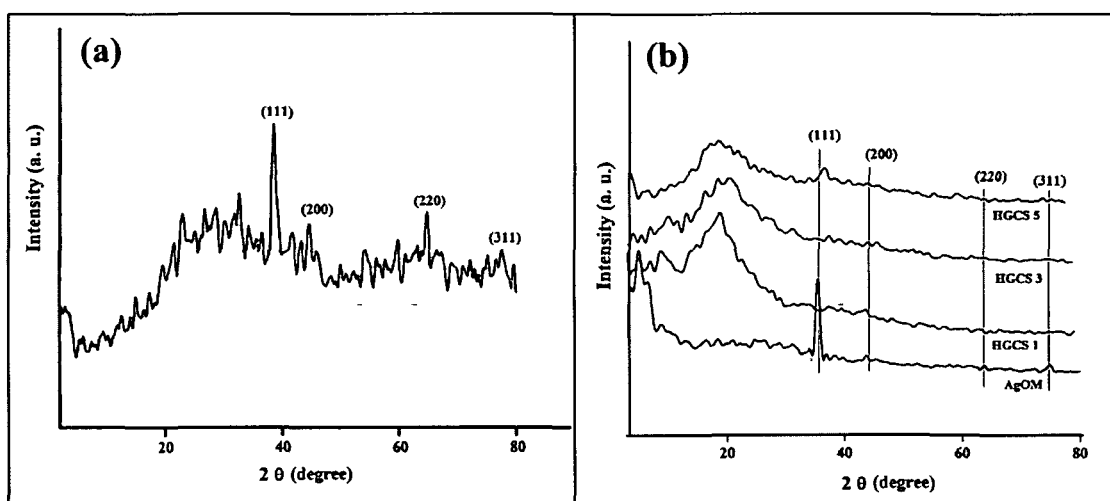


Figure 4.3: XRD patterns of (a) AgNP and (b) AgOM and HGCS

4.3.3.4. Morphological study

SEM micrographs disclose the morphology of HGCS, where the distribution of the nanohybrid is visible (Figure 4.4 a-b). Surface of HGCS exhibited a rough morphology, while a smooth surface was observed in case of the pristine epoxy. Distribution of AgOM in the matrix can be seen from the SEM image.

Chapter 4

Again, well dispersed spherical colloidal AgNP within a narrow size window (7-14 nm) could be observed from the TEM micrograph of AgNP (Figure 4.5 a) with maximum number of particles having average diameter of 9.8 nm. However, to confirm the interfacial distance, distribution of AgOM and their sizes in HGCS, TEM micrographs were taken (Figure 4.5 b-c). This study showed partially exfoliated clay layers (with interlayer spacing of 3.3 nm), in the epoxy matrix.⁹ Further, AgNP (within a narrow size spectrum of 1-10 nm) distributed uniformly over the clay layers can also be observed from these images. Partially exfoliated clay layers prevented agglomeration of the nanoparticles by embedding them within the layers, which is supported by the XRD study. Such distribution of AgNP embedded in the clay layers would be helpful to confer good biological activities to the NC.

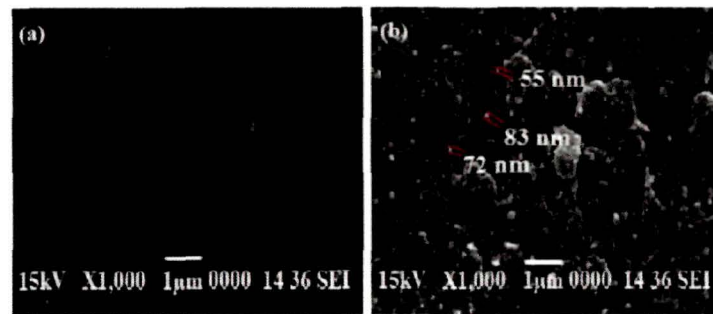


Figure 4.4: SEM micrographs of (a) HGE5 and (b) HGCS5

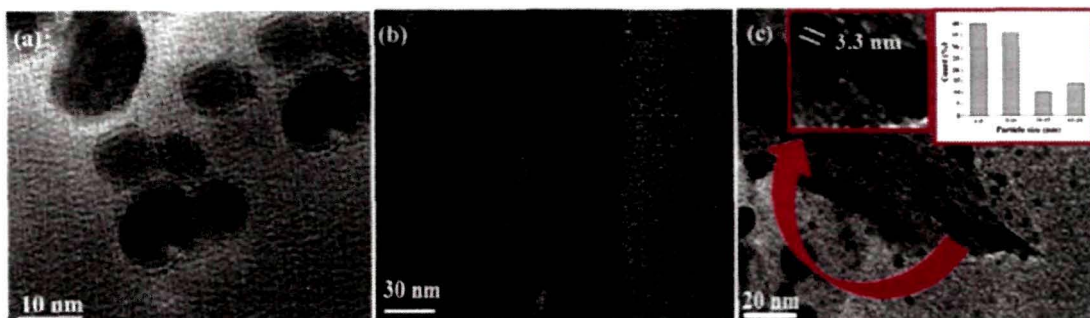


Figure 4.5: TEM micrographs of (a) AgNP and (b-c) HGCS5

4.3.4. Curing study and mechanical properties

Curing time decreased for HGCS in comparison to the pristine epoxy system as observed in the previous chapter. The hard drying times were recorded for HGCS1, HGCS3 and

Chapter 4

HGCS5 (Table 4.1) and only subtle differences were noticed. This is because of the presence of same amount of nanoclay in each case. However, the adsorption of different plant components on the surface of AgNP may play a minimal role in the crosslinking process. In all the cases, 70-80% crosslinking was obtained which is desirable for optimal properties of the NC.

Table 4.1: Curing parameters and performance of HGE5 and HGCS

Property	HGE5 [#]	HGCS1	HGCS3	HGCS5	LSD
Curing time at 120 °C (min)	24±0.58	15±0.63	14±0.48	12±0.37	0.41
Swelling (%)	22.7±0.43	26.2±0.23	24.4±0.31	23.5±0.74	0.73
Tensile strength (MPa)	38.4±0.84	54.8±0.51	56.8±0.65	60.9±0.18	0.64
Elongation at break (%)	21.3±0.57	16.2±0.29	15.2±0.39	14.6±0.041	0.39
Impact resistance (m)*	>1	>1	>1	>1	-
Scratch hardness (kg)*	>10	>10	>10	>10	-
Bending (mm)*	<1	<1	<1	<1	-
Adhesive strength (MPa)	768	2029±0.17	2223±0.43	2419±0.78	42.87

*Instrumental limits: Scratch hardness=10 kg, Impact resistance=1 m and bending test mandrel=1 mm

[#]As reported in Chapter 2, Table 2.2.

The values for the mechanical properties of the HGCS are provided in Table 4.1. Incorporation of 5 weight% M-OMMT improved the tensile strength up to 51 MPa in HGEMC as shown in Chapter 3, section 3.3.3. Intercalation and partial exfoliation of clay layers inside HGE5 contributed to the enhancement of mechanical properties. However, AgOM embedded epoxy NC exhibited marginal increment of tensile strength from the earlier NC with increase in AgNP loading. This predicts that the clay layers basically confer mechanical strength to the NC.⁹ AgNP further reinforced the systems. Elongation at break decreased with increase in loading of AgOM. Further, excellent flexibility was witnessed from the bending values of HGCS as they can be folded up to 180° without

Chapter 4

fracture. The exact values for impact resistance and scratch hardness could not be measured because of instrumental limits as stated earlier.

Excellent lap shear tensile adhesive strength of HGCS was observed in case of wood substrates (Table 4.1). This increase in adhesive strength is because of the interaction of the polar groups of wood substrate with those of the HGE5 matrix. Further, the interactions of AgOM with the epoxy matrix play vital roles in augmentation of the adhesive properties. Data presented in Table 4.1 are significantly different in each case, as their difference is quite higher than the LSD values. Further, statistically significant ($p < 0.05$) difference was witnessed for each case.

4.3.5. In vitro biocompatibility assessment

Myriads of reports on the applications of AgNP particularly in the biomedical domain but nowhere the toxicity assessment was reported properly. Therefore cytocompatibility was assessed for L929 cell line by incubating with the prepared AgNP (Figure 4.6 a). Treatment of the cells with AgNP up to 50 $\mu\text{g/mL}$, showed no significant decrease in the cell survival rate. However, increasing the concentration up to 75 $\mu\text{g/mL}$ led to considerable loss in cell viability (by almost 50%) as evident from the MTT assay. Thus, these results suggest that there exists a direct correlation between dose and toxicity of the nanoparticles.⁸ At this juncture, it is worthy to state that the response of a single cell line towards a particular nanomaterial is not representative of all the plausible outcome of the events at the bio-nanomaterial interface.

MTT assay was carried out to ascertain the cytocompatibility of the prepared NC with primary cardiac and liver cell lines (Figure 4.6 b). AgOM showed 88% cell compatibility. On average, HGCS showed a cell survival rate above 90%, which confirms the *in vitro* biocompatibility of them. However, better compatibility was witnessed in case of cardiac cell line. Compatibility of the materials is due to the presence of the biocompatible moiety glycerol in the structure. Also nanoclay is known to possess good compatibility at bio-nano-interface. As described in the previous chapter, HGEMC exhibited 91% compatibility. Further, the cytocompatibility of AgNP is confirmed from the aforementioned assay. Therefore, it is predictable that HGCS would show good compatibility with biological systems.

Chapter 4

In both the cases, cell survival rate was comparable to that of control (<LSD) with $p < 0.05$.

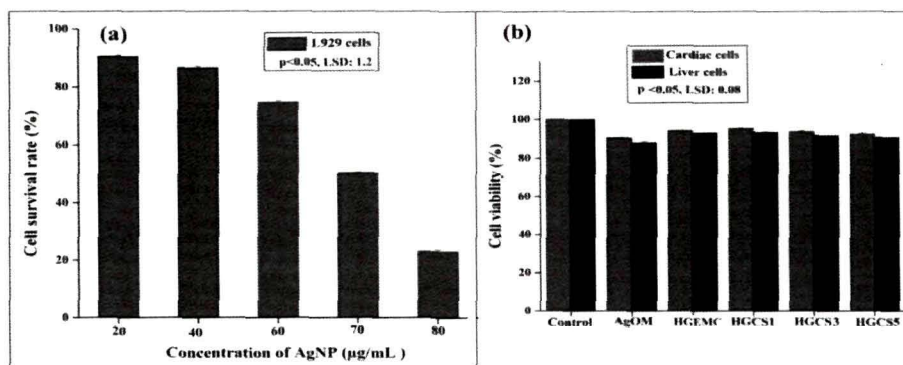


Figure 4.6: Cytotoxicity assessment (% cell viability) of (a) AgNP and (b) AgOM, HGEMC and HGCS

4.3.6. Antimicrobial assays

Thuja finds its use as an adjuvant to antibiotics in severe bacterial infections as reported in literature.⁷ However, no zone of inhibition was noted for *S. aureus* and *E. coli* when treated only with the aqueous leaf extract. On the other hand, AgNP showed antibacterial efficacy for both the Gram positive and negative species under consideration (Figure 4.7). It is well reported that AgNP could inhibit the growth and reproduction of bacteria. High aspect ratio and the crystallographic structure of the nanoparticles govern their antimicrobial potency which is favored by (111) facets.¹⁹ Recent reports focused that silver ions react with SH groups of proteins and inhibit the bacterial metabolism.²⁰⁻²² Permeability of bacterial cell membrane to phosphate is inhibited by oxidative phosphorylation upon exposure to AgNP. The prepared AgNP exhibited antibacterial efficacy almost at par with the positive controls (ampicillin and gentamicin) used.

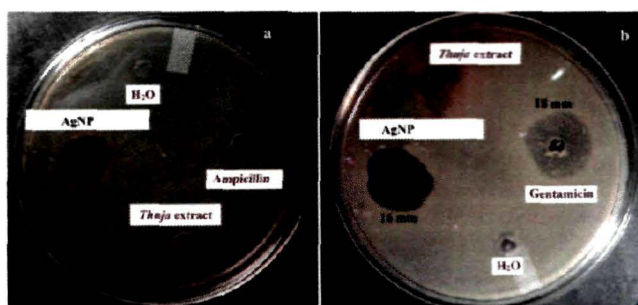


Figure 4.7: Antibacterial activity of the prepared AgNP against (a) *S. aureus* and (b) *E. coli*

Chapter 4

The differential interaction of the nanoparticles with the two groups of the bacterial species has remained an intriguing observation for a couple of years. Differential expression of molecular moieties at the surface of the respective group may be influential in dictating the antimicrobial activity of the nanoparticles. The basic architectural differences between the cell walls may be another major player.

The postoperative wounds may lead to severe infections which affect the surgical implant. Evolution of infection is caused by biofilm formation around the implanted device.²³ So, it is very important to protect the implant surface from such infections. Basu et al. recently designed a peptide immobilized antimicrobial polymeric surface.²⁴ They observed that the membrane integrity of *E. coli* was lost on contact with that surface. Fate of *E. coli* is studied in the present investigation upon interaction with the HGCS surfaces. The SEM images showed good bacterial adhesion on the surface of HGE5 (Figure 4.8). However, morphological alteration, membrane disintegration and wrinkling were witnessed for the bacteria that came in contact with HGCS (Figure 4.8). Further, no indication of bacterial-biofilm formation was observed on interaction with the HGCS surfaces. Thus, such surfaces could be applied for the prevention of surgical infections caused by this bacterium. Further, MIC was determined for HGCS against *S. aureus*, *E. coli* and *C. albicans*. AgOM exhibited an increase in inhibitory effect as compared to the bare AgNP and M-OMMT. HGCS, however showed subtle decrement in the inhibitory effect which may be due to the slow release of AgNP from the epoxy matrix. An increase in silver content increased the antimicrobial effect. MIC values for the tested microorganisms are presented in Figure 4.9. Significant difference in the MIC values was noticed for the studied materials ($p < 0.05$).

Further, HGCS were incubated with the test strains to monitor the microbial growth in their presence. The CFU per milliliter was counted for each treatment (Table 4.2). A significant decrement was observed in the microbial growth. Reduction of the microbial colonies clearly indicates the profound antimicrobial activity of HGCS. However, a differential effect was witnessed for each microorganism, which is attributed to the different cellular organizations of the microorganisms.

A clear indication is obtained from the study that the material can be used as a microbial-infection-resistant surface in biomedical applications. Such materials may be

Chapter 4

applied to biomedical implants and devices to prevent acute and chronic infections after scrutinizing their compatibility with *in vivo* system.

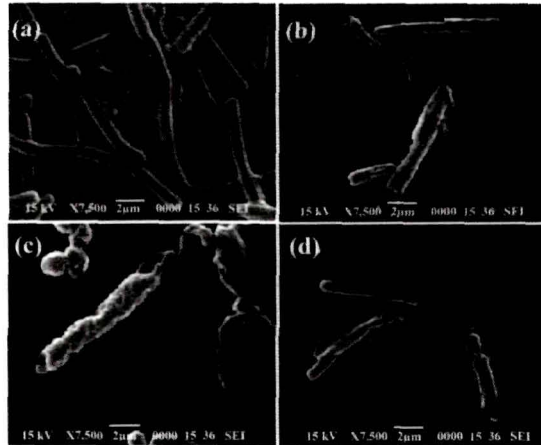


Figure 4.8: SEM images of *E. coli* cells incubated with (a) HGE5, (b) HGCS1, (c) HGCS3 and (d) HGCS5

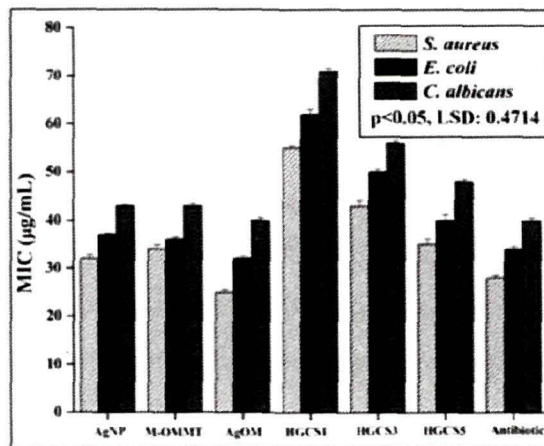


Figure 4.9: MIC values against *S. aureus*, *E. coli* and *C. albicans*

Table 4.2: Antimicrobial activity (CFU mL⁻¹)

Microorganisms	AgOM	HGCS1	HGCS3	HGCS5	Control
<i>S. aureus</i>	2.6×10^4	1.8×10^7	1.5×10^6	2.8×10^6	1.0×10^8
<i>E. coli</i>	3.4×10^4	1.4×10^7	1.2×10^6	3.2×10^5	1.0×10^8
<i>C. albicans</i>	2.8×10^4	2.1×10^7	1.9×10^6	3.5×10^5	1.0×10^8

Chapter 4

4.3.7. Wound healing analysis

Wound healing was monitored *in vivo* by analyzing the image of the wound area. The wound area shrank with time in the scaffold treated as well as untreated group. However, infection was observed in the latter one. Efficient antimicrobial activity of HGCS5 scaffold prevented infections at the wound sites. This is quite obvious because of the proficient activity of the material against the microbes responsible for surgical infections. Complete healing was acquired within 21 days from implantation in the treated group. The percentage of wound contraction is presented in Table 4.3. The results ascertained that the scaffold helped in early healing of the wound. Reconstruction of skin with time can be clearly visible from Figure 4.10.

Adherence of skin tissues over the implanted scaffold was observed after 21 days of implantation. The scaffold was taken out from the sacrificed rat and fixed in glutaraldehyde (2.5%). This was then observed under a scanning electron microscope (Figure 4.11). The image showed adherence of cells over the scaffold surface. Cell attachment was excellent on the matrix. The rough surface with porous structure of nanoclay helps the cells to anchor on. There was no infiltration of inflammatory cells on the material. This signifies the potential of HGCS5 as an implantable skin tissue scaffold. HGCS5 thus provides a compatible surface for the growth of skin cells, which is a prime criterion for implantable scaffold materials.

Table 4.3: Percentage of wound contraction

Days	Healed wound area (%)	
	Treated	Untreated
0	0	0
7	51±2.57	19.76±0.82
14	96±2.61	55.24±1.60
21	99.1±2.31	72.4±0.98

4.3.8. Hematological and histopathological examinations

Hematological parameters recorded after 21 days of implantation are presented in Table 4.4. The results indicate that the parameters are within the normal range in case of HGCS5

Chapter 4

treated rats. These observations suggest that no immune response was generated after implantation of the material. However, in case of the untreated group, a clear increase in the levels of monocytes and eosinophils was observed. This is due to infection at the wound sites. Other parameters also did not show much difference.

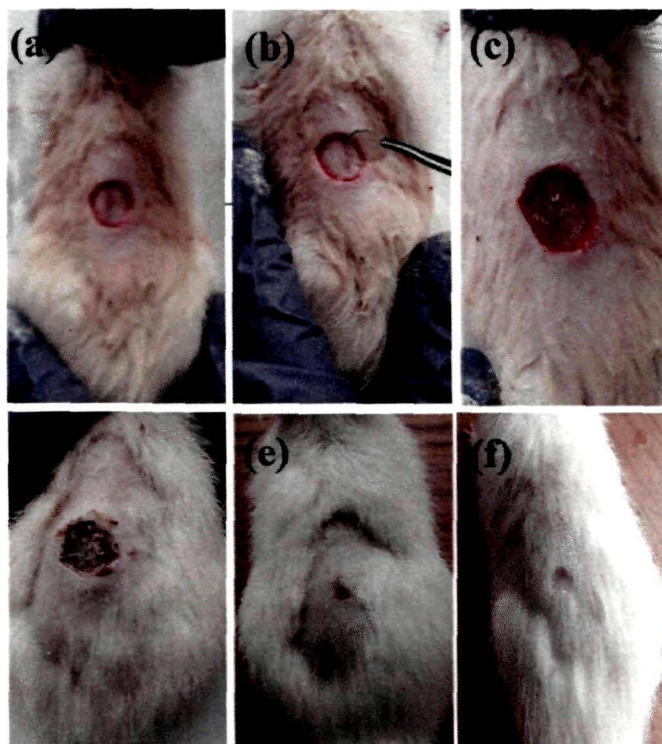


Figure 4.10: (a) Creation of wound, (b) HGCS5 scaffold implantation and wound contraction on (c) 0 day, (d) 7 days, (e) 14 days and (f) 21 days

Wound healing involves different phases such as inflammation, tissue granulation and reconstruction.²⁵ This is termed as hypertrophic scarring in the literature, which causes increased collagen production. Fibroblasts are mainly responsible for collagen production. This leads to fibrosis and reconstruction of the skin starts. In this process the present scaffold acts as an extracellular matrix to support the proliferation of the fibroblasts, which in turn help in fast contraction of the wound. At 7 days after surgery the presence of inflammatory cells was evident from the skin section (Figure 4.12). It was observed that during that time, re-epithelialization was not completed and a disrupted dermis and epidermal layers were seen. After 2 weeks, a loosely packed dermis was visible. Re-

Chapter 4

epithelialization was in progress and immature hair follicles started to develop. A regularly packed dermis and complete regeneration of the epidermis were seen at the 21st postoperative day. This section also shows neovascularization, mature hair follicles and intact epidermis. Vascularization helps in carrying the essential nutrients to the wound site and harnesses the healing process. The histological study thus supports the wound contraction analysis presented in Table 4.4.

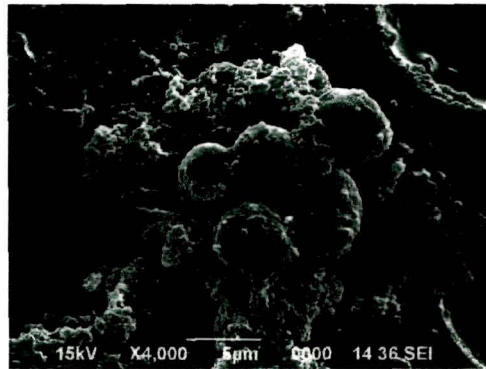


Figure 4.11: SEM image, showing the adherence of dermatocytes on the surface of HGCS5

Table 4.4: Hematological parameters after 21 days of implantation

Parameters	Treated	Untreated	Normal range
Lym (%)	74.28±0.87	78.34±0.34	65-85
Mon (%)	4.5±0.43	9.8±0.54	0-5
Neu (%)	10.75±0.12	9.5±0.52	9-34
Eo (%)	4.6±0.56	12.9±0.29	0-6
Ba (%)	0.4±0.45	0.3±0.87	0-0.7
RBC (m/mm ³)	9.25±0.18	8.78±0.63	7-10
MCV (fl)	65.7±0.24	63.61±0.55	65-70
Hct (%)	46.32±0.64	45.84±0.94	30-39
MCH (pg)	21.9±0.29	18.65±0.87	22-24
MCHC (g/dL)	32.8±0.95	29.2±0.59	34-37
Hb (g/dL)	13.6±0.68	12.1±0.62	11-18
Pct (%)	1.54±0.18	0.78±0.62	-

Chapter 4

Again, histopathological study of the other major organs set evidence for the *in vivo* compatibility of HGCS5. Representative images of heart, liver and brain sections of the treated animals are shown in Figure 4.13. A fine stained section of heart clearly shows the presence of nuclei and intercalated disc without any damage. Similar observation was made for the liver section, where portal veins, sinusoids and hepatocytes are clearly distinguishable. A normal arrangement of the nerve cells was observed, which showed that the material did not induce neurotoxicity in the host.

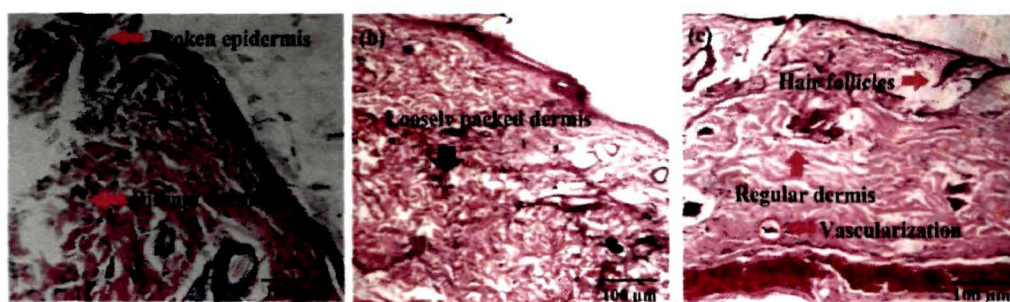


Figure 4.12: Hematoxylin and eosin stained histopathological sections of skin, showing contraction of the wound at (a) 7 (b) 14 and (c) 21 days after surgery

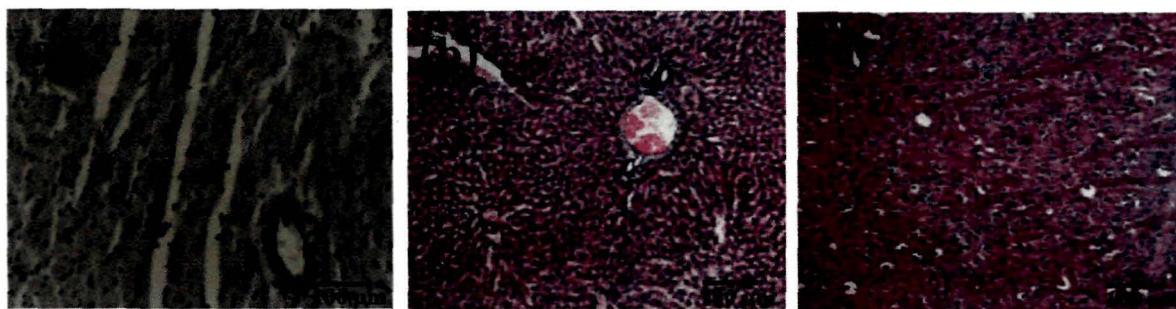


Figure 4.13: Representative histopathological sections of HGCS5 treated rats: (a) heart, (b) liver and (c) brain

4.4. Conclusion

‘Green nanotechnology’ and ‘nanotoxicology’ are two important areas of nanomaterial research. Herein, the colloidal AgNP were prepared through greener routes with desirable material features (e.g., good stabilization within narrow size spectrum) and profound biomedical implications. Further, a high performance, biocompatible HGE5/clay-AgNP NC

Chapter 4

is projected here as an implantable skin scaffold. The scaffold provided an infection-resistant surface which could prevent the growth of pathogenic microbes at the wound site. Biocompatibility of the material was established by *in vitro* and *in vivo* toxicity analyses. Furthermore, HGCS5 helped in wound healing by supporting skin reconstruction in wistar rat. The study showed that the reported material may find utility as a microbial-infection-resistant tissue scaffold or can modify the surfaces of conventional implants.

References

1. Percival, S.L., et al. *Int. Wound J.* **4** (2), 186--191, 2007.
2. Tuan, T.Q., et al. *J. Hazard. Mater.* **192** (3), 1321--1329, 2011.
3. Sondi, I. & Salopek-Sondi, B. *J. Colloid Interface Sci.* **275** (1), 177--182, 2004.
4. Zhang, Y., et al. *J. Colloid Interface Sci.* **325** (2), 371--376, 2008.
5. Kumar, V. & Yadav, S.K. *J. Chem. Technol. Biotechnol.* **84** (2), 151--157, 2009.
6. Rai, M., et al. *Biotechnol. Adv.* **27** (1), 76--83, 2009.
7. Naser, B., et al. *Alternat. Med.* **2** (1), 69--78, 2005.
8. Vasilev, K., et al. *Nano Lett.* **10** (1), 202--207, 2010.
9. Roy, B., et al. *Bioresour. Technol.* **127**, 175--180, 2013.
10. Ahmed M.B., et al. *Am. J. Appl. Sci.* **6** (11), 1909--1914, 2013.
11. Shameli K., et al. *Int. J. Nanomed.* **5** (1), 1067--1077, 2010.
12. Shameli K., et al. *Int. J. Nanomed.* **5** (1), 875--887, 2010.
13. Schierholz, J.M. & Beuth, J. *J. Hosp. Infect.* **49** (2), 87--93, 2001.
14. de Mel, A., et al. *J. Biomed. Mater. Res. A* **100** (9), 2349--2349, 2012.
15. An, J., et al. *Polym. Int.* **59** (1), 62--70, 2010.
16. Dohmen, P.M. *J. Hosp. Infect.* **70** (1), 15--20, 2008.
17. Upadhyay, A., et al. *J. Ethnopharmacol.* **146** (2), 490--494, 2013.
18. Miyoshi, H., et al. *J. Colloid Interface Sci.* **345** (2), 433--441, 2010.
19. Wiley, B.Y., et al. *Chem. Eur. J.* **11** (2), 454--463, 2005.
20. Feng, Q., et al. *J. Biomed. Mater. Res.* **52** (4), 662--668, 2000.
21. Liao, S., et al. *Appl. Microbiol.* **25** (4), 279--283, 1997.
22. Mathew, T.V. & Kuriakose, S. *Colloid Surf. B* **101**, 14--18, 2013.
23. Darouiche, R.O., et al. *N. Engl. J. Med.* **350** (14), 1422--1429, 2004.

Hyperbranched epoxy/silver-reduced graphene oxide-curcumin nanocomposite as an advanced antimicrobial material

Highlights

This chapter deals with the preparation and characterization of a glycerol based hyperbranched epoxy/silver-reduced graphene oxide-curcumin NC. This NC is investigated here as a highly efficient antimicrobial material with potential utility in biomedical devices and implants. Silver-reduced graphene oxide nanohybrid was prepared by simultaneous reduction of graphene oxide and silver salt, using the aqueous extract of *Colocasia esculenta* leaf, wherein curcumin was immobilized sonochemically. The immobilized system was incorporated to the hyperbranched epoxy matrix in 1, 2 and 3 weight%. UV-visible spectroscopy, FTIR, XRD, SEM and TEM analyses ascertained the interaction of the immobilized system with the matrix. Cured thermosets showed superior mechanical behavior as that of the pristine system. *In vitro* and *in vivo* assessments revealed the biocompatibility of the material. Further, the material inhibited the growth of the microorganisms mostly responsible for surgical site infections, by both *in vitro* and *in vivo* studies.

Parts of the chapter are published in

Barua, S., Thakur, S., Aidew, L., Buragohain, A.K., Chattopadhyay, P. & Karak, N. *RSC Adv.* **4** (19), 9777--9783, 2014.

Barua, S., Chattopadhyay, P., Phukan, M.M., Konwar, B.K., Islam, J. & Karak, N. *RSC Adv.* **4** (88), 47797--47805, 2014.

Chapter 5

5.1. Introduction

Microbial biofouling is a serious problem associated with biomedical devices, implants, marine coatings, food packaging materials etc. Formation of microbial biofilms over biomedical devices and implants causes severe infections at surgical sites.¹ Again, surfaces that are regularly in contact with the aquatic environment are vulnerable to the growth of marine algae, microorganisms etc. which causes severe crisis in marine industry. Hence, it needs proper attention to find a suitable way to address such problems. Antimicrobial thin films and surfaces with differential properties have been designed to tackle the abovementioned inconvenience.²⁻⁴ Use of metals in such thin film applications was preferred till the last decade.^{5, 6} However, induction of toxicity to non-target organisms restricted their uses.

On the contrary, biocompatible metal nanoparticles based thin film with efficient antimicrobial activity may be a good alternative to the conventionally used systems. Chapter 4 shows the competence of AgNP in this regard. Interestingly, AgNP prepared via 'greener' routes were found to be compatible with the eco-system.⁷ However, incorporation of metal nanoparticles into a polymeric system rarely contributes to the mechanical strength of the system.⁸ Thus, carbon based nanomaterials like CNT, graphene etc. may be considered to enjoy the twin goals of efficient antimicrobial activity and high mechanical attributes. Limited literature demonstrated the augmentation of thermo-mechanical properties of graphene based epoxy NC as to that of the pristine polymer.⁹

Graphene has recently been added to the family of nanomaterials. Being a nano-dimensional carbon based material; its compatibility with biological systems may be interesting and relevant to investigate. Outstanding attributes of graphene, including antimicrobial activity, are also present in RGO.¹⁰ There are several reports on the preparation of RGO by direct reduction of graphene oxide (GO), using different reducing agents like sodium borohydride, hydrazine, hydroquinone etc.¹¹⁻¹³ Retention of trace amount of the reducing agents may be toxic to biological systems. In this context, attempts have been made to use benign materials, such as aqueous leaf extracts.¹⁴ Recently, RGO has also been used to sequester some metal nanoparticles to obtain materials with multifaceted attributes.¹⁵

Chapter 5

Amongst different metal nanoparticles, AgNP have been widely used for various material and biomedical applications.¹⁶ Antimicrobial potency of these nanoparticles has attained copious attention of the scientific community.¹⁷ Therefore, it was considered worthwhile to obtain a RGO-silver nanohybrid (Ag-RGO) to study whether there would be any synergistic effect with respect to the antimicrobial potency of the material. In this respect, the simultaneous reduction of GO and silver salt was reported in literature.^{18, 19} Liu et al. recently reported the preparation of metal nanoparticles decorated with graphene by liquid phase exfoliation at 150 °C.¹⁰ Baby and co-workers also synthesized similar material by using a mixture of NaBH₄ and NaOH as the reducing agents.¹⁷ Further, Xu et al. projected an idea for preparing a silver decorated graphene oxide NC at 60 °C.¹⁸ On the contrary, the present method proposes the use of an aqueous plant extract as the reducing agent, which could simultaneously reduce GO and silver salt under ambient conditions.

Further, immobilization of biomolecules onto nanomaterials confers interesting attributes to the resulted system. Here, curcumin would be immobilized onto Ag-RGO (Ag-RGO-Cur) which is expected to enhance antimicrobial efficacy of the system. Curcumin is a traditionally known molecule of turmeric (*Curcuma longa*), a natural preservative and ingredient of common food items that possesses tremendous antimicrobial activity.²⁰

From the previous chapters, it is abundantly clear that HGE5 has immense potential as a biomaterial. Thus, it would be interesting to study the biocompatibility and antimicrobial activity of HGE5/Ag-RGO-Cur NC which would endorse the material for advanced biomedical applications.

5.2. Experimental

5.2.1. Materials

Graphite flakes (60 mesh, 99% purity) were procured from Loba Chemie, India. Graphite is the most stable allotrope of carbon under ambient conditions. It has a planer structure arranged in honeycomb fashion. Two common forms of graphite are hexagonal and rhombohedral, both of which are highly thermostable. It has broad utility in batteries, lubricants, steel industries, composites etc. Here it was used as the precursor for RGO.

Chapter 5

The extract was prepared by stirring 2 g of finely ground *Colocasia esculenta* leaves (collected from Tezpur University campus, Assam, India) in 25 mL of water at 50 °C. Subsequent filtration by a muslin cloth yielded the aqueous leaf extract. This extract was used for the simultaneous reduction of GO and AgNO₃.

Turmeric was sun dried and ground to powder. Curcumin was extracted from 25 g of turmeric powder using solvent (toluene) extraction technique.²¹ Obtained curcumin was dried at room temperature. Curcumin structure consists of aromatic ring systems such as phenols, connected by two α , β -unsaturated carbonyl groups. It has shown significant effect against pancreatic cancer, colon cancer, arthritis, myelodysplastic syndromes and Alzheimer's disease, Here it was used as an antimicrobial agent.

The chemicals and reagents like glycerol, BPA, epichlorohydrin, THF, toluene, sodium hydroxide, poly(amido amine) etc. were of the same grade as mentioned in Chapter 2, section 2.2.1 and Chapter 3, section 3.2.1.

To assess the compatibility of Ag-RGO with mammalian peripheral blood mononuclear cells (PBMC), goat blood was collected in a citrated container. For *in vitro* biocompatibility assessment of the NC, William medium, low-glucose DMEM medium, MTT etc. were taken as mentioned in Chapter 2, section 2.2.1. For antimicrobial assays, *Staphylococcus aureus* (ATCC 11632), *Escherichia coli* (ATCC 10536), *Candida albicans* (ATCC 1023) and *Chlorella* sp. MP-1 (Genbank entry KJ499988) were taken as the test microbes. Required agar and media such as Luria Bertani broth, Potato Dextrose broth and agar (HiMedia, India), Bold Basal medium etc. were provided by the Department of Molecular Biology and Biotechnology, Tezpur University, Assam.

5.2.2. Animals

Wistar rats (male) used for *in vivo* compatibility assessment of the materials, were provided by the Laboratory Animal Resources, Division of Pharmaceutical Technology, Defence Research Laboratory, Tezpur, Assam, India as described in Chapter 3, section 3.2.2.

5.2.3. Instruments

Chapter 5

UV-visible, FTIR, XRD, SEM and TEM analyses were carried out under the same conditions as stated in Chapter 4, section 4.2.3, by using the same instrumental specifications.

Mechanical properties like tensile strength and elongation at break as well as lap shear tensile adhesive strength of the prepared NC were evaluated by using the UTM and procedures, as mentioned in Chapter 2, section 2.2.2. For the tests, samples were prepared as described in the section. Bending, impact resistance and scratch hardness of the NC were measured under the same conditions as described in that section by using the same instruments.

5.2.4. Methods

5.2.4.1. Preparation of Ag-RGO

GO was prepared by a modified Hummers method from graphite.¹⁴ GO (50 mg) was well dispersed in 100 mL of distilled water by ultrasonication for 20 min. Ten milliliters of the aqueous extract of *C. esculenta* leaves was added into the solution with constant stirring by a magnetic stirrer. After 10 min, 0.01 M AgNO₃ solution was added to the reaction vessel and allowed to stir for another 8 h under the same reaction conditions. On completion of the reduction, Ag-RGO settled down and it was washed several times with distilled water to remove undesired residual components followed by vacuum drying. For comparison, AgNP and RGO were separately prepared by using the same extract under ambient conditions.

5.2.4.2. Preparation of Ag-RGO-Cur

Ag-RGO (0.5 g) was dispersed in 15 mL of THF by sonicating it for 15 min. An amount of 0.25 g of curcumin was dissolved separately in 5 mL of THF and added to the above dispersion. The dispersion was stirred at room temperature for 4 h, followed by 30 min of ultrasonication (amplitude: 60% and cycles: 0.5). It was then centrifuged for 15 min at 1006 × g (3000 rpm) and the supernatant (in THF) was discarded. The process was repeated to discard the undesired components. The immobilized system (Ag-RGO-Cur) was collected and allowed to dry at room temperature.

Chapter 5

5.2.4.3. Preparation of the NC

Ag-RGO-Cur was dispersed in THF and incorporated into HGE5 resin in 1, 2 and 3 weight%, separately. The mixture was stirred at 50 °C for 4 h. Then, it was ultrasonicated for 15 min in each case under the same conditions as stated earlier. Prepared NC were coded as HGGs1, HGGs2 and HGGs3 for 1, 2 and 3 weight% of Ag-RGO-Cur respectively. The prepared NC are collectively termed as HGGs in this chapter.

5.2.4.4. In vitro biocompatibility assessment

To assess the compatibility of the nanomaterials with mammalian PBMC, goat blood was collected in a citrated container and diluted to 1:1 ratio with PBS. The suspension was centrifuged at 3000 rpm (400 × g) for 15 min. Without disturbing the interface, plasma-PBS was carefully removed and diluted to 20 mL in a serum free RPMI-1640 medium. The PBMC were cultured in RPMI-1640 in a 6 well plate (1 × 10⁵ cells per well). Samples were added to the wells and the plate was incubated in a CO₂ incubator for 24 h at 37 °C. Cells were stained with trypan blue and counted on a hemocytometer. PBMC without sample was used as controls. To evaluate the cell viability in the cultured PBMC, an MTT assay was performed. Twenty microlitres of a sterile MTT solution in PBS was added into each well. Formation of formazan crystals was observed after 4 h of incubation. These crystals were dissolved in DMSO and absorbance was measured at a wavelength of 540 nm on an ELISA plate reader (Thermo Scientific, India). Relative cell viability (%) was calculated by the formula mentioned in Chapter 2, section 2.2.3.4.

Biocompatibility of HGGs was assayed with wistar rat primary heart cell line following the same protocol as described in Chapter 2, section 2.2.3.4.

5.2.4.5. In vivo biocompatibility assessment

In vivo toxicity was assessed by implanting HGGs3 films (10 mm × 10 mm × 0.25 mm) subcutaneously into wistar rats (number, n= 6). Rats (n=6) without implants were kept as control. Two vital factors of the implanted rats were taken under consideration. Blood parameters and histomorphological changes were studied as stated in Chapter 3, section 3.3.4.4. Further, liver function, lipid and kidney profiles were tested by collecting the blood serum after 30 days of implantation. Blood samples were collected in vacuum blood

Chapter 5

collection tubes (Peerless Biotech, India). The tubes were allowed to stand at room temperature and serum was collected by centrifugation at 3000 rpm ($400 \times g$) after the blood had clotted. Serum biochemistry was examined in a Coralyzer-100 (Tulip Diagnostics, India) with the help of commercially available biochemical kits.

5.2.4.6. Antimicrobial assays

MIC of the nanomaterials against the mentioned strains was determined using a micro-dilution technique. Stock solutions (20 mg mL^{-1}) were prepared for the samples. These were then diluted with 1% DMSO to obtain concentrations ranging from $1\text{-}40 \text{ }\mu\text{g mL}^{-1}$. Samples ($100 \text{ }\mu\text{L}$) were added in the wells in various concentrations. Again, $100 \text{ }\mu\text{L}$ of the microbial inocula, corresponding to 10^7 CFU per mL, was added to each well. DMSO (1%) was taken as the negative control and streptomycin and nystatin were taken as the positive controls. The assay was carried out according to the procedure described in Chapter 3, section 3.3.4.5.

Again, the zones of inhibition for the microorganisms were measured by incubating with the nanomaterials according to the protocol explained in Chapter 4, section 4.3.4.5.

MIC of HGGS was estimated against *S. aureus* and *C. albicans*. Moreover, the efficacy of the thermosets was determined by monitoring the microbial growth profiles in their presence. *S. aureus* and *C. albicans* were cultured in 15 mL test tubes in Luria Bertani (LBB) and Potato Dextrose broth (PDB) respectively. Tubes were incubated for 24 and 48 h respectively. Absorbances were recorded at 600 nm for bacteria and 620 nm for fungi to observe the absorbance variations in the growth profiles of the tested microorganisms. Similar test was also carried out for the microalgae, *Chlorella* sp. by culturing it in Bold's Basal Medium (BBM) followed by 15 days of incubation.

Another assay was carried out to examine their growth in the proximity of HGGS surface. The bacterial and fungal strains ($100 \text{ }\mu\text{L}$) were spread over solidified agar, while $500 \text{ }\mu\text{L}$ (exponentially growing microalgal culture, 82×10^6 cells per mL) of the fresh microalgal suspension was spread over solidified BBM. A piece ($10 \text{ mm} \times 10 \text{ mm} \times 0.25 \text{ mm}$) of the most effective HGGS was laid on the plates just before solidification. Plates were kept in an incubator for 24 and 48 h respectively for *S. aureus* and *C. albicans*. The

Chapter 5

microalgal plates were incubated for 15 days. Growth of microorganisms over the films was monitored by the images captured by a Nikon Coolpix-S3000 camera.

Again, *S. aureus* was considered as the representative microbe to ascertain the efficacy of HGGS under *in vivo* condition. A 2 cm incision was made on the dorsal side of rats of two groups (n=6, in each group). In one group, HGGS3 films were implanted and the other group was closed as such by suturing. Inoculum of *S. aureus* (10^7 CFU mL⁻¹) was cultured overnight in LBB and applied to the surgical area of each group by swabbing with sterile cotton. After 24 h, a piece of moist cotton was used to swap the surgical area and it was dipped in LBB. The cotton was removed subsequently, after shaking the media with a vortex shaker. This was tested for CFU mL⁻¹ count to ensure the total microbial colonies.²² After 3 days, the animals were sacrificed and a small portion was taken from the surgical area to analyze the presence of microbes. The skin sample was fixed in 2.5% gluteraldehyde solution and dehydrated in alcohol (70-100%). SEM micrographs were taken to see the inhibitory effect of HGGS3 on *S. aureus*.

5.2.4.7. Statistical analysis

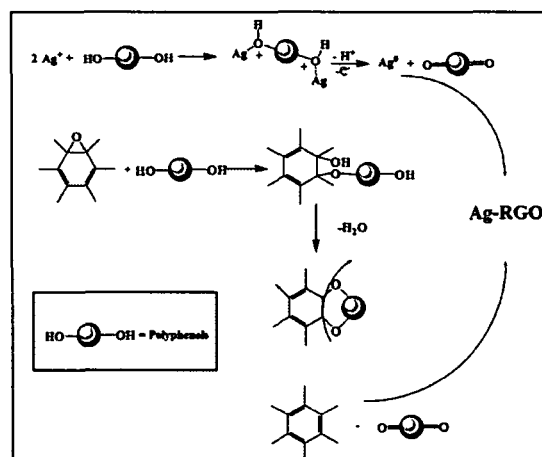
Obtained results were presented as mean±SD, from triplicate data. One or two way ANOVA was carried out to determine the LSD amongst the data.

5.3. Results and discussion

5.3.1. Preparation of Ag-RGO

In the previous chapter, preparation of AgNP was demonstrated by utilizing the aqueous extract of *T. occidentalis* leaf. In this study, endeavor was made to prepare an Ag-RGO nanohybrid by a single step method using the aqueous leaf extract of *C. esculenta* as the reducing agent. The extract is a natural source of many polyphenolic compounds.²³ As described in the last chapter, these compounds have an affinity to form complexes with metal ions. The mechanism of reduction of silver salt was described in Chapter 4, section 4.3.1. Simultaneous reduction of GO and silver salt is schematically presented in Scheme 5.1. The present method depicts a greener and sustainable process, which is also cost effective one for the preparation of such nanohybrids.

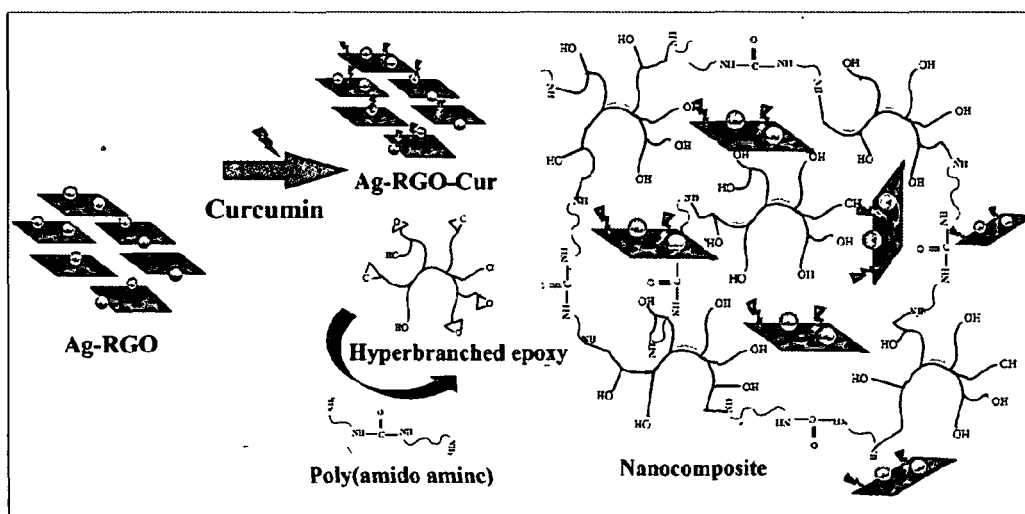
Chapter 5



Scheme 5.1: A probable mechanism for the simultaneous reduction of GO and Ag^+ by the *C. esculenta* leaf extract

5.3.2. Preparation of HGGS

In the present investigation, interest was drawn to immobilize curcumin on the surface of Ag-RGO. Structure of curcumin possesses aromatic and aliphatic unsaturation, which helps to interact with RGO by π - π electronic stacking.²⁰ Thus, it holds a strong binding with Ag-RGO. Ultrasonication is an efficient ‘green’ tool for immobilization of biomolecules onto nanomaterials. The immobilized system again interacts with HGE5 via surface hydroxyl functionalities and by π -electron affinity. This provides adequate stability to HGGS which would be reflected in their performance in regard of mechanical attributes and antimicrobial efficacy. The preparative protocol of HGGS is presented in Scheme 5.2.



Chapter 5

Scheme 5.2: Preparative protocol of HGGS

5.3.3. Characterization

5.3.3.1. UV-visible spectroscopy

UV-visible spectroscopy is an important tool to characterize nanomaterials, which is governed by the response of the electrons present in the nanomaterial surface to the incident UV radiation. Here UV-visible spectra demonstrated clear evidence of the simultaneous reduction of AgNO_3 and GO. Characteristic peaks for GO were observed at 228 nm and 302 nm, which are due to the $\pi\text{-}\pi^*$ and $n\text{-}\pi^*$ electronic transitions of the aromatic C=C bond and C=O bond respectively (Figure 5.1).¹⁴ A red shift was observed for the first peak at 265 nm after formation of Ag-RGO. This confirms the restoration of the electronic conjugation after reduction of GO to RGO. A peak at around 429 nm in the spectrum of Ag-RGO was observed, which indicates the formation of AgNP.

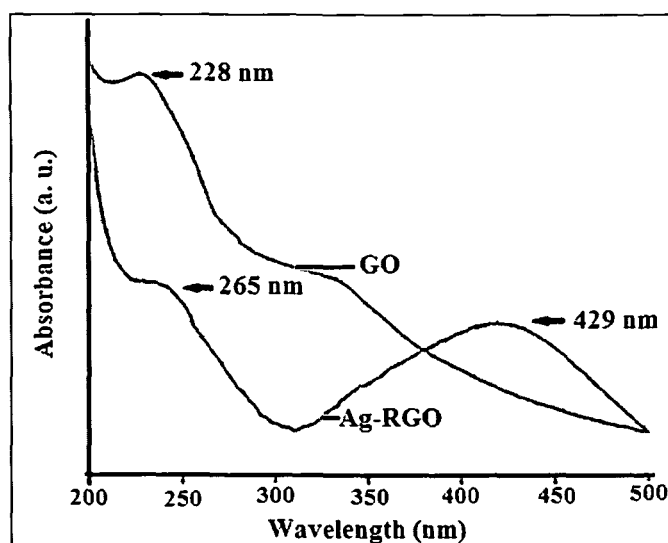


Figure 5.1: UV-visible spectra of GO and Ag-RGO

Again, UV-visible spectrum of bare curcumin showed a broad peak at around 418 nm (Figure 5.2 a), which upon deconvolution split to three peaks at 400, 418 and 439 nm (Figure 5.2 b). Characteristic peaks at 408 and 330 nm were observed for Ag-RGO. The second peak is due to the $n\text{-}\pi^*$ electronic transitions of the aromatic C=C bond of RGO.¹⁴ In case of Ag-RGO-Cur, the total peak area was broadened. This upon deconvolution showed four peaks at 388, 402, 422 and 441 nm. The surface plasmon peak of AgNP in Ag-

Chapter 5

RGO-Cur showed a blue shift from 408 to 388 nm, which is because of the oxygenous groups present in the curcumin structure (Figure 5.2 c).²⁴ This clearly indicates the interaction of curcumin with Ag-RGO. Similarly the peaks at 338 and 419 nm indicates the presence of Ag-RGO-Cur in HGGS (Figure 5.2 d).

5.3.3.2. FTIR study

FTIR spectra of GO and Ag-RGO are shown in Figure 5.3 a. Presence of the bands at 1049 (C–O stretching), 1224 (C–O–C stretching) and 1720 cm^{-1} (C=O stretching) with the broad band at around 3400 cm^{-1} (–OH stretching) confirmed the presence of carbonyl, carboxylic, epoxy and hydroxyl moieties in GO.¹⁴ Removal of these oxygen-containing moieties of GO in Ag-RGO are clearly reflected by the absence of the aforementioned bands. Relative decrease in the intensity of the broad band at 3400 cm^{-1} for the hydroxyl group is attributed to the successful reduction of GO.

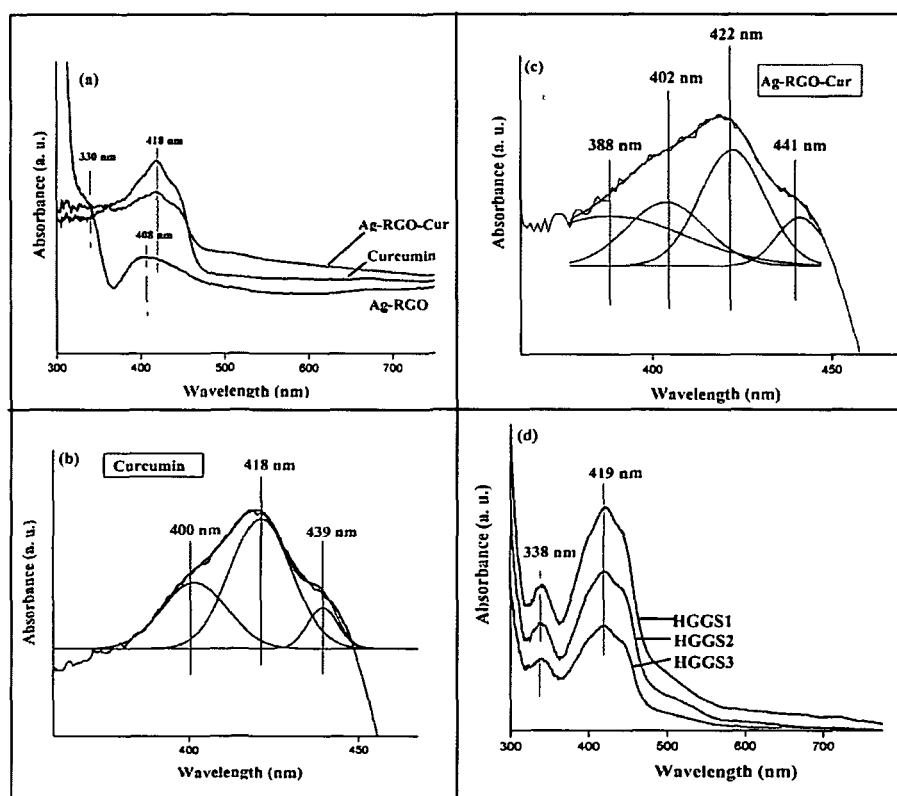


Figure 5.2: (a) UV-visible spectra of curcumin, Ag-RGO and Ag-RGO-Cur, (b) deconvoluted spectrum of curcumin, (c) deconvoluted spectrum of Ag-RGO-Cur and (d) spectra of HGGS

Chapter 5

Again, in the FTIR spectrum of curcumin, vital bands were observed at 3420, 1720, 1510, 1286, 1137 and 1033 cm^{-1} . These bands correspond to the $-\text{OH}$, $-\text{C}=\text{O}$, $-\text{C}-\text{H}$, $\text{C}-\text{O}$ groups of curcumin (Figure 5.3 b).²⁵ This confirms the successful extraction of curcumin from turmeric. All these bands are also present in the other spectra which confirmed the presence of curcumin in the immobilized nanohybrid as well as in HGGS3. In case of Ag-RGO-Cur, two characteristic bands were observed at 2871 and 2919 cm^{-1} , which are due to the symmetric and asymmetric vibrations of $-\text{CH}$ groups of the polyphenolic compounds of the plant extract. In the region 3300–3450 cm^{-1} , a broad band was observed which is attributed to the $-\text{OH}$ stretching of curcumin and other polyphenolic compounds. Bands for oxirane ring at around 915 and 839 cm^{-1} confirms the presence of epoxy groups in HGGS3. Contrarily, their absence in the spectra of the cured HGGS3 proves the successful crosslinking of the NC by reacting with poly(amido amine).

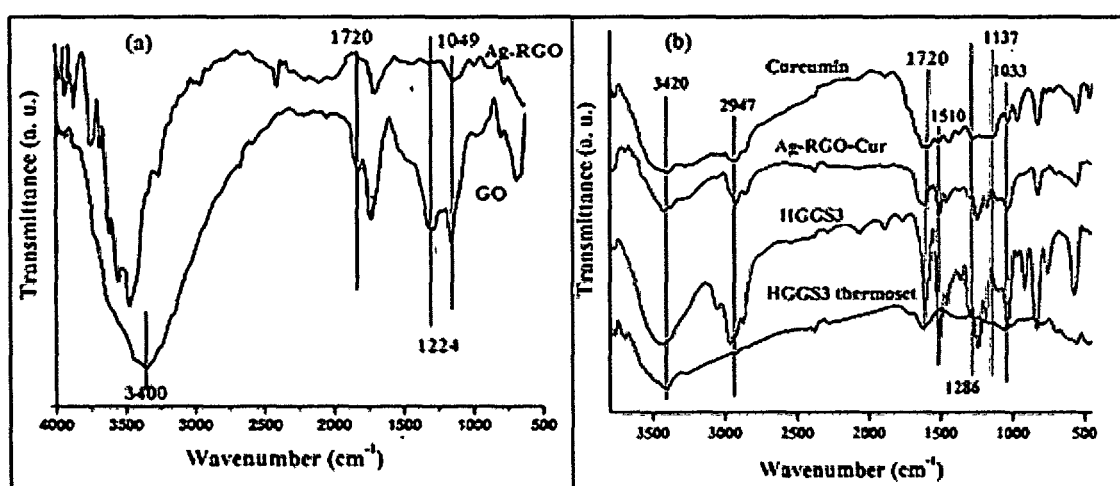


Figure 5.3: FTIR spectra of (a) GO and Ag-RGO and (b) Curcumin, Ag-RGO-Cur and the cured and uncured HGGS3

5.3.3.3. XRD analysis

XRD patterns of Ag-RGO clearly indicated the presence of silver within it (Figure 5.4 a). In Ag-RGO, basal reflection peaks of fcc silver were visible at 2θ positions of 38.4, 44.2, 64.4 and 74.3°, which correspond to the (111), (200), (220) and (311) Bragg lattices (JCPDS 89-3722). This confirmed that AgNP with different average crystallite domain sizes were loaded onto RGO.

Chapter 5

Similar diffraction pattern was observed in case of Ag-RGO-Cur with basal peaks at 2θ values of 37.8 , 44.9 , 64.2 and 76.4° (Figure 5.4 b). This again, ascertained the presence of AgNP within the curcumin immobilized nanohybrid system. Further, literature reports the crystalline nature of curcumin.²⁶ However, in the present case no distinct crystalline peak was visible for curcumin in Ag-RGO-Cur. Interaction of this biomolecule with the nanohybrid is attributed to this fact. XRD patterns of HGGs did not show any characteristic peak as that of Ag-RGO-Cur (Figure 5.4 c). The presence of very low amount of Ag-RGO-Cur in the HGE5 matrix induces a masking effect, which dictates the diffraction behavior. However, amorphous nature of HGE5 can be predicted from the broad peaks at around 2θ value of 20 - 22° in HGGs.

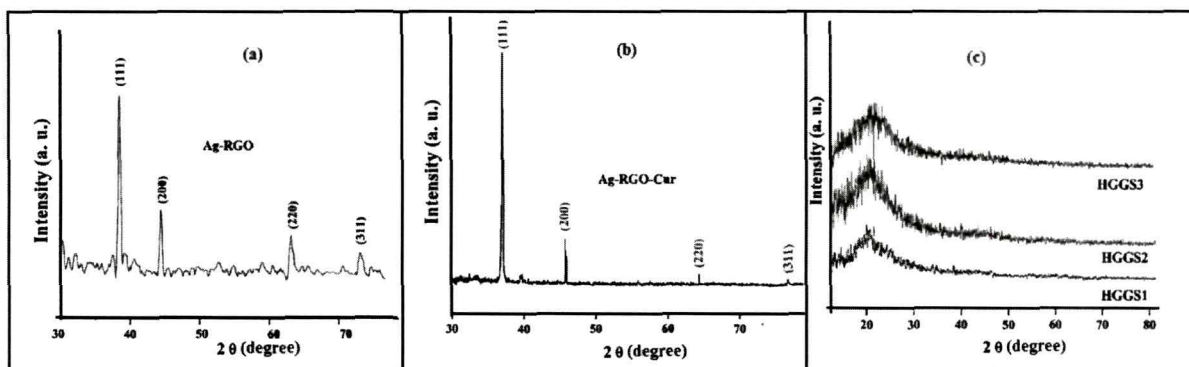


Figure 5.4: XRD patterns of (a) Ag-RGO, (b) Ag-RGO-Cur and (c) HGGs

5.3.3.4. Morphological study

HRTEM images of Ag-RGO are presented in Figure 5.5. These indicate that AgNP with almost spherical morphology were impregnated within the RGO sheets. The histogram shows a narrow size distribution of AgNP; where most of the particles range from 15-20 nm with average particle size of 17.2 nm. A 0.270 nm lattice fringe spacing was observed for the particles, which represents the fcc lattice of AgNP (Figure 5.5 b, inset). It was observed that a nanoparticle was residing between the two sheets of RGO with two different lattice fringe spacings of 0.345 and 0.364 nm.

TEM micrographs of HGGs3 are shown in Figure 5.5 b-d. Narrow size distribution of AgNP was clearly visible from the histogram, where maximum particles lie between 10-15 nm. Moreover, these particles are embedded within the RGO sheets. Again, uniform distribution of Ag-RGO within the HGE5 matrix was witnessed from the micrographs. This

Chapter 5

indicated sufficient interactions between Ag and RGO, which are also retained after immobilization of curcumin. Further, Ag-RGO-Cur strongly interacts with the epoxy matrix. The π - π electron affinity plays the vital role in this case. The micrographs showed no sign of agglomeration of AgNP. Thus, this is validated that anchoring of AgNP onto RGO surface confers stability to the nanoparticles. Again, functionalities of curcumin also aids to the strong interactive forces of the immobilized nanohybrid system towards the hyperbranched matrix. These types of interactions lead to the enhancement of mechanical attributes in NC as well as offers interesting biological activities.

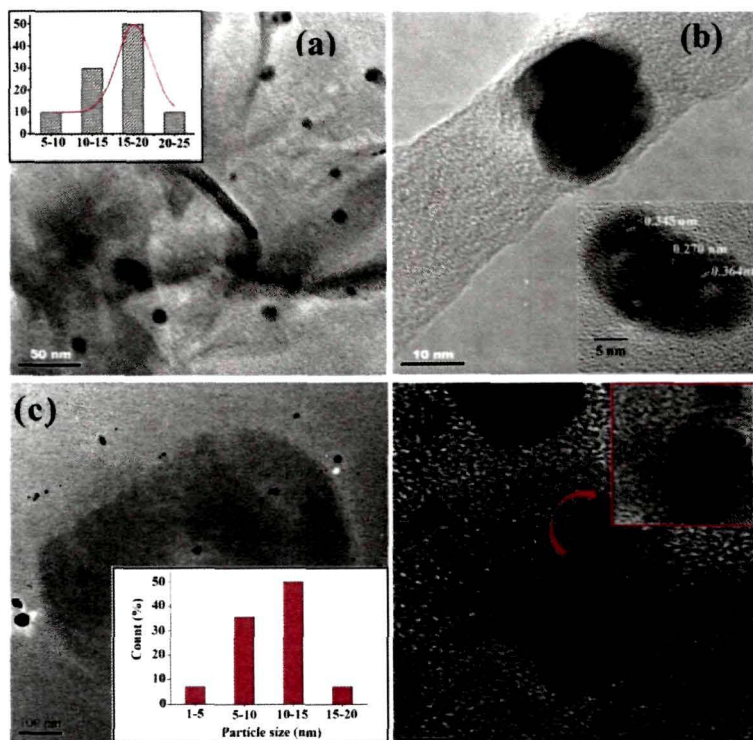


Figure 5.5: HRTEM images of (a) Ag-RGO, Inset: histogram of the size distribution of AgNP, (b) a nanoparticle residing between sheets of RGO, (c) distribution of Ag-RGO-Cur in HGG3 and (d) RGO sheet with lattice fringe spacing of 0.68 nm over AgNP

5.3.4. Curing study and mechanical performance

HGGs were crosslinked at 120 °C and their curing times are given in Table 5.1. Curing time decreased with the loading of Ag-RGO-Cur for HGGs. Hydroxyl groups of curcumin may have taken part in the crosslinking process besides the functionalities of HGE5. That is

Chapter 5

why the aforesaid linear relationship was evident. All the NC showed adequate crosslinking (between 70-80%) which was observed from the swelling values (Table 5.1).

Literature reports that epoxy/graphene NC exhibited augmentation of mechanical properties.²⁷ The data in Table 5.1 reveals the increment of tensile strength of HGGS with increase in loading of Ag-RGO-Cur. Layered RGO sheets embedded with AgNP improved the interfacial interaction with the hyperbranched matrix. As a result, this enhancement of tensile strength was witnessed. Loading of Ag-RGO-Cur however, restricts the epoxy chains due to which elongation at break gets decreased. Beyond this level of loading (3 weight%), phase separation was observed after HGGS were cured. However, the HGGS films could be folded up to a curvature of 180°, without any fracture. Values of scratch hardness and impact resistance were above the instrumental limits (limits of the instruments: impact resistance 1 m, scratch hardness 10 kg). Thus, considering the mechanical attributes, HGGS3 can be considered as the best performing HGGS.

Table 5.1: Curing parameters and performance of HGE5 and HGGS

Property	HGE5 [#]	HGGS1	HGGS2	HGGS3	LSD
Curing time at 120 °C (min)	24±0.58	20.6±1.5	18.6±0.57	15.5±0.5	0.81
Swelling (%)	22.6±0.43	25.1±0.7	23.5±0.12	24.2±1	0.76
Tensile strength (MPa)	38.4±0.84	54.3±0.5	59.6±0.45	65.5±0.3	0.35
Elongation at break (%)	21.3±0.57	20.7±0.6	19.2±0.26	17.7±0.45	0.38
Impact resistance (m)*	>1	>1	>1	>1	-
Scratch hardness (kg)*	>10	>10	>10	>10	-
Bending (mm)*	<1	<1	<1	<1	-
Adhesive strength (MPa)	768	2210±2	2328.6±2.5	2570.6±2.5	31.23

*Instrumental limits: Scratch hardness=10 kg, Impact resistance=1 m and bending test mandrel=1 mm

[#]As reported in Chapter 2, Table 2.2.

Lap shear tensile adhesive strength augmented with increase in the loading of Ag-RGO-Cur. Increase in functionalities on the surface of HGGS is directly attributed to this enhancement. Further, significant differences were noticed for each case ($p < 0.05$).

Chapter 5

5.3.5. *In vitro* biocompatibility test

A material to be used in biomedical field demands compatibility with biological systems. Cytotoxicity of the nanomaterials was evaluated with mammalian PBMC to get a better comparison with *in vivo* systems. These cells are responsible for wound contraction and healing. No alteration of the cell morphology was witnessed when treated with the materials (Figure 5.6). It is quite interesting to note that AgNP, RGO and Ag-RGO proved excellent compatibility with the cells. ‘Green’ route mediated synthetic protocol may have the prime role for such biological activity. Further, MTT assay revealed that the cell survival rate of the treated groups was almost comparable with that of the control (Figure 5.7 a). This test provides evidence for the potential of the nanomaterials for utilization in biomedical applications.

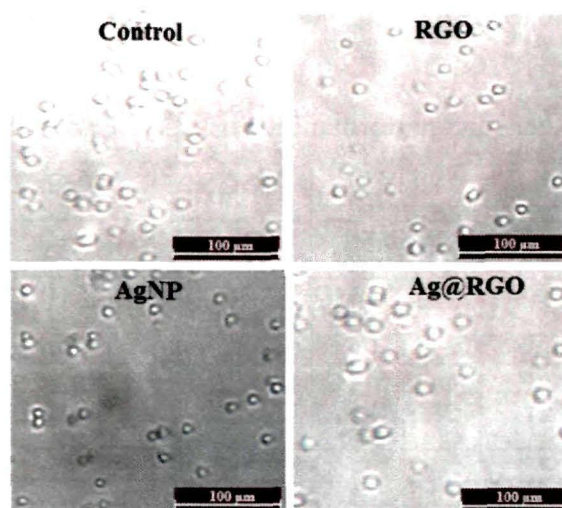


Figure 5.6: Microscopic images of trypan blue stained PBMC (control and treated)

Again, to examine the *in vitro* toxicity of the materials, mammalian primary heart cells were considered. RGO showed 72% compatibility with the cells (Figure 5.7 b). Upon formation of Ag-RGO, this was increased to 83.2%. Again, immobilization of curcumin increased this value to 84.7%, where content of curcumin was 33%. Compatibility of Ag-RGO with mammalian PBMC was observed from the above assay. Further, curcumin is a common ingredient of regular food items. Therefore, Ag-RGO-Cur showed good compatibility with mammalian cell lines (with 66% of Ag-RGO and 33% of curcumin in

Chapter 5

the system). HGE5 possesses good biocompatibility with its glycerol based architecture as evident from the assay described in Chapter 2, section 2.3.9. Thus, HGGs demonstrated more than 89% cell viability. Only subtle difference was observed amongst the three NC, due to small scale loading of Ag-RGO-Cur, as observed from the LSD value ($p < 0.05$). This assay ascertained the *in vitro* biocompatibility of HGGs, which is a primary criterion for a material to be used in biomedical domain. However, for actual endorsement of such materials to the real field, *in vivo* compatibility assessment is a prerequisite.

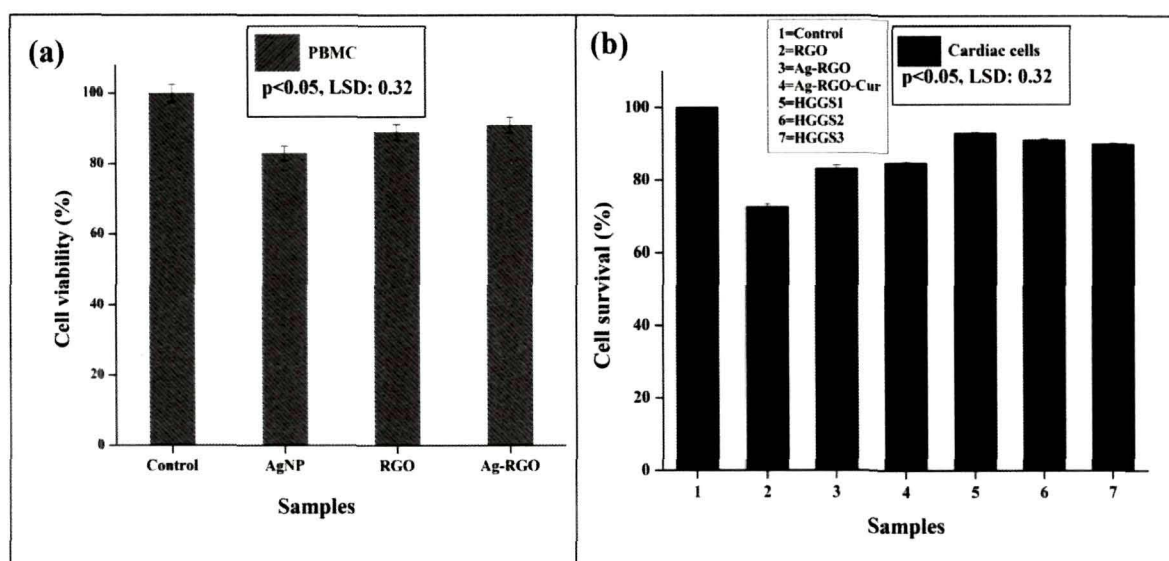


Figure 5.7: Cell survival (%) of (a) PBMC and (b) primary cardiac cell line of wistar rat

5.3.6. *In vivo* biocompatibility test

Hematological parameters regulate different physiological functions of the body. Changes in their values from the normal range may cause heavy damage to the body. Therefore, it is important to check these parameters after implantation of a biomaterial into the host body. Table 5.2 provides a clear picture of the hematological parameters of HGGs3 implanted rats which are nearly comparable to that of the control. However, the parameters suggested initial marginal increment (up to 15 days) in the level of macrophage (matured monocytes), neutrophil or lymphocytes, which is due to the surgery and introduction of the foreign polymeric NC. However, their gradual normalization after 15 days, indicated the immunocompatibility of this material within the host body.

Chapter 5

Further, lipid and kidney profiles and liver function of the implanted rats were determined and compared with the control parameters, by analyzing the serum biochemistry of their blood. Lipid profile (LDL, HDL, Chol and TGL) can help in screening the abnormality of body lipids which can lead to cardiovascular disorder.²⁸ Again, ALT/SGPT and AST/SGOT are the biomarkers of animal liver function. Table 5.3 shows comparable results of lipid profile and liver function test values of the implanted and control rats. Besides, Gluc, urea, UA and Cre values confirms no induction abnormality in the kidney profiles of the rats after implantation of HGGS3.

Table 5.2: Hematological parameters of the control and HGGS3 implanted rats

Parameter	0 day		15 days		30 days	
	Control	HGGS3	Control	HGGS3	Control	HGGS3
Lym (%)	30.1±0.2	28.4±0.5	29.1±0.2	33.6±0.73	30.7±1.22	29.4±0.5
Mon (%)	18.4±0.2	18.2±0.2	19.9±0.2	23.8±0.3	19.5±0.15	19.0±0.2
Neu (%)	59.8±0.5	60.4±0.3	56.3±0.37	66.3±0.15	58.3±0.55	59.5±0.15
Eo (%)	8.6±0.3	7.5±0.26	9.1±0.15	10.1±0.1	7.1±0.15	8.1±0.15
Ba (%)	0.6±0.01	0.7±0.05	0.8±0.05	0.7±0.05	0.7±0.05	0.7±0.05
RBC (m/mm ³)	9.6±0.3	7.8±0.35	9.7±0.34	8.6±0.25	9.3±0.1	8.7±0.36
MCV (fl)	58.3±0.3	56.4±0.41	58.3±0.25	57.2±0.3	59.5±0.26	56.4±0.37
Hct (%)	42.2±0.5	46.5±0.2	46.4±0.26	48.3±0.2	47.5±0.41	46.4±0.3
MCH (pg)	18.6±0.3	16.5±0.2	18.3±0.32	16.4±0.35	17.3±0.15	17.5±0.36
MCHC (g/dL)	31.4±0.5	33.4±0.32	35.5±0.45	35.5±0.36	36.6±0.43	36.5±0.25
Hb (g/dL)	15.7±0.2	16.3±0.28	17.7±0.15	16.2±0.25	18.4±0.15	17.6±0.26
Pct (%)	0.51±0.2	0.55±0.04	0.56±0.03	0.55±0.02	0.61±0.02	0.63±0.03

These findings were further validated by the histopathological studies of the treated rats (Figure 5.8). Skin was taken from the area near the implant. On 7th day of post

Chapter 5

implantation, disrupted striated skin muscles were seen. However, no infiltration of immune cells was visible, which is supported by the hematological parameters.

Table 5.3: Liver function, kidney and lipid profiles of HGG3 implanted rats

Parameter	Control	HGGS3
Low density lipoprotein (mg/dL)	115.8±0.5	118.1±0.81
High density lipoprotein (mg/dL)	47.2±0.80	46.5±0.27
Cholesterol (mg/dL)	39.2±0.32	35.3±0.37
Triglycerides (mg/dL)	9.2±0.2	8.7±0.15
Glucose (mg/dL)	112.5±0.25	110.6±0.2
Urea (mg/dL)	70.7±0.41	69.7±0.35
Total protein (g/dL)	5.7±0.15	6.3±0.5
Uric acid (mg/dL)	1.14±0.05	1.74±0.03
Alanine aminotransferase (U/L)	78.7±0.45	75.5±0.4
Aspartate aminotransferase (U/L)	110.6±0.3	112.3±0.45

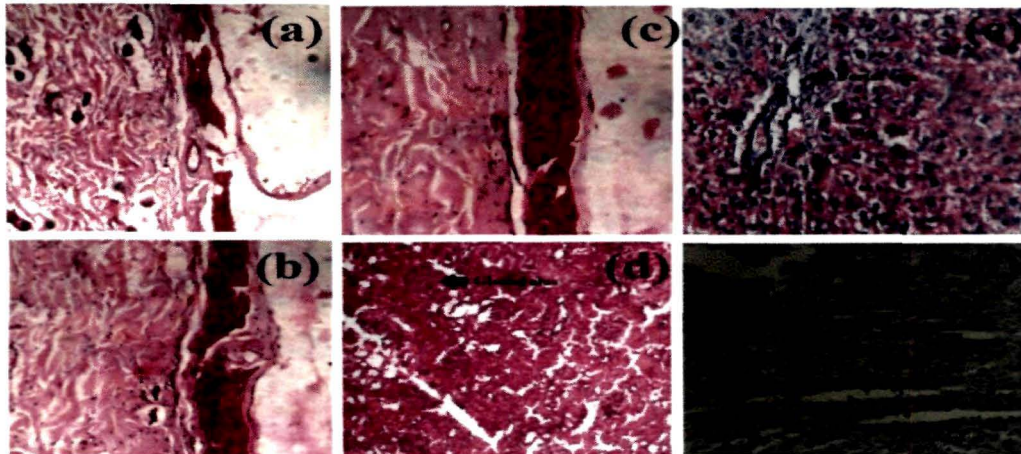


Figure 5.8: Representative histopathological sections of skin (a) 7, (b) 15 and (c) 30 days to post implantation and (d) kidney, (e) liver and (f) heart sections of the implanted rats

The figure also shows the skin sections on 15th and 30th days of implantation. Different epithelial layers are clearly visible in the representative skin sections. Also, the absence of any capsule formation suggested good integration of the material with the

Chapter 5

surrounding host tissues.²⁹ Similarly, liver and kidney sections represent normal cellular organizations like hepatocytes and glomerulus etc. Heart section was observed with regular nuclei and intercalated discs. The overall *in vivo* findings demonstrated the potential utility of HGGS3 in the field of biomedical applications, as an efficient thin film material over implant devices.

5.3.7: Antimicrobial assays

Antimicrobial activity of the nanomaterials was evaluated by calculating MIC values for each microbe (Table 5.4). From the table it can be assumed that Ag-RGO system has greater antimicrobial activity than both of the individual nanomaterials. This is reflected by the lower concentration of Ag-RGO which showed an inhibitory effect to microbial growth. This is due to the fact that Ag-RGO may have wrapped around the microbial cells, resulting in the intimate contact of silver with the microbial cell membranes.¹⁰

Table 5.4: MIC ($\mu\text{g/mL}$) of the nanomaterials against bacteria and fungus

Test Organism	RGO	AgNP	Ag-RGO	Antibiotic
<i>S. aureus</i>	16 \pm 0.83	20 \pm 0.34	12.5 \pm 0.32	8 \pm 0.68
<i>E. coli</i>	21 \pm 0.71	25 \pm 0.51	20 \pm 0.74	10 \pm 0.23
<i>C. albicans</i>	19 \pm 0.56	20 \pm 0.87	16 \pm 0.18	6 \pm 0.65

Zones of inhibition for each microorganism were determined at the MIC values of the nanomaterials (Figure 5.9). Ag-RGO showed higher zones of inhibition than any of the individual nanomaterial. Thus the formation of the nanohybrid possesses advantageous attributes compared to the individual nanomaterials from two perspectives; (1) this prevents the agglomeration of the nanoparticles and (2) it synergistically increases the antimicrobial potency.

Again, MIC was calculated for HGGS against *S. aureus*, and *C. albicans* (Figure 5.10). The above assay demonstrated enhanced inhibitory effect of Ag-RGO over the individual components. Ag-RGO showed MIC against *S. aureus* and *C. albicans* at 12.5 and 16 $\mu\text{g mL}^{-1}$. After immobilization of curcumin, these values were reduced to 7 and 10

Chapter 5

$\mu\text{g mL}^{-1}$ respectively, which showed clear enhancement of antimicrobial activity. Curcumin is a renowned antimicrobial agent found abundantly in nature. Again, immobilization of biomolecules onto the nanomaterial surface increases its efficacy by synergistic effect at bio-nano-interface. Ag-RGO provides a high surface area, which complemented the activity of curcumin. However, in case of HGGs, lower MIC values were observed, which can be attributed to the indirect exposure of the active components to the microbes. Additionally, the significant reduction in the amount of Ag-RGO-Cur with respect to the matrix is also responsible for the above finding. Profound antimicrobial activity was witnessed with increase in the amount of Ag-RGO-Cur in HGGs. HGGs3 showed MIC at 38 and 41 $\mu\text{g mL}^{-1}$ against *S. aureus* and *C. albicans* respectively. Thus, HGGs sufficiently inhibited bacterial and fungal fouling at 3 weight% loading of Ag-RGO-Cur. Statistically significant differences were found in the MIC values, with LSD: 0.81 and p values <0.05 .

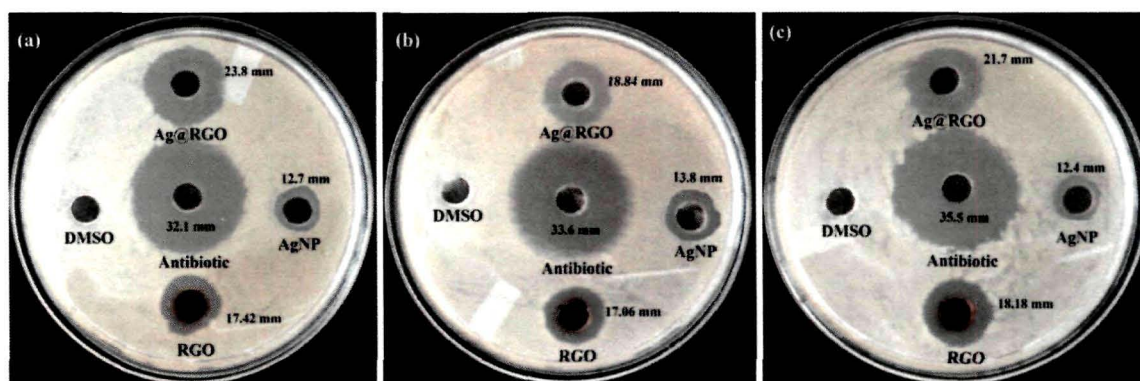


Figure 5.9: Representative antimicrobial activity of the nanomaterials against (a) *S. aureus*, (b) *E. coli* and (c) *C. albicans*

Again, Figure 5.11 indicates clear decrement of the microbial growth with time when incubated with HGGs3 film. Absorbance for *S. aureus* shows exponential growth with time in case of the control. On the other hand, their growth decreases and comes to a steady state in presence of HGGs3. This ascertains that HGGs3 possesses sound antibacterial activity. Similar absorbance profile was witnessed for *C. albicans*. Adherence of microbes to the NC surface causes microbial cell lysis, which leads to a decrease in their population and stops further growth.³⁰ This type of activity is essential for an antimicrobial material, which could prevent infection at surgical sites.

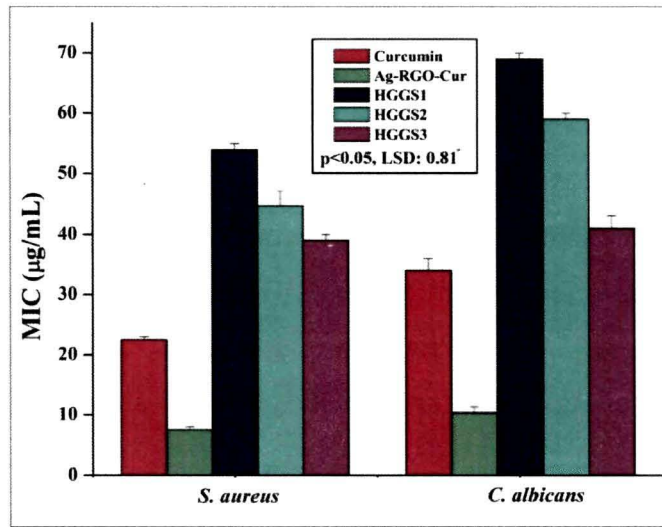


Figure 5.10: MIC against *S. aureus* and *C. albicans*

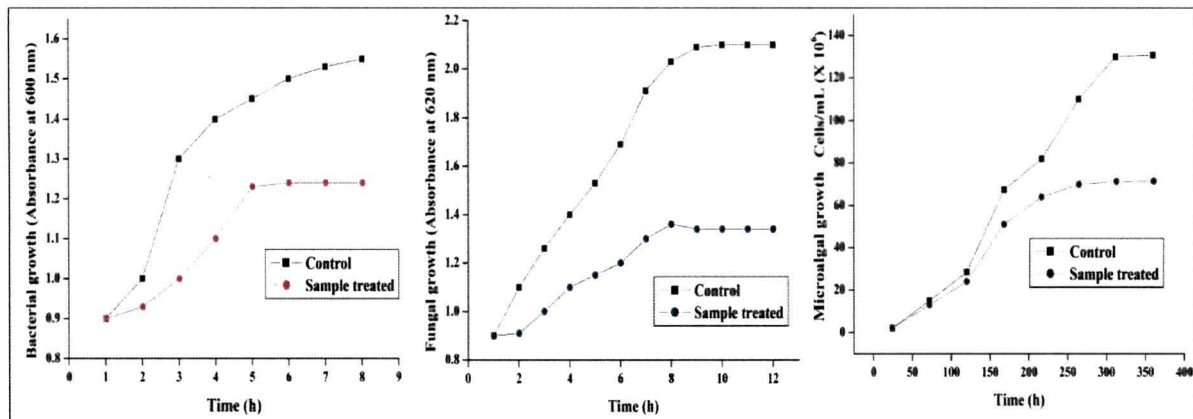


Figure 5.11: Inhibition of growth of (a) *S. aureus* (b) *C. albicans* and (c) *Chlorella sp.* in presence of HGGS3

Unlike bacteria and fungi, the growth of microalgae was not monitored spectrophotometrically. Microalgal growth was recorded by measuring the cell concentration in a Neubauer haemocytometer (in triplicates) at regular intervals of 50 h for 15 days. From Figure 5.11, a gradual decline in microalgal growth is evident. This may be attributed to the fact that the microalgae could not adhere to the HGGS3 surface and deposited at the bottom of the test tubes, whereby demonstrating competitive growth inhibition.³¹ Additionally, the light absorbing capacity of RGO may also help in the prevention of microalgal growth.³²

Chapter 5

Hence, HGGS3 has the potential to provide a surface that could prevent microalgal growth. Marine coatings with such properties may help in resisting the growth of different fouling microalgae.

Moreover, assays were carried out to examine the possibility of microbial growth in the proximity of HGGS3. Figure 5.12 shows clear evidence that neither *S. aureus* nor *C. albicans* could grow on the surface of HGG3 within an area of 1 cm². On the other hand, their uniform growth is visible throughout the rest parts of the plates. Although the microalgal growth is not uniform, no growth is seen on the surface of HGGS3 within an area of 1 cm². Thus, the aforesaid assays confirmed that HGGS3 could prevent the growth of the two most notorious microorganisms responsible for causing infection at surgical sites. This may be utilized to design protective coatings for surgical implants and devices. Moreover, the surface was able to inhibit microalgal fouling over it, which may endorse the same material for utilization in advanced marine coatings.

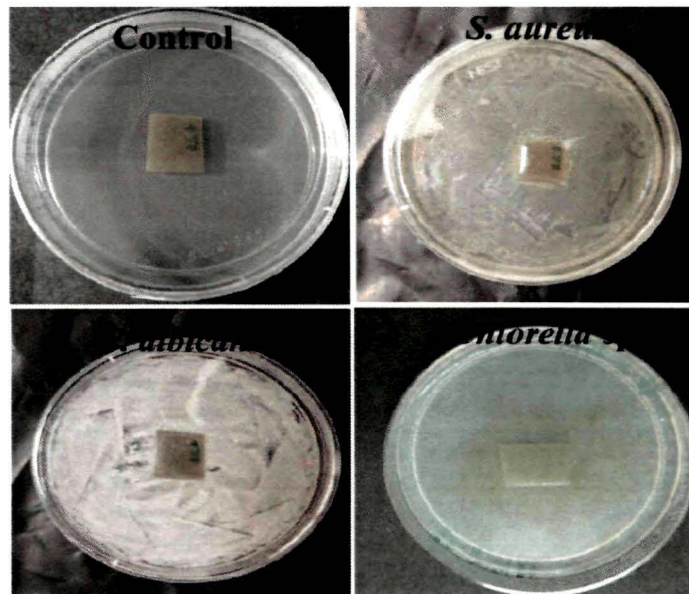


Figure 5.12: Antimicrobial activity of HGGS3 in the proximities of *S. aureus*, *C. albicans* and *Chlorella* sp.

Again, *in vivo* antimicrobial activity was analyzed, where no infection was evident visually in the HGGS3 implanted rats, while un-implanted rats faced severe infection (Figure 5.13). Acute edema and erythema were visible in the infection area of the latter group. This clarifies the microbial infection resistance ability of HGGS3, which is a very

Chapter 5

important criterion for an implantable biomaterial. Further, colonies recovered from the animals were presented in Table 5.5. It was observed that bacterial colonies were decreased with time in HGGS3 implanted rats. Again, SEM micrographs of the un-implanted sample showed abundant growth of *S. aureus* without losing their cellular integrity. Contrarily, disruption, morphological alteration and agglomeration of bacterial cells were seen in case of the HGGS3 implanted rats.

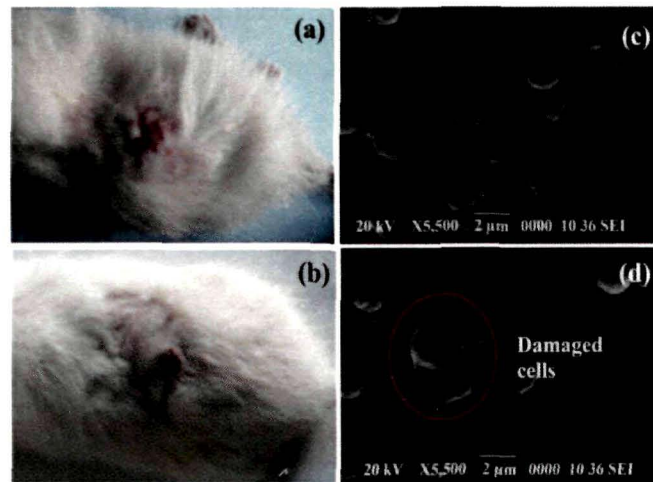


Figure 5.13: (a) Severe infection on un-implanted rat, (b) no sign of infection on HGGS3 implanted rat and SEM micrographs of (c) un-implanted skin, (d) implanted skin

Table 5.5: CFU/mL count for *in vivo* antimicrobial assay against *S. aureus*

Time (h)	Un-implanted	Implanted
24	5.0×10^7	4.2×10^6
48	3.0×10^8	1.2×10^5
72	7.4×10^8	2.3×10^4

Above assays thus confirmed the antimicrobial efficacy of the material under *in vitro* as well as *in vivo* conditions.

5.4. Conclusion

A single-step 'green' protocol was presented to synthesize an Ag-RGO nanohybrid using *C. esculenta* leaf extract. The characterization tools sufficed the formation of the

Chapter 5

nanohybrid. The material possesses good antimicrobial activity. The cytocompatibility profile was found to be excellent for mammalian PBMC. Further, an efficient biocompatible material based on HGE5/Ag-RGO-Cur is put forward for advanced antimicrobial applications. Properties of Ag-RGO were complemented by the immobilization of a naturally abundant biomolecule, curcumin. HGGs inhibited bacterial, fungal and microalgal growth on its surface. Moreover, *in vitro* and *in vivo* assays confirmed the biocompatibility of the material with mammalian hosts. Present findings suggest the potential of HGGs3 as a thin film material in the domain of biomedical implants and devices. Further, the properties of the same material could be utilized to design a microbial fouling resistant marine coating.

References

1. Xiao, L., et al. *ACS Appl. Mater. Interfaces* **5** (20), 10074--10080, 2013.
2. Statz, A., et al. *Biofouling* **22** (5-6), 391--399, 2006.
3. Roosjen, A., et al. *Langmuir* **20** (25), 10949--10955, 2004.
4. Perrino, C., et al. *Langmuir* **24** (16), 8850--8856, 2008.
5. Schiff, K., et al. *Mar. Pollut. Bull.* **48** (3-4), 371--377, 2004.
6. Silver, S., et al. *J. Ind. Microbiol. Biotechnol.* **33**(7), 627--634, 2006.
7. Pauksch, L., et al. *Acta Biomater.* **10** (1) 439--449, 2014.
8. Dallas, P., et al. *Adv. Colloid Interface Sci.* **166** (1-2), 119--135, 2011.
9. Yang, S-Y., et al. *Carbon* **49** (3) 793--803, 2011.
10. Liu, S., et al. *ACS Nano* **5** (9), 6971--6980, 2011.
11. Si, Y. & Samulsk, E.T. *Nano Lett.* **8** (6), 1679--1682, 2008.
12. Wang, G., et al. *J. Phys. Chem. C* **112** (22), 8192--8195, 2008.
13. Muszynski, R., et al. *J. Phys. Chem. C* **112** (14), 5263--5266, 2008.
14. Thakur, S. & Karak, N. *Carbon* **50** (14), 5331--5339, 2012.
15. Liu, K., et al. *J. Mater. Chem.* **22** (38), 20342--20352, 2012.
16. Yang, Z., et al. *J. R. Soc. Interface* **7** (4), S411--S422, 2010.
17. Baby, T.T. & Ramaprabhu, S. *J. Mater. Chem.* **21** (26), 9702--9709, 2011.
18. Xu, W.P., et al. *J. Mater. Chem.* **21** (12), 4593--4597, 2011.
19. Robinson, J.T., et al. *Nano Lett.* **8** (10), 3137--3140, 2008.

Chapter 5

20. De, R., et al. *Antimicrob. Agents Chemother.* **53** (4), 1592--1597, 2009.
21. Almeida, L.P., et al. *Food Res. Int.* **38** (8-9), 1039--1044, 2005.
22. Elsome, A.M., et al. *J. Antimicrob. Chemother.* **37** (5), 911--918, 1996.
23. Hussain, M., et al. *J. Sci. Food Agric.* **35** (10), 1112--1119, 1984.
24. Pol, V.G., et al. *Langmuir* **18** (8), 3352--3357, 2002.
25. Brahatheeswaran, D., et al. *Biomed. Mater.* **7** (4), 045001--045016, 2012.
26. Sahu, A., et al. *J. Biomater. Appl.* **25** (6), 619--639, 2011.
27. Shen, X.J., et al. *Compos. Sci. Technol.* **72** (13), 1581--1587, 2012.
28. J. Santos, *Int. J. STD AIDS* **16** (10), 677--680, 2005.
29. Deitch, E.A. et al. *J. Trauma* **27** (3), 301--304, 1987.
30. Knetsch, M.L.W. & Koole, L.H. *Polymers* **3** (1), 340--366, 2011.
31. Lam, C.W.Y. & Silvester, W.B. *Hydrobiologia* **63** (2), 135--143, 1979.
32. Bai, X., et al. *J. Phys. Chem. C* **115** (23), 11673--11677, 2011.

Hyperbranched epoxy/MWCNT-CuO-nystatin nanocomposite as a high performance, biocompatible, antimicrobial material

Highlights

This chapter includes the preparation of a high performance, advanced antimicrobial material based on hyperbranched epoxy/MWCNT-CuO-nystatin NC. The material showed significant improvement of mechanical properties over the pristine system without effecting elongation. MWCNT was modified by a non-ionic surfactant, triton X-100, wherein copper oxide nanoparticles were anchored *in situ* by a 'green' method. Further, sonochemical immobilization of nystatin enhanced the stability of the system. The immobilized nanohybrid system was incorporated into the hyperbranched matrix at 1, 2 and 3 weight%. The resultant system proved its ability to prevent bacterial, fungal and microalgal fouling against the tested strains, *Staphylococcus aureus*, *Candida albicans* and *Chlorella* sp. Additionally, this system is quite compatible with rat heart cells. Furthermore, *in vivo* assessment showed that this could be utilized as an implantable antimicrobial biomaterial. Thus, the overall study pointed out that the prepared material may have immense utility in biomedical domain to address microbial fouling, without inducing any toxicity.

Parts of the chapter are published in

Barua, S., Chattopadhyay, P., Phukan, M.M., Konwar, B.K., & Karak, N. *Mater. Res. Express* 1 (4), 045402--045419, 2014.

Chapter 6

6.1. Introduction

Advancement of nanotechnology in association with the development of polymer science has brought about myriads of relieving measures to longstanding human problems. Microbial infections and contamination cause devastating loss to health and materials. Recent investigations reported that more than 15% mortality occurs worldwide due to *S. aureus* infections.¹ Further, higher death rate arises because of post-surgical or hospital related infections. Thus, there is a strong probability of microbial attack through medical implants and devices, which raised the concern of protecting such appliances with antimicrobial coatings.² However, development of such coatings is hindered by the fact that most of them are banned by different regulatory authorities due to their extensive toxicity.³

4

Hence, designing of high performance antimicrobial surface with adequate biocompatibility may be applied to medical implants and devices to combat this issue. Polymeric materials with multifaceted properties are being utilized in the fabrication of antimicrobial scaffolds, implants and implant-coatings etc.^{5, 6} Chapter 5 dealt with the potential of HGE5/Ag-RGO-Cur NC as a profound antimicrobial material for biomedical use. Therein it was observed that incorporation of RGO augmented the mechanical properties of the pristine system. The key strategy applied in the present study is the incorporation of another carbon based nanomaterial, MWCNT into the HGE5 matrix. Extraordinary mechanical, electrical and physico-chemical properties have endorsed MWCNT as a central point of attraction in the field of nanotechnology.⁷ Allaoui et al. reported many fold increment of mechanical properties of epoxy upon incorporation of 1-4 weight% of MWCNT.⁸ Again, Gojny and co-workers witnessed improvement of thermo-mechanical properties of MWCNT-epoxy NC over the pristine system.⁹ MWCNT thus can be used in advanced polymeric NC as a nano-reinforcing agent. However, inherent inertness is a challenge for its efficient utility, particularly in polymer technology. Proper functionalization of the nanotubes makes them compatible with polymeric systems. Covalent functionalization of MWCNT involves harsh chemical treatments.¹⁰ However, recent reports put forward some alternative ways such as ultrasonication, microwave irradiation, plasma treatment etc. to achieve covalent modification of MWCNT surface.¹¹⁻¹³ Non covalent modification, contrarily implicates the use of macromolecules, surface

Chapter 6

adsorption, π -stacking interactions etc.¹⁴ In this regard, Triton X-100 is a non-ionic surfactant that has been used widely for the stabilization of MWCNT.¹⁵

Further, the previous chapter ascertained the inhibitory effect of AgNP, coated over RGO against bacteria and fungi. In this study interest was focused on the utility of another class of metal nanoparticles, CuO for attaining microbial fouling preventing potency. Copper and CuO are used in a number of antimicrobial commercial products such as Super KL K90 Red, Nordox etc.¹⁶ Recently, Perelshtein et al. reported a CuO/cotton NC with efficient activity against *S. aureus* and *E. coli*.¹⁷ CuO impregnated matrices exhibited excellent antibacterial as well as antifungal behavior. Nagarajan et al. further demonstrated the potential of such nanoparticles in biomedical applications.¹⁸ Although most of the copper based microbial-antifouling materials are banned due to their highly toxic nature, CuO nanoparticles prepared through 'green' routes have proved their compatibility at the bio-interface.¹⁹ Therefore, it would be a good proposition to anchor CuO onto MWCNT, via 'green' methodology to achieve antimicrobial activity and biocompatibility of the resultant nanohybrid system (CNT-CuO).

Moreover, immobilization of a natural component, curcumin complemented the properties of Ag-RGO, as evident from the last chapter. Therefore, another antimicrobial molecule, nystatin is proposed to immobilize on CNT-CuO. Nystatin is a broad spectrum antifungal agent with 'polyene' structural backbone. Immobilization of this may serve a dual purpose of modifying MWCNT surface with π - π electronic interaction as well as imparting antifungal activity to the system. In the present investigation, the effect of the immobilized nanohybrid system (CNT-CuO-Nys) was studied after incorporating it into HGE5 matrix.

6.2. Experimental

6.2.1. Materials

MWCNT with ~95% purity was procured from Hanwha Nanotech Corp., Korea. These are generally synthesized by laser ablation, arc discharge, chemical vapor deposition and high-pressure carbon monoxide disproportionation methods. Owing to extraordinary thermo-

Chapter 6

mechanical attributes, MWCNT find huge applications in polymer technology as a nano-reinforcing agent.

Copper acetate was purchased from Merck, India. It has broad utilities as fungicide and green pigments from ancient times. Melting and boiling points of copper acetate are 115 and 240 °C, with density 1.882 g/cm³. It is industrially synthesized by reacting copper(II) hydroxide or copper(II) carbonate with acetic acid, at high temperature. Now a days, this is widely used as a precursor to synthesize Cu/CuO/Cu₂O nanoparticles.

Triton X-100 was obtained from HiMedia, India with molecular weight 640 g/mol. This is a non ionic surfactant containing a hydrophilic poly(ethylene oxide) chain and a hydrophobic aromatic hydrocarbon group. It is a clear viscous liquid with an approximate viscosity of 270 centipoise at 125 °C. Its melting and boiling points are 6 and 270 °C, while density is 1.07 g/cm³. It is soluble in water, xylene, toluene, ether, trichloroethylene, ethanol, ethylene glycol, isopropyl alcohol etc. Triton X-100 has been utilized as a modifier for carbon based nanomaterials to enhance their stability in solution.

Nystatin was procured from HiMedia, India. It is a broad spectrum antifungal agent derived from *Streptomyces noursei*. It is a long chain polyene molecule with molecular weight of 926.09 g/mol. Nystatin is highly effective in healing fungal infections of skin, mouth, esophagus and vagina. In the present study, it is used to attain profound antifungal activity of the NC.

Terminalia chebula fruits were collected from Tezpur University campus, Assam, India and sun dried. About 2 g of the fruit was washed and ground in a domestic blender. It was stirred for about 30 min in 100 mL of water at 40 °C. The aqueous extract was filtered through a muslin cloth. The pH of the extract was found to be 7.4, which is near to neutral.

The required chemicals and reagents such as glycerol, BPA, epichlorohydrin, THF, toluene, sodium hydroxide, poly(amido amine) etc. were of the same specifications as stated in Chapter 2, section 2.2.1 and Chapter 3, section 3.2.1.

William medium and low-glucose DMEM medium, MTT etc. used to evaluate the *in vitro* biocompatibility of the prepared NC are of same specifications as described in Chapter 2, section 2.2.1

The microbial test organisms used in the present investigation were *Staphylococcus aureus* (ATCC 11632), *Candida albicans* (ATCC 10231) and *Chlorella* sp. MP-1

Chapter 6

(Genbank entry: KJ499988). *S. aureus* was cultured in Luria Bertani broth (LBB, HiMedia, India) and *C. albicans* in Potato Dextrose broth (PDB, HiMedia, India). The bacterial culture was incubated at 37 °C (for 24 h), whereas the fungal culture was at 28 °C (for 48 h) for assessing the antibacterial and antifungal activities of the NC. The microalga, *Chlorella* sp. was cultured in Bold Basal medium (BBM) for 15 days as per the prescribed protocol.²⁰

6.2.2. Animals

Male wistar rats with average body weight of 250 g were obtained from the same source as stated in Chapter 3, section 3.2.2.

6.2.3. Instruments

UV-visible, FTIR, XRD, SEM and TEM analyses were performed by using the same instruments, under the same test conditions as described in Chapter 4, section 4.2.3.

Tensile strength, elongation at break and lap shear tensile adhesive strength were determined for the NC, by using the UTM, as specified in Chapter 2, section 2.2.2. Samples were prepared with the same dimensions as mentioned in that section. Similarly, bending, impact resistance and scratch hardness tests were carried out for the prepared NC by using the same process as described there.

6.2.4. Methods

6.2.4.1. Preparation of CNT-CuO-Nys

MWCNT (0.5 g) was dispersed in water by employing ultrasonication for 45 min. Triton X-100 (0.15 g, 30 weight% of MWCNT) was added into the dispersion and stirred mechanically for 3 h at 60 °C. CuO nanoparticles were prepared *in situ* as follows. Copper acetate (1.42 g) was dissolved in the aforementioned dispersion using a magnetic stirrer. The amount was taken at 2:1 ratio of MWCNT to CuO. Then, 1 mL of *T. chebula* fruit extract was added to the reaction mixture and stirred for another 2 h at room temperature. The mixture was sonicated for 30 min (amplitude 60% and cycles 0.5). Then, the suspension was centrifuged for 10 min at $1006 \times g$ (3000 rpm). This was repeated several

Chapter 6

times to remove unwanted components. Finally the residue was washed with THF for 2-3 times and allowed to dry at room temperature to obtain the desired nanohybrid (CNT-CuO).

CNT-CuO was then dispersed in THF by sonication for 10 min. Then, 0.5 g of nystain was added to the dispersion and stirred at room temperature for 3 h, followed by ultrasonication for 15 min. Prepared CNT-CuO-Nys was again centrifuged at $1006 \times g$ (3000 rpm) for 15 min. The residue was collected and dried at room temperature.

6.2.4.2. Preparation of NC

Three NC were prepared by incorporating 1, 2 and 3 weight% of CNT-CuO-Nys to 5 g of HGE5 resin in each case, separately and encoded as HGCC1, HGCC2 and HGCC3 respectively. The systems were allowed to stir for 5 h at 50 °C followed by sonication for 15 min. All the NC together was denoted as HGCC in this chapter.

6.2.4.3. Antimicrobial assays

To determine the efficacy of the resinous HGCC, MIC was calculated against *S. aureus* and *C. albicans* by micro-dilution technique. Stock solutions of concentration 30 mg mL^{-1} were prepared for each sample and diluted with 1% DMSO to yield a final concentration range of $10\text{-}100 \text{ }\mu\text{g mL}^{-1}$. Samples ($100 \text{ }\mu\text{L}$) were added to the wells of 96 well plates. Aforementioned microbial strains ($100 \text{ }\mu\text{L}$) were then added to the wells and the plates were incubated separately. The test was performed by using the procedure described in Chapter 3, section 3.3.4.5.

Further, growth profiles of the microbial species were recorded in presence of HGE5 and HGCC3 films. *S. aureus* and *C. albicans* were cultured in the aforementioned media in 15 mL test tubes. This assay was done by the same procedure as mentioned in Chapter 5, section 5.2.4.6.

Another assay was carried out to investigate the growth of the above microorganisms in close vicinity of HGCC3 thermoset. For this test, $100 \text{ }\mu\text{L}$ of the bacterial and fungal strains were spread over agar plates, by using a spreader. Then, pieces of HGE5 and HGCC3 films ($10 \text{ mm} \times 10 \text{ mm} \times 0.25 \text{ mm}$) were laid on the plates. After incubating for specified times, microbial growth was inspected by capturing images of the plates with a Nikon Coolpix-S3000 camera as described in Chapter 5, section 5.2.4.6.

Chapter 6

Again, to scrutinize the activity of HGCC3 against the microalga, similar tests were carried out as that for bacteria and fungi. The microalga was cultured in 15 mL test tubes in BBM culture media and incubated for 15 days in presence of the pristine and HGCC3 films. The microalgal growth was monitored haemocytometrically and compared with that of the control (tube without film). Growth of the microalga was checked in the proximity of the films by the same method as described in the previous chapter. Here, the film was laid on solidified BBM, where 500 μL of the microalgal culture (cell density of 89.5×10^5 cells mL^{-1}) was spread. Possibility of microalgal growth in vicinity of the films was examined by capturing the photographs of the plates at the end of microalgal growth phase.

6.2.4.4. In vitro biocompatibility assessment

In vitro biocompatibility of HGCC was assayed against primary heart cell line of wistar rat by following the same method as described in Chapter 2, section 2.2.3.4. For this assay direct contact method was employed as stated in that section. Finally, cell viability (%) was calculated after adding MTT by monitoring the UV absorbance at 540 nm.

6.2.4.5. In vivo biocompatibility assessment

To investigate the compatibility of HGCC, a representative sample (HGCC3) was considered for *in vivo* implantation. Wistar rats (n=6) were taken for implantation and the same number of animals were kept as control. HGCC3 (films with dimension 10 mm \times 10 mm \times 0.25 mm) was implanted into the rats subcutaneously. Blood parameters were evaluated for both the groups at 0, 15 and 30 days of implantation, by following the method as described in the previous chapter, section 5.2.4.5. Test animals were sacrificed on the 30th day of implantation and histomorphological sections were studied under a microscope, after following the staining with hematoxylin and eosin.

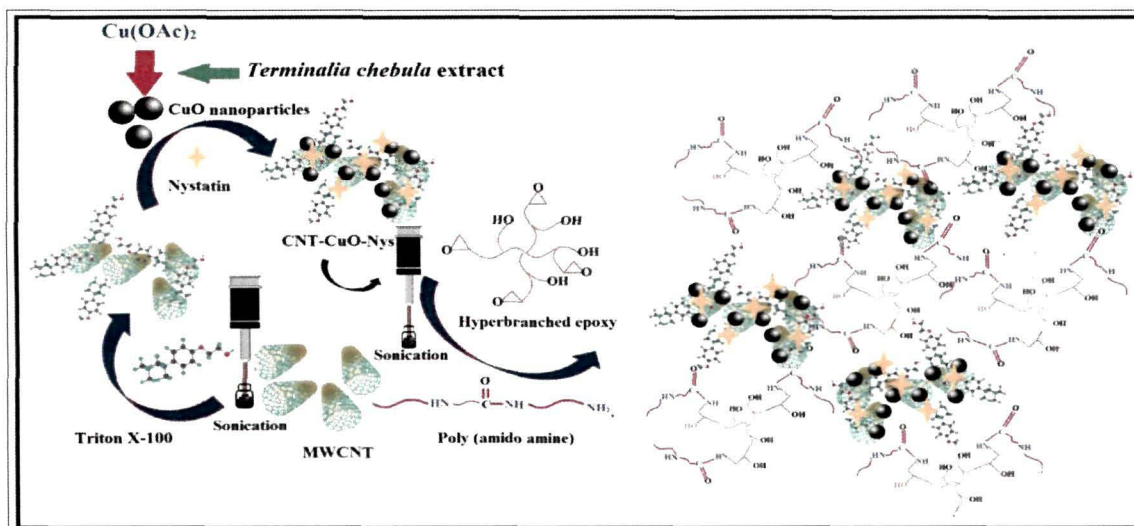
6.2.4.6. Statistical analysis

All the data were presented as mean \pm SD after taking the results in triplicate. Statistical methods (one way and two way ANOVA) were employed to calculate the LSD.

6.3. Results and discussion

6.3.1. Preparation of HGCC

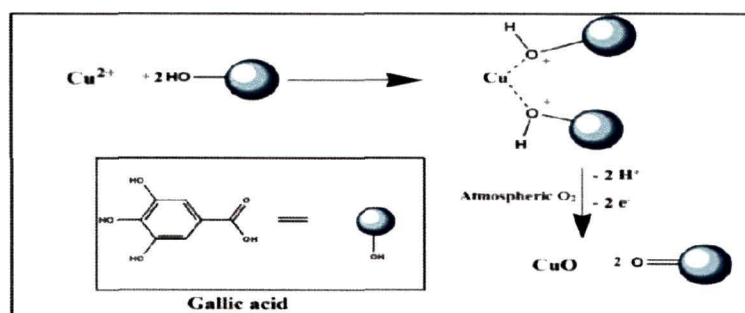
Inertness of MWCNT is a major problem for preparation of polymeric NC with this nanomaterial. The preparative protocol of HGCC is presented in Scheme 6.1. Triton X-100, being a non-ionic surfactant, cannot produce any charge attraction with the tubes.²¹ However, poly(ethylene glycol) based structure provides compatibility with aqueous solutions and again the hydrocarbon tail of the surfactant physically interacts with the hydrophobic surface of MWCNT. Moreover, π -electronic affinity of this surfactant towards the aromatic rings of MWCNT is also significant. The above effects increase the adsorption of the surfactant onto the nanotubes. Again, the hydrophilic end offers compatibility towards the continuous aqueous phase and forms a stable dispersion in water.



Scheme 6.1: Preparative protocol of HGCC

In situ generation of CuO nanoparticles was achieved by utilizing the reductive potency of *T. chebula* fruit extract. The fruit extract was well reported to possess many polyphenol compounds, where gallic acid is the major component. The mechanism of formation of CuO nanoparticles is depicted in Scheme 6.2, where gallic acid is considered as the active component. Cu subsequently oxidizes to CuO in presence of the oxidative environment (open atmosphere) due to low stability of metallic copper.²² Stability of the nanoparticles was enhanced by MWCNT surface, where electrostatic interaction plays the vital role. Triton X-100 modified nanotube surface is a good platform to anchor metal oxide nanoparticles. CNT-CuO is expected to serve a dual purpose; increment of mechanical

properties and acquirement of strong antimicrobial efficacy. Again, nystatin was immobilized to CNT-CuO, to attain a strong antifungal activity within HGCC. The π - π electronic interaction between the nanotubes and nystatin further helps in the stability of nanotubes.



6.3.2. Characterization

6.3.2.1. UV-visible spectroscopy

UV-visible spectroscopy is a valuable tool to detect the generation of metal nanoparticles. MWCNT did not show any peak in the UV-visible region, due to its poor stability in the aqueous medium (Figure 6.1). In the figure, it is clearly visible that the characteristic plasmon peaks of CuO were present in case of CNT-CuO at 232 and 325 nm. Again, CNT-CuO-Nys showed subtle blue shift of the former peak to 227 nm, along with the multiple peaks of nystatin at 289, 303 and 318 nm. Similar spectral behavior was evidenced for HGCC3. This indicates the presence of CNT-CuO-Nys in HGCC3.

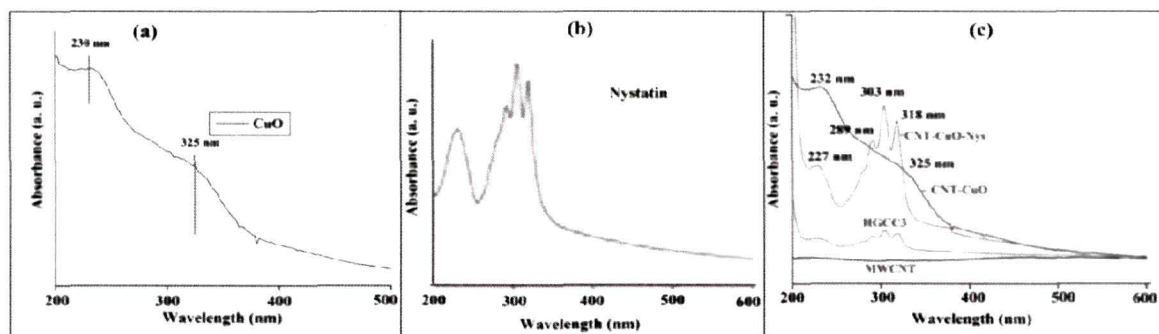


Figure 6.1: UV-visible spectra of (a) CuO, (b) Nystatin and (c) MWCNT, CNT-CuO, CNT-CuO-Nys, HGCC3

Chapter 6

6.3.2.2. FTIR study

FTIR spectra were recorded and presented in Figure 6.2 a. Triton X-100 modified MWCNT showed the presence of characteristic bands of poly(ethylene glycol) at 3422 (-OH stretching) and 1137 cm^{-1} (C-O stretching). These bands were visible for all the samples. Presence of C=C bonds of MWCNT is shown by the band at around 1653 cm^{-1} . This band sharpened in case of the nanohybrid and HGCC, which may be due to the combined effect of nystatin and MWCNT. Other characteristic bands of nystatin were observed at 2880 and 2943 cm^{-1} , due to the symmetric and asymmetric vibrations of -CH₂ groups.²³ These bands are clearly visible in case of HGCC thermosets. The bands for epoxy ring are generally observed at around 915 and 839 cm^{-1} . Absence of these bands ascertains the successful curing of HGCC.

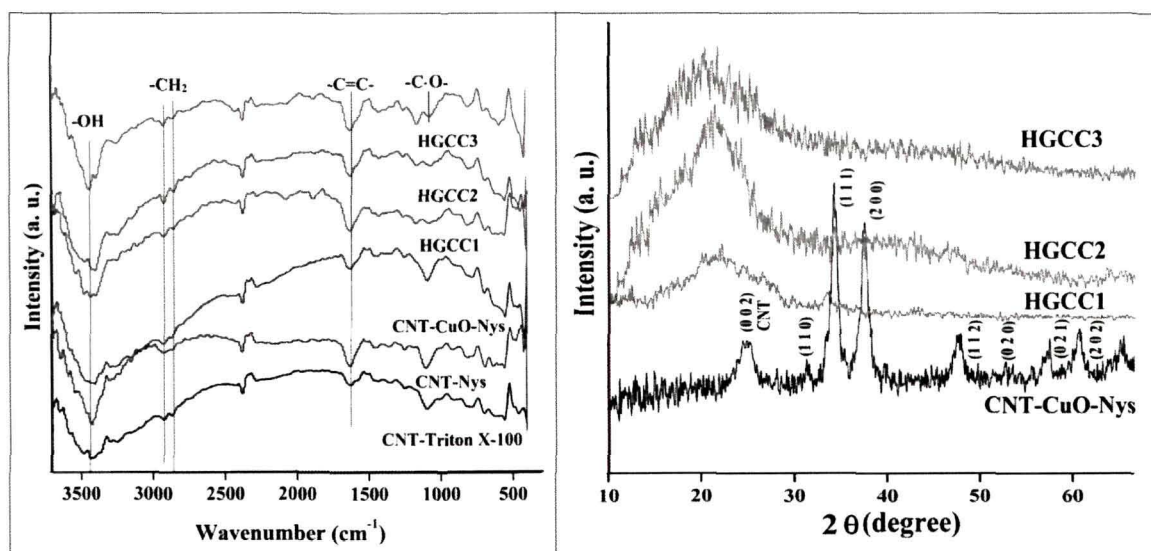


Figure 6.2: (a) FTIR spectra of modified CNT, CNT-CuO, CNT-CuO-Nys and thermosetting HGCC and (b) XRD patterns of CNT-CuO-Nys and HGCC

6.3.2.3. XRD analysis

XRD patterns of CNT-CuO-Nys showed a peak at 2θ value of 24.7°, due to the presence of the graphitic structure of MWCNT (Figure 6.2 b). The pattern showed distinct peaks at around 31.23, 34.16, 37.52, 47.81, 53.38, 57.54 and 60.43°, corresponding to the monoclinic structure of CuO, with Bragg's reflection planes of (110), (111), (200), (112), (020), (021) and (202) (JCPDS No. 80-1917). These peaks were not distinctly visible in

case of HGCC which may be due to the masking effect induced by the HGE5 matrix. This is attributed to the efficient interaction of the nanohybrid with the HGE5 matrix. However, a small amount of nanomaterials and their embedded structure within the epoxy matrix directly influences their XRD patterns. A broad peak was observed at around 2θ value 23° , which stands for the amorphous nature of hyperbranched epoxy system.

6.3.2.4. Morphological study

Figure 6.3 shows the TEM images of pristine MWCNT (a) and HGCC3 (b)-(d). A micrograph (Figure 6.3 c) indicated the presence of 16 layers of the dispersed MWCNT in HGCC. External and internal diameters of the tubes were 18 and 4.9 nm, respectively. Elongated sphere-shaped CuO nanoparticles (width 6.7 nm) were residing inside the walls of the tube. Also, spherical particles (diameter 7.1 nm) were visible within the tubes. The aqueous solution, containing the Cu precursor may have entered the tubule and subsequently got reduced in presence of the reducing agent.²⁴

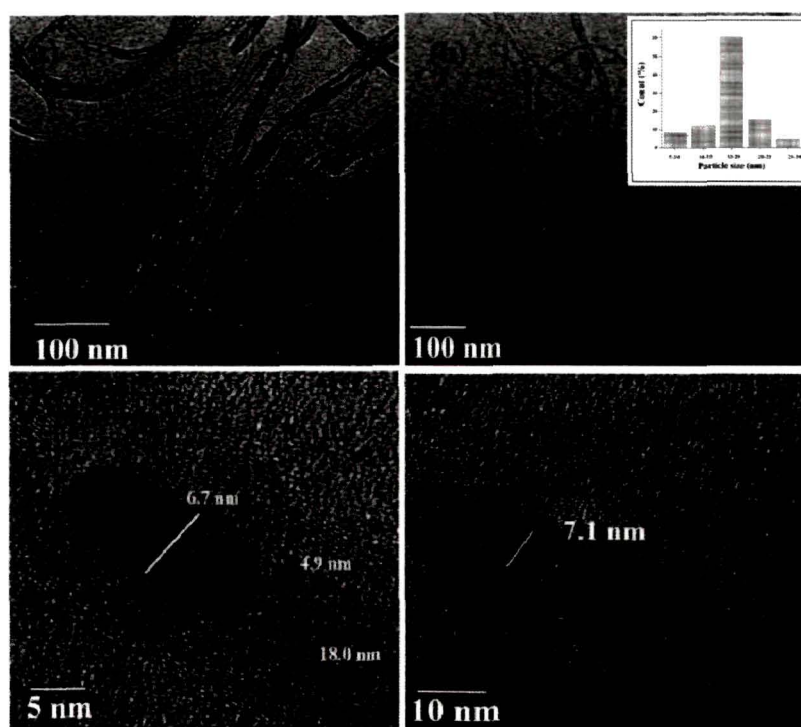


Figure 6.3: TEM micrographs of (a) pristine MWCNT, (b) distribution of CNT-CuO-Nys within HGCC matrix (onset: particle size distribution histogram), (c) and (d) CuO nanoparticles inside the tubule of MWCNT

Chapter 6

Nanoparticles were found to be residing 'in and on' the nanotubes. The overall distribution is shown in Figure 6.3 b, where it is clear that CNT-CuO-Nys is uniformly located within the HGE5 matrix. The π - π electronic interaction of the nanotubes with triton X-100 and nystatin helps in the proper stability of CNT-CuO-Nys system. Further, the HGE5 matrix stabilized it sterically as well as via π - π stacking. These interactions aid the mechanical properties of HGCC.

6.3.3. Curing study and mechanical performance

Curing time of HGCC at 120 °C decreased with increase in the amount of CNT-CuO-Nys (Table 6.1). Functional groups of HGE5 take part in the crosslinking process with the amine hardener. Again, hydroxyl groups of nystatin and triton X-100 enhance the curing reaction. Extent of curing was determined by swelling values, which ensures sufficient crosslinking in the thermosets.

Tensile strength augmented to a significant extent upon formation of HGCC (Table 6.1) from the pristine system. This increment was directly proportional to the loading of CNT-CuO-Nys into the epoxy matrix. In this case, MWCNT plays the leading role. It is well known to the scientific community that incorporation of CNT abets the mechanical strength of a polymeric system.⁸ However, elongation and flexibility generally get decreased. In the present case, use of triton X-100, helps in maintaining the elongation and flexibility, due to its long flexible chain structure.¹⁵ Further, nystatin also aids to the augmentation of this property. Therefore, it was witnessed that both tensile strength and elongation at break increased from the pristine matrix on loading of 1 and 2 weight% CNT-CuO-Nys in HGCC. However, on 3 weight% loading, though the tensile strength increased, a slight decrement of the elongation value was observed. Competition between the restriction of molecular mobility and plasticization affects this phenomenon, where the former overcomes the latter. Loading beyond this value showed phase separation at the time of curing. Thus, HGCC3 could be considered as the best performing NC, in regard of the overall mechanical properties. Moreover, the thermosetting HGCC could be folded to 180° curvature without any damage. The variations of scratch hardness and impact resistance values were not possible to detect due to the limits of the instruments (instrumental limits: scratch hardness 10 kg and impact resistance 1 m). Lap shear tensile

Chapter 6

adhesive strength of HGCC also increased to many folds over the pristine epoxy thermoset. Polar functionalities of triton X-100, nystatin as well as of HGE5 help in the augmentation of adhesive strength.¹⁵ With increase in loading of CNT-CuO-Nys, these functionalities increase. Thus, they cause extensive interaction with the polar groups of wood substrate by secondary forces. One way ANOVA suggested that the results presented in Table 6.1 are significantly different in each case, with p value < 0.05 . Performance of HGCC reflects their potential as excellent materials for thin film applications. Further, focusing on the targeted field of application, their antimicrobial efficacy and biocompatibility are to be monitored carefully.

Table 6.1: Curing parameters and performance of HGE5 and HGCC

Property	HGE5 [#]	HGCC1	HGCC2	HGCC3	LSD
Curing time at 120 °C (min)	24±0.58	20.33±0.57	19±0.6	15.5±1.8	1.0
Swelling (%)	22.6±0.43	24.8±0.5	23.1±0.32	23±1	0.57
Tensile strength (MPa)	38.4±0.84	51.7±1.99	55.7±0.7	63.7±0.6	1.04
Elongation at break (%)	21.3±0.57	24.7±0.56	28.5±0.23	21.5±0.4	0.35
Impact resistance (m)*	>1	>1	>1	>1	-
Scratch hardness (kg)*	>10	>10	>10	>10	-
Bending (mm)*	<1	<1	<1	<1	-
Adhesive strength (MPa)	768	2560.3±2.5	2652.6±2.5	2829±2.6	2.09

*Instrumental limits: Scratch hardness=10 kg, Impact resistance=1 m and bending test mandrel=1 mm

[#]As reported in Chapter 2, Table 2.2.

6.3.4. Antimicrobial assay

In Chapter 3, section 3.3.8., it was observed that HGE5 did not show any inhibitory effect against *S. aureus* and *C. albicans* up to a concentration of 500 $\mu\text{g mL}^{-1}$. Here, MIC values of the nanomaterials and HGCC are presented in Figure 6.4. Inhibitory effect of MWCNT increased upon formation of CNT-CuO. CuO and copper are used in a number of commercial products as antimicrobial agents, which prevent the growth of a broad spectrum of microbes. Thus, the increment is obvious in case of CNT-CuO. Immobilization

Chapter 6

of nystatin further enhanced this efficacy. However, activity of the material was found to be stronger against *C. albicans*. HGCC showed inhibitory effect within the concentration range of 75-54 $\mu\text{g mL}^{-1}$. HGCC3 showed the lowest MIC value amongst the studied NC, which is owing to the amount of CNT-CuO-Nys within the matrix. Higher MIC values for the NC are attributed to the reduction in the amount of CNT-CuO-Nys as compared to that of HGE5. Significant differences were observed in the inhibitory concentrations, with LSD: 0.42 (p values <0.05).

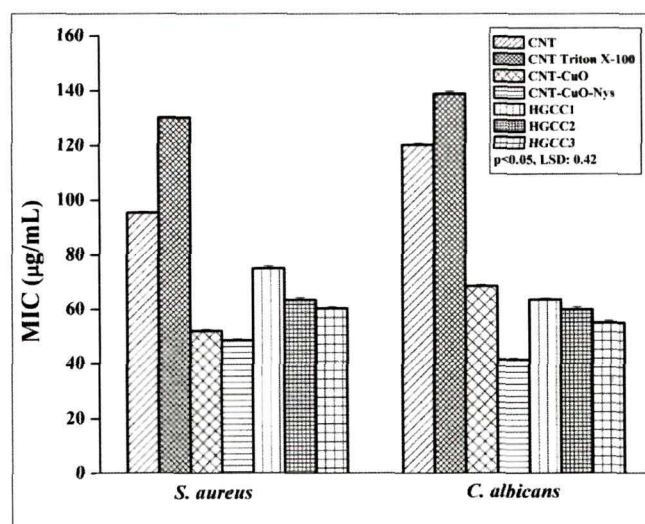


Figure 6.4: MIC of pristine CNT, CNT-CuO, CNT-CuO-Nys and HGCC against *S. aureus* and *C. albicans*

Further, microbial growth with time was monitored in presence of the pristine and HGCC3 systems. Both *S. aureus* and *C. albicans* grew in exponential manner in the control. Similar growth profile was also observed in case of pristine matrix. Contrarily, in presence of HGCC3, growth was hindered and a clear decrement in absorbance was witnessed (Figures 6.5 a-b). Reported literature suggests that adherence of microorganisms to antimicrobial surfaces cause cell-lysis, which restricts their proliferation upon it.²⁵ Here, also SEM micrographs show alteration of cell membranes in case of *S. aureus* and *C. albicans* (Figures 6.5 c-d). In the figure, red-marked portions clearly indicate fragmentation, disruption and morphological alteration of the microbial cells on adherence to HGCC3 surface. Thus, their growth was inhibited in presence of HGCC3. This assay

Chapter 6

confirms that HGCC3 can prevent the growth of both *S. aureus* and *C. albicans*. Materials with this kind of activity may be useful in biomedical domain to design antimicrobial surface over implants and devices. Interestingly, HGCC3 inhibited the growth of *S. aureus* and *C. albicans* that cause most of the severe infections at surgical sites.

Figures 6.5 e-f clearly indicates the growth of bacteria and fungi over the pristine matrix, which is not visible in the close vicinity of HGCC3 surfaces (Figures 6.5 g-h), though the growth was observed on the rest parts of the plates. This again affirms the aforesaid observation that HGCC3 surface could prevent both bacterial and fungal growth over it.

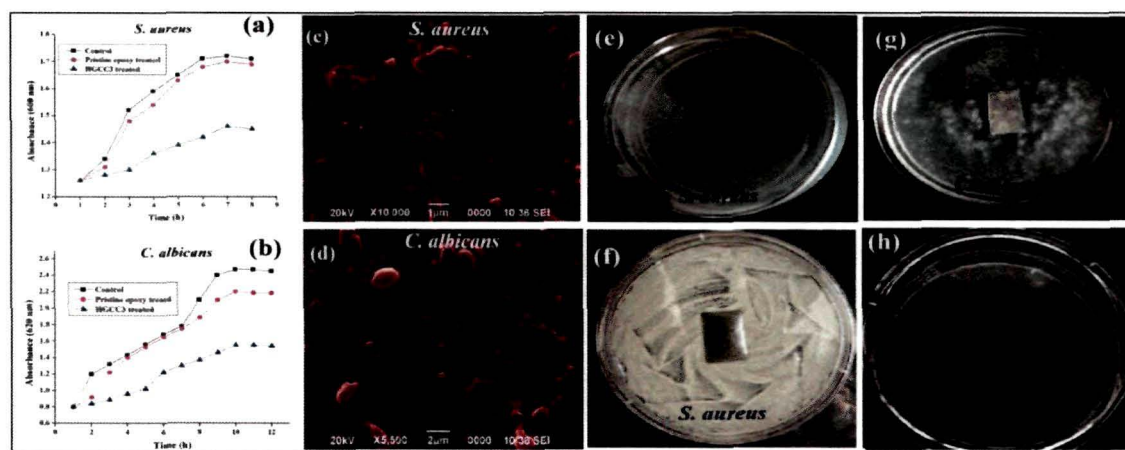


Figure 6.5: Inhibition of growth of (a) *S. aureus*, (b) *C. albicans*; SEM images of cell morphology alteration of (c) *S. aureus*, and (d) *C. albicans* adhered on HGCC3 and (e, f) growth of *S. aureus* and (g, h) *C. albicans* in the close vicinity of HGE5 and HGCC3 respectively

Figure 6.6 shows the growth curve for *Chlorella* sp. (for the control, pristine and HGCC3 treated samples) in BBM culture media. As evident from the curve, a decrement in growth was observed for the HGCC3 treated samples. At the end of the 13th day, maximum cell density of 129.9×10^5 cells mL⁻¹ was achieved in case of the control as well as in the pristine epoxy system which corresponds to a growth rate of ~ 0.215 per day. The maximum cell density for the HGCC3 treated sample was 74.8×10^5 cells mL⁻¹ at the end of the 13th day which corresponds to a growth rate of ~ 0.191 per day. SEM micrographs showed shrinkage of the microalgal cells when they were adhered to HGCC3 surface

Chapter 6

(Figure 6.6 b). Complete disintegration of the nuclei is clearly visible from the figure (red marked). Thus, this confirmed that HGCC3 could prevent the proliferation *Chlorella* sp. on its surface, which may be highly useful in marine industry to prevent algal biofouling.

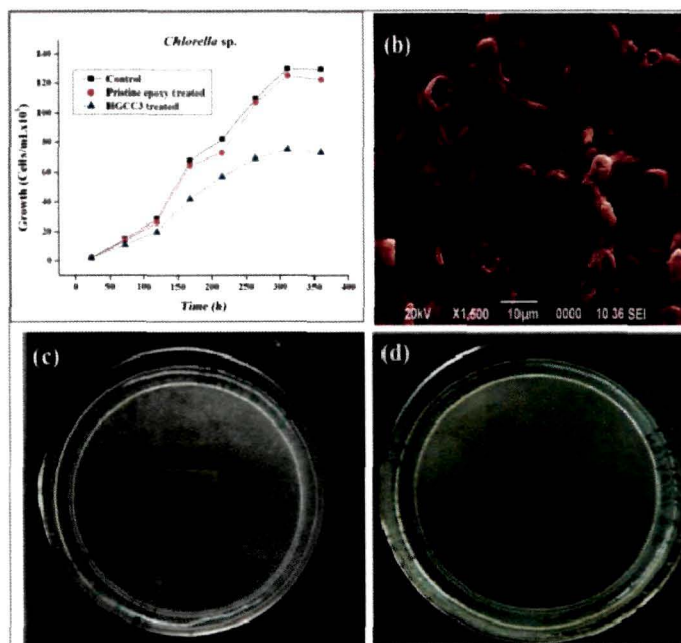


Figure 6.6: (a) Growth inhibition of *Chlorella* sp. in presence of pristine epoxy and HGCC3, (b) SEM micrographs of microalgal cells, adhered onto HGCC3 surface, and (c and d) growth of the microalga in the proximity of HGE5 and HGCC3

From Figure 6.6 c and d, it is clearly visible that the microalga could grow on the edges of the pristine film, while no microalgal growth was evident in close proximity of the HGCC3 film. These observations revealed that HGCC3 possessed inhibitory activity that prevents the growth of microalgae in its vicinity. From the overall antimicrobial assay it is ascertained that HGCC3 could prevent bacterial, fungal and microalgal fouling. This activity endorses the material for multifaceted advanced applications in the domains of biomedical science.

6.3.5. *In vitro* biocompatibility assessment

Cytocompatibility was assessed for HGCC along with CNT-CuO-Nys and pristine MWCNT. Pristine MWCNT showed 68% compatibility with the primary heart cells (Figure 6.7). Toxicity of CNT is a major concern for their utility in biomedical domain.²⁶

Chapter 6

Upon modification with triton X-100, compatibility was increased to 81%. CNT-CuO showed 79% compatibility, which was enhanced by the immobilization of nystatin to 83%. The immobilized system was found to be better than CNT-CuO, which may be due to the minimization of surface energy upon immobilization.²⁷ The MTT assay showed significant difference amongst the cell survival rates (LSD: 0.33; $p < 0.05$). In Chapter 2, section 2.3.9., compatibility of rat heart cell was observed to be more than 98% when incubated with HGE5. Here, HGCC also exhibited more than 85% cytocompatibility. However, with increase in loading, the cell viability decreased to a small extent. The overall compatibility of HGCC was satisfactory. Such high performing biocompatible materials could be put forward to advanced fields of applications after determining their *in vivo* compatibility.

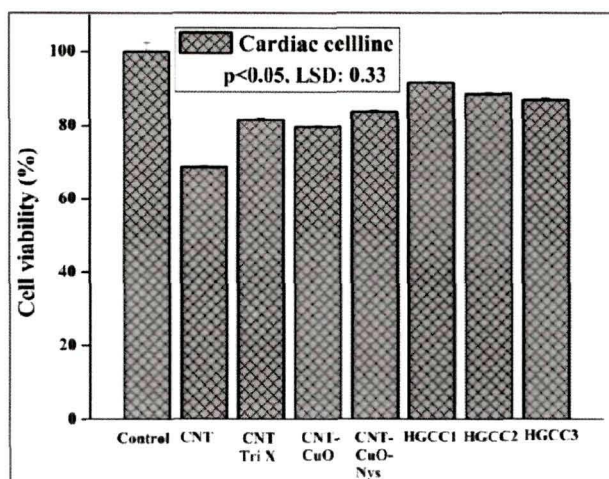


Figure 6.7: Cell viability (%) of the rat primary heart cells

6.3.6. *In vivo* biocompatibility assessment

A biocompatible polymeric material enjoys utility in different domains of applications. Their applications in biomedical coatings, implant devices, tissue scaffold materials etc. need a scrutiny of *in vivo* compatibility.^{28, 29} Previous chapters suggested that HGE5 based NC have potential utility as implantable scaffold materials. In the present case also, *in vivo* testing was carried out by following the same protocol. Hematology and histopathology of the tested animals are the two vital parameters considered in the test after subcutaneous implantation of HGCC3 as the representative NC.

Hematological parameters were evaluated and compared with that of the control (Table 6.2). Their values suggested that no abnormality in the blood parameters was

Chapter 6

induced upon implantation of HGCC3. White blood cell components like lymphocytes, monocytes, neutrophil etc. represent the immunogenic response of the body against any xanobiotic material. However, the parameters indicated no induction of immunity as evident from the levels of the implanted rats. The other parameters also did not show significant difference from that of the control, which ensures the *in vivo* hemocompatibility of HGCC3.

Table 6.2: Hematological parameters of HGCC3 implanted rats

Parameter	0 day		15 days		30 days	
	Control	HGCC3	Control	HGCC3	Control	HGCC3
Lym (%)	35.5±0.41	30.8±0.17	36.9±0.5	32.4±0.63	32.9±0.78	35.8±0.45
Mon (%)	18.2±0.18	19.5±0.59	18.4±0.21	17.8±0.16	19.4±0.92	18.3±0.56
Neu (%)	60.8±0.65	63.2±0.34	61.8±0.78	62.8±0.68	65.9±0.98	63.9±0.79
Eo (%)	7.9±0.32	8.1±0.77	7.1±0.34	8.8±0.32	7.1±0.34	9.1±0.29
Ba (%)	0.9±0.32	0.8±0.2	0.9±0.12	0.9±0.81	0.9±0.18	0.9±0.46
RBC (m/mm ³)	9.7±0.39	8.1±0.51	9.6±0.11	8.4±0.98	9.3±0.23	9.1±0.93
MCV (fl)	61.4±0.19	59.2±0.9	62.4±0.51	60.8±0.72	62.9±0.65	61.2±0.47
Hct (%)	45.4±0.54	46.5±0.21	46.2±0.81	47.9±0.64	46.5±0.12	45.3±0.18
MCH (pg)	14.8±0.72	15.2±0.43	15.1±0.79	15.2±0.54	16.7±0.29	16.8±0.17
MCHC (g/dL)	34.5±0.34	37.0±0.87	34.2±0.56	32.4±0.34	35.8±0.48	33.9±0.21
Hb (g/dL)	11.8±0.74	17.9±0.82	12.2±0.6	18.1±0.28	12.6±0.15	18.6±0.73
Pct (%)	0.78±0.25	0.83±0.37	0.79±0.54	0.87±0.97	0.78±0.56	0.84±0.98

Again, histopathological sections of the rat organs ascertained no infiltration of inflammatory cells (Figure 6.8). Their cellular organizations remained intact after implantation. Skin shows intact epidermis and dermis, while distinct portal vein and hepatocytes were observed in the liver section. In the brain section clear hippocampus was visible with undamaged brain cells. Heart also showed unaltered nuclei and intercalated disks. Thus, this assay established the compatibility of HGCC3 with mammalian cells as

well as with their *in vivo* conditions. Potential of the material as an implantable biomaterial is strongly supported by its compatibility.

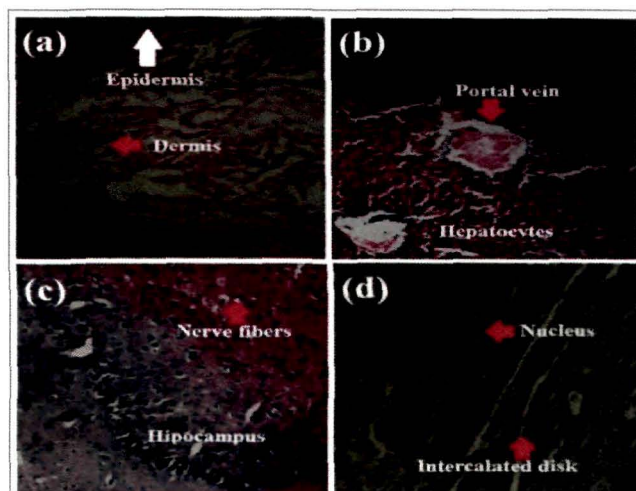


Figure 6.8: Representative histopathological sections of (a) skin, (b) liver, (c) brain and (d) heart of HGCC3 implanted rat

6.4. Conclusion

A high performance material with excellent antimicrobial attributes and good biocompatibility was prepared by utilizing the combined merits of hyperbranched architecture and CNT-CuO-Nys. The material showed antimicrobial activity against bacteria, fungi and microalgae. *In vitro* and *in vivo* assays indicated that HGCC3 could be used as a biocompatible, antimicrobial implantable material. The same material can further be utilized for designing efficient coating in marine industry to prevent microalgal growth. This multifaceted material further needs critical scrutiny regarding its compatibility with non-target organisms, before being applied to the real field.

References

1. Cosgrove, S.A., et al. *Clin. Infect. Dis.* **36** (1), 53--59, 2003.
2. Banerjee, I., et al. *Adv. Mater.* **23** (6), 690--718, 2011.
3. Hagger, J.A., et al. *Aquat. Toxicol.* **57** (4), 243--255, 2012.
4. Chesworth, J.C., et al. *Aquat. Toxicol.* **66**, 293--305, 2004.
5. Liu, Z., et al. *J. Med. Chem.* **49** (12), 3436--3439, 2006.
6. Schmidmaiera, G., et al. *Injuri* **37** (2), S105--S112, 2006.

Chapter 6

7. Park, J.S., et al. *J. Mater. Chem.* **22** (25), 12695--12700, 2012.
8. Allaoui, A., et al. *Compos. Sci. Technol.* **62** (15), 1993--2015, 2002.
9. Gojny, F.H., et al. *Chem. Phys. Lett.* **370** (5-6), 820--824, 2003.
10. Karousis, N. & Tagmatarchis, N. *Chem. Rev.* **110** (9), 5366--5397, 2010.
11. Park, C., et al. *Chem. Phys. Lett.* **364** (3-4), 303--308, 2002.
12. Felten, A., et al. *Nanotechnology* **17** (8), 1954--9, 2006.
13. Pramanik, S., et al. *Carbon* **55**, 34--43, 2013.
14. Wu, X., et al. *Ind. Eng. Chem. Res.* **50** (2), 891--897, 2011.
15. Vaisman, L., et al. *Adv. Funct. Mater.* **16** (3), 357--363, 2006.
16. Anyaogu, K.C., et al. *Langmuir* **24** (8), 4340--4346, 2008.
17. Perelshtein, I., et al. *Surf. Coat. Tech.* **204** (1-2), 54--57, 2009.
18. Nagarajan, S. & Yong, Z. *Recent Pat. Biomed. Eng.* **1** (1), 1874--7647, 2008.
19. Valodkar, M., et al. *Mater. Chem. Phys.* **128** (1), 83--89, 2011.
20. Phukan, M.M., et al. *Appl. Energy* **88** (10), 3307--3312, 2011.
21. Li, N., et al. *Langmuir* **26** (12), 9315--9320, 2010.
22. Yang, J.G., et al. *Chem. Lett.* **35** (10), 1190--1191, 2006.
23. Mandru, M., et al. *Cellulose Chem. Technol.* **47** (1-2), 5--12, 2013.
24. Tessonnier J-P., et al. *ACS Nano* **3** (8), 2081--2089, 2009.
25. Sivakumar, P.M., et al. *Biomater. Sci.* **2** (7), 990--995, 2014.
26. Wu, H., et al. *J. Mater. Chem.* **20** (6), 1036--1052, 2010.
27. Liu, S., et al. *ACS Nano* **3** (12), 3891--3902, 2009.
28. Smith, W.E., et al. *ACS Nano* **6** (11) 9475--9484, 2012
29. Freed, L.E., et al. *J. Biomed. Mater. Res.* **27** (1), 11--23, 1993 .

Antimicrobial hyperbranched epoxy/CuO-nanofibrillar cellulose nanocomposite as a potential implantable scaffold for tissue regeneration

Highlights

This chapter highlights the potentiality of a glycerol based hyperbranched epoxy/CuO-nanofibrillar cellulose based NC as an implantable muscle tissue scaffold material. Nanofibrillar cellulose was isolated from an abundant natural source, *Colocasia esculenta*, by a chemical method. The nanofibrils were decorated with CuO nanoparticles through a 'green' technique by using the aqueous extract of *Terminalia chebula* fruit. Prepared NC demonstrated the betterment of mechanical performance over the pristine system upon incorporation of 0.1-0.5 weight% of the nanohybrid. *In vitro* studies revealed that the material supported the growth and proliferation of L6 muscle cells, without causing any detriment to the cell morphology. Further, *in vitro* and *in vivo* toxicity assessments ascertained the biocompatibility of the material. No sign of immunogenesis was witnessed after implanting the material to wistar rat. Moreover, the NC exhibited profound inhibitory effect against *Staphylococcus aureus*, *Escherichia coli* and *Candida albicans*, the microorganisms responsible for various surgical site infections. Thus, the overall study endorses the NC as a high performance, antimicrobial scaffold material for reconstruction of muscle cells.

Parts of the chapter are published in

Barua, S., Das, G., Aidew, L., Buragohain, A.K. & Karak, N. *RSC Adv.* **3** (35), 14997--15004, 2013.

Barua, S., Gogoi, B.J., Aidew, L., Buragohain, A.K., Chattopadhyay, P. & Karak, N. *ACS Biomater. Sci. Eng.* 2014 (*Under review*).

Chapter 7

7.1. Introduction

Scaffolds are the basic platforms for tissue engineering research. Reconstruction of damaged organ is possible at present time with the aid of implantable tissue scaffolds. Skeletal muscles are the voluntarily controlled strained muscle tissues, which cover maximum part of the body. Due to trauma, burn or some congenital anomalies, muscles may be damaged.¹ Regeneration of damaged muscles has been a longstanding problem in medical science due to many post operative cosmetic disorders.² However, this is possible to address by the help of a suitable tissue engineering technique. Fabrication of three dimensional polymeric scaffold is a promising measure to culture smooth muscle tissues *in vitro* to foster cell growth.³⁻⁵ Subsequent implantation of such scaffold within host body offers clean reconstruction of muscle cells (myocytes), without inducing any cosmetic defect. Biodegradable polymeric scaffolds are advantageous in numerous ways over the conventional implants. They provide good compatibility with the host body; overrule the necessity of repeated surgery, help in early reconstruction of tissues and most interestingly offer tunable surface properties.^{6,7} In this context, polyester based scaffolds were prepared which showed good adhesion of smooth muscle cells (SMC).³ Again, polyglycolic acid (PGA) fiber meshes were utilized to fabricate implantable device, which supported the growth of SMC.⁸ Hydrogel based scaffolds are also used as good extracellular matrices for regenerating bone, cartilage and muscle tissues.⁹ Moreover, some materials of natural origin like collagen, elastin, fibrin etc. were exploited for muscle tissue engineering research.¹⁰ However, these materials are not able to provide adequate mechanical strength. Further, fabrication of implantable scaffolds has challenges in overcoming infection at surgical sites, inadequate mechanical performance and induction of toxicity to the host body.¹¹

Highly compatible, infection resistant tough polymeric scaffolds are desired for tissue engineering applications to evade post surgical complications and sound recovery of damaged tissues. Previous chapters demonstrated that HGE5 based NC showed immense potential to regenerate skin. Here, the prospect of HGE5 based NC would be investigated for muscle tissue reconstruction. Further, the emphasis on utilization of sustainable resources motivated the researchers to explore inexpensive bioresources. Cellulose, being the most abundant organic polymer in nature, drew considerable attention in this regard.

Chapter 7

Plant cellulose generally forms a native composite with lignin and other carbohydrates (e.g. hemicelluloses) from which it can be isolated by various physico-chemical techniques.¹² A scrutiny of literature reveals limited number of reports on the isolation of micro and nanofibrillar cellulose (NFC) from natural and industrial wastes.^{13, 14} Recently, Mandal and Chakrabarty reported the isolation of nanocellulose from waste sugarcane bagasse by an acid hydrolysis method.¹⁵ Apart from plants, certain non-pathogenic bacteria, algae and fungi found in fruits, vegetables etc. have been reported to be used in the isolation of cellulose.^{16, 17} However, crystallinity and fiber size depend on the isolation conditions as well as the post- and pre-treatments.¹⁸ Another vital factor that dictates these features is the original source from which it is isolated. *Colocasia esculenta* is an abundantly grown plant in the tropical regions across the globe. Nutrient composition and cellulose content of this plant have already been evaluated thoroughly.¹⁹ In the present study, isolation of NFC would be carried out from *C. esculenta* stem by a chemical method using alkali and acid treatments.

Again, the previous chapter clearly proved the antimicrobial potency of CuO nanoparticles, prepared through a greener route. Thus, interest would be paid on decorating the isolated NFC by CuO nanoparticles to achieve microbial inhibition. This nanohybrid system (CuO-NFC) is expected to show high mechanical performance with efficient antimicrobial efficacy when incorporated into HGE5. Cellulosic scaffolding is an interesting area from the perspective of biomedical applications.²⁰ Reported literature showcases the utility of this bioresource in the fabrication of cardiac and bone tissue scaffolds.²¹ In this study, CuO-NFC based HGE5 NC would be studied for evaluating its potentiality as a scaffold for SMC regeneration.

7.2. Experimental

7.2.1. Materials

C. esculenta stems were collected from Tezpur University (Assam, India) campus and were cut, sun dried and washed. The dried sample was ground with a domestic blender.

The chemicals used for the extraction of fibers and preparation of NFC were sodium hydroxide, glacial acetic acid and hydrogen peroxide obtained from Merck, India. Acetic

Chapter 7

acid is a colourless liquid with molecular weight of 60.05 g/mol. It has broad utility in the production of poly(vinylacetate) and cellulose acetate. Melting and boiling points of acetic acid are 16-17 and 118-119 °C respectively. It is a mild acid (pKa 4.76) with a density of 1.049 g/cm³. Vinegar (3-5% acetic acid) is a common preservative for packaged food items. Glacial acetic acid is referred to as the anhydrous form which is widely used as an analytic reagent in chemical laboratories.

Hydrogen peroxide (H₂O₂) is a simple form of peroxide which is colourless in its neat form. Molecular weight of H₂O₂ is 34.0147 g/mol, melting and boiling points are -0.43 and 150.2 °C. H₂O₂ is a strong oxidizing agent and used as a bleaching agent and disinfectant. It is industrially produced by the hydrolysis of ammonium peroxydisulfate. However, presently, it is manufactured by the reduction of anthraquinone via hydrogenation using palladium catalyst. Anthrahydroquinone undergoes autoxidation, regenerating the starting compound, where H₂O₂ is produced as a by-product.

BPA, epichlorohydrin, THF, toluene, sodium hydroxide, poly(amido amine) etc. used for the synthesis of HGE5 were of the same specifications as referred to in Chapter 2, section 2.2.1 and Chapter 3, section 3.2.1.

To assess the compatibility of CuO-NFC with PBMC, goat blood was collected from a slaughterhouse in containers, containing 5% sodium citrate. *In vitro* biocompatibility of the NC were assessed by an MTT assay by culturing primary rat hepatocytes in low-glucose DMEM medium with the same protocol as mentioned in Chapter 2, section 2.2.1.

Staphylococcus aureus (ATCC 11632), *Escherichia coli* (ATCC 10536) and *Candida albicans* (ATCC 1023) were considered for examining the antimicrobial activity of CuO-NFC and the NC. For these assays, the required media and agar were provided by the Department of Molecular Biology and Biotechnology, Tezpur University, Assam, India with the same grades as stated in Chapter 5, section 5.2.1.

The L6 cell line was procured from National Centre for Cell Science, Pune, India, in association with the Department of Molecular Biology and Biotechnology, Tezpur University, Assam, India. Trypsin-EDTA solution required for the L6 cell adherence test was procured from Sigma, USA.

Chapter 7

7.2.2. Animals

Male wistar rats of weight 200-250 g were acquired from the Laboratory Animal Resources, Division of Pharmaceutical Technology, Defence Research Laboratory, Tezpur, Assam, India. Animals were utilized for the *in vivo* biocompatibility assessment of the materials, as stated in Chapter 3, section 3.2.2 with due permission from the Institutional Animal Ethics Committee.

7.2.3. Instruments

FTIR, UV-visible spectrophotometer, XRD, SEM and TEM with same instrumental specifications as stated in Chapter 4, section 4.2.3., were used for the characterization of the prepared NC, under the same test conditions.

Tensile and lap shear tensile adhesive strengths with elongation at break were determined for the NC by using the same UTM, as stated in Chapter 2, section 2.2.2. Scratch hardness, bending and impact resistance of the NC were evaluated by using the same instruments as described in that section.

7.2.4. Methods

7.2.4.1. Isolation of NFC from *C. esculenta* stems

Ground mass of *C. esculenta* stems was bleached with a 7% H₂O₂ solution (pH 5, adjusted with glacial acetic acid), maintaining a fiber to solution ratio (1:50) for 2 h at 45 °C. This was followed by successive washing with water to maintain a neutral pH. The treatment facilitated the removal of lignin from the fibers and helped in partial removal of hemicelluloses. For complete delignification of the fibers, a 5% NaOH solution was used. Fibers were soaked in 250 mL alkaline solution for 2 h at 45 °C. The residue was collected by filtration through a micro filter and washed several times with water. The residue was then air dried and treated with 50% DMSO, at 80 °C for 2 h.⁴ This was again filtered and washed with distilled water. The delignified cellulose fibers were treated with 50% glacial acetic acid for 2 h at 50 °C. The acid treated fibers were washed with water until the medium reached the neutral pH. The acid hydrolysis reaction was quenched by pouring water to the reactor and allowed to cool at room temperature. The fibrils were collected by

Chapter 7

centrifugation and washed several times with distilled water. Then, fibrils were mechanically dispersed in water to obtain a suspension of NFC. The NFC suspension was frozen by lowering the pressure under vacuum, followed by sublimation of water using a lyophilizer (Labtech Freeze dryer, Daihan Labtech Co. L-DF5512). This resulted in a dry NFC powder.

7.2.4.2 Preparation of CuO-NFC

T. chebula fruit extract was prepared by the method described in Chapter 6, section 6.2.1. A copper acetate solution was prepared in water (10% w/v), by stirring for 15 min at room temperature. NFC (4 g) was dispersed in water by ultrasonication for 30 min. Copper acetate solution was poured onto the dispersed NFC and stirred at room temperature for 2 h. The *T. chebula* fruit extract (1 mL) was added to the above solution and stirred for another 6 h at room temperature. Color of the solution was changed from blue to dark brown on completion of the reaction. The solution was centrifuged and fibers were washed with water. CuO-NFC thus prepared was mechanically dispersed in water and freeze dried under vacuum using a lyophilizer as mentioned above.

7.2.4.3 Preparation of NC

CuO-NFC was dispersed in THF in three different proportions 0.1, 0.3 and 0.5 weight% with respect to HGE5 resin separately by the aid of ultrasonication for 1 h. The resin was added to each system in the mentioned ratios and magnetically stirred for 4 h at 70 °C. This was followed by 45 min of ultrasonication to allow efficient dispersion of CuO-NFC within the epoxy matrix. Finally, the NC were dried at 70 °C for 24 h inside a heat convection oven (Eyela, NBO-710, Japan). Three NC were coded as HGCNF1, HGCNF2 and HGCNF3 for 0.1, 0.3 and 0.5 weight% loading of CuO-NFC respectively. These NC is termed as HGCNF in general in this chapter.

7.2.4.4. *In vitro* biocompatibility assessment

In vitro biocompatibility of the nanomaterials was tested by incubating the samples with mammalian PBMC by using the same protocol as mentioned in Chapter 5, section 5.2.4.4. Again, HGCNF were tested for their *in vitro* biocompatibility against primary rat

hepatocytes. The test was carried by an MTT assay as described in Chapter 2, section 2.2.3.4. Direct contact method was employed for the assay. Cell viability (%) was determined by monitoring the UV absorbance at 540 nm.

7.2.4.5. Adhesion of L6 muscle cells on HGCNF3 scaffold

Cell adhesion was studied by seeding L6 cells on HGCNF3 films followed by inverted microscopic and SEM analyses. The L6 cell line was cultured at 37 °C under a continuous supply of 5% CO₂ using DMEM media containing 10% FBS. Approximately $1 \times 10^5 \text{ mL}^{-1}$ cells were seeded in a 6 well cell culture plate containing HGCNF3 films (5 mm × 5 mm × 0.25 mm). The plate was incubated for 96 h under the same condition. After termination of the incubation period, cells were observed under an Axiovert A1 inverted microscope (Carl Zeiss, Germany). The media from the wells were discarded and washed with PBS (pH 7.4). Cells were then fixed with glutaraldehyde (2.5%) solution. Excess solution was discarded and the films were analyzed under SEM for studying cell adherence on it. The microscopic images were visualized by using a software, Fiji, 13 that rendered colour to the images.

Further, a trypsin-EDTA solution was used to detach the adhered cells from HGCNF3 surface and rinsed in PBS. Cell count was taken each day (from 0 to 4th day) of incubation by using a haemocytometer.²²

7.2.4.6. In vivo implantation of HGCNF3 and host response

Implantable biomaterials require immunocompatibility with the host systems. To assess the *in vivo* response of the present material, HGCNF3 was implanted within rat. A group of animals (number, n=6) was considered for the test and films were implanted subcutaneously. Another group with the same number of animals was kept as control. Immunocompatibility was analyzed by recording the hematological parameters of both the groups at 0th, 15th and 30th post implantation days.

To analyze the effect of HGCNF3 on the host tissues, histopathological study of the major organs like skin, liver, kidney and brain was carried out. On the 30th post implantation day, the organs were extracted and fixed with 10% formaldehyde solution and dehydrated with alcohol. Organs were embedded by paraffin and sectioned in a microtome.

Chapter 7

Sections were studied under a microscope after staining with hematoxylin and eosin.

7.2.4.7. Antimicrobial assays

Zones of inhibition for NFC and CuO-NFC as well as HGCNF were measured against *S. aureus*, *E. Coli* and *C. albicans* by following the same protocol as described in Chapter 3, section 3.3.4.5.

MIC of CuO-NFC and HGCNF were determined against the aforementioned microbes to examine the effect of the material on both Gram positive and negative bacteria as well as on fungi. Micro-dilution technique was adopted to quantify the MIC, as elaborated in Chapter 3, section 3.3.4.5.

Further, microbial growth inhibition activity of HGCNF3 surface was studied against *S. aureus*. The bacterium was cultured for 24 h at 37 °C in nutrient broth (HiMedia, India) and centrifuged, followed by re-suspension in PBS (pH 7.4). Then the bacterium was again incubated in presence of HGCNF films of dimension 10 mm × 10 mm × 0.3 mm for 24 h. The films were then fixed with 2.5% gluteraldehyde solution and treated with increasing alcohol gradient (70-100%). Fate of the bacteria on interaction with HGCNF3 surface was studied by SEM.

7.2.4.8. Statistical analysis

Results are presented here as mean±SD. One or two way ANOVA was employed to determine the LSD amongst the data.

7.3. Results and discussion

7.3.1. Preparation of CuO-NFC

H₂O₂ is used extensively for bleaching lignocellulosic materials.²³ Lignin was partly removed from the cellulosic fiber in this step. Again, alkali treatment accelerated the removal of lignins whereas hemicellulose was partially removed. Finally, the paracrystalline regions of the fibers got hydrolyzed preferentially by acid treatment, while the crystalline regions were resistant to the acid attack.²⁴ Further, the use of *T. chebula* extract is a greener trial to generate CuO nanoparticles. Mechanism of formation of CuO

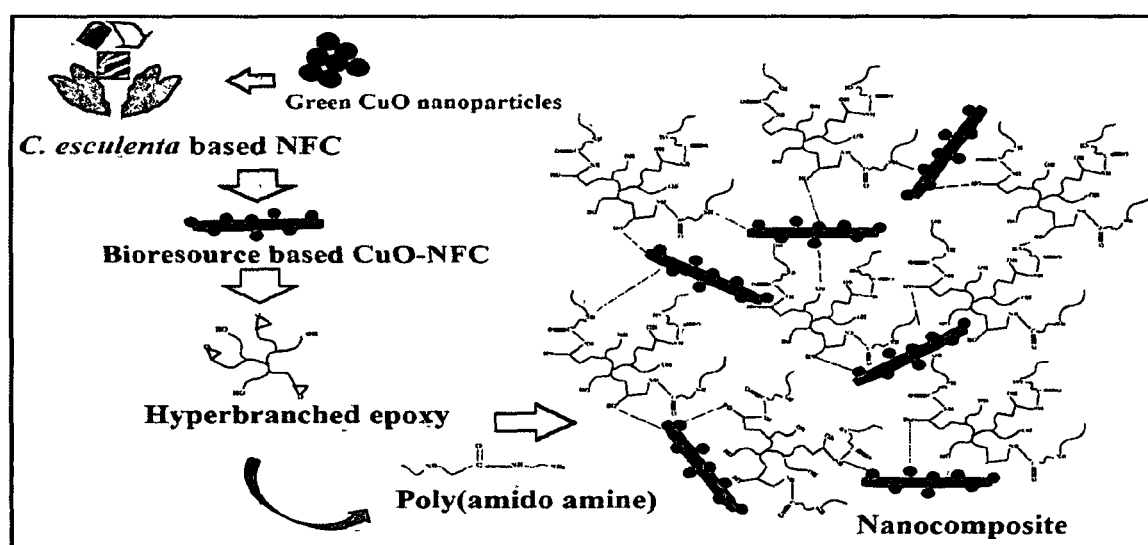
was well documented in Chapter 6. Interaction of the nanoparticles with NFC matrix was previously shown by Jia et al.²⁵ In the present study, CuO-NFC is incorporated into HGE5 matrix to fabricate a biocompatible, microbial infection resistant smooth muscle scaffold. The difficulty of dispersion of CuO-NFC was overcome by minimal incorporation of the nanohybrid to the matrix. Beyond 0.5 weight%, dispersion was quite difficult and a clear phase separation was observed during the crosslinking process. Scheme 7.1 represents the preparative protocol of HGCNF.

Cellulose based nano-reinforcing agent was selected for the present purpose because of its compatibility with biosystems.²⁶ Further, 'green' route mediated preparation of metal nanoparticles showed good biocompatibility with different cell lines as well as with *in vivo* systems.²⁷

7.3.2. Characterization

7.3.2.1. UV-visible spectroscopy

Presence of CuO-NFC in HGCNF was preliminarily examined by the help of UV-visible spectroscopy. Characteristic plasmon peaks for CuO were observed at 256 and 330 nm in case of CuO-NFC (Figure 7.1). HGCNF also revealed the existence of CuO-NFC within their matrices by exhibiting similar kind of spectral behaviours. However, slight deviations were observed for the plasmon peak positions in each material.



Scheme 7.1: Schematic protocol for the preparation of HGCNF

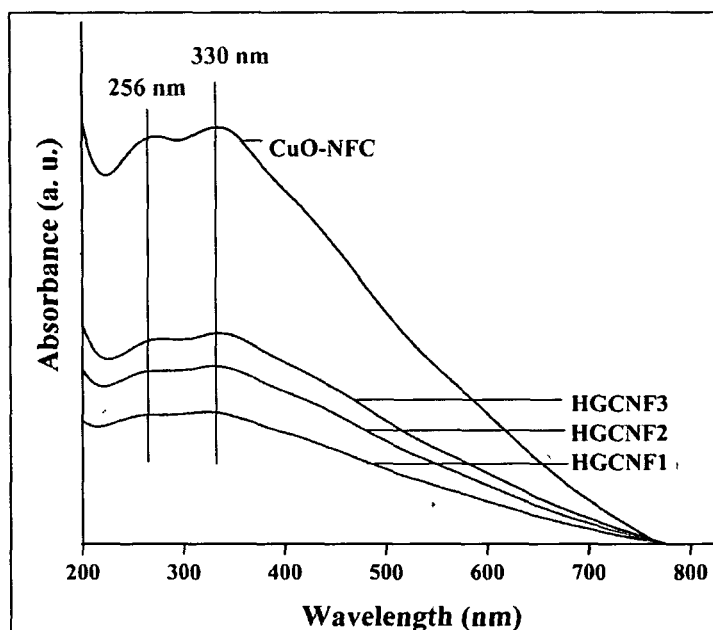


Figure 7.1: UV-visible spectra of CuO-NFC and HGCNF

7.3.2.2. FTIR study

FTIR is a potential tool in cellulose research.²⁸ The chemical changes in the cellulose fibers during the treatments are shown in Figure 7.2 a. The band observed for all the samples at 1051 cm^{-1} is assigned to the -C-O-C stretching vibration of the pyranose ring. The glycosidic ether components seemed to be diminished gradually in NFC because of the loss of molecular weight during hydrolysis, which was clearly indicated by the band sharpness at 1159 cm^{-1} . Only NaOH treated fibers were showing the aromatic methyl groups associated with lignin at 1427 cm^{-1} , which disappeared gradually during the acid treatment and finally became negligible in case of NFC. The absorption band at 1610 cm^{-1} is associated with the -C=C symmetrical stretching of the aromatic rings present in lignin.¹³ Thus, hemicellulose was removed predominantly after base treatment as compared to the samples subjected to the acid treatment. The characteristic -C-H stretching vibration around 2919 cm^{-1} was common for all the cases. Mandal et al. recently reported that the absorption band at 902 cm^{-1} was continuously increased during alkaline and acid hydrolysis.¹⁵ A slight broadening of the peak associated with the β -glycosidic linkages between the glucose units in cellulose, was observed around $898\text{-}912\text{ cm}^{-1}$ for the base treated cellulose and around $878\text{-}927\text{ cm}^{-1}$ for NFC. This indicates the formation of

Chapter 7

cellulose II.²³ FTIR study was also carried out for CuO-NFC (Figure 7.2 b). A broad band ranging from 3200 to 3600 cm^{-1} is a clear indication of adsorption of the polyphenolic compounds of the extract on the surface of the nanohybrid.²⁸ Bands at 1640 cm^{-1} corresponds to the stretching vibrations of the carbonyl groups of gallic acid, the major component of the extract. The bands for Cu–O were observed at around 461, 521 and 668 cm^{-1} .²⁹

Again, FTIR spectra revealed the functionalities associated with HGCNF (Figure 7.2 c). Sharp band at 1047 cm^{-1} stands for the -C-O-C stretching of pyranose ring. β -Glycosidic linkages within the glucose units of cellulose is shown by the band at 909 cm^{-1} . The band at 1607 cm^{-1} is due to the aromatic -C=C stretching of the cellulose units. Characteristic -C-H vibration band of cellulose was witnessed at around 2979 cm^{-1} . Further, bands at 3350-3500 cm^{-1} show the absorption of different polyphenolic compounds of *T. chebula* extract on the surface of CuO-NFC. Cu-O linkage was confirmed from the band at 537 cm^{-1} . Characteristic bands for oxirane ring were observed at 921 and 840 cm^{-1} in the uncured HGCNF3. Their absence in the thermoset abundantly clarifies the successful crosslinking of HGCNF3.

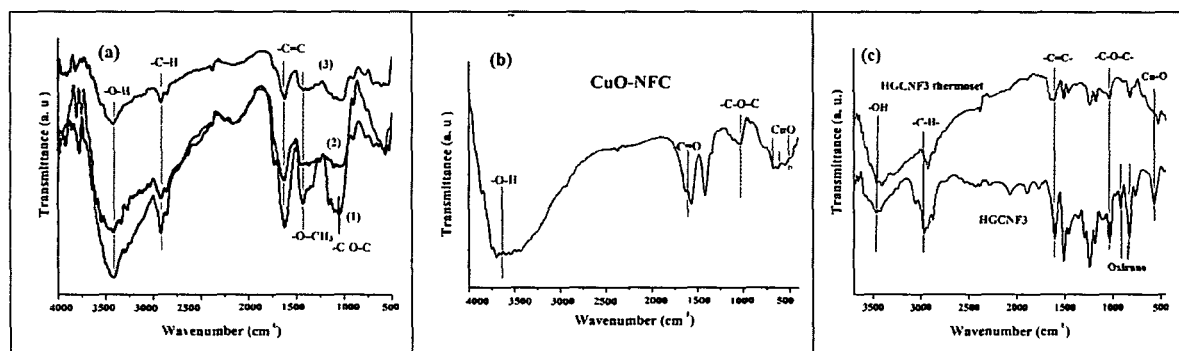


Figure 7.2: FTIR spectra of (a) base treated fibers (1), acid treated fibers (2) and NFC (3), (b) CuO-NFC and (c) cured and uncured HGCNF3

7.3.2.3. XRD analysis

The diffractogram in Figure 7.3 a shows well-defined peaks at around 2θ values 16.46 and 22.25° for the (110) and (200) characteristic planes of cellulose.¹⁵ The diffractogram of CuO-NFC showed distinct peaks at 2θ values 30.49, 36.12, 40.60, 47.26, 52.27 and 56.66°, corresponding to the (110), (111), (200), (112), (020) and (021) Bragg reflection planes of the monoclinic structure (JCPDS data file 80-1917) of CuO respectively (Figure 7.3 b).

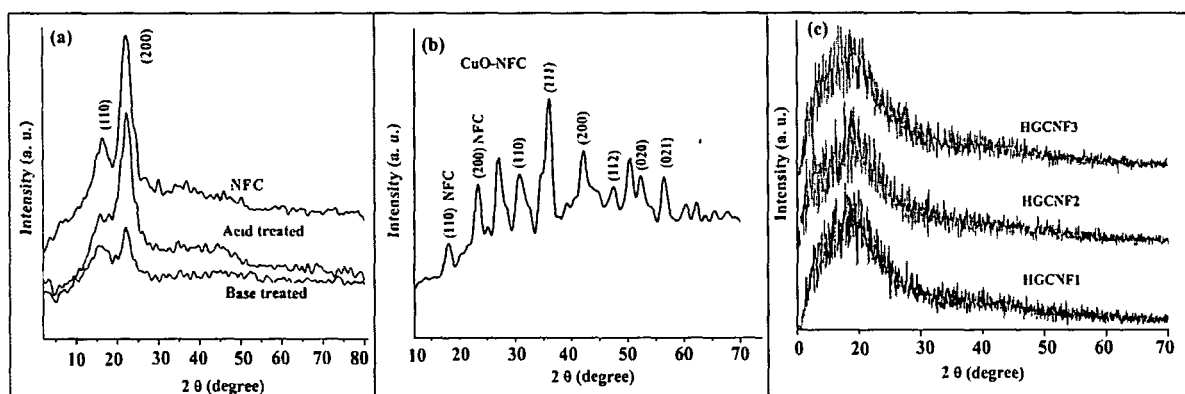


Figure 7.3: XRD patterns for (a) NFC, (b) CuO-NFC and (c) HGCNF

Again, the XRD patterns of HGCNF showed no distinct characteristic feature of CuO-NFC (Figure 7.3 c). This is attributed to the masking effect induced by the HGE5 matrix. Only 0.5 weight% loading of the nanohybrid could not show the Bragg's lattice reflection planes for CuO and NFC. However, the broad diffraction peaks around 2θ value 21° were observed due to presence of the amorphous hyperbranched matrix.

7.3.2.4. Morphological study

Distribution of CuO-NFC within the matrix is depicted in the TEM micrographs (Figure 7.4). Fibers were seen with diameter, ranging from 10-80 nm. CuO nanoparticles were decorated over NFC in uniform manner. Particle size distribution histogram demonstrated that maximum particles lie within a size spectrum of 5-10 nm. Dispersion of cellulose in polymeric system is very difficult due to high density of hydroxyl functionalities in cellulose, which imparts intramolecular hydrogen bonding.³⁰ However, in the present case amount of NFC is quite less as compared to the matrix. This confers good dispersibility of CuO-NFC within the epoxy system, as reflected by the TEM micrographs.

7.3.3. Curing study and performance of HGCNF

HGCNF were cured at 120°C by reacting with poly(amido amine) hardener. Cellulose possesses lots of hydroxyl groups which take part in the curing reaction. Thus, curing time decreased with increase in CuO-NFC loading (Table 7.1). Effect of CuO may be minimal in the crosslinking process. Besides, functionalities of HGE5 minimize the curing time. Successful curing was confirmed from the swelling values, which showed 70-80%

crosslinking in each case.

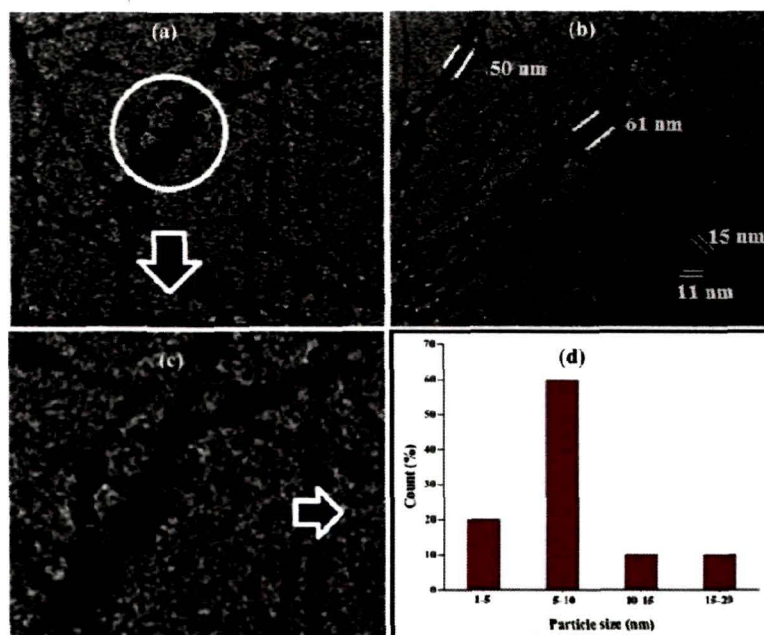


Figure 7.4: TEM images of (a-b) Distribution of CuO-NFC within the matrix, (c) Enlarged area of a and (d) particles size distribution histogram

Tensile strength increased with increase in the amount of CuO-NFC in HGCNF (Table 7.1). Interaction of NFC with epoxy and poly(amido amine) functionalities forms a rigid three dimensional network, which showed high stress bearing capacity. Again, electrostatic interaction of CuO with NFC and HGE5 further aid to the increment of tensile strength. Elongation at break signifies the amount of strain the material can withstand before the point of break. Increasing amount of CuO-NFC decreased the elongation value to a little extent. However, the bending test confirmed excellent flexibility of the materials, which can be folded to 180° curvature without crack. The strength and flexibility of HGCNF suggested that they can be used as a tough scaffold material, after assessing their bioactivities.

Adhesive strength also augmented with increase in the loading of CuO-NFC. Functional groups of HGCNF interact with the polar groups of woods by means of different secondary bonding forces. The overall mechanical study showed that formation of NC, enhanced the performance of the material to a significant extent ($p < 0.05$) over the pristine

Chapter 7

epoxy system.

Table 7.1: Curing parameters and performance of HGE5 and HGCNF

Property	HGE5 [#]	HGCNF1	HGCNF2	HGCNF3	LSD
Curing time at 120 °C (min)	24±0.58	22.93±0.4	20.83±0.45	19.17±0.4	0.345
Swelling (%)	22.6±0.43	23.2±1.08	24.47±1.45	23.7±1.07	0.992
Tensile strength (MPa)	38.4±0.84	44.3±0.86	50.7±0.56	55.4±0.68	0.58
Elongation at break (%)	21.3±0.57	20.67±0.61	18.2±0.2	15.7±0.2	0.318
Impact resistance (m)*	>1	>1	>1	>1	-
Scratch hardness (kg)*	>10	>10	>10	>10	-
Bending (mm)*	<1	<1	<1	<1	-
Adhesive strength (MPa)	768	2233±2.64	2382±2	2432±2	1.82

*Instrumental limits: Scratch hardness=10 kg, Impact resistance=1 m and bending test mandrel=1 mm

[#]As reported in Chapter 2, Table 2.2.

7.3.4. *In vitro* biocompatibility assessment

PBMC are the blood cells with a round nucleus, such as lymphocytes, monocytes etc. These blood cells have a critical role in the immune system and wound contraction.³¹ Thus, it is quite relevant to undertake a compatibility assessment of the nanomaterials with PBMC, which may reveal their potential to be used in advanced biomedical applications. Biocompatibility of CuO-NFC was examined through their interaction with PBMC. It is clear from Figure 7.5 that there is no change in the morphology of the cells after treating with CuO-NFC. Cell survival rate was found to be almost equal as to the control as evident from the MTT assay (Figure 7.6 a).

Cellulose fibers of nano dimension proved their compatibility in different *in vitro* tests. NFC thus exhibited 99% cell viability when incubated with wistar rat primary hepatocytes (Figure 7.6 b). However, a little decrement of viable cells was observed in case of CuO-NFC, which may be due to the high surface activity of the nanohybrid. Loading of CuO-NFC into HGE5 up to 0.5 weight% induced no significant toxicity to the hepatocytes. Hence, more than 89% cell survival was witnessed when incubated with HGCNF. The

differences might be due to the variable amounts of CuO-NFC within the matrices. One way ANOVA revealed that cell viability percentages are not significantly different from each other, with LSD 0.35 ($p < 0.05$).

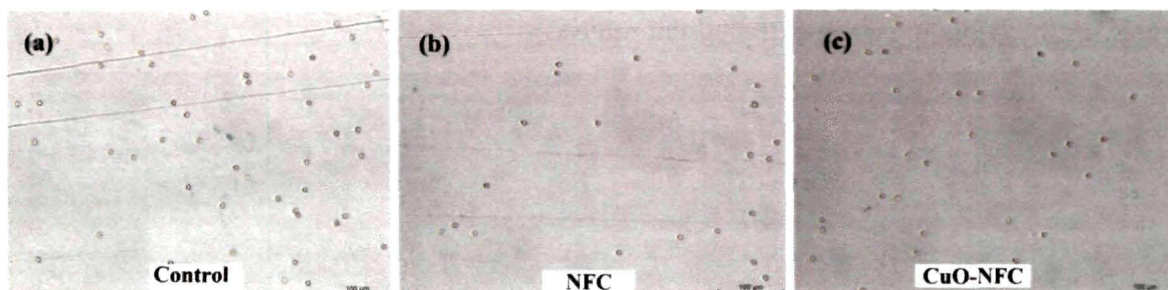


Figure 7.5: Microscopic images of Trypan Blue stained PBMC treated with NFC and CuO-NFC

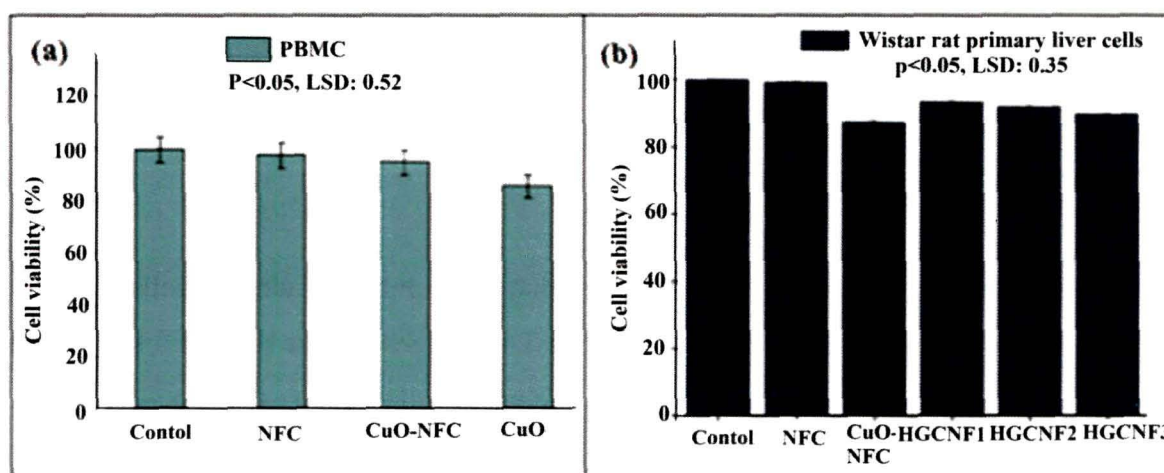


Figure 7.6: Cell survival (%) of (a) PBMC and (b) rat primary liver cells

7.3.5. Adhesion of L6 muscle cells on HGCNF3 scaffold

Cellulose based scaffolds are explored for the reconstruction of cardiovascular, bone and skin damages.³⁰ However, existing literature showcase very few reports regarding the use of cellulose based polymeric scaffolds for SMC regeneration.³² Microscopic images showed well adhered L6 cells on the HGCNF3 surface (Figure 7.7 a-d). No morphological alteration was witnessed for the adhered myocytes. This affirmation was further supported by the SEM micrographs where elongated myocytes were seen adhering on the surface of HGCNF3 (Figure 7.7 e-h). The vital characteristics of a scaffold material are to provide

mechanical toughness as well as compatible surface where cells can anchor on easily. Porous structure of cellulose helps the cells to adhere onto the HGCNF3 scaffold surface. Thus, HGCNF3 can provide a surface which supports the adherence and growth of myocytes, by behaving as an extracellular matrix.

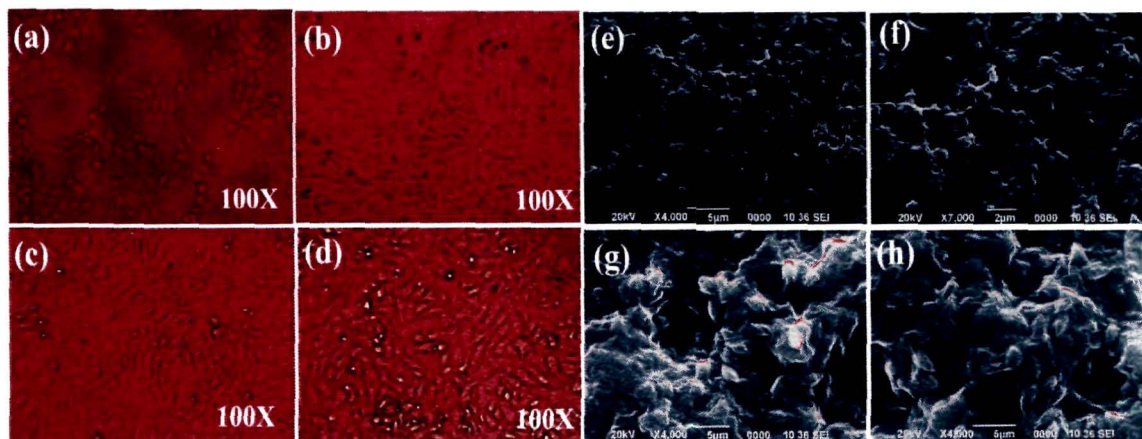


Figure 7.7: (a-d) Inverted microscope images of L6 cells adhered onto HGCNF3 on 1st to 4th day of incubation and (e-h) SEM images of L6 cells adhered onto HGCNF3 on 1st to 4th day of incubation

During the experiment, it was observed that the number of adhered cells increased with the increase of incubation time (Figure 7.8). This suggested that HGCNF3 surface can aid to the proliferation of myocytes, without inducing any abnormality to the cells.

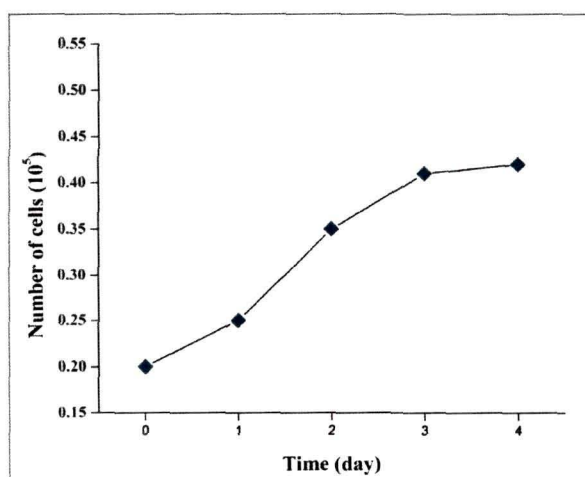


Figure 7.8: Growth rate of L6 cells on the surface of HGCNF3

7.3.6. *In vivo* implantation of HGCNF3 and host response

Chapter 7

Hematological parameters govern many important physiological functions in animal body. Abnormality to any of the parameter may lead to drastic disorder of metabolic system. The white blood cell components, such as monocytes, neutrophils and eosinophils respond to any xenobiotic material that enters the body and generate immunity against it. A change in their normal level is reflective of immune response to that material. In the present study, no sign of immunogenesis was observed from the hematological parameters of the rats after HGCNF3 implantation (Table 7.2). Further, all the parameters lie in the range that is comparable to that of control. This strongly affirms that HGCNF3 can be implanted into host body as an immunocompatible biomaterial.

Table 7.2: Hematological parameters of HGNFC3 implanted rats

Parameter	0 day		15 days		30 days	
	Control	HGCNF3	Control	HGCNF3	Control	HGCNF3
Lym (%)	39.1±0.18	37.5±0.6	40.4±1.5	39.8±0.7	39.2±0.7	40.2±0.40
Mon (%)	19.7±0.34	19.5±0.5	20.3±0.1	19.4±0.6	20.8±0.9	19.9±0.63
Neu (%)	64.48±0.5	63.9±0.3	62.5±0.5	63.4±0.8	65.1±0.4	64.3±0.56
Eo (%)	6.2±0.22	7.1±0.37	7.2±0.54	7.3±0.12	7.9±0.83	7.1±0.29
Ba (%)	0.5±0.19	0.6±0.51	0.7±0.21	0.8±0.48	0.9±0.78	0.9±0.39
RBC (m/mm ³)	8.2±0.74	8.3±0.21	8.8±0.23	8.1±0.89	8.2±0.52	8.3±0.93
MCV (fl)	65.2±0.89	64.7±0.9	66.4±0.7	64.1±0.6	64.1±0.8	64.1±0.82
Hct (%)	43.5±0.68	43.8±0.8	44.2±0.8	45.4±0.8	46.1±0.7	45.8±0.48
MCH (pg)	16.2±0.7	17.9±0.1	17.2±0.6	18.1±0.6	18.8±0.9	17.8±0.65
MCHC (g/dL)	38.59±0.3	37.1±0.3	37.2±0.7	39.1±0.6	39.2±0.1	38.9±0.87
Hb (g/dL)	14.6±0.56	15.1±0.5	14.2±0.1	15.1±0.8	14.5±0.8	15.8±0.81
Pct (%)	0.75±0.91	0.78±0.7	0.76±0.2	0.78±0.9	0.77±0.3	0.80±0.54

Again, toxicity of a material triggers many histological disorders. Histopathological study is therefore another vital tool for scrutinizing the host response to an implanted biomaterial. Here, skin section provides a clear picture of normal dermatocytes with intact epidermis and dermis (Figure 7.9). Similarly, liver and kidney sections showed regular

arrangement of portal vein, hepatocytes and glomerulus respectively. Normal brain cells are visible from the image of the brain section. Thus, a clear picture was obtained from the histopathological evaluations regarding the *in vivo* compatibility of HGCNF3. The study put forward HGCNF3 as a potential implant material in biomedical applications. However, microbial infection resisting capacity of an implant is desired to avoid post surgical complications.

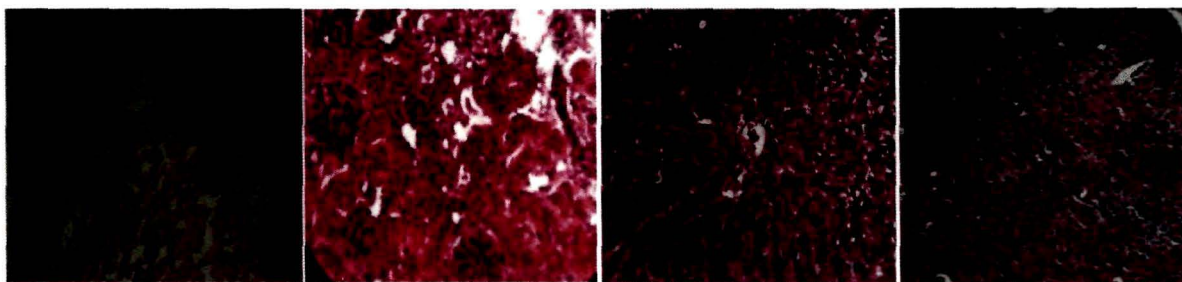


Figure 7.9: Histopathological sections of (a) skin, (b) kidney (c) liver and (d) brain of HGCNF3 implanted rat

7.3.7. Antimicrobial assay

MIC of the nanomaterials and HGCNF were calculated against *S. aureus*, *E. coli* and *C. albicans*. CuO nanoparticles showed the highest inhibitory effect against all the tested strains (Figure 7.10). Copper based antimicrobial materials are already commercialized for their efficient activity. Further, CuO nanoparticles were also well reported to possess excellent antimicrobial efficacy.³³ Surface activity of the nanoparticles basically causes damage to the microbes, by penetrating through their cell membranes. Again, nanohybrid formation caused a slight decrement of the MIC values against the strains. Further, indirect exposure of CuO-NFC suppressed the inhibitory effect to a small extent in case of HGCNF. However, all the materials showed significant detriment to bacteria and fungi. Statistically significant ($p < 0.5$) difference ($LSD = 0.81$) was witnessed for the MIC values in each case.

Zone of inhibition assay demonstrated no effect of NFC on both bacteria and fungus. Contrarily, CuO-NFC showed profound antimicrobial efficacy (Figure 7.11). HGCNF3 exhibited significant zones of inhibition in all the cases. However, the effect was stronger against Gram negative bacteria than the Gram positive one and weaker against the fungi. Greater zones were observed for CuO-NFC with respect to CuO. Exposure of the microbes to higher surface area of the nanohybrid might have affected this. The above two

Chapter 7

assays confirmed proficient activity of HGCNF against both Gram positive and negative bacteria as well as fungi.

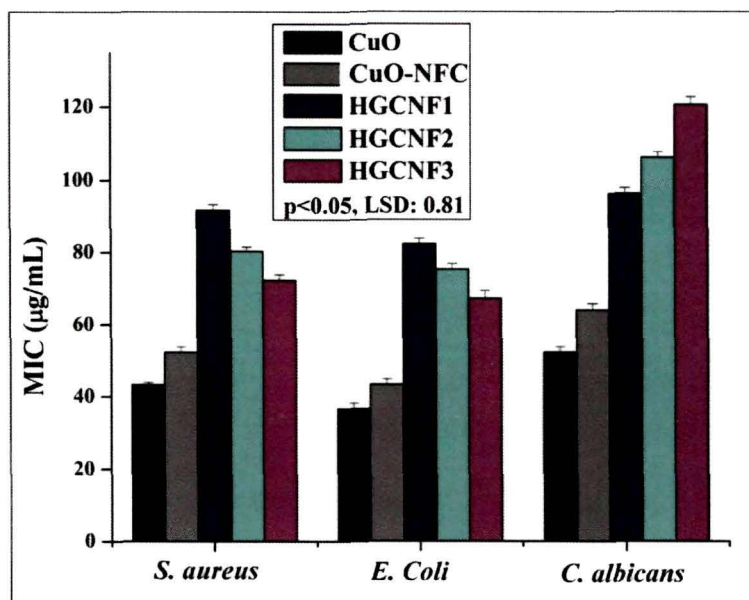


Figure 7.10: MIC values against *S. aureus*, *E. coli* and *C. albicans*

Activity of the HGCNF thermosets was analyzed against *S. aureus*, by incubating HGE5 and the HGCNF with the bacterium. The SEM micrographs showed clear morphological alteration of cells when incubated with the HGCNF, while contrary result was noticed for HGE5. The red marks (Figure 7.12) indicated the shrinkage and membrane disruption of *S. aureus* cells that were adhered to the HGCNF surfaces. The inhibitory effect shows clear increment from HGCNF1 to HGCNF3, which is owing to the increase in loading of CuO-NFC.

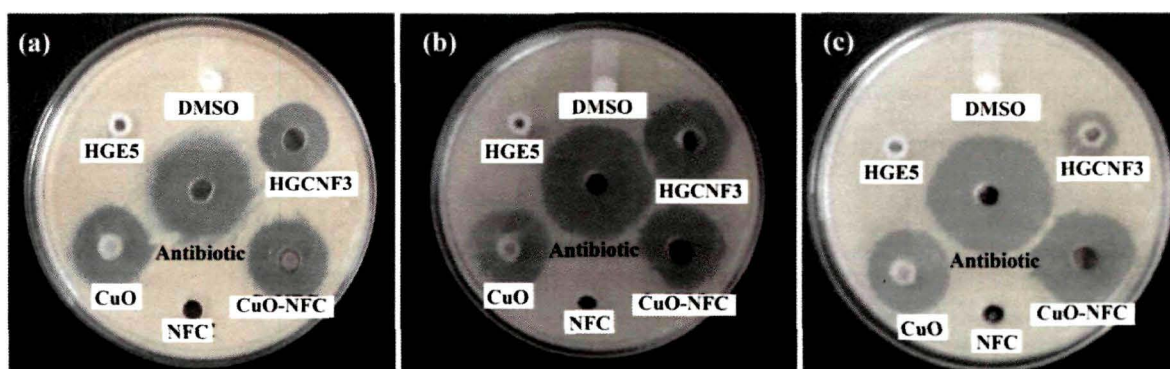


Figure 7.11: Zones of inhibition against (a) *S. aureus*, (b) *E. coli* and (c) *C. albicans*

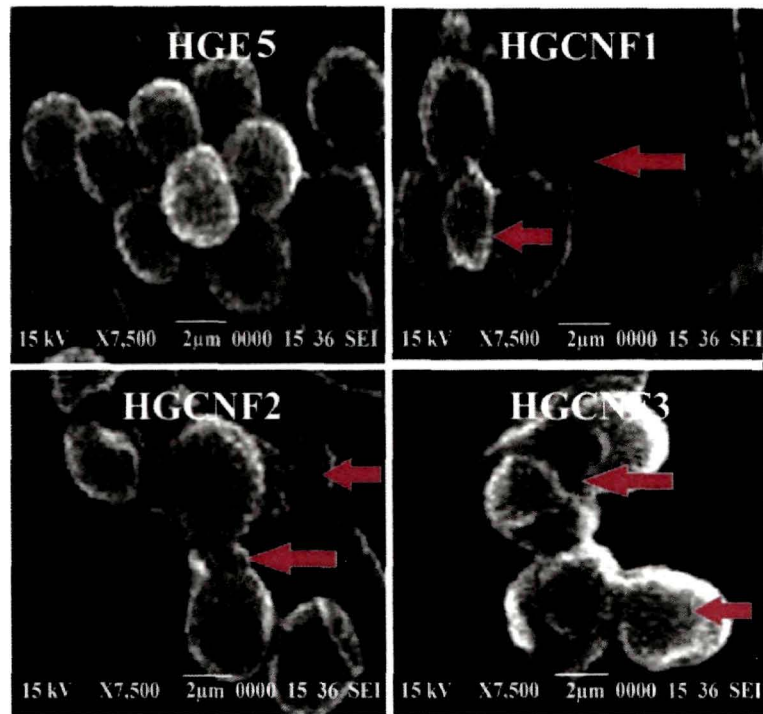


Figure 7.12: SEM micrographs of *S. aureus* adhered to HGE5 and HGCNF

7.4. Conclusion

The study showed the unison of polymer science and nanotechnology to fabricate an antimicrobial implantable biomaterial. NFC was isolated from *C. esculenta* stems by a chemical method and CuO nanoparticles were decorated on the surface of the nanofibrils. The advantageous attributes of HGE5 and CuO-NFC conferred HGCNF high strength and flexibility as well as efficient antimicrobial property. HGCNF3 supported the growth and proliferation of L6 muscle cells, by providing a compatible surface. Cytocompatibility of the material was confirmed by incubating with mammalian PBMC and primary hepatocytes. Moreover, HGCNF3 exhibited positive host response when implanted within rat host. The overall study thus forwards an antimicrobial, non toxic implantable scaffold material for muscle tissue reconstruction.

References

1. Campbell, K.P. *Cell*, **80** (5), 675--679, 1995.
2. Cassell, C.S.O., et al. *J. Plast. Surg.* **55** (8), 603--610, 2002.
3. Nikolovski, J. & Mooney, D.J. *Biomaterials* **21** (20), 2025--2032, 2000.

Chapter 7

4. Dennis, R.G. & Cosnik, P.E. *Biol. Anim.* **36** (5), 327--335, 2000.
5. Danielsson, C., et al. *Biomaterials* **27** (8), 1410--1415, 2006.
6. Cheung, H., et al. *Compos. Part B-Eng.* **38** (3), 291--300, 2007.
7. Hutmacher, D.W., et al. *J. Biomater. Sci. Polym. Ed.* **12** (1), 107--124, 2001.
8. Mooney, D.J., et al. *Biomaterials* **17** (2), 115--124, 1996.
9. Drury, J.L. & Mooney, D.J. *Biomaterials* **24** (24), 4337--4351, 2003.
10. Koning, M., et al. *J. Tissue. Eng. Regen. Med.* **3** (6), 407--415, 2009.
11. Chaturvedi, V., et al. *Aust. Biochem.* **42** (3), 8--10, 2011.
12. Klemm, D., et al. *Adv. Polym. Sci.* **205**, 49--96, 2006.
13. Moran, J.I., et al. *Cellulose* **15** (1), 149--159, 2008.
14. Bai, W., et al. *Cellulose* **16** (3), 455--465, 2009.
15. Mandal, A. & Chakrabarty, D. *Carbohydr. Polym.* **86** (3), 1291--1299, 2011.
16. Alemdar, A. & Sain, M. *Bioresour. Technol.* **99** (6), 1664--1671, 2008.
17. Kramer, F., et al. *Macromol. Symp.* **244** (1), 136--148, 2006.
18. Dong, X.M., et al. *Cellulose* **5** (1), 19--32, 1998.
19. Hussain, M., et al. *J. Sci. Food Agric.* **35** (10), 1112--1119, 1984.
20. Mano, J.F., et al. *J. R. Soc. Interface* **4** (17), 999--1030, 2007.
21. Petersen, N. & Gatenholm, P. *Appl. Microbiol. Biotechnol.* **91** (5), 1277--1286, 2011.
22. Michael, L.F., et al. *PNAS* **98** (7), 3820--3825, 2001.
23. Hamed, O.A., et al. *BioResources* **7** (3), 1490--4201, 2012.
24. Habibi, Y., et al. *Chem. Rev.* **110** (6), 3479--3500, 2010.
25. Jia, B., et al. *ACS Appl. Mater. Interfaces* **4** (6), 2897--2902, 2012.
26. Muller, F.A., et al. *Biomaterials* **27** (21), 3955--3963, 2006.
27. Mattoussi, H., et al. *Adv. Drug. Deliver. Rev.* **64** (2), 138--166, 2012.
28. Rathinamoorthy, R., et al. *J. Pharma. Sci. Nanotech.* **4**, 1549--1556, 2012.
29. Rahman, A., et al. *Indo. J. Chem.* **9** (3), 355--360, 2009.
30. Kondo, T. *J. Polym. Sci., Part B: Polym. Phys.* **35** (4), 717--723, 1997.
31. Yang, L., et al. *Lab. Invest.* **82**, 1183--1192, 2002.
32. Petersen, N. & Gatenholm, P. *Appl. Microbiol. Biotechnol.* **91** (5), 1277--1286, 2011.
33. Azam, A., et al. *Int. J. Nanomed.* **7**, 3527--3535, 2012.

Chapter 8

Conclusion and future scopes

Highlights

The present chapter summarizes the thesis with the remarks of the present investigation. Results of the study are compiled with an emphasis on the potential biomedical applications of the prepared materials. Chapter wise findings are briefed and concluding remarks are drawn out based on the obtained results. Finally, a few future directions of the present investigation are mentioned, which may be studied for further exploration of such hyperbranched epoxy thermosets.

Chapter 8

8.1. Summery and conclusions

The thesis explicates the utility of glycerol based hyperbranched epoxy thermoset and its NC for potential biomedical applications. The effect of incorporation of different nanomaterials on the properties of the NC was analyzed extensively. The first chapter depicted a general introduction to the development of biomaterials with time. A brief review on the emergence of polymeric biomaterials is taken into account with special emphasis on epoxy thermosets. Further, prospect of HE in biomedical domain is discussed in the chapter. On the basis of reported literature, preparation, characterization, properties and applications of epoxy/NC based biomaterials are briefly addressed. Objectives and plans of works for the present investigation were set in relevance to the importance of the proposed research.

Various methodologies have been applied to synthesize HE, by varying the reactants and reaction strategies. In this respect, the second chapter described the synthesis of a glycerol based HE via $A_2 + B_3$ approach, following a single step polycondensation reaction. Three HGE systems were synthesized by varying the amount of the environmentally benign moiety, glycerol. The synthesized resins were characterized with various analytical and spectroscopic techniques. Thermo-mechanical properties as well as *in vitro* biocompatibility of the materials are reported thoroughly in this chapter.

Application of HE based NC in the domain of biomedical research is rare in literature. Thus, the preparation of an antimicrobial biomaterial based on HGE5/clay NC is described in the third chapter. *H. aromatica* rhizome oil modified bentonite and OMMT clay were incorporated into HGE5 matrix to study the property enhancement of the NC systems. Further, *in vitro* and *in vivo* studies established the compatibility of the material with mammalian system. The best performing NC supported the growth of dermatocytes on its surface, without induction of any detriment to the cells. The material also exhibited profound antimicrobial efficacy against bacteria and fungi.

Chapter 4 demonstrated the preparation and characterization of HGE5/clay-silver NC based infection resistant tough implantable scaffold material. 'Green' AgNP were synthesized by using the aqueous extract of *T. occidentalis* leaves and decorated onto M-OMMT. The nanohybrid embedded NC showed augmentation of mechanical properties and imparted excellent antimicrobial activity. *In vivo* implantation of the material fostered the

Chapter 8

wound healing in wistar-rats by acting as an extra cellular matrix for skin regeneration. No sign of toxicity was witnessed after implantation of the material to the rat host.

A highly efficient antimicrobial implantable material is reported in the fifth chapter based on HGE5/Ag-RGO-Cur NC. Ag-RGO was synthesized by simultaneous reduction of AgNO₃ and GO, by the aid of *C. esculenta* leaf extract. A naturally abundant biomolecule, curcumin was sonochemically immobilized to the nanohybrid, which upon incorporation into HGE5 exhibited improvement of material properties as compared to the pristine matrix. The NC strongly inhibited the growth of bacteria, fungi and microalgae on its surface. Further, *in vitro* and *in vivo* assessment confirmed excellent biocompatibility of the NC.

The sixth chapter included the description of an advanced antimicrobial biomaterial based on HGE5/CNT-CuO-Nys NC. CuO nanoparticles were anchored *in situ* onto MWCNT by a 'green' approach, whereon an antifungal agent, nystatin was immobilized. Incorporation of this nanomaterial into HGE5 resulted tremendous increment of mechanical performance as well as antimicrobial efficacy against bacteria, fungi and microalgae. Biocompatibility of the material was ascertained by *in vitro* and *in vivo* assessments.

The seventh chapter described the isolation of NFC from a very common natural bioresource, *C. esculenta* by a facile chemical method. CuO nanoparticles were decorated onto NFC surface and the nanohybrid was utilized to prepare HGE5/NFC-CuO NC. The NC exhibited excellent antimicrobial properties with high mechanical attributes. The material supported the growth and proliferation of L6 muscle cells on its surface without causing any damage to the cells. Further, the material did not induce any sign of toxicity when tested both *in vitro* and *in vivo*.

Concluding remarks of the present thesis are briefed herein.

- i) The study describes the successful synthesis of a glycerol based biocompatible HE resin via single step polycondensation reaction, following an A₂ + B₃ approach.
- ii) HGE system proved superiority over the conventional linear analog in regard of mechanical strength and flexibility.
- iii) Incorporation of *H. aromatica* rhizome oil modified OMMT into HGE5 resulted a tough, biocompatible NC, which supported the growth of dermatocytes on its surface. Utility of the oil further conferred antimicrobial efficacy to the implantable biomaterial.

Chapter 8

- iv) Silver embedded modified OMMT clay based HGE5 NC served as a tough, infection resistant implantable scaffold material, which enhanced the wound healing in wistar rats.
- v) Ag-RGO-Cur based HGE5 NC proved its efficiency as an antimicrobial biomaterial with high mechanical attributes. The NC showed proficient inhibitory effect against bacteria, fungi and microalgae, without induction of toxicity as tested both *in vitro* and *in vivo*.
- vi) A CNT-CuO nanohybrid immobilized nystatin reinforced HGE5 matrix showed tremendous increment of mechanical performance. This NC system was highly effective against *S. aureus* and *C. albicans*, the microorganisms mostly responsible for surgical site infections. Again, the same material prevented the growth of the microalgae, *Chlorella* sp. on its surface. Further, no toxic effect was noticed for the material on implantation within wistar rat.
- vii) Natural resource based NFC on decoration with 'green' CuO nanoparticles served as an efficient nanohybrid for advanced applications. This nanohybrid based HGE5 NC supported the growth of L6 muscle cells without hindering their normal cellular behavior. Further, the material served as an antimicrobial scaffold with excellent mechanical strength.

The overall investigation demonstrated the potential utility of thermosetting epoxy based NC in various domains of biomedical science. Throughout the thesis, emphasis was given to achieve 'green' credentials in the synthetic approaches, by using benign materials as well as methodologies. Glycerol based HGE5/NC thus can be endorsed as multifaceted biomaterials with various advantageous attributes over the prevailing materials in the domain. However, it is mandatory to carry out clinical trials critically before applying to actual fields.

8.2. Future scopes

The thesis compiles a comprehensive study regarding the potential use of HGE5 NC based biomaterials in possible domains. However, the work may establish a platform for future research, which would be quite relevant for the development of such materials.

- i) Carbon dot based NC can be prepared by using the HGE5 matrix, which would impart fascinating optical properties with a great room for utility in biomedical imaging.

Chapter 8

- ii) Detailed clinical testing can be performed for the prepared biomaterials for their actual endorsement to the real fields of applications.
- iii) Extensive investigation can be made for studying the antimicrobial behavior of the materials against a broad spectrum of microbes.
- iv) The skin and muscle tissue scaffolds can be implanted to higher animals like rabbit and pig to observe the efficacy of the materials.

List of publications

In Journals

From thesis

- 1) Barua, S., Dutta, G. & Karak, N. *Chem. Eng. Sci.* **95**, 138--147, 2013.
- 2) Barua, S., Dutta, N., Karmakar, S., Chattopadhyay, P., Aidew, L., Buragohain, A.K. & Karak, N. *Biomed. Mater.* **9**, 025006--025019, 2014.
- 3) Barua, S., Konwarh, R., Bhattacharya, S.S., Das, P., Devi, K.S.P., Maiti, T.K., Mandal, M. & Karak, N. *Colloids Surf., B* **105**, 37--42, 2013.
- 4) Barua S., Chattopadhyay, P., Aidew, L., Buragohain, A.K. & Karak, N. *Polym. Int.* DOI: 10.1002/pi.4790, 2014.
- 5) Barua, S., Thakur, S., Aidew, L., Buragohain, A.K., Chattopadhyay, P. & Karak, N. *RSC Adv.* **4** (19), 9777--9783, 2014.
- 6) Barua, S., Chattopadhyay, P., Phukan, M.M., Konwar, B.K., Islam, J. & Karak, N. *RSC Adv.* **4** (88), 47797--47805, 2014.
- 7) Barua, S., Chattopadhyay, P., Phukan, M.M., Konwar, B.K., & Karak, N. *Mater. Res. Express* **1** (4), 045402--045419, 2014.
- 8) Barua, S., Das, G., Aidew, L., Buragohain, A.K. & Karak, N. *RSC Adv.* **3** (35), 14997--15004, 2013.
- 9) Barua, S., Gogoi, B.J., Aidew, L., Buragohain, A.K., Chattopadhyay, P. & Karak, N. *ACS Biomater. Sci. Eng.* 2014 (*Under review*)

Other related publications

- 1) Barua, S., Konwarh, R., Mandal, M., Gopalakrishnan, R., Kumar, D. & Karak, N. *Adv. Sci. Eng. Med.* **5** (4) 291--298, 2013.
- 2) Barua, S., Sengupta, A., Banerjee, P.P., Chatterjee, S., Sarkar, S., Barman, S., Chattopadhyay, A., Bhattacharya, S., Mondal, N.C. & Karak, N. 2014(*Communicated*).
- 3) Gogoi, S., Barua, S. & Karak, N. *Prog. Org. Coat.* **77** (9), 1418--1427, 2014.
- 4) Gupta, K., Barua, S., Hazarika, S.N., Manhar, A.K., Nath, D., Karak, N., Namsa, N.D., Mukhopadhyay, R., Kalia, V.C. & Mandal, M. *RSC Adv.* **4** (95) 52845--52855, 2014.
- 5) Thakur, S., Barua, S. & Karak, N. *RSC Adv.* DOI: 10.1039/C4RA11730A, 2014.
- 6) Gogoi, S., Barua, S. & Karak, N. *Chem. Eng. Sci.* 2014(*Under review*).

In conferences

1. Barua, S., Konwarh, R., Mandal, M. & Karak, N. Greener approach to prepare polymer stabilized biocidal silver nanoparticles, National workshop on recent trends in nanoscience and technology (RETNAT-11), Jorhat (Assam), 2011.
2. Barua, S., Konwarh, R., Devi, K.S P., Maiti, T. & Karak, N. Biomimetically prepared antibacterial and anti-cancerous PEG@Ag nanoparticles, National workshop on emerging trends in nanochemistry (NWETNC- 11), Shillong (Meghalaya), 2011.
3. Barua, S., Das, I. & Karak, N. Epoxy cured, pumpkin seed oil modified polyester resin as surface coating material, National conference on chemistry, chemical technology and society (NCCCTS-11) Tezpur (Assam), 2011.
4. Barua, S., Chottapadhyay, P. & Karak, N. Bio-resource based thermostable and cytocompatible micro-crystalline cellulose, 100th Indian science congress, Kolkata, 2013.
5. Barua, S., Chottapadhyay, P. & Karak, N. Hyperbranched epoxy clay nanocomposite as tissue scaffold material, National conference on health and hygiene (TEZCON-12), Defence Research Laboratory, Tezpur (Assam), 2012.
6. Barua, S. & Karak, N. Carbon nanotube copper oxide nanohybrid immobilized antibiotic as an efficient antimicrobial agent, 3rd International conference on advanced nanomaterials and nanotechnology (ICANN-13), Guwahati (Assam), 2013.
7. Barua, S. & Karak, N. Hyperbranched epoxy/clay nanocomposite as an efficient antimicrobial coating material, APA International Conference on Polymers : Vision & Innovations, Delhi, 2014.